

On the Present and Future Changes in Climate Extremes Over India

Author:

Marc Norgate

Supervised by:

Dr. P. R. Tiwari

Prof. R. S. Sokhi

Centre for Atmospheric and Climate Physics Research

Centre for Climate Change Research

Department of Physics, Astronomy and Mathematics

School of Physics, Engineering and Computer Science

University of Hertfordshire

*Submitted to the University of Hertfordshire in partial fulfilment of the requirements of
the degree of Doctor of Philosophy*

October 2024

Abstract

This work uses state-of-the-art Global and Regional Climate Models to assess present and future changes in climate extremes over India. India has the world's largest population and many of the people there are extremely vulnerable to future changes in Climate extremes.

The fidelity of general circulation models (GCMs) from the Coupled Model Intercomparison Project version 6 (CMIP6), to simulate temperature and precipitation over India. The period of study is split into three parts, historical (1984-2014), near-future (2030-2060) and far-future (2070-2100). The models are found to have varying biases, and the computation of a multi-model mean shows an improvement upon these biases. Future projections make use of the newest Shared Socioeconomic Pathways (SSPs), which generally show an increase in both mean and extreme climate variables. This increase is most extreme under the high emission scenario SSP5-8.5 for both temperature and precipitation.

Due to the coarse resolution of GCMs, dynamical downscaling (at 25 km resolution) is applied with the use of the Regional Climate Model version 4.7 (RegCM4.7) from The Abdus Salam International Centre for Theoretical Physics (ICTP). Sensitivity experiments have been carried out to better tune RegCM4.7 to the Indian domain. Orography representation, cumulus convection schemes and land surface schemes are tested, and the best schemes are selected for the purpose of model parameterisation. A better representation of moisture transport, surface fluxes and soil moisture are shown to improve the simulation of temperature and precipitation extremes in the RCM. Envelop orography treatment (i.e. increasing orography from model mean height) by 10%, the use of the Grell over land and Emanuel over ocean cumulus schemes and the Community Land Model land surface scheme are found to give the best results over the Indian domain.

The aforementioned RCM is found to improve upon all tested GCMs in the simulation of temperature and precipitation over India. For future simulations, heat waves are found to increase in both frequency and duration when compared to the present climate. The areas most affected by this increase are along the Indo-Gangetic plane, where most of the Indian population resides. Future temperature extremes projected by the RCM are greater than those of the GCMs and heat wave frequency and duration is more severe in RCM simulations. Precipitation intensity is greater in the RCM than the GCM for the PR, however most regions (CNE, HR, NE and NW) are shown to have a decrease in mean precipitation. The areas most impacted by this increase are along the Westcoast of India, where most of the monsoon rainfall occurs. Extreme precipitation is greater during the near future in the RCM for all SSPs and the increase from near to far future is lesser than what is shown by the GCMs. The increases in both climate extremes are found to be worsened when using the high emission scenario SSP5-8.5 and are shown to improve when using the sustainable scenario SSP1-2.6 towards the end of the century.

Overall, this study highlights the importance of dynamical downscaling as an important tool for predicting climate extremes over India and understanding the impacts of climate change over this region. These results emphasise the importance of sufficient mitigation strategies to lessen the impact of climate extremes over India and the urgent need to act sooner rather than later.

Declaration

I declare that no part of this work is being submitted concurrently for another award of the University or any other awarding body or institution. This thesis contains a substantial body of work that has not previously been submitted successfully for an award of the University or any other awarding body or institution.

The following parts of this submission have been published previously and/or undertaken as part of a previous degree or research programme:

1. Chapters 1 and 2: Marc Norgate, P. R. Tiwari, S. Das and D. Kumar (2024). On the heat waves over India and their future projections under different SSP scenarios from CMIP6 models. *International Journal of Climatology, Royal Meteorological Society*, 44(3). doi.org/10.1002/joc.8367
2. Chapters 1 and 3: Marc Norgate, P. R. Tiwari and S. Das (2024). On the present and future changes in Indian summer monsoon precipitation characteristics under different SSP scenarios from CMIP6 models. *Climate Dynamics*, Springer, (Accepted, in press).
3. Chapter 4: Marc Norgate, P.R. Tiwari, S. Das (2024). Sensitivity experiment with orography, convective and land surface schemes in the regional climate model driven by HadGEM3-GC31-LL, *International Journal of Climatology, Royal Meteorological Society*, (to be submitted)
4. Chapter 5: Marc Norgate, P.R. Tiwari, S. Das (2024). On the present and future changes in climate extremes over India using the dynamical downscaling approach, *Quarterly Journal of the Royal Meteorological Society, Royal Meteorological Society* (to be submitted)
5. Chapter 5: P. Maharana, D. Kumar, S. Das, P. R. Tiwari., Marc Norgate & V. Raman (2024). Projected changes in heatwaves and its impact on human discomfort over India due to global warming under the CORDEX-CORE framework. *Theor Appl Climatol, Springer*, 155, 2775–2786

Except where indicated otherwise in the submission, the submission is my own work and has not previously been submitted successfully for any award.

Acknowledgements

I would like to thank the following people, who I would not have been able to complete this thesis without. My supervisor Dr. Raj Tiwari for all his help and support throughout my PhD and the countless meetings throughout the years that were essential for my development in research. Dr. Sushant Das, who provided valuable feedback throughout my PhD. Dr. Dharendra Kumar, who answered many of my coding questions towards. Prof. Ranjeet Sokhi for his support as my secondary supervisor. Finally, to my friends and family who have shown endless support and encouragement during my PhD and who I am extremely grateful for.

Contents

Abstract	i
Declaration	iii
Acknowledgements	iv
Contents	v
List of Figures	viii
List of Tables	xiv
List of Abbreviations	xv
1 Introduction	1
1.1 Background	2
1.2 Characteristics of Summertime Circulation and Associated Temperature and Precipitation	3
1.2.1 General Circulation	3
1.2.2 Regional Circulation	5
1.2.3 Temperature Extremes	6
1.2.4 Precipitation Extremes	7
1.2 Climate Modelling	8
1.3.1 Coupled Model Intercomparison Project (CMIP)	10
1.3.2 Regional Climate Modelling	11
1.3.2.1 Dynamical Downscaling	12
1.3.2.2 Statistical Downscaling	13
1.4 Objective and Scope	13
2 Fidelity of CMIP6 Models in Simulating Temperature and Associated Extremes Over India	15
2.1 Introduction	17
2.2 Methodology	18
2.2.1 Indian Temperature Homogenous Regions and Observed Data	18
2.2.2 CMIP6 Experiments	19
2.2.3 Shared Socioeconomic Pathways	21
2.3 Results and Discussion	23
2.3.1 Temperature Biases of CMIP6 Models	23
2.3.2 Statistical Analysis of CMIP6 Models	27
2.3.3 Future Changes in Temperature	30
2.3.3.1 Extreme Temperature Analysis	38
2.4 Conclusion	48

3 Fidelity of CMIP6 Models in Simulating Precipitation and Associated Extremes Over India	50
3.1 Introduction	52
3.2 Methodology.....	53
3.2.1 Indian Precipitation Homogenous Regions and Observed Data.....	53
3.2.2 CMIP6 Experiments	54
3.2.3 Future Scenarios and Extreme Precipitation Variables	55
3.3 Results and Discussion.....	57
3.3.1 CMIP6 Performance in Capturing ISM Characteristics.....	57
3.3.2 Future Changes ISM Characteristics over South Asia.....	64
3.3.2.1 Future Changes in JJAS Extreme Precipitation.....	68
3.4 Conclusion.....	75
4 Customization of RCM Through Sensitivity Experiments	77
4.1 Introduction	79
4.2 Methodology.....	82
4.2.1 Hadley Centre Global Environment Model Version 3 (HadGEM3)	82
4.2.2 Regional Climate Model.....	83
4.3 Experimental Framework and Data	84
4.4 Results and Discussion	90
4.4.1 Himalayan Orography Representation.....	90
4.4.1.1 Zonal Moisture Transport	90
4.4.1.2 Precipitation	90
4.4.2 Convective Parameterization Schemes	95
4.4.2.1 Circulation Features.....	95
4.4.2.2 Precipitation	97
4.4.2.2.1 Precipitation Distribution	97
4.4.2.2.2 Statistical Analysis of Precipitation Simulation in RegCM4.....	98
4.4.3 Land Surface Schemes	99
4.4.3.1 Analysis of Soil Moisture and Sensible Heat Flux	100
4.4.3.2 Precipitation Statistical Evaluation	102
4.5 Conclusion.....	103
5 Dynamical Downscaling of Climate Extremes Over India and Future Scenarios using SSP's	105
5.1 Introduction	107
5.2 Methodology.....	108
5.2.1 RCM Configuration.....	108
5.2.2 Observed Data and Future Temperature and Precipitation Simulations	109

5.3 Results and Discussion.....	110
5.3.1 Temperature Extremes using RCM Simulations.....	110
5.3.1.1 HadGEM and RegCM4 Historical Analysis	110
5.3.1.2 RegCM4 Future Projections over India	112
5.3.1.2.1 Future Changes in Heat Wave Characteristics	113
5.3.2 Precipitation extremes using RCM simulations	120
5.3.2.1 HadGEM and RegCM4 Historical Analysis	120
5.3.2.2 Future Changes in Precipitation.....	122
5.3.2.2.1 Extreme Precipitation	125
5.4 Conclusion.....	127
6 Conclusion and Future Scope	130
Appendix	135
Python Code	135
Time Average Computation.....	135
Probability Density Function.....	135
Spatial Map.....	136
Time Series	137
Diagonal Correlation Matrix	138
Vertically Integrated Moisture Transport Calculation	140
References.....	142

List of Figures

1. **Figure 1.1** - General circulation. Hadley Cells are between the equator and a latitude of 30°, Mid-latitude cells are between 30° and 60°, and polar cells at higher latitudes. North-easterly and south-easterly trade winds occur in the lower parts of the Hadley Cells, which meet in the Inter Tropical Convergence Zone (ITCZ). Air rises to form frequent thunderstorms and heavy rainfall.
2. **Figure 1.2** – Precipitation, SST and wind speed over South Asia for winter (1.2a) and summer (1.2b). Precipitation and SST are shown over land and ocean respectively.
3. **Figure 1.3** – Observed (CRU) mean temperature (1901-2014) during JJA over the Indian temperature homogenous regions.
4. **Figure 1.4** - Observed (CRU) mean precipitation (1901-2014) during JJAS over the Indian precipitation homogenous regions.
5. **Figure 2.1** - Study area and different temperature homogenous regions over India.
6. **Figure 2.2** - Schematic diagram showing the methodology used for the analysis.
7. **Figure 2.3** - Annual mean near surface temperature difference of models compared to observation for the period 1984-2014. Ensemble mean of 13 CMIP6 models (a) and individual CMIP6 models used in ensemble (b-n). The dots represent the grid points with significant differences at 95% significance level.
8. **Figure 2.4** -JJA mean near surface temperature difference of models compared to observation for the period 1984-2014. Ensemble mean of 13 CMIP6 models (a) and individual CMIP6 models used in ensemble (b-n). The dots represent the grid points with significant differences at 95% significance level.
9. **Figure 2.5** - Annual maximum (a, b, c), mean (d, e, f) and minimum (g, h, i) temperature (°C) over the temperature homogenous regions of India for the historical period (1984-2014). Column (a, d, g) shows observed temperature, column (b, e, h) shows the ensemble mean of CMIP6 models and column (c, f, i) shows the difference between the models and observed temperature. The dots represent the grid points with significant differences at 95% significance level.
10. **Figure 2.6** - JJA maximum (a, b, c), mean (d, e, f) and minimum (g, h, i) temperature over the temperature homogenous regions of India for the historical period (1984-2014). Column (a, d, g) shows observed temperature, row (b, e, h) shows the ensemble mean of CMIP6 models and column (c, f, i) shows the difference between the models and observed temperature. The dots represent the grid points with significant differences at 95% significance level.
11. **Figure 2.7** - Taylor diagram showing the annual (a, b, c) and JJA (d, e, f) maximum (a, d) mean (b, e) and minimum (c, f) temperature over India. The correlation coefficient and normalised standard deviation for 13 CMIP6 models compared to observations are shown. The grey curved lines show the root mean square error (RMSE).
12. **Figure 2.8** - Diagonal correlation matrix for JJA tas (a, c) and tasmx (b, d) over the Indian temperature homogenous regions. Correlation is shown for the individual models (columns 2-14) and the ensemble mean of these models (column 1) compared to observed values for the

historical period (1984-2014). Fig a and b show the spatial correlation and fig c and d show the temporal correlation.

13. **Figure 2.9** - Annual (a) and JJA (b) mean near surface temperature over India. The solid grey line shows observed temperature, and the dashed grey line shows the present ensemble mean temperature for the historical period (1984-2014). The green, blue and red lines represent SSP1-2.6, SSP2-4.5 and SSP5-8.5. For the SSPs a solid line represents the NF (2030-2060), and a dashed line represents the FF (2070-2100).
14. **Figure 2.10** - JJA mean near surface temperature for each temperature homogenous region over India. The solid grey line shows observed temperature, and the dashed grey line shows the present ensemble mean temperature for the historical period (1984-2014). The green, blue and red lines represent SSP1-2.6, SSP2-4.5 and SSP5-8.5. For the SSP scenarios a solid line represents the NF (2030-2060), and a dashed line represents the FF (2070-2100).
15. **Figure 2.11** - Annual mean near surface temperature for each temperature homogenous region over India. The solid grey line shows observed temperature, and the dashed grey line shows the present ensemble mean temperature for the historical period (1984-2014). The green, blue, and red lines represent SSP1-2.6, SSP2-4.5 and SSP5-8.5. For the SSP scenarios a solid line represents the NF (2030-2060), and a dashed line represents the FF (2070-2100).
16. **Figure 2.12** - The difference in JJA Tmax for each SSP1-2.6 (a, b), SSP2-4.5 (c, d) and SSP5-8.5 (e, f) compared to the historical period from the ensemble mean. The first column (a, c, e) shows the NF difference, and the second column (b, d, f) shows the FF difference.
17. **Figure 2.13** - JJA maximum (a), mean (b) and minimum (c) near surface temperature over India for historical (1984-2014) and future (2015-2100). The magenta line is the observed temperature, and all others are an ensemble mean of 13 CMIP6 models. Near future (NF) is shown from 2030-2060 and far future (FF) is shown from 2070-2100. Grey represents the historical time period, and the green, blue and red lines represent SSP1-2.6, SSP2-4.5 and SSP5-8.5 respectively.
18. **Figure 2.14** - Annual maximum (a), mean (b) and minimum (c) near surface temperature over India for historical (1984-2014) and future (2015-2100). The magenta line shows the observed temperature, and all others are an ensemble mean of 13 CMIP6 models. Near future (NF) is shown from 2030-2060 and far future (FF) is shown from 2070-2100. The black line shows the historical time period, and the green, blue and red lines represent SSP1-2.6, SSP2-4.5 and SSP5-8.5 respectively. The shaded regions show the 95% confidence interval using the student-t test.
19. **Figure 2.15** - Consecutive summer days index per summer season difference compared to the ensemble mean of the historical period (1984-2014) for SSP1-2.6 (a, b), SSP2-4.5 (c, d) and SSP5-8.5 (e, f). The first column shows the difference over the NF period (a, c, e) and the second column shows the difference over the FF period (b, d, f).
20. **Figure 2.16** - Warm days percent with reference to the 90th percentile of the summer season difference compared to the ensemble mean of the historical period (1984-2014) for SSP1-2.6 (a, b), SSP2-4.5 (c, d) and SSP5-8.5 (e, f). The first column shows the difference over the NF period (a, c, e) and the second column shows the difference over the FF period (b, d, f).

21. **Figure 2.17** - Warm spell days index with reference to the 90th percentile of the summer season difference compared to the ensemble mean of the historical period (1984-2014) for SSP1-2.6 (a, b), SSP2-4.5 (c, d) and SSP5-8.5 (e, f). The first column shows the difference over the NF period (a, c, e) and the second column shows the difference over the FF period (b, d, f).
22. **Figure 2.18** - Heat waves per summer season (where $TX > TX_{norm} + 5^{\circ}C$ for 7 consecutive days) difference compared to the ensemble mean of the historical period (1984-2014) for SSP1-2.6 (a, b), SSP2-4.5 (c, d) and SSP5-8.5 (e, f). The first column shows the difference over the NF period (a, c, e) and the second column shows the difference over the FF period (b, d, f).
23. **Figure 2.19** - Heat waves per summer season (where $TX > TX_{norm} + 5^{\circ}C$ for 3 consecutive days) difference compared to the ensemble mean of the historical period (1984-2014) for SSP1-2.6 (a, b), SSP2-4.5 (c, d) and SSP5-8.5 (e, f). The first column shows the difference over the NF period (a, c, e) and the second column shows the difference over the FF period (b, d, f).
24. **Figure 2.20** - Heat waves per summer season (where $TX > TX_{norm} + 5^{\circ}C$ for 5 consecutive days) difference compared to the ensemble mean of the historical period (1984-2014) for SSP1-2.6 (a, b), SSP2-4.5 (c, d) and SSP5-8.5 (e, f). The first column shows the difference over the NF period (a, c, e) and the second column shows the difference over the FF period (b, d, f).
25. **Figure 2.21** - Heat wave duration index with reference to the mean of the summer season (where $TX > TX_{norm} + 5^{\circ}C$ for 7 consecutive days) difference compared to the ensemble mean of the historical period (1984-2014) for SSP1-2.6 (a, b), SSP2-4.5 (c, d) and SSP5-8.5 (e, f). The first column shows the difference over the NF period (a, c, e) and the second column shows the difference over the FF period (b, d, f).
26. **Figure 2.22** - Heat wave duration index with reference to the mean of the summer season (where $TX > TX_{norm} + 5^{\circ}C$ for 3 consecutive days) difference compared to the ensemble mean of the historical period (1984-2014) for SSP1-2.6 (a, b), SSP2-4.5 (c, d) and SSP5-8.5 (e, f). The first column shows the difference over the NF period (a, c, e) and the second column shows the difference over the FF period (b, d, f).
27. **Figure 2.23** - Heat wave duration index with reference to the mean of the summer season (where $TX > TX_{norm} + 5^{\circ}C$ for 5 consecutive days) difference compared to the ensemble mean of the historical period (1984-2014) for SSP1-2.6 (a, b), SSP2-4.5 (c, d) and SSP5-8.5 (e, f). The first column shows the difference over the NF period (a, c, e) and the second column shows the difference over the FF period (b, d, f).
28. **Figure 3.1** – Six precipitation homogenous regions of India.
29. **Figure 3.2** – JJAS precipitation over South Asia (1984-2014) for observed (a), MME (b) and individual models (c-n).
30. **Figure 3.3** – JJAS precipitation bias over South Asia (1984-2014) for observed (a), MME (b) and individual models (c-n). The dots represent the grid points with significant differences at 95% significance level.

31. **Figure 3.4** – JJAS precipitation spatial correlation for MME and individual models compared to observed data over each Indian precipitation homogenous region.
32. **Figure 3.5** – Taylor diagram for precipitation over India landmass compared to observed data for 17 CMIP6 models.
33. **Figure 3.6** - JJAS windspeed (850hPa) bias over South Asia (1984-2014) for MME (a) and individual models (b-m) compared to observed values from CRU. Arrows show absolute values.
34. **Figure 3.7** - JJAS specific humidity (850hPa) bias over South Asia (1984-2014) for MME (a) and individual models (b-m) compared to observed values.
35. **Figure 3.8** – Vertically integrated moisture transport bias compared to ERA5 for MME (a) and individual models (b-m) over South Asia. The arrows show the absolute values, both bias and absolute values are shown from 1000-100hPa.
36. **Figure 3.9** – Mean precipitation difference over South Asia for SSP1-2.6 (a, b, c, d), SSP2-4.5 (e, f, g, h) and SSP5-8.5 (I, j, k, l). The first and second columns show the absolute values for NF (a, e, i) and FF (b, f, j) respectively. The third and fourth columns show the precipitation difference for NF (c, g, k) and FF (d, h, l) respectively when compared to the historical period. The dots represent the grid points with significant differences at 95% significance level.
37. **Figure 3.10** – Vertically integrated moisture transport difference compared to the historical period from 1000-1hPa over South Asia. SSP scenarios SSP1-2.6 (12a, b), SSP2-4.5 (12c, d) and SSP5-8.5 (e, f) are used. The SSPs are split into NF (a, c, e) and FF (b, d, f).
38. **Figure 3.11** – PDF distribution of precipitation over Indian precipitation homogenous regions (a-f) and India landmass (g). The black lines represent the historical period (1984-2014). The solid and dashed black lines show observed and MME data respectively. For the SSP scenarios green, blue, and red represent SSP126, SSP245 and SSP585 respectively. For the SSPs a solid line shows the NF time period, and a dashed line shows the FF time period.
39. **Figure 3.12** – Extremely wet days with reference to the 99th percentile of reference period (1984-2014). The first column (a, c, e) shows the NF and the second column (b, d, f) shows the FF for SSP126 (a, b), SSP245 (c, d) and SSP585 (e, f).
40. **Figure 3.13** – Precipitation percent due to R95p days. The first column (a, c, e) shows the NF and the second column (b, d, f) shows the FF for SSP126 (a, b), SSP245 (c, d) and SSP585 (e, f).
41. **Figure 3.14** – Percentage difference compared to the historical period for the number of cwd periods with more than 5 days per JJAS season. The first column (a, c, e) shows the NF and the second column (b, d, f) shows the FF for SSP126 (a, b), SSP245 (c, d) and SSP585 (e, f).
42. **Figure 3.15** – Wet days Index per JJAS season over India. The first column (a, c, e) shows the NF and the second column (b, d, f) shows the FF for SSP126 (a, b), SSP245 (c, d) and SSP585 (e, f).
43. **Figure 4.1** – Model domain and orography (m) as used in RegCM4.

44. **Figure 4.2** – Model orography (m) from HadGEM3 (a) and RegCM4 (b) models.
45. **Figure 4.3** – Difference in height (m) over the Himalayan region between RegCM4 model mean height and a 5% (P5), 10% (P10), 15% (P15), 20% (P20) increase in mean height. There is a contour interval of 100m.
46. **Figure 4.4** – JJAS differences between wet and dry years for zonal moisture transport at 500hPa. Observation and different Himalayan orography representations (M20, M15, M10, M5, CNTRL, P5, P10, P15, P20) are shown.
47. **Figure 4.5** – JJAS precipitation over India using observed and RegCM4 simulations with different Himalayan orography representations (M20, M15, M10, M5, CNTRL, P5, P10, P15, P20) for nine distinct years (three years each for wet, normal and dry).
48. **Figure 4.6** – Western Himalayan (71°E-84°E; 28°N-38°N) area averaged JJAS mean precipitation computed for different Himalayan orography representations (M20, M15, M10, M5, CNTRL, P5, P10, P15, P20) using RegCM4. The y-axis shows precipitation (mm/day).
49. **Figure 4.7** – Hit Rate (y-axis) versus False Alarm Rate (x-axis) for nine different Himalayan orography representations (M20, M15, M10, M5, CNTRL, P5, P10, P15, P20).
50. **Figure 4.8** – Equitable Threat Score (ETS) for nine different Himalayan orography representations (M20, M15, M10, M5, CNTRL, P5, P10, P15, P20). ETS is considered for days where the observed precipitation is greater than 3mm/day.
51. **Figure 4.9** – JJAS mean vertical pressure velocity (Pa/s) at 500 hPa pressure level of Obs (a), RegCM4 simulations at 25km resolution using SC1 (b), SC2 (c), SC3 (d) and SC4 (e) cumulus schemes for a composite (wet-dry) precipitation year.
52. **Figure 4.10** – JJAS mean precipitation over India from observed values and SC1, SC2, SC3, and SC4 cumulus schemes for wet, normal and dry precipitation years.
53. **Figure 4.11** – Taylor diagram showing the correlation coefficient, normalised standard deviation and root mean square error for SC1, SC2, SC3 and SC4 when compared to observed values for JJAS precipitation.
54. **Figure 4.12** – Equitable threat score (ETS) for precipitation simulations using RegCM4 with SC1, SC2, SC3 and SC4 schemes for dry, normal and wet years.
55. **Figure 4.13** – JJAS average soil moisture for composite precipitation years using observed (a), BATS (b) and CLM (c) schemes.
56. **Figure 4.14** – JJAS sensible heat flux difference for composite precipitation years obtained for observed (a), BATS (b) and CLM (c) schemes.
57. **Figure 5.1** – JJA tmax (a, b, c), tas (d, e, f) and tasmin (g, h, i) for observed (a, d, g), RCM (b, e, h) and RCM bias (c, f, i) during the historical period (1984-2014). The dots represent the grid points with significant differences at 95% significance level.

58. **Figure 5.2** – Spatial correlation coefficient for both the HadGEM3-GC31-LL (1st row) and RCM (2nd row) compared to the observed (CRU) dataset for JJA tasmax (a), tas (b) and tasmin (c) over the Indian temperature homogenous zones for the historical period.
59. **Figure 5.3** – PDF for JJA tasmax over the Indian temperature homogenous regions during the historical, NF and FF periods using SSP1-2.6 (green), SSP2-4.5 (blue) and SSP5-8.5 (red). The historical period shows both observed values (solid black) and RCM values (dashed black). SSPs show solid lines for NF and dashed lines for FF.
60. **Figure 5.4** – Heat waves per summer season (where $TX > TX_{norm} + 5^{\circ}C$ for 7 consecutive days) difference compared to the present climate for SSP1-2.6 (a, b), SSP2-4.5 (c, d) and SSP5-8.5 (e, f). The first column shows the difference over the NF period (a, c, e) and the second column shows the difference over the FF period (b, d, f).
61. **Figure 5.5** – Heat waves per summer season (where $TX > TX_{norm} + 5^{\circ}C$ for 5 consecutive days) difference compared to the present climate for SSP1-2.6 (a, b), SSP2-4.5 (c, d) and SSP5-8.5 (e, f). The first column shows the difference over the NF period (a, c, e) and the second column shows the difference over the FF period (b, d, f).
62. **Figure 5.6** – Heat waves per summer season (where $TX > TX_{norm} + 5^{\circ}C$ for 3 consecutive days) difference compared to the present climate for SSP1-2.6 (a, b), SSP2-4.5 (c, d) and SSP5-8.5 (e, f). The first column shows the difference over the NF period (a, c, e) and the second column shows the difference over the FF period (b, d, f).
63. **Figure 5.7** – Heat wave duration index with reference to the mean of the summer season (where $TX > TX_{norm} + 5^{\circ}C$ for 7 consecutive days) difference compared to the present climate (1984-2014) for SSP1-2.6 (a, b), SSP2-4.5 (c, d) and SSP5-8.5 (e, f). The first column shows the difference over the NF period (a, c, e) and the second column shows the difference over the FF period (b, d, f).
64. **Figure 5.8** – JJAS mean precipitation over the Indian precipitation homogenous regions for observed (a), RCM (b) and RCM bias (c) for the historical period (1984-2014). Here the observed data is taken from IMD. The dots represent the grid points with significant differences at 95% significance level.
65. **Figure 5.9** – Taylor diagram showing JJAS mean precipitation over India for the historical period (1984-2014) for 17 CMIP6 models and the RCM compared to the IMD observed dataset.
66. **Fig. 5.10** – JJAS mean precipitation difference over Indian precipitation homogenous regions for SSP1-2.6 (a, b), SSP2-4.5 (c, d) and SSP5-8.5 (e, f). The first and second columns show the precipitation difference for NF (a, c, e) and FF (b, d, f) respectively when compared to the historical period.
67. **Fig. 5.11** – PDF for JJAS mean precipitation over the Indian precipitation homogenous regions during the historical, NF and FF periods using SSP1-2.6 (green), SSP2-4.5 (blue) and SSP5-8.5 (red). The historical period shows both observed values (solid black) and RCM values (dashed black). SSPs show solid lines for NF and dashed lines for FF.
68. **Fig. 5.12** – Extremely wet days with reference to the 99th percentile of reference period (1984-2014). The first column (a, c, e) shows the NF and the second column (b, d, f) shows the FF for SSP126 (a, b), SSP245 (c, d) and SSP585 (e, f).

List of Tables

1. **Table 1.1** - Summary of efforts to study climate extremes using GCMs and RCMs and the associated human health impacts of these extremes.
2. **Table 2.1** - CMIP6 GCMs used in this work.
3. **Table 2.2** - Heat wave variables calculated using CDO (Schulzweida et al. 2021).
4. **Table 3.1** - CMIP6 models used in study.
5. **Table 3.2** - Extreme precipitation indices definitions calculated using CDO (Schulzweida et al. 2021).
6. **Table 3.3** - Precipitation increase (%) per region compared to historical period (1984-2014).
7. **Table 3.4** - Extreme wet days difference (%) per region compared to historical period (1984-2014).
8. **Table 3.5** - Consecutive dry days difference (%) per region compared to historical period (1984-2014).
9. **Table 3.6** - Consecutive wet days difference (%) per region compared to historical period (1984-2014).
10. **Table 4.1** – The RegCM4 configuration used.
11. **Table 4.2** - Different cumulus scheme experiments with RegCM4 simulations at a 25 km resolution.
12. **Table 4.3** – Land Surface Parameterisation Schemes (CLM and BATS).
13. **Table 4.4** – Root mean square error (RMSE) and correlation for wet, dry and normal precipitation years when compared to observed values using BATS and CLM schemes.
14. **Table 4.5** - Skill scores for wet, normal and dry precipitation years over India (where rainfall ≥ 2 mm/day for a wet day).
15. **Table 5.1** - Configuration of RegCM4.7 model used in the present study.
16. **Table 5.2** – JJAS mean precipitation increase (%) per region compared to historical period (1984-2014). Positive (negative) values show an increase (decrease) in precipitation.

List of Abbreviations

Acronym	What it stands for
AR4	IPCC Fourth Assessment Report
BATS	Biosphere-Atmosphere Transfer Scheme
CC	Correlation Coefficient
CDD	Consecutive Dry Days
CDO	Climate Data Operator
CLM	Community Land Model
CMIP	Coupled Model Intercomparison Project
CNE	Central Northeast
CORDEX	Coordinated Regional Climate Downscaling Experiment
CRU	Climatic Research Unit
CWD	Consecutive Wet Days
EC	East coast
ERA5	European Centre for Medium-Range Weather Forecasts Reanalysis version 5
ETS	Equitable Threat Score
EWD	Extremely Wet Days
FAR	IPCC First Assessment Report
FAR	False Alarm Rate (Used in Chapter 4 only)
FF	Far Future
GCM	General Circulation Model
GHG	Greenhouse Gases
HR	Himalayan Region
HR	Hit Rate (Used in Chapter 4 only)
HW	Heat Wave
HWDI	Heat Wave Duration Index
IMD	Indian Meteorological Department
IOA	Index of Agreement
IOD	Indian Ocean Dipole
IP	Interior Peninsula
IPCC	Intergovernmental Panel on Climate Change

ISM	Indian Summer Monsoon
JJA	June, July, August
JJAS	June, July, August, September
LSPS	Land Surface Parameterization Scheme
LW	Long Wave
MME	Multi-Model Ensemble
NC	North Central
NF	Near Future
NW	Northwest
PDF	Probability Density Function
PR	Peninsular Region
RCM	Regional Climate Model
RCP	Representative Concentration Pathway
RegCM	International Centre for Theoretical Physics Regional Climate Model
RMSE	Root Mean Square Error
SC	Cumulus Scheme
SD	Standard Deviation
SRES	Special Report on Emission Scenario
SSP	Shared Socioeconomic Pathway
SST	Sea Surface Temperature
SW	Short Wave
TAR	IPCC Third Assessment Report
tas	Mean Near-Surface Air Temperature
tasmax	Maximum Near-Surface Air Temperature
tasmin	Minimum Near-Surface Air Temperature
VIMT	Vertically Integrated Moisture Transport
WC	West Coast (for temperature homogenous region)
WC	West Central (for precipitation homogenous region)
WDI	Wet Days Index
WH	Western Himalaya

Introduction

1.1 Background

There is high confidence that climate change has caused irreversible damage to terrestrial, freshwater, and coastal and open marine ecosystems. A warming of approximately $\sim 0.85^{\circ}\text{C}$ has occurred globally in the last 40 years and without sufficient mitigation strategies global surface temperatures will continue to rise. It is extremely likely that human influence is responsible for the rise in global temperature as well as an increase in extreme events such as warm temperature extremes (IPCC, 2022).

South Asia is one of the most vulnerable regions in the world to the impacts of climate change (Sivakumar and Stefanski, 2010) with signs of warming trends and a consistent increase in temperature extremes (IPCC, 2022). Climate change has been shown to affect the food production, putting this region at risk of a food shortage by 2030 and creating food security concerns in the future (Acharya et al. 2014; Bandara and Cai, 2014). Extreme temperatures, heavy rainfall, flooding, and droughts negatively affect agriculture and can sometimes even destroy harvests (Gornall et al., 2010). Generally, both extreme precipitation (Almazroui et al., 2020, Mondal et al., 2022, Shahi et al., 2021) and extreme temperature (Almazroui et al., 2020, Dong et al. 2021, Meehl and Tebaldi 2004) have been shown to increase in the future more with continued warming. India's population is particularly vulnerable to extreme temperatures and an increase in heat wave severity has been linked to an increase in heat-related mortality over India (Mazdiyasi et al., 2017).

Agriculture in India relies on the Indian summer monsoon (ISM) and is an important part of the Indian economy, which many people rely on for their livelihood (Krishna Kumar et al., 2004). Rice is one of the main crops grown in the region and is highly susceptible to changes in rainfall (DeFries et al., 2016). Changes to the amount of rainfall can have a damaging effect on the population, with too much or too little rainfall leading to events such as flooding, landslides, droughts and crop failure (Shonk, 2022, Webster et al., 1998). Historically, it has

been shown that global monsoon land precipitation has been decreasing, with the South Asian monsoon being one of the primary causes (Zhou, Zhang and Li, 2008). There has been an increase in extreme precipitation over most of India in the past 120 years, with urbanisation correlating to an increase in the intensity of these extreme events (Falga and Wang, 2022).

1.2 Characteristics of Summertime Circulation and Associated Temperature and Precipitation

1.2.1 General Circulation

The general circulation of the atmosphere (Fig. 1.1) is important to study how the surface climate may change in the future and the past, as well as to assess the effects on meteorology, weather and on the lives of the human population (Schneider 2006). George Hadley was the first scientist with early works on the features of the atmospheric flows. While looking for an explanation for the trade wind circulation he noticed that the solar heating might produce a direct meridional cell in each hemisphere (Holton 2004) (Lorenz 1967).

The atmosphere receives heat by incoming short wave (SW) radiation and loses heat by outgoing long wave (LW) radiation. To reach thermal equilibrium the net radiative heating of the Earth-Atmosphere system as whole must be zero. This only happens globally, but not regionally (Holton 2004) (Salby 2012).

During winter the low latitudes experience radiative heating which is seen from the observed net radiation. This means that they receive more energy by absorbing more SW radiation than the LW radiation they emit. The mid and high latitudes experience radiative cooling at this time, which is most noticeable in the winter hemisphere, meaning they will emit more LW radiation than the SW radiation they absorb. These local imbalances are compensated by a poleward transfer of heat which preserves thermal equilibrium. This is achieved by the general circulation of the Earth-Atmosphere system. The heat transfer is made by a steady

circulation between the equator and poles, which is driven by the atmospheric heating in the tropics and cooling in the extratropics. Atmospheric heating at low latitudes is caused by latent heat releasing inside centres of convection. This paired with the radiative cooling at high latitudes forces vertical motions across isentropic surfaces. This is compensated by a horizontal motion called the Meridional Overturning Circulation. Hadley Circulation occurs at lower latitudes. The heating at these low latitudes causes air to flow poleward and sink at around 30° in both hemispheres. Between the mid to high latitudes lies the Mid-Latitude Cell. The hot air transferred from the Hadley Cell is slightly cooler, which sinks and flows poleward inside the Mid-Latitude Cell. Cold air from the Polar Cell flows south inside the same cell. The warm and

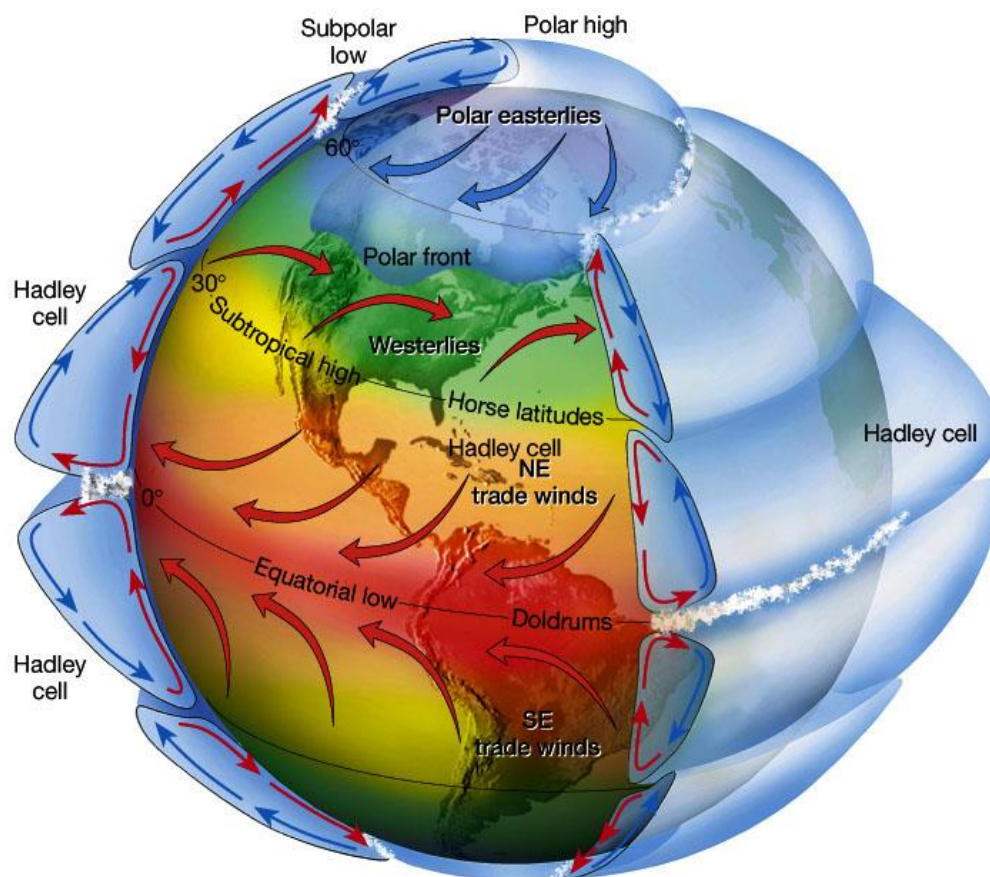


Fig. 1.1 - General circulation. Hadley Cells are between the equator and a latitude of 30° , Mid-latitude cells are between 30° and 60° , and polar cells at higher latitudes. North-easterly and south-easterly trade winds occur in the lower parts of the Hadley Cells, which meet in the Inter Tropical Convergence Zone (ITCZ). Air rises to form frequent thunderstorms and heavy rainfall.

Source: The Atmosphere, 8th edition, Lutgens and Tarbuck, 8th edition, 2001.

cold air meet forcing the warm air to rise over the denser cold air and then cools down, causing precipitation (Holton 2004) (Salby 2012) (Peixoto et al. 1992).

1.2.2 Regional Circulation

South Asia receives significant warming towards the end of Spring as the northern hemisphere summer approaches. This leads to increased sea surface temperatures in the northern hemisphere and cooler temperatures in the southern hemisphere, creating temperature pressure gradients between the north and south. Most of the year India receives strong westerly winds (fig. 1.2a), but during the monsoon season the pressure gradient causes a shift from west to east in the lower troposphere (fig. 1.2b). These easterly winds then transport vast amount of water vapor over India causing the Indian summer monsoon, which then continue through parts of southeast Asia.

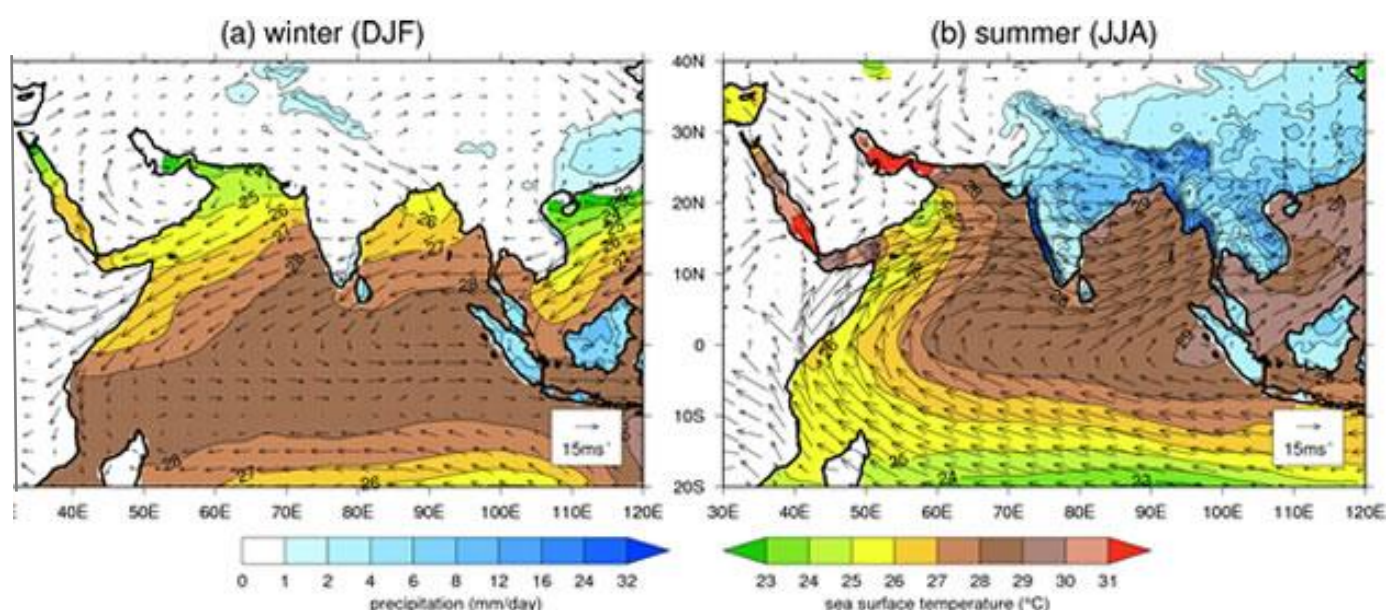


Fig. 1.2 – Precipitation, SST and wind speed over South Asia for winter (1.2a) and summer (1.2b). Precipitation and SST are shown over land and ocean respectively.

Source: <https://www.rmets.org/metmatters/indian-monsoon-changing-climate>

1.2.3 Temperature Extremes

Heat waves have caused many deaths over India in the last 100 years (De et al., 2005). Mortality related to heat waves in India has increased between 1970-2019. The impact of heat waves compared to other extreme weather events varies per state. For instance, Andhra Pradesh is the most affected where the mortality rate due to heat waves increased by 60% followed by Odisha with an increase of 20% (Ray et al., 2021). Most of the heat waves in India usually occur in the pre-monsoon season (April, May and June) and can cover a large portion of the country (Pai et al., 2013). However, the high temperatures can still persist during the summer monsoon (June, July and August, JJA) season and therefore it is critical to estimate such occurrences as there is possible climate shift in future scenarios. For example, the monsoon precipitation which occurs actively during JJA over India exhibits a temporal shift in onset

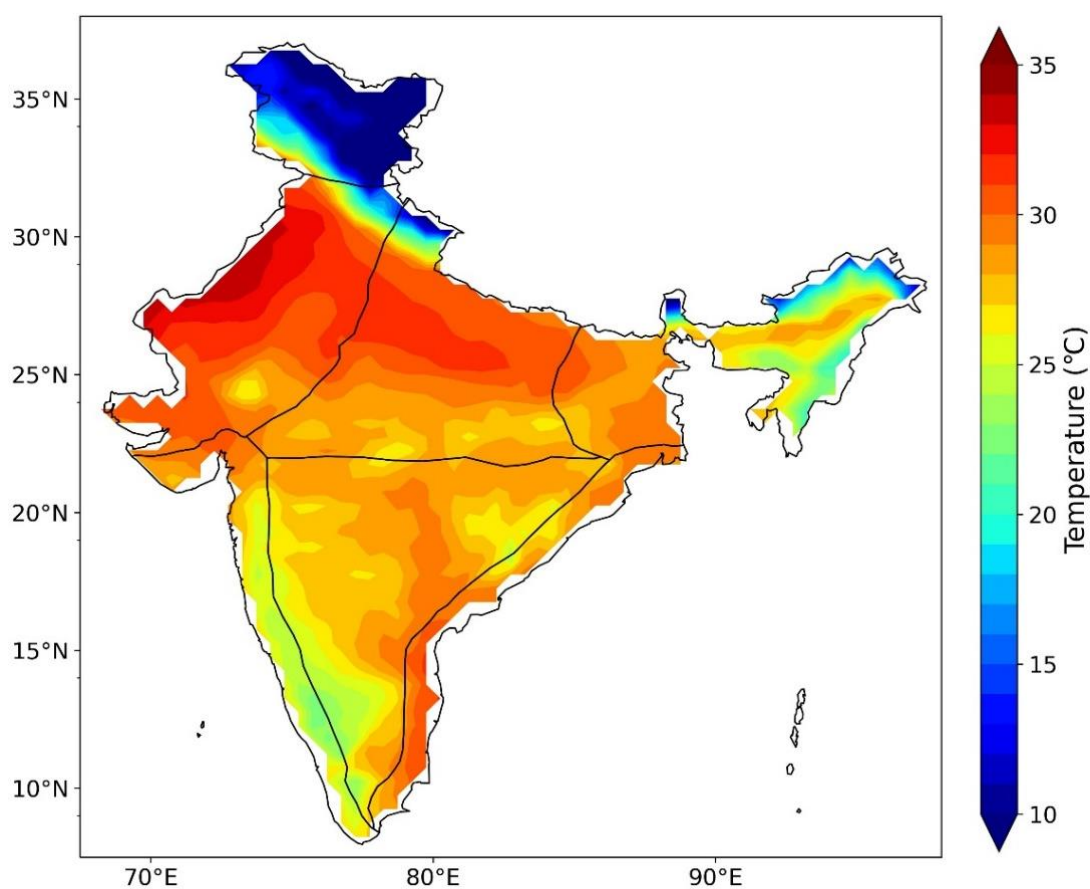


Fig. 1.3 – Observed (CRU) mean temperature (1901-2014) during JJA over the Indian temperature homogenous regions.

dates as well as the precipitation maxima under RCP 8.5 (Ashfaq et al., 2021, Shahi et al., 2021). The dryness induced in the future could inculcate extreme temperature conditions over India during summer monsoon season.

1.2.4 Precipitation Extremes

The Indian summer monsoon (ISM) falls between June, July, August, September (JJAS) and provides about 80% of the total annual rainfall over India (Kripalani et al., 2003). There are many factors that can affect the ISM such as the topography of the region (Medina et al., 2010) and soil moisture (Asharaf et al., 2012) making it a very complex system to model and understand. It has been shown that increasing the orography in the model leads to an increase in ISM precipitation, and a decreasing the orography shows a decrease in ISM precipitation (Sinha et al., 2010, Song et al., 2009). This has also been shown by Tiwari et al., (2016) for winter precipitation over India. This means that the model's ability to correctly represent the Himalayas has a significant impact on precipitation results. The Asian Monsoon shows a higher sensitivity to global warming when compared to other monsoon domains (Kitoh et al., 2013) meaning an increase in greenhouse gas (GHG) emissions could lead to a more intense ISM in the future. Various studies have been conducted reflecting monsoon rainfall and its simulation over South Asia and India (Almazroui et al., 2020, Asharaf and Ahrens, 2015, Katzenberger et al., 2021, Menon et al., 2013, Sharmila et al., 2015). Global and regional climate models have been used to look at future changes in precipitation over India until the end of the century with a general agreement that precipitation will increase during this time period.

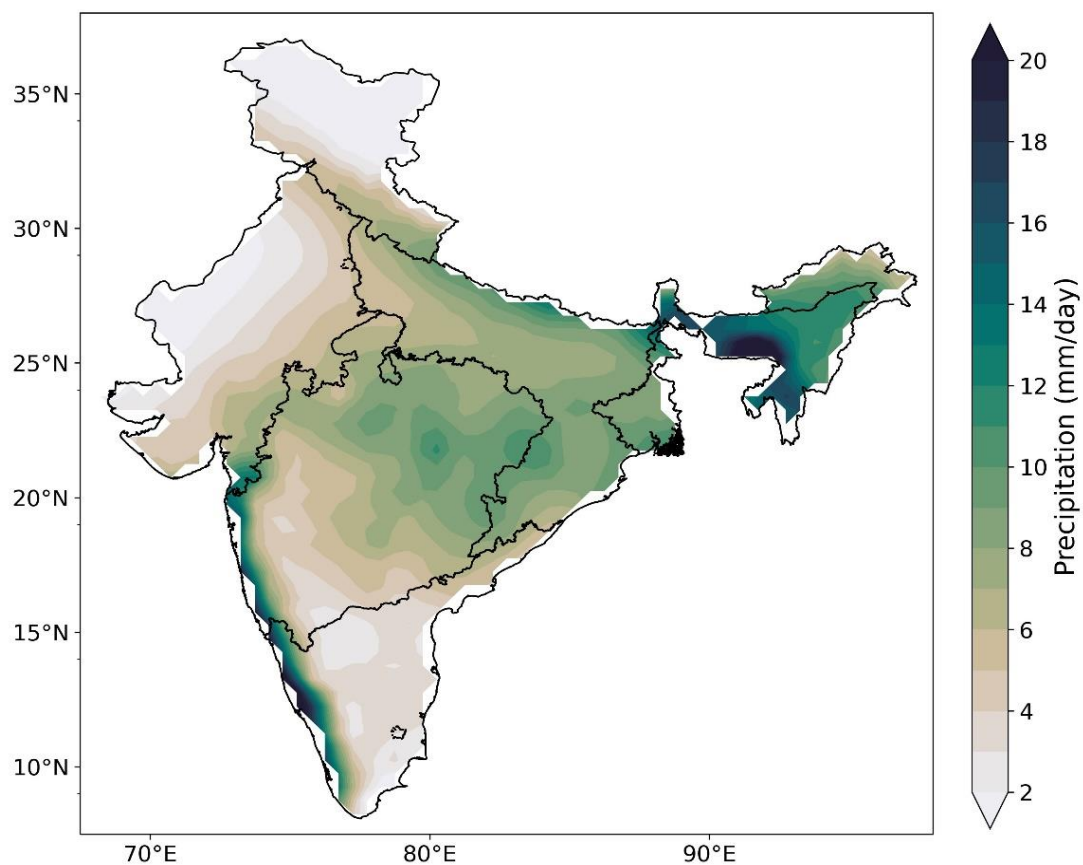


Fig. 1.4 - Observed (CRU) mean precipitation (1901-2014) during JJAS over the Indian precipitation homogenous regions.

1.3 Climate Modelling

Table 1.1 - Summary of efforts to study climate extremes using GCMs and RCMs and the associated human health impacts of these extremes.

Reference	Study Period	Models Used	Significant Findings
Giorgi et al. 1999	1994-1995	RegCM	Model predicts precipitation over the east Asian domain, however it over predicts the intensity of the east Asian monsoon. Highlights the importance of cloud radiation processes in models.

Pal et al. 2000	1986-1990 and 1993	RegCM	Model better represents mean and extreme precipitation over North America with the added cloud and precipitation scheme coupled to RegCM.
Li and Xie, 2012	1970-1999	CMIP3 and CMIP5 ensemble	Two types of biases found for SST over the tropics using CMIP. One is linked to cloud cover and the other is the thermocline depth.
Im, Pal, and Eltahir, 2017	2017	MIT Regional Climate Model (MRCM)	Wet-bulb temperature is shown to increase most over India under RCP8.5 in the far future and is shown to exceed 35°C. The increase is smaller under RCP4.5.
Zhao, Bollasina, and Stevenson, 2019	2019	Community Earth System Model Large Ensemble (CESM-LE)	Changes to heatwave magnitude are mostly caused by greenhouse gases, however aerosol reductions have a significant impact over the northern hemisphere.
Sousa et al. 2020	2020		Reduced soil moisture promotes warming and future extreme heat episodes could be further intensified by the increasing severity of drought events.
Zhang, Held, and Fueglistaler, 2021	2021	22 CMIP5 ensemble	Slowing the effects of global warming will also slow the maximum wet-bulb temperature over the tropics.

1.3.1 Coupled Model Intercomparison Project (CMIP)

The Coupled Model Intercomparison Project (CMIP) models are global climate models (GCMs) created by modelling groups around the world and are useful tools for assessing changes in past, present and future climate. CMIP first began in 1995 and CMIP models have received various improvements over the years with CMIP6 (Eyring et al., 2016) being the newest iteration of these models.

The earliest form of climate models were simple energy balance models, which didn't consider climate system dynamics and only considered ingoing and outgoing radiation at the Earth's surface. One of the earliest examples of future climate predictions is from Sawyer, 1972, who predicted that the Earth would receive 0.6°C warming between 1969 and 2000. The observed warming during this period was around 0.54°C, putting Sawyers estimate very close to the actual value. His estimate for CO₂ concentrations was higher than the actual value. This overestimation of CO₂ concentrations is also seen in the IPCC First Assessment Report (FAR). The FAR estimated a climate sensitivity of 2.5°C for doubled CO₂, which is close to the 3°C which is used today (IPCC, 1992).

The IPCC Third Assessment Report [TAR (IPCC, 2001)] and IPCC Fourth Assessment Report [AR4 (IPCC, 2007)] made use of new socioeconomic emission scenarios (SRES) which included four different future emission pathways. These SRES were included in the newer and more sophisticated GCMs and were ways to look at future warming for different possible futures. CMIP5 models were used in the IPCC AR5 report (IPCC, 2014) and replaced SRES with newer Representative Concentration Pathways (RCPs) which are four scenarios with different concentrations of greenhouse gases.

CMIP5 and CMIP6 models have been used in the latest IPCC AR6 report (IPCC, 2022) when looking at past and future climate. In CMIP models, the bigger challenges are to simulate

variables at a regional to local scale accurately. They struggle to accurately represent processes such as clouds which occur on a smaller scale than the GCMs resolutions, which in turn lead to larger uncertainties between models (IPCC, 2014).

CMIP6 models incorporate the newest form of future emission scenarios called Shared Socioeconomic Pathways (SSPs). There are five different SSPs that represent different challenges to both mitigation and adaptation. SSP1 is the best-case scenario and represents a sustainable future. Here the world is more focused on human well-being and a lower resource and energy requirement. This scenario shows low challenges to both adaptation and mitigation. SSP2 is a middle road scenario with medium challenges to adaptation and mitigation. Here progress towards a sustainable future is slower and not all countries are progressing at the same rate. SSP3 is the worst-case scenario with high challenges to mitigation and adaptation. This scenario sees climate change as a low priority and prioritises security and conflict, with large material consumption. SSP4 represents low challenges to mitigation but high challenges to adaptation. This scenario focuses on inequality where part of the population is progressing rapidly leaving the rest of the population behind. SSP5 represents a fossil-fuelled future, with high challenges to mitigation and low challenges to adaptation. The world progresses rapidly on a global scale and quality of life generally improves; however, the consumption of fossil fuels persists.

1.3.2 Regional Climate Modelling

Climate modelling is an important tool for increasing our understanding of the Earth's climate and climate change. However, there are limitations to GCMs, mainly due to their coarse resolution. This means they fail to capture smaller scale processes (IPCC 2013) leading to a less accurate representation of the Earth's climate. Downscaling is a way to create high

resolution simulations over a smaller region. There are two types of downscaling, dynamical and statistical downscaling.

1.3.2.1 Dynamical Downscaling

RCMs are used to create high resolution simulations on a local scale. Dynamical downscaling can better represent small-scale processes due to the increased resolution. Generally, an RCM is scaled over a specified region (known as nesting) at an increased resolution and is driven by initial and time-dependant lateral boundary conditions of either GCM or observed datasets (Giorgi, 2019), however this uses considerable computing power. The reliance on GCM data means that it is important that a good performing GCM must be selected to get more reliable RCM results. The increased resolution gained by dynamical downscaling is an important tool for better understanding regional climate.

There are a number on institutions that have created RCMs for better understanding regional climate events. For example, RegCM from the Abdus Salam International Centre for Theoretical Physic (ICTP, Elguindi et al., 2017), COSMO-CLM from the Climate Limited-area Modelling Community (CLM-Community, Rockel and Geyer, 2008), REMO from the Max Planck Institute for Meteorology (MPIfM, Jacob and Podzun, 1997), HadCM3 from the UK Met Office (Gordon et al., 2000) and the HIRHAM Regional Climate Model from the Danish Meteorological Institute (Bøssing et al., 2007)

It is commonly accepted that GCMs struggle to capture the ISM, particularly over north India which has more complex topography (Mishra et al., 2018). Dynamical downscaling has been shown to improve ISM simulations (Agrawal et al., 2021, Dobler and Ahrens 2010, Lucas-Picher et al., 2011, Seo et al., 2023), however these models still show biases over this region.

1.3.2.2 Statistical Downscaling

Another way to create higher resolution simulations using GCMs is the use of statistical downscaling. Here a statistical relationship between observed and GCM variables is formed during the historical period using methods such as multiple linear regression, artificial neural networks, multi-model ensemble, stepwise regression etc. and is often paired with bias correction techniques. The GCM is then used to simulate future climate, with the statistical relationships being used to better represent smaller-scale processes that the GCMs cannot capture.

1.4 Objective and Scope

This thesis aims to find a better understanding on how the characteristics of climate extremes will change in the future over India and its relevant homogenous regions due to human induced climate change and how these changes will affect the population of this region.

The objectives of this project are:

- Utilise state-of-the-art climate model CMIP6 simulations to assess how climate extremes and climate extreme events will change in the future.
- Assess the role of physical processes through various sensitivity experiments (cumulus scheme, land surface scheme and orography representation).
- Undertake high-resolution climate model simulations (CORDEX framework) to examine the extent, severity, and probability of climate extreme episodes in India and how they will respond to future changes in emission pathways. Connect the changes in extremes in line with possible emission pathways and assess the associated human health risk over the region of interest.

Chapter 2 uses thirteen of the latest Coupled Model Intercomparison Project phase 6 (CMIP6) models have been used to model mean, maximum, and minimum temperature over the 7 homogenous temperature regions of India for both annual and summer season consisting of months June, July and August (JJA) time periods. The fidelity of these models was assessed by comparing them with observed temperature from the Climate Research Unit (CRU) dataset. A multi-model mean of the thirteen CMIP6 models was found to reduce temperature biases and was used to assess future changes in temperature extremes and heatwave characteristics using SSPs.

The ability of twelve CMIP6 models to represent the Indian summer monsoon (ISM) precipitation, vertically integrated moisture transport and windspeed over the Indian precipitation homogenous zones during June, July, August and September (JJAS) is shown in chapter 3. To test the fidelity of these models, they were compared to observed values from the CRU dataset and a multi-model mean was used for future analysis. Changes in future precipitation and extreme precipitation variables are then shown for future periods using SSPs.

Sensitivity experiments were used to assess the role of physical processes in chapter 4 with the addition of some machine learning techniques.

Dynamical downscaling for both temperature and precipitation extremes is shown in chapter 5. Here the RegCM4.7 regional climate model is used at a 25km resolution, driven by the HadGEM3-GC31-LL global climate model. The RCM was compared to its driving model for the historical period and then used to assess future changes in temperature and precipitation, as well as heat wave duration and intensity and extremely wet days.

Fidelity of CMIP6 Models in Simulating Temperature and Associated Extremes Over India

This chapter is based on the paper:

- Marc Norgate, P. R. Tiwari, S. Das and D. Kumar (2024). On the heat waves over India and their future projections under different SSP scenarios from CMIP6 models. *International Journal of Climatology, Royal Meteorological Society*, 44(3). doi.org/10.1002/joc.8367

Abstract

The multi-model ensemble (MME) mean of 13 CMIP6 models was calculated for present (1984–2014), near (2030-2060) and far (2070-2100) future scenarios and the models showed larger warm biases during the JJA time period. Although the models could simulate the spatial variability of the mean and maximum temperature over most of the homogeneous regions, they do not compare well for representing the temporal variability. We have found that CNRM-CM6 is comparably the best performing model for spatial temperature trends over India although all models struggle with representing temperature characteristics over the east coast of India. HadGEM3-GC31-LL, KACE-1-0G and UKESM1-0-LL are comparably the best performing models for temporal temperature trends over India. The annual maximum temperature during the far-future (FF) period is projected to increase by 1.5°C, 2.3°C and 4.1°C for the FF Shared Socioeconomic Pathways (SSPs) SSP1-2.6, SSP2-4.5 and SSP5-8.5 respectively. The JJA mean temperature for SSP5-8.5 shows an increase of 3.8°C for Interior Peninsula (IP), 5.6°C for Western Himalaya (WH), 3.9°C for North West (NW), 3.6°C for West Coast (WC), 3.6°C for East Coast (EC), 3.6°C for North East (NE) and 3.8°C for North Central (NC) in FF compared to present period implying WH being more sensitive to climate change. The frequency of heat waves is also projected to increase, with the most affected areas showing more than three heat waves per summer season when compared to historical values. The northern territory of India consisting of NW, NC, NE and part of IP are found to be the most affected regions, where week-long heat wave duration is expected at higher emission scenario affecting larger portion of population (~ 50% of India's population). Such unprecedented impacts seem to be less profound in case of abatement scenarios such as the SSP1-2.6. Our findings support the urgent need for more ambitious mitigation and adaptation strategies to minimize the public health impacts of climate change.

2.1 Introduction

A rise in temperature can be seen globally and it is likely that heat waves have increased in large parts of Asia (IPCC, 2022). Heat waves are a type of extreme weather event, generally defined as an extended period of extreme temperature (Perkins and Alexander, 2013). The frequency, intensity and duration of extreme heat events have increased globally (Perkins and Alexander, 2013) in South Asia (Dong et al., 2021), which is likely caused by an increase in anthropogenic emissions (Collins et al., 2013, Pattnayak et al., 2017, Meehl and Tebaldi, 2004). Zhao et al., (2019) suggest that these extreme heat events will continue to increase into the future under the RCP 8.5 scenario. They have a significant impact on human health (Arbutnott and Hajat, 2017, Haines et al., 2006, Patz et al., 2005, Zeng et al., 2016) and have caused many deaths globally, with a greater impact on the elderly, women, and those suffering from chronic respiratory disorders (Dippoliti et al., 2010). This poses a risk to the world's population, especially those in developing countries who will struggle to mitigate this increase in heat wave severity.

There is a link between the warming of the Indian Ocean and El-Nino events with heat waves over India (Rohini et al., 2016). The surface temperature of the Indian Ocean is projected to continue to rise in the future (Pattnayak et al., 2017) increasing the likelihood of heat waves over India in the near future. India has a population of over 1.3 billion putting a large portion of the world's population at risk to an increase in extreme temperature events. The most densely populated parts of India are in the Indo-Gangetic plain where approximately half the population lives.

Considering such risks to the large population over a vulnerable region like south Asia, it becomes important to investigate the utility of the available modelling tools for understanding the present and future climate change. To aid this, a wide range of climate model simulations are produced through the coordinated efforts worldwide. Coupled Model Intercomparison

Project (CMIP) has been around since the mid 1990's and makes use of General Circulation Models (GCMs) simulations to improve our understanding of the climate system (Stouffer et al., 2017). CMIP models have received many improvements over the years such as improved resolution, improvements in the representation of the physical processes and different climate forcings. Representative Concentration Pathways (RCPs, Moss et al., 2010) were introduced in CMIP5 (Taylor et al., 2012) to explore different future scenarios for different radiative forcing pathways. In the present work we will be using the latest Coupled Model Intercomparison Project 6 (CMIP6; Eyring et al., 2015) dataset over India which has been used in many studies globally looking at both temperature and precipitation (Almazroui et al., 2021, Maharana et al., 2018, Pattnayak et al. 2019, You et al. 2016). One of the most notable additions compared to CMIP5 are the Shared Socioeconomic Pathways (SSPs, Riahi et al., 2017) which represent five different narratives for future socioeconomic scenarios (O'Neill et al., 2017). The main aim of this chapter is to study present and future changes (near and far future) in mean, max, min temperature over India's homogeneous temperature regions using state-of-the-art CMIP6 models.

2.2 Methodology

2.2.1 Indian Temperature Homogenous Regions and Observed Data

Thirteen CMIP6 models (see Table 2.1) are used in investigating the maximum, mean and minimum temperature over India and its 7 homogeneous temperature regions (Fig 2.1). The Indian Institute of Tropical Meteorology at Pune has defined these 7 homogenous regions which are specified based on spatial and temporal variations of surface air temperature (Dash and Mamgain, 2011). The 7 homogenous temperature regions are the Western Himalaya (WH), North West (NW), North Central (NC), North East (NE), West Coast (WC), East Coast (EC) and Interior Peninsula (IP) regions. Similar homogenous regions have been used when assessing temperature over India (Dilepkumar et al., 2018). The CMIP6 data used in this work

can be found from the CMIP6 database (<https://esgf-node.llnl.gov/search/cmip6/>). All models have been re-gridded to the observed grid (Climatic Research Unit (CRU) data, Harris et al., 2017) which has resolution of 0.5° using the bilinear interpolation method. CRU has been used in various studies over India (Dileepkumar, et al. 2018, Kumar et al. 2013, Ullah et al. 2022).

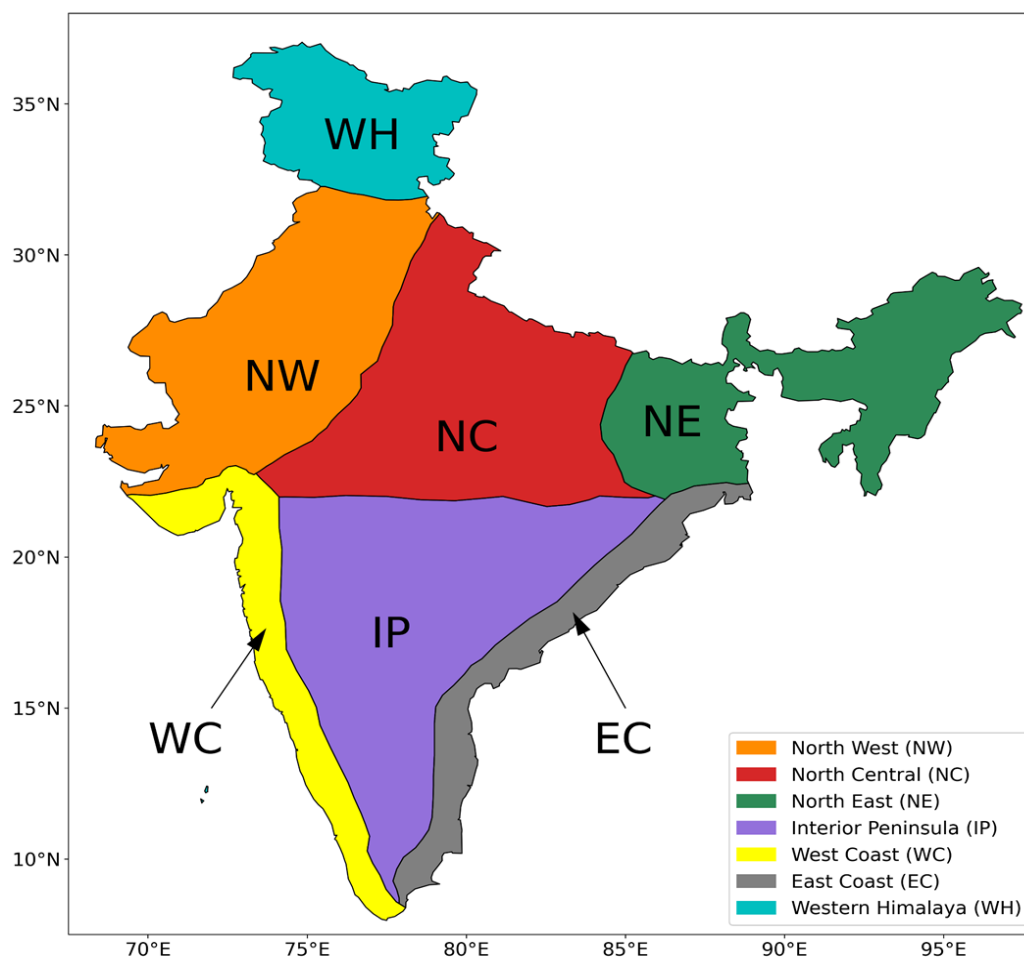


Fig. 2.1 - Study area and different temperature homogenous regions over India

2.2.2 CMIP6 Experiments

The historical analysis is from 1984–2014 and this time period is used to examine the performance of the models in representing different characteristics of temperature variations over the region. Besides the individual experiment, we also compute the multi-model ensemble (MME) from the 13 experiments. Daily data is required for the temperature variables seen in Table 2. Due to limited data availability only 9 models are used for the daily MME. The models

used in the daily data MME are CMCC, CNRM, GFDL, HadGEM, INM, KACE, MIROC6, MPI and UKESM. The method for projecting these extreme temperatures is shown in figure2.2.

Table 2.1 - CMIP6 GCMs used in this work

Model	Country	Horizontal Resolution (lon and lat)
ACCESS-CM2	Australia	192 x 144
CANESM5-CanOE	Canada	128 x 64
CMCC-ESM2	Italy	288 x 192
CNRM-CM6-1	France	362 x 294
FIO-ESM-2-0	China	192 x 288
GFDL-ESM4	USA	360 x 180
GISS-E2-1-H	USA	144 x 90
HadGEM3-GC31-LL	UK	192 x 144
INM-CM5-0	Russia	180 x 120
KACE-1-0-G	South Korea	192 x 144
MIROC6	Japan	256 x 128
MPI-ESM1-2-LR	Germany	192 x 96
UKESM1-0-LL	UK	192 x 144

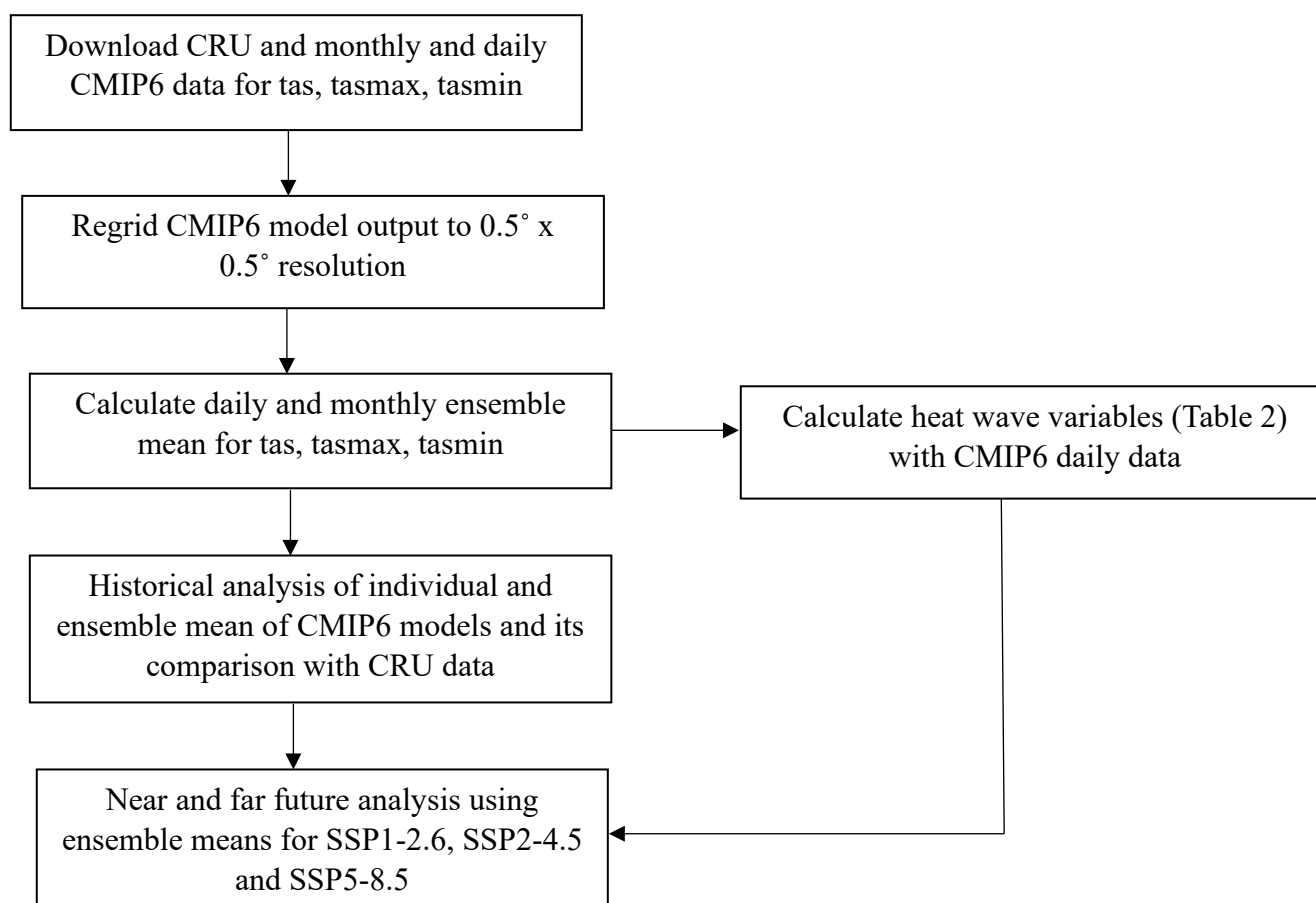
The monthly maximum, mean and minimum near-surface air temperature from CRU (Harris et al., 2017) at a resolution of $0.5^{\circ} \times 0.5^{\circ}$ is used to evaluate the individual model and their MME. CRU is a well trusted source of historical observations (Mitchell and Jones, 2005) and has been used in many previous studies (Maharana et al., 2018, Pattnayak et al., 2017a, Panda et al. 2020).

2.2.3 Shared Socioeconomic Pathways

We first evaluate the models in terms of their capabilities in representing the climatological mean annually and during the summer season (June, July, and August), mean annual cycle, Taylor's metrics and representation of the probability distribution over individual temperature homogeneous regions over India. To further understand the model's capabilities in representing the mean patterns spatially, we compute the differences of the mean for the present climate (with respect to observation) and future climate (with respect to present climate). To assess the changes during the future, we make use of three different Shared Socioeconomic Pathways namely: SSP1-2.6, SSP2-4.5 and SSP5-8.5 where SSP1-2.6 represents a "green road", SSP5-8.5 represents fossil-fuelled development and SSP2-4.5 represents a middle road (Riahi et al., 2017). The SSPs used represent low (SSP1-2.6), medium (SSP2-4.5) and high (SSP5-8.5) emission scenarios making SSP5-8.5 the most aggressive scenario in terms of emissions. To highlight the spatial heterogeneity in the differences, we compute the significance of differences in the mean by applying the student t-test and have identified the areas having significant differences at 95% level. All SSPs represent the future time period 2015-2100 and have been split into near-future [NF (2030-2060)] and far-future [FF (2070-2100)] to evaluate future changes in maximum, mean and minimum temperature over India. We looked at projected changes in annual and seasonal temperatures. To analyse future changes in temperature distribution over India and different homogeneous regions, we used spatial, time series and probability density function (PDF) figures using the SSP scenarios. Further we have used CDO (Schulzweida et al. 2021) to compute different heat wave variables which is shown in Table 2.2.

Table 2.2 - Heat wave variables calculated using CDO (Schulzweida et al. 2021)

Consecutive summer days index per summer season	Warm days percent wrt 90th percentile of the summer season	Warm spell days index wrt 90th percentile of the summer season	Heat waves per summer season	Heat wave duration index wrt the mean of the summer season
The largest number of consecutive summer days per summer season. In this case a summer day is where $T_{max} > 31^{\circ}\text{C}$ (31°C is the mean of T_{max} for the historical period).	The percentage of time where $T_{mean} > T_{mean90}$. T_{mean90} is the 90th percentile of daily T_{mean} for a five-day window centered on each calendar day for the historical period.	The number of days where $T_{mean} > T_{mean90}$ in intervals of 6 consecutive days. T_{mean90} is the same as warm days percent.	The number of heat waves equal to, or longer than n days per summer season. In this case a heat wave is where $T_{max} > T_{maxNorm} + 5^{\circ}\text{C}$ for n consecutive days. $T_{maxNorm}$ is the mean of T_{max} of a five-day window centered on each calendar day for the historical period. We calculated results for $n=3, 5$ and 7 days.	Number of heat wave days equal to, or longer than n days per summer season. Uses the same heat wave definition as heat waves per summer season.

**Fig. 2.2** - Schematic diagram showing the methodology used for the analysis

2.3 Results and Discussion

2.3.1 Temperature Biases of CMIP6 Models

Figures 2.3 and 2.4 show the biases in MME and individual CMIP6 models in simulating annual and JJA mean temperatures over the homogenous temperature regions of India. The annual T_{mean} show large variation of hot and cold biases for individual models. MIROC6 (Fig 2.3n) has a very high warm bias most notably over the NW region, whereas CNRM (Fig 2.3e) and GFDL (Fig 2.3i) have a cold bias over almost all of India compared to the observations. For JJA T_{mean} (Fig 2.4) there are larger warm biases in most models when compared to annual T_{mean} (Fig 2.3). MIROC6 consistently shows the largest warm bias again in the NW region. The CANESM and GISS models have a much higher warm bias to the east of the NC and IP regions compared to their annual counterparts. These models are likely contributing to the biases of the MME and there is large inter-model variability over the different homogenous regions. Using the MME reduces the biases overall, especially when studying long-term climate trends for both annual and JJA time periods.

The observed climatology of annual maximum, mean and minimum (T_{max}, T_{mean} and T_{min}) over the homogenous temperature regions of India is shown in Fig. 2.5 (a, d, g) and MME (Fig. 2.5b, e, h). The annual temperature ranges from below 5°C to 37°C for the entirety of India, with the highest temperatures being from the NW (37°C) and IP (36°C). The difference between the MME and observed data can be seen in Fig. 2.5c, f, i. Generally, the models are good at representing the temperature over India as there are significant values (at 95% significance level) in all regions. The NC region results are mostly significant for annual T_{max} and T_{mean} but show much less significant values when looking at T_{min}. There is a large cold bias (> 5°C) from the models over the northernmost regions for T_{max} (Fig. 2.5a, b, c), T_{mean} (Fig 2.5d, e, f) and T_{min} (Fig. 2.5g, h, i). This might be related to the snow cover,

the aspect, slope and complex topography of these regions, and the coarser resolution of these GCMs cannot capture (Das et al. 2021, Tiwari et al .2016, Tiwari et al .2017). A larger warm bias (up to 3°C) from the models can be seen in the Tmax mostly over the NC, NW, and NE regions, whereas the Tmin has mostly a cold bias over these. There is a high aerosol load over the Indo-Gangetic plains which stretches over these three regions (Dey and Di Girolamo, 2010) and could explain the warm biases seen which are not considered in these set of CMIP6 models.

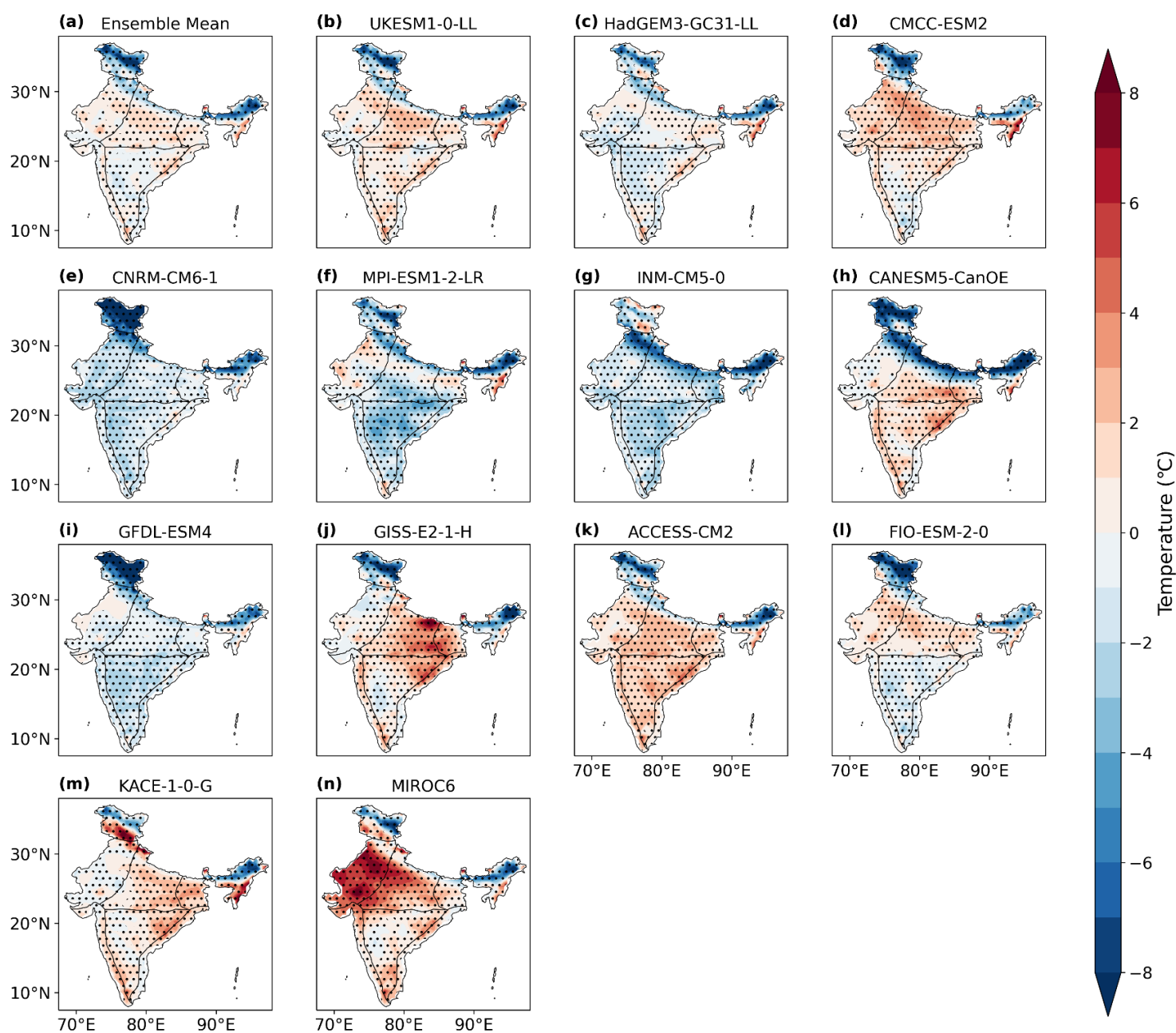


Fig. 2.3 - Annual mean near surface temperature difference of models compared to observation for the period 1984-2014. Ensemble mean of 13 CMIP6 models (a) and individual CMIP6 models used in ensemble (b-n). The dots represent the grid points with significant differences at 95% significance level.

A similar analysis for the JJA period (Fig. 2.6) shows much larger warm biases for Tmax, Tmean and Tmin. This further suggests that the MME are substantially overestimating both hot and cold temperatures in the present.

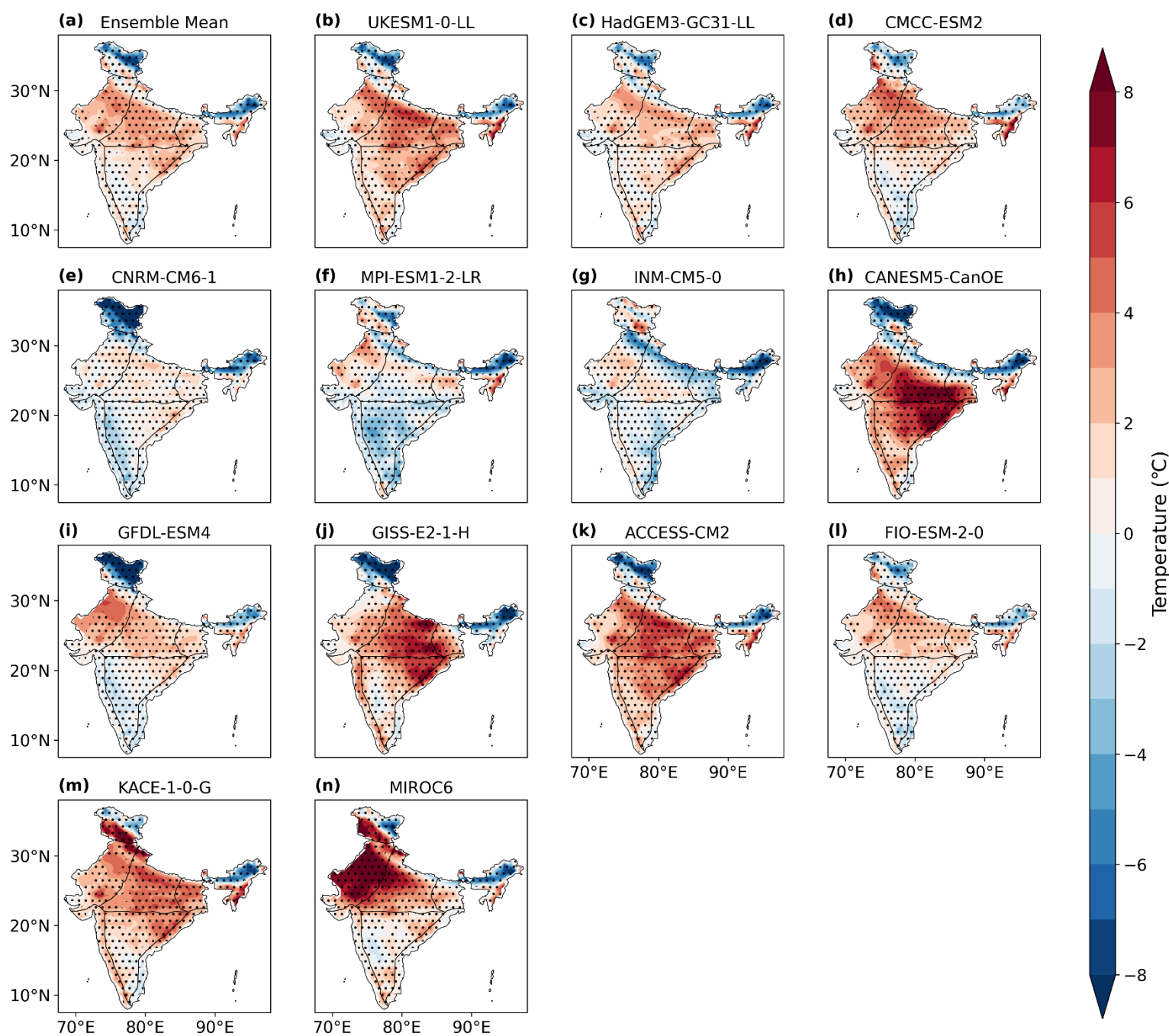


Fig. 2.4 -JJA mean near surface temperature difference of models compared to observation for the period 1984-2014. Ensemble mean of 13 CMIP6 models (a) and individual CMIP6 models used in ensemble (b-n). The dots represent the grid points with significant differences at 95% significance level.

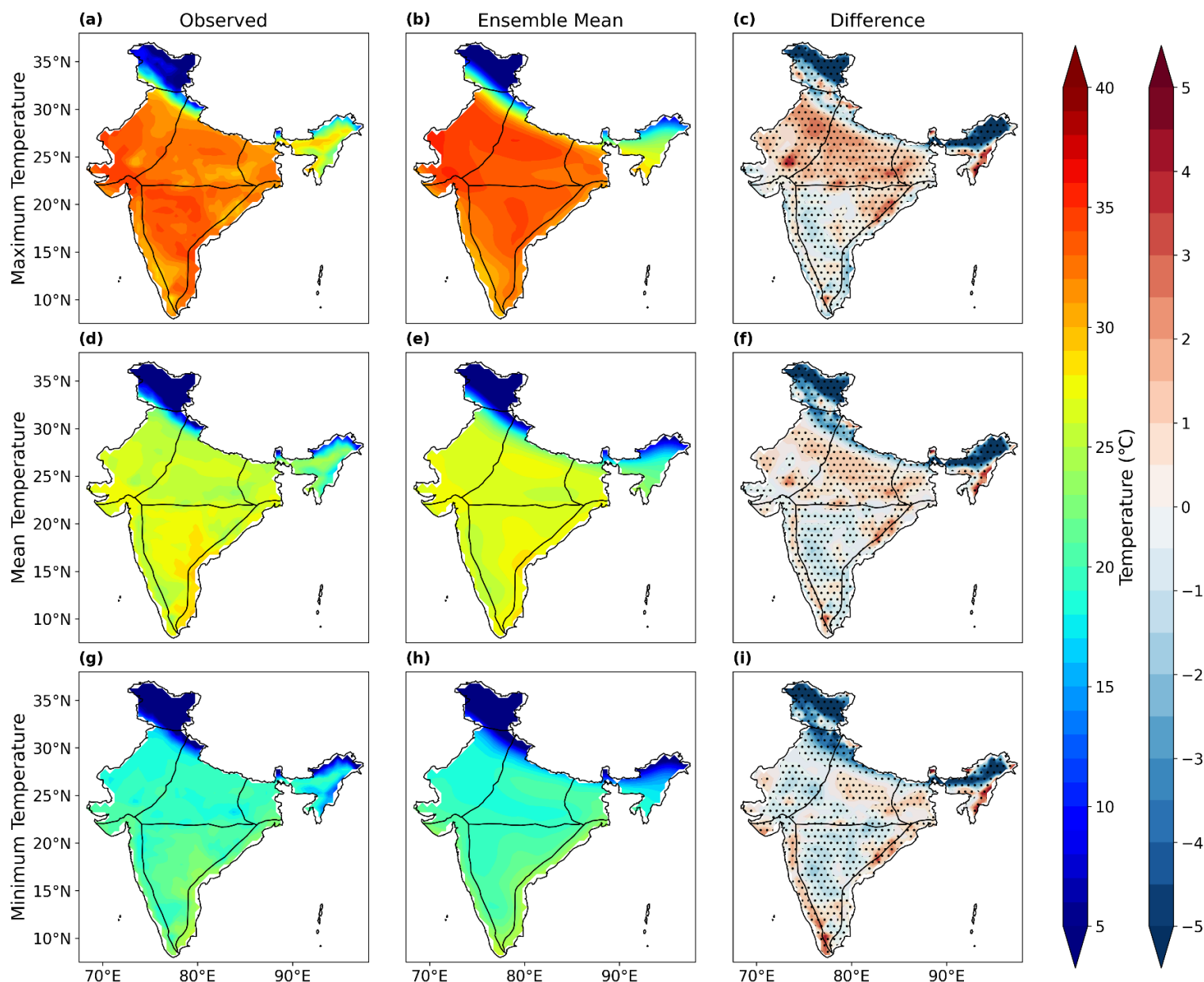


Fig. 2.5 - Annual maximum (a, b, c), mean (d, e, f) and minimum (g, h, i) temperature ($^{\circ}\text{C}$) over the temperature homogenous regions of India for the historical period (1984-2014). Column (a, d, g) shows observed temperature, column (b, e, h) shows the ensemble mean of CMIP6 models and column (c, f, i) shows the difference between the models and observed temperature. The dots represent the grid points with significant differences at 95% significance level.

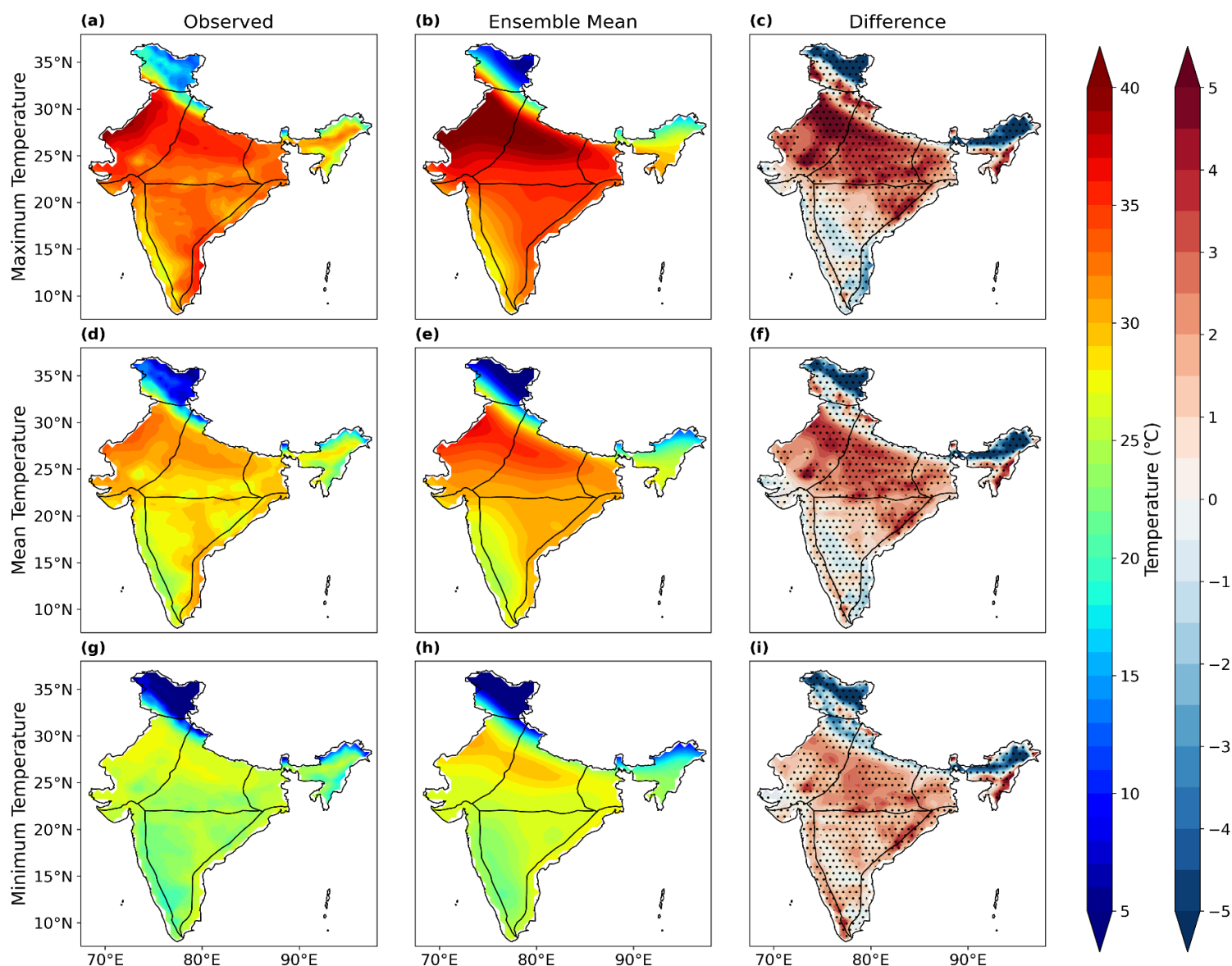


Fig. 2.6 - JJA maximum (a, b, c), mean (d, e, f) and minimum (g, h, i) temperature over the temperature homogenous regions of India for the historical period (1984-2014). Column (a, d, g) shows observed temperature, row (b, e, h) shows the ensemble mean of CMIP6 models and column (c, f, i) shows the difference between the models and observed temperature. The dots represent the grid points with significant differences at 95% significance level.

2.3.2 Statistical Analysis of CMIP6 Models

A Taylor diagram (Taylor, 2001) is presented in Figure 2.7. In this diagram, the performance of individual models in simulating Tmax, Tmean and Tmin during the annual (Fig 2.7a, b, c) and JJA (Fig 2.7d, e, f) periods in terms of the correlation coefficient (CC), root mean square error (RMSE) and normalised standard deviation (SD) is shown. A model that is closest to a SD of 1 and CC of 1 is closest to the observed values. Models perform reasonably

well when capturing Tmax, Tmean and Tmin for both time periods and the models tend to give results closer to observation for annual compared to JJA. There is more of a spread in CC and SD values for JJA compared to annual which highlights the inter-model differences. Almost all models have a CC of over 0.95 for the annual period and over 0.9 for JJA. The SD is generally between 1 and 1.4 for all models for both annual and JJA. Most models have an RMSE of less than 0.4 for the annual period but have a larger RMSE of between 0.4 and 0.8 for JJA. For JJA Tmin, RMSE is smallest for all models. The MME outperforms the individual model experiments and is closer to the observed values in most cases. The FIO and CMCC models perform comparatively better during the JJA period with the FIO model outperforming the MME. The performance of CANESM5 and MIROC6 models in simulating temperature over India is poor compared to the rest of the CMIP6 models used in this study.

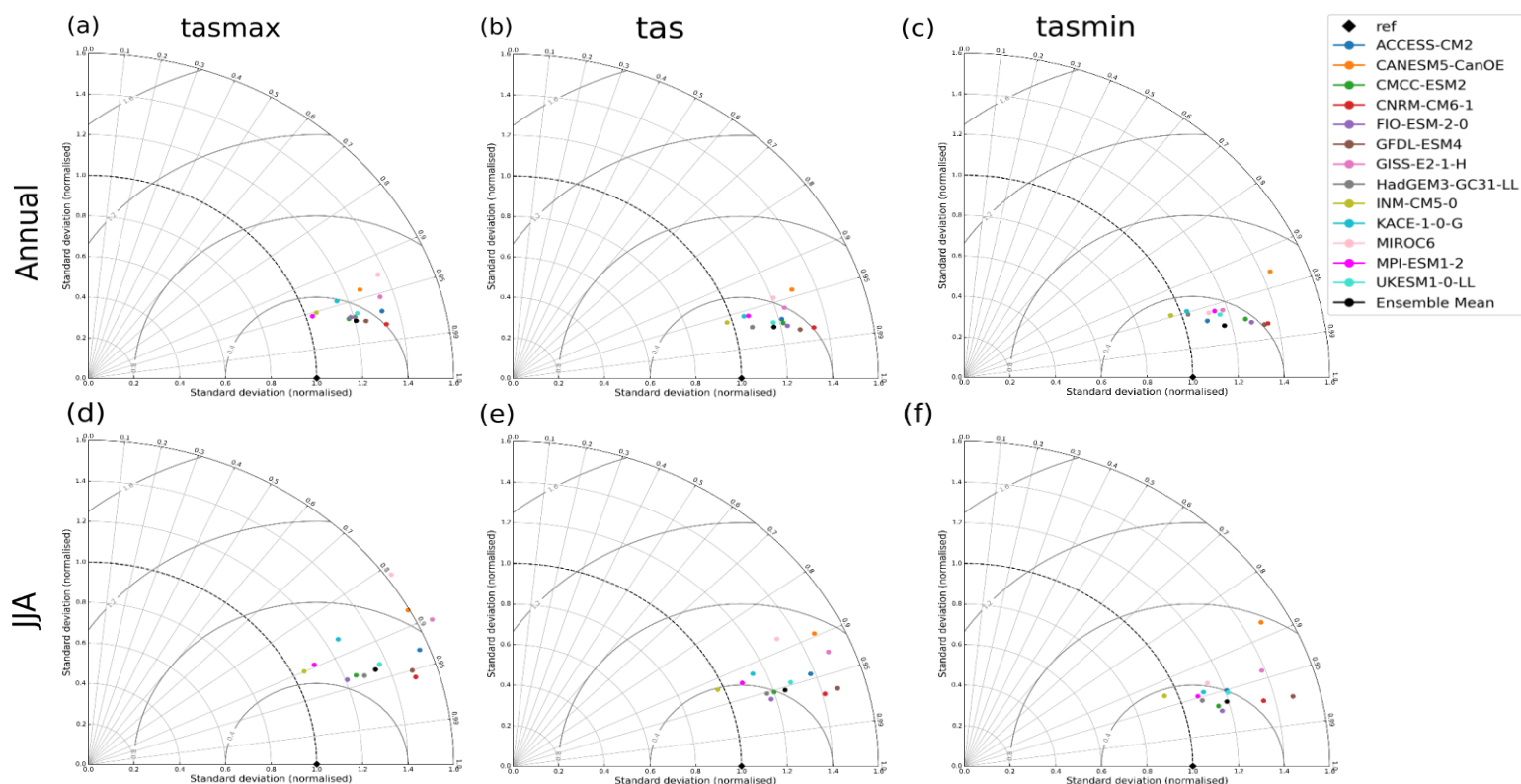


Fig. 2.7 - Taylor diagram showing the annual (a, b, c) and JJA (d, e, f) maximum (a, d) mean (b, e) and minimum (c, f) temperature over India. The correlation coefficient and normalised standard deviation for 13 CMIP6 models compared to observations are shown. The grey curved lines show the root mean square error (RMSE).

The models do well at simulating temperature spatially however, they struggle much more temporally for JJA tas and tasmax (Fig 2.8). When looking at the spatial patterns of temperature (Fig 2.8a, b), models show good CC (0.7+) for the WH, NW, WC, NC, and NE regions. The IP shows slightly lower CC of 0.5 compared to other regions. All models appear to struggle with the EC region with the lowest values being from the CanESM, KACE and GISS models with a correlation of -0.5 for both tas and tasmax. Moving onto temporal correlations, almost all models give low values for all regions. The only models that give CC values over 0.5 are the HadGEM, KACE and UKESM models. This is the same for both temporal tas and tasmax. These results suggest that the models are much better at representing the temperature spatially as opposed to temporally when looking at the individual temperature homogenous regions.

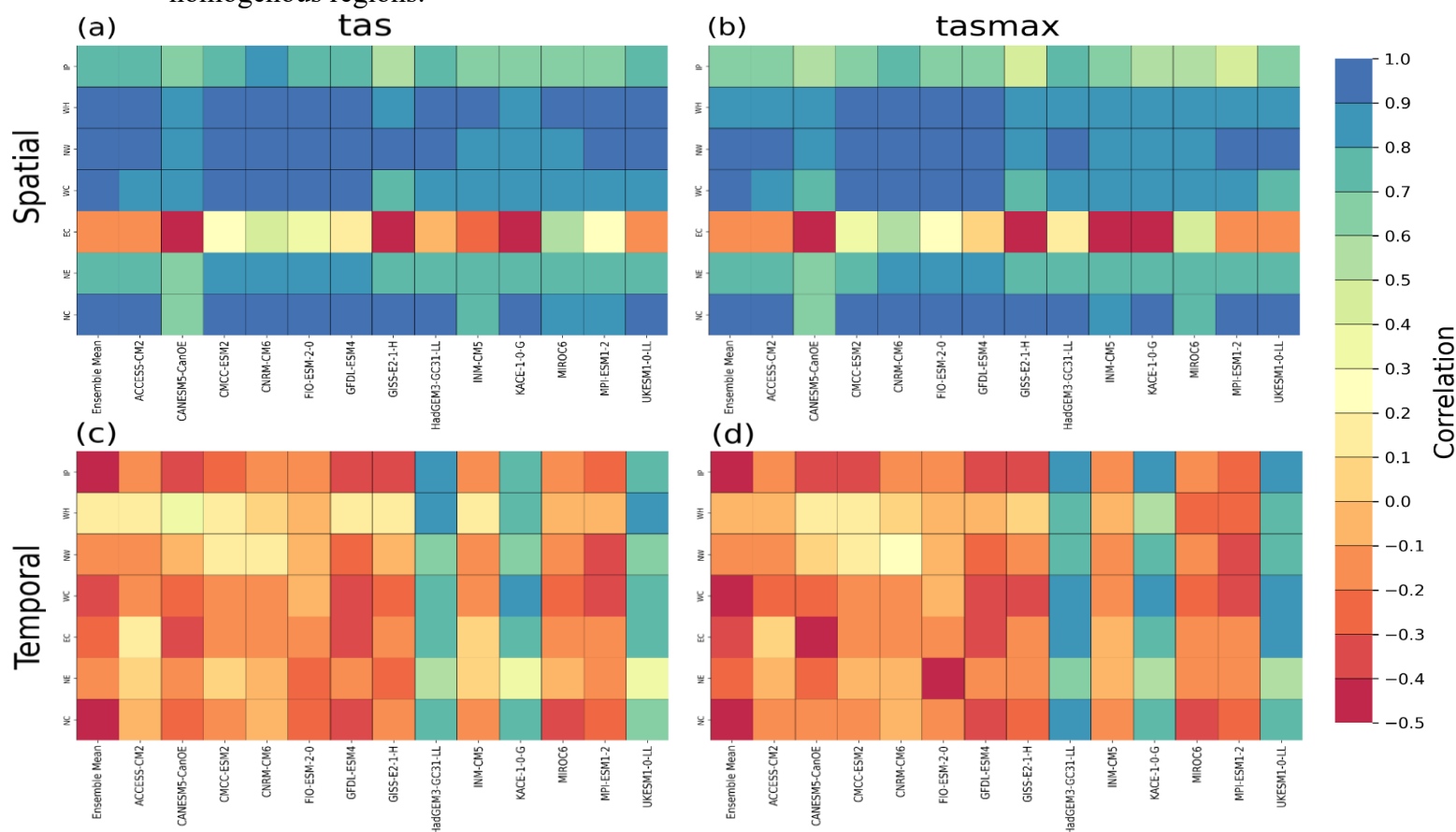


Fig. 2.8 - Diagonal correlation matrix for JJA tas (a, c) and tasmax (b, d) over the Indian temperature homogenous regions. Correlation is shown for the individual models (columns 2-14) and the ensemble mean of these models (column 1) compared to observed values for the historical period (1984-2014). Fig a and b show the spatial correlation and fig c, and d show the temporal correlation.

2.3.3 Future Changes in Temperature

The PDF distributions of the Tmean over India using present and three different SSP scenarios for both annual and JJA periods is shown in figure 2.9. The MME underestimates the annual Tmean with a difference of 0.5°C and overestimates the JJA Tmean with a difference of 2.1°C when compared to observed values. SSP1-2.6, SSP2-4.5 and SSP5-8.5 are split into near-future (NF) and far-future (FF), with a shift in annual Tmean of 0.8°C, 0.9°C and 1.2°C for NF respectively and 1.1°C, 2°C and 4°C for FF respectively compared to observed values. FF SSP5-8.5 shows the largest shift in Tmean and a noticeably higher temperature distribution compared to all other scenarios. The difference between NF and FF SSP5-8.5 is also very large

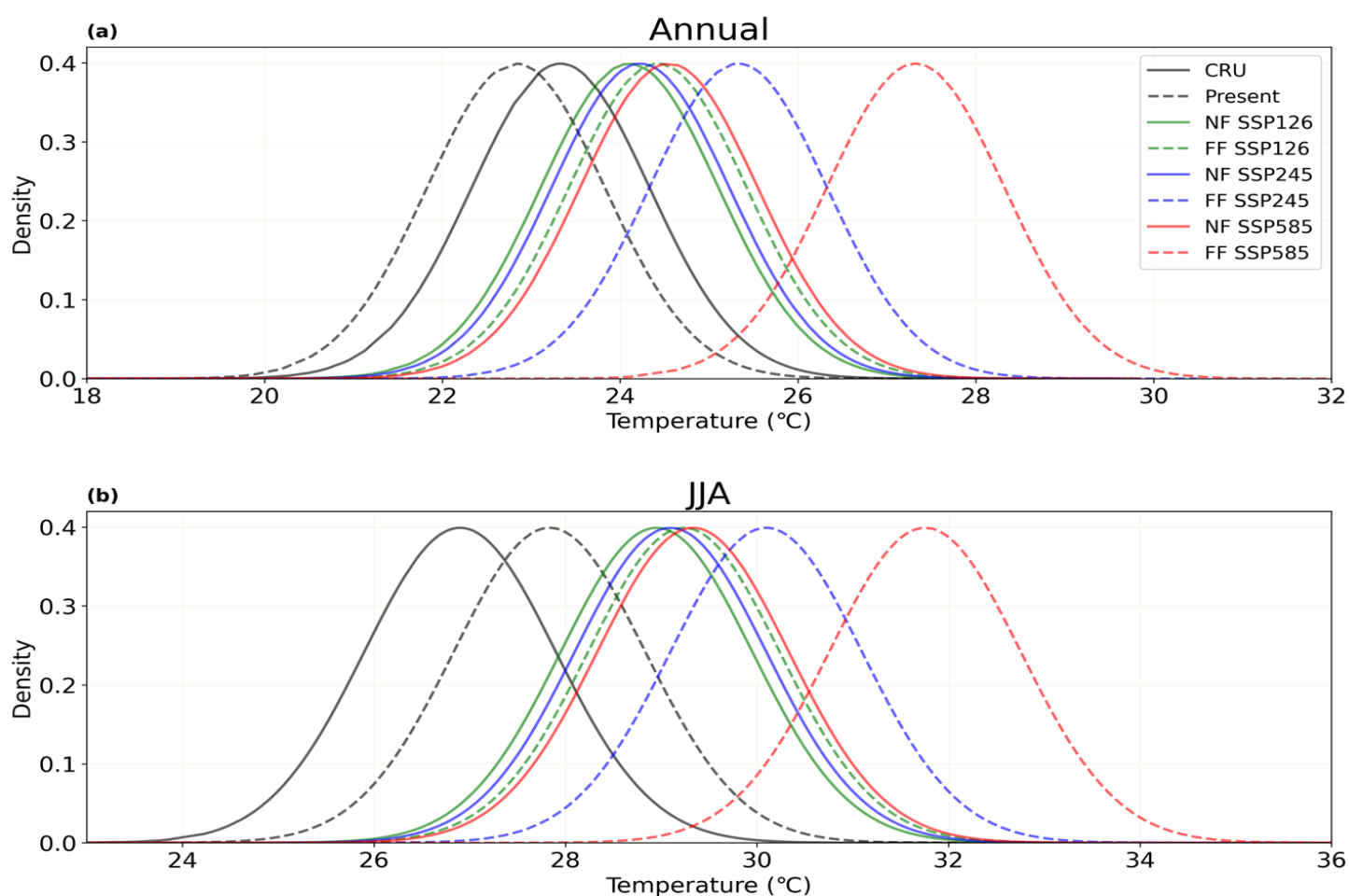


Fig. 2.9 - Annual (a) and JJA (b) mean near surface temperature over India. The solid grey line shows observed temperature, and the dashed grey line shows the present ensemble mean temperature for the historical period (1984-2014). The green, blue and red lines represent SSP1-2.6, SSP2-4.5 and SSP5-8.5. For the SSPs a solid line represents the NF (2030-2060), and a dashed line represents the FF (2070-2100).

compared to other scenarios with a difference of 2.8°C compared to 0.3°C for SSP1-2.6 and 1.1°C for SSP2-4.5. This suggests that under SSP5-8.5 there will be much more warming towards the end of the century. Similarly, when comparing JJA Tmean with observed values, a shift of 2.1°C, 2.2°C and 2.4°C can be seen for NF and 2.3°C, 3.2°C and 4.9°C can be seen for FF SSP1-2.6, SSP2-4.5 and SSP5-8.5 respectively. Both annual and JJA show similar increases in Tmean between NF and FF SSP1-2.6, SSP2-4.5 and SSP5-8.5 with FF SSP5-8.5 showing a noticeably warmer climate compared to present day. The JJA shift in Tmean is larger for both NF and FF compared to the annual period. The NF SSP5-8.5 distribution shows a warmer climatology than FF SSP1-2.6 for both annual and JJA periods suggesting that with sufficient mitigation we can significantly reduce the amount of warming by the end of the century.

Further, the PDF over individual homogeneous regions is discussed in Fig. 2.10 for the JJA and Fig. 2.11 for annual season. For JJA Tmean, the regions with the highest observed Tmean are the NW (30.3°C) and EC (29.5°C). The coldest region is the WH with a Tmean of 11.8°C. For annual Tmean the regions with the highest observed Tmean are the EC (27.6°C) and IP (26.9°C). The coldest region is the WH with a Tmean of 2.4°C. For most regions the historical values from the MME during the annual period are very close to observed values, NW and EC show negligible temperature bias, IP shows a cold bias of 0.2°C, WC shows a warm bias of 0.2°C, NC shows a cold bias of 0.4°C and NE shows a cold bias of 1.4°C. The WH region has a much larger cold bias of 4.3°C. During JJA there are slightly higher warm biases across most regions of 1.0°C (IP), 2.1°C (NW), 0.5°C (WC), 0.6°C (EC) and 2.5°C (NC). The WH and NE have a cold bias of 2.8°C and 0.3°C respectively. Both for annual and JJA periods there is an increase in Tmean between NF and FF for all SSPs over all regions. There is a small increase between NF and FF SSP1-2.6 and SSP2-4.5. The difference between NF and FF SSP5-8.5 is larger than the other two scenarios and FF SSP5-8.5 shows the highest shift in Tmean compared to observed values. The largest increases in Tmean are shown by FF

SSP5-8.5, with an annual increase of 4.3°C (IP), 5.6°C (WH), 4.8°C (NW), 4.0°C (WC), 3.7°C (EC), 4.3°C (NE) and 4.6°C (NC) when compared to the historical Tmean of the MME. This means that the largest shift in Tmean can be seen over the WH region with the NW being close behind. JJA FF SSP5-8.5 compared to the historical Tmean of the MME shows an increase of 3.8°C (IP), 5.6°C (WH), 4.0°C (NW), 3.6°C (WC), 3.6°C (EC), 3.6°C (NE) and 3.8°C (NC). When looking at NF Tmean changes the WH, and NW regions show the largest shift from both annual and JJA Tmean of 2.3°C and 1.9°C (annual) and 2.5°C and 1.5°C (JJA) respectively under SSP5-8.5.

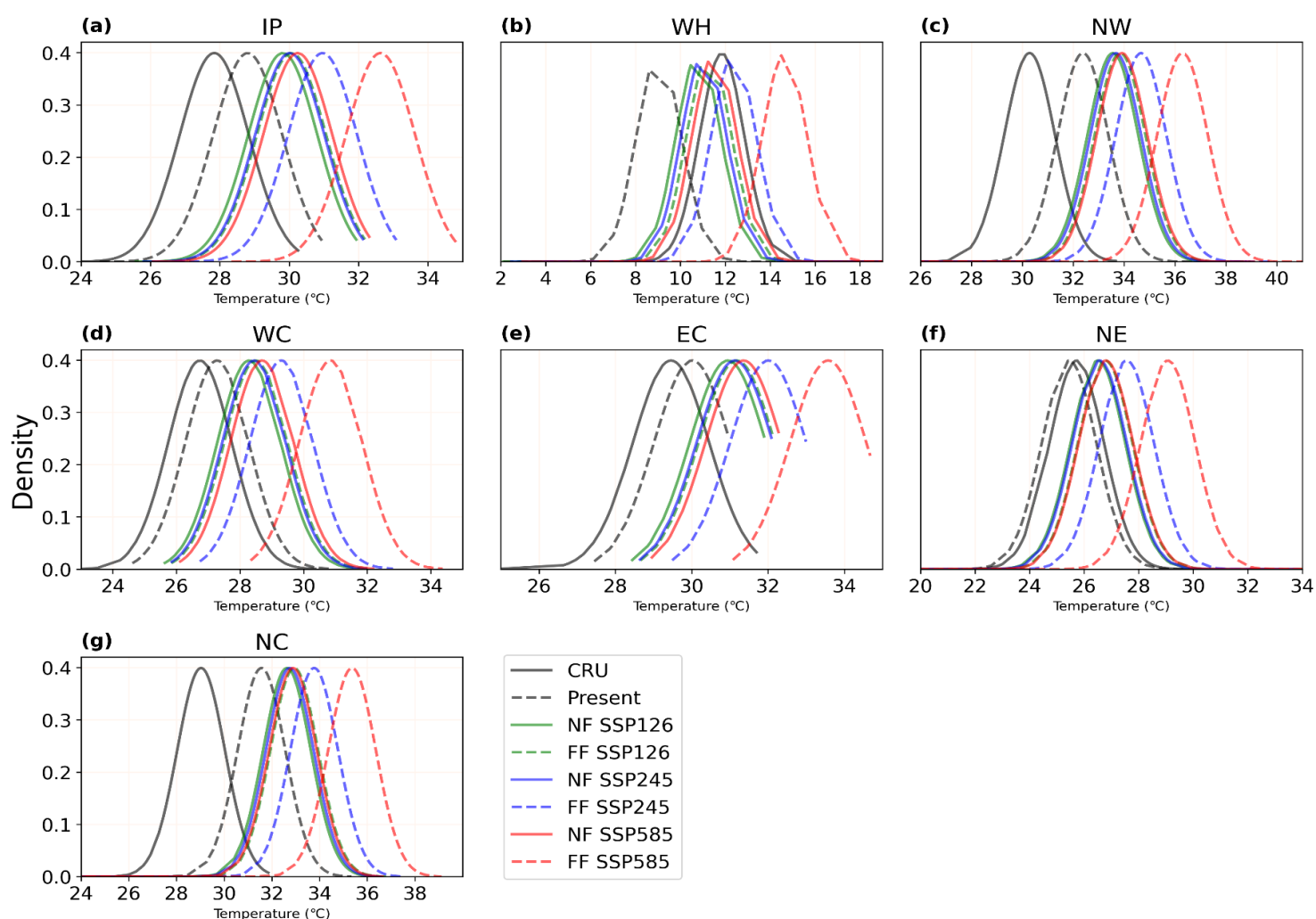


Fig 2.10 - JJA mean near surface temperature for each temperature homogenous region over India. The solid grey line shows observed temperature, and the dashed grey line shows the present ensemble mean temperature for the historical period (1984-2014). The green, blue and red lines represent SSP1-2.6, SSP2-4.5 and SSP5-8.5. For the SSP scenarios a solid line represents the NF (2030-2060), and a dashed line represents the FF (2070-2100).

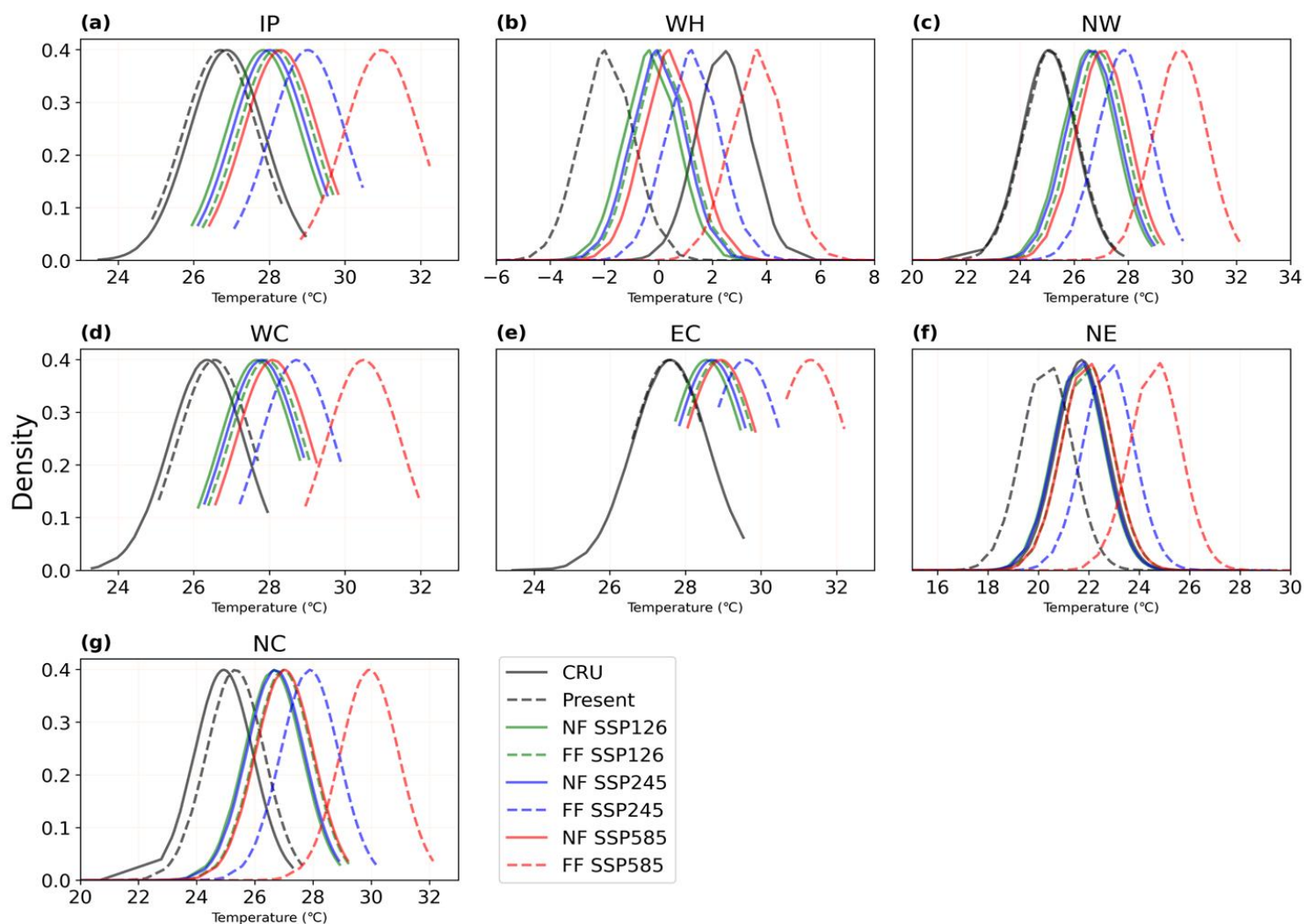


Fig. 2.11 - Annual mean near surface temperature for each temperature homogenous region over India. The solid grey line shows observed temperature, and the dashed grey line shows the present ensemble mean temperature for the historical period (1984-2014). The green, blue, and red lines represent SSP1-2.6, SSP2-4.5 and SSP5-8.5. For the SSP scenarios a solid line represents the NF (2030-2060), and a dashed line represents the FF (2070-2100).

The MME of NF and FF changes in JJA Tmax for all the scenarios over India compared to the present is shown in Fig 2.12. The difference in temperature ranges from $<1^{\circ}\text{C}$ to $>6^{\circ}\text{C}$ over different regions under various scenarios. The regions that show strong differences are the WH, east of NW, west of NC, west and central IP and parts of EC and NE regions. All SSPs over all regions show warming compared to the present Tmax and there is warming when comparing NF SSP1-2.6, SSP2-4.5, SSP5-8.5 and FF SSP1-2.6, SSP2-4.5, SSP5-8.5 respectively, with the increase in temperature being the largest between NF and FF SSP5-8.5.

Under FF SSP5-8.5 parts of the Western Himalaya region are projected to warm by over 6°C and all other regions show a warming of 4-6°C when compared to present day temperatures. The warming is much lower for FF SSP1-2.6 and SSP2-4.5 with an increase over India of 1-3°C and 2-5°C respectively. NF SSP5-8.5 shows similar warming to FF SSP1-2.6 meaning that SSP5-8.5 is projected to reach the same temperature increase as FF SSP1-2.6 30 years earlier.

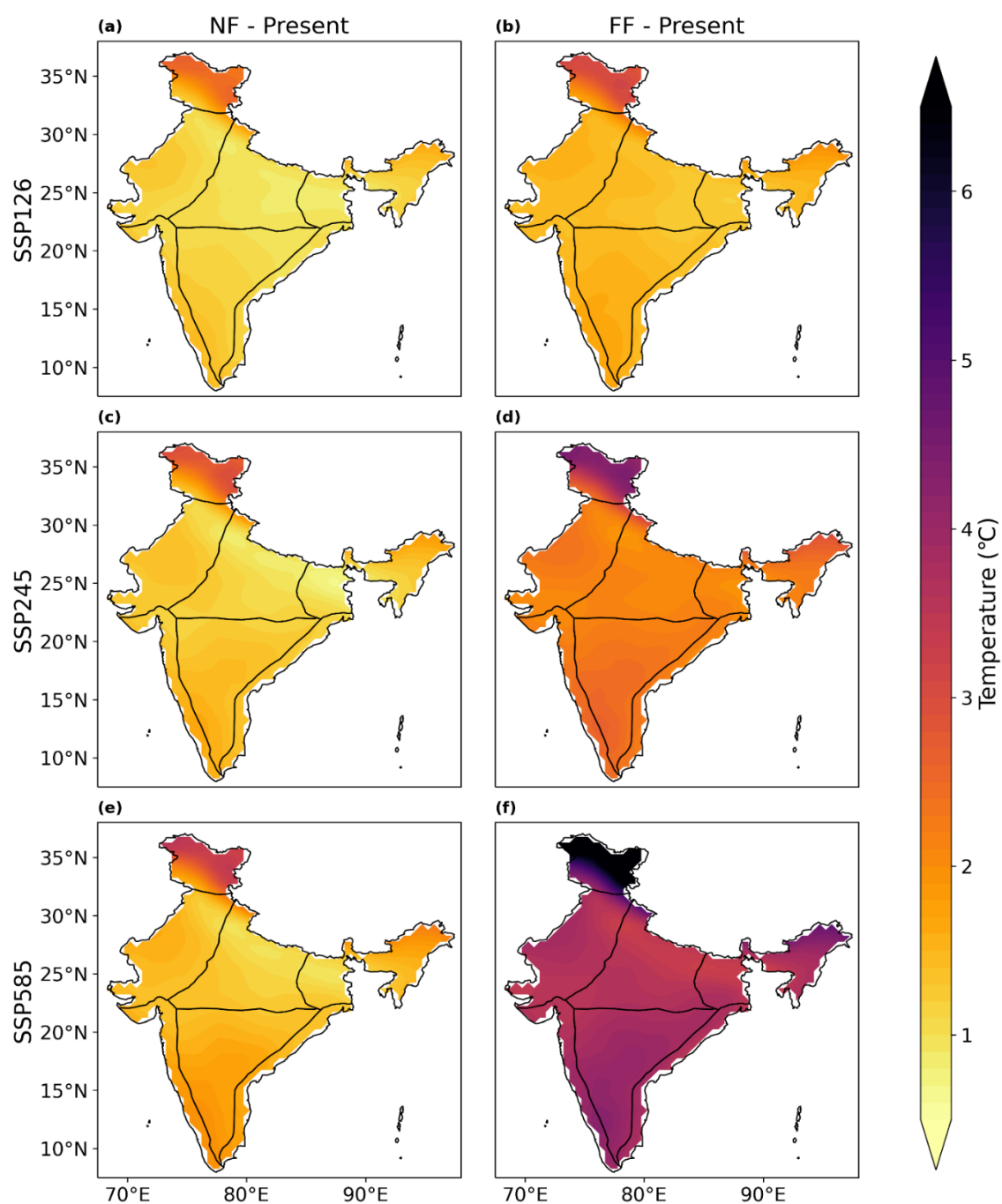


Fig. 2.12 - The difference in JJA Tmax for each SSP1-2.6 (a, b), SSP2-4.5 (c, d) and SSP5-8.5 (e, f) compared to the historical period from the ensemble mean. The first column (a, c, e) shows the NF difference, and the second column (b, d, f) shows the FF difference.

In order to further investigate the rising temperatures, we analysed the JJA, and annual time series averaged over India for all the variables as shown in Fig. 2.13 and 2.14 respectively. Comparing the observed series for the period 1984-2015, the MME series are consistently warmer than the observation for all the present years. This is due to the fact that MME are warmer over major parts of India as discussed previously. However, for the annual timeseries (Fig. 2.14) the MME annual means are colder than the observation. However, such differences are not much profound for the annual series. Annual Tmean is projected to increase by 1.3°C, 1.4°C and 1.7°C for NF and 1.6°C, 2.5°C and 4.5°C for FF. The annual Tmax is projected to increase by 1.1°C, 1.2°C and 1.6°C for NF and 1.5°C, 2.3°C and 4.1°C for FF. The annual Tmin is projected to increase by 1.4°C, 1.6°C and 2.0°C for NF and 1.7°C, 2.7°C and 5°C for FF. The above values are for SSP1-2.6, SSP2-4.5 and SSP5-8.5 respectively and compare the mean of the NF and FF temperatures to the mean of the historical period. The SSPs show relatively similar temperatures till around 2040. The temperature rises for SSP1-2.6 levels off at around 2060 and the temperature rise for SSP2-4.5 decreases, almost levelling off by 2100, however the temperature for SSP5-8.5 continues to steadily rise until the end of the century. A similar plot was created using the JJA period (Fig 2.10). During the JJA period the MME over predicts the temperature for Tmax, Tmean and Tmin. JJA Tmean is projected to increase by 1.2°C, 1.3°C and 1.5°C for NF and 1.4°C, 2.3°C and 4°C for FF. The JJA Tmax is projected to increase by 0.9°C, 1.1°C and 1.3°C for NF and 1.3°C, 2.1°C and 3.7°C for FF. The JJA Tmin is projected to increase by 1.2°C, 1.4°C and 1.7°C for NF and 1.4°C, 2.3°C and 4.1°C for FF. The above values are for SSP1-2.6, SSP2-4.5 and SSP5-8.5 respectively. Annual and JJA periods show similar temperature increases for all SSPs. As expected, SSP5-8.5 shows the greatest increase in temperature by the end of the century for all temperatures for both annual and JJA periods. All SSPs show a higher temperature than present day showing that warming

is inevitable, but the amount of warming can be reduced significantly with sufficient mitigation strategies. Similar increases in annual Tmean over India can be seen in Almazroui et al. (2020).

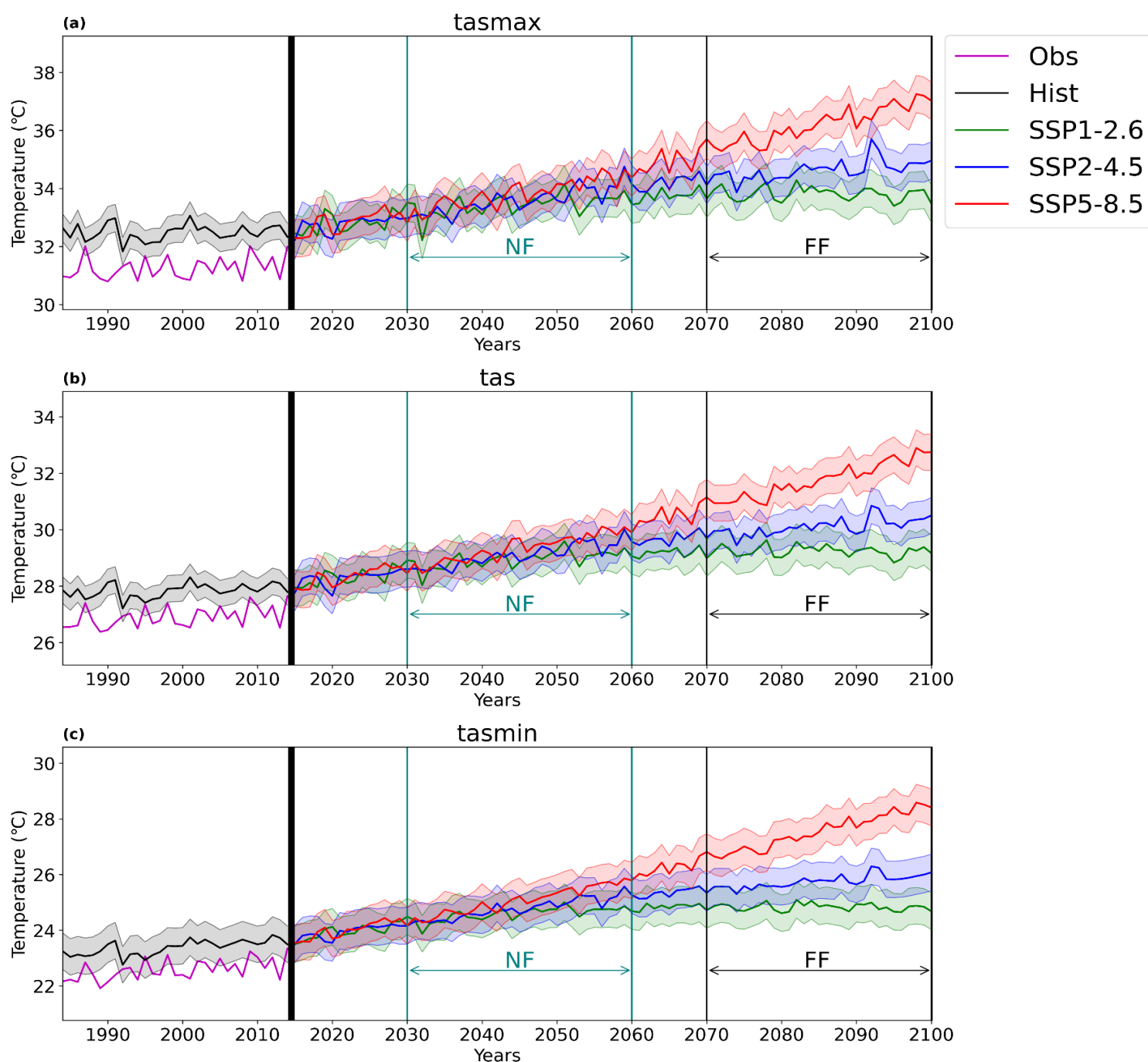


Fig. 2.13 - JJA maximum (a), mean (b) and minimum (c) near surface temperature over India for historical (1984-2014) and future (2015-2100). The magenta line is the observed temperature, and all others are an ensemble mean of 13 CMIP6 models. Near future (NF) is shown from 2030-2060 and far future (FF) is shown from 2070-2100. Grey represents the historical time period, and the green, blue and red lines represent SSP1-2.6, SSP2-4.5 and SSP5-8.5 respectively.

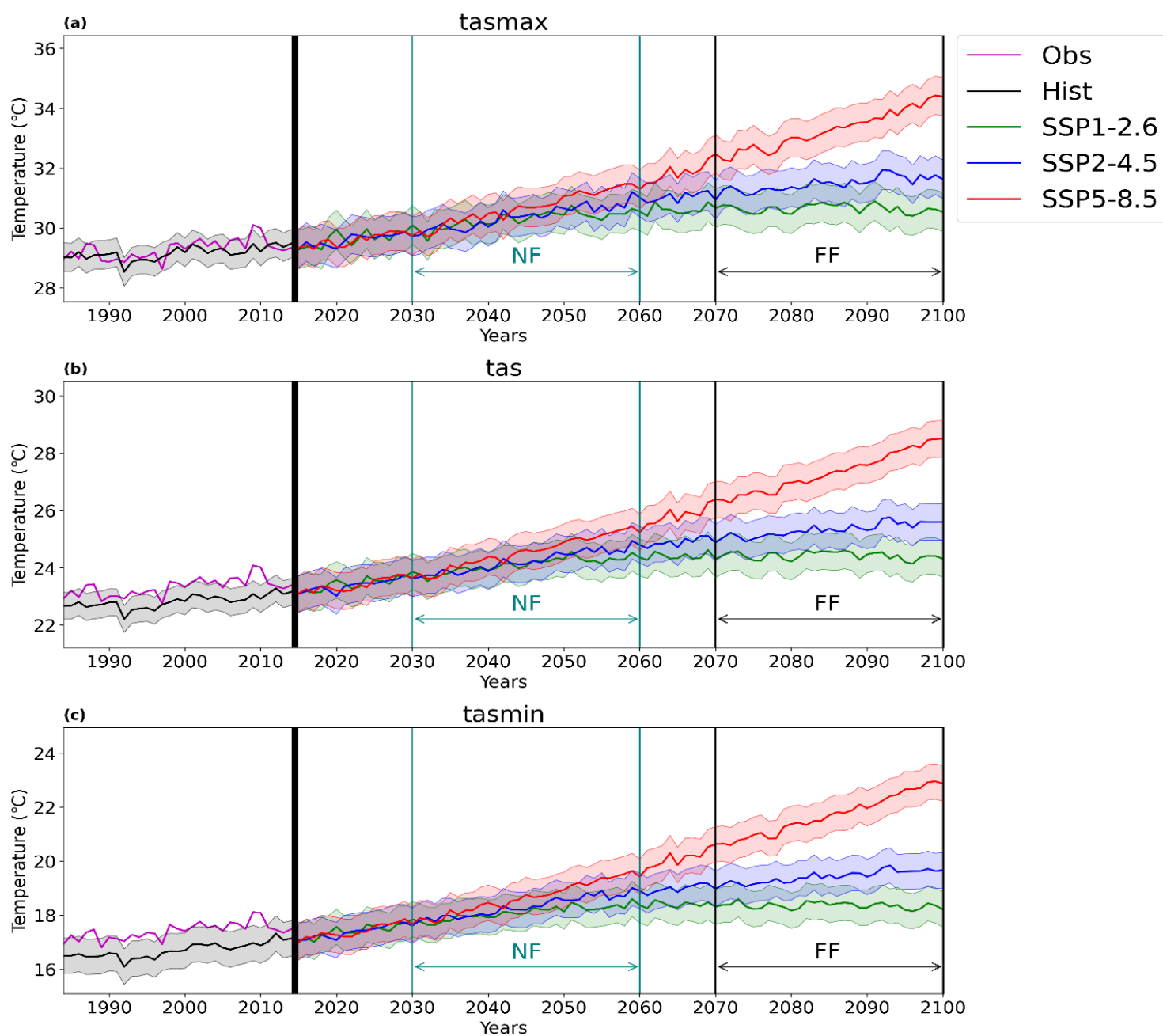


Fig 2.14 - Annual maximum (a), mean (b) and minimum (c) near surface temperature over India for historical (1984-2014) and future (2015-2100). The magenta line shows the observed temperature, and all others are an ensemble mean of 13 CMIP6 models. Near future (NF) is shown from 2030-2060 and far future (FF) is shown from 2070-2100. The black line shows the historical time period, and the green, blue and red lines represent SSP1-2.6, SSP2-4.5 and SSP5-8.5 respectively. The shaded regions show the 95% confidence interval using the student-t test.

2.3.3.1 Extreme Temperature Analysis

The changes in the consecutive summer days are projected to decrease for the NF and increase for the FF over India for all SSPs when compared to the historical period (Fig 2.15). In the near future, the NC, east of NW, and west of NE regions show the largest decrease of around 30-40 consecutive summer days for all SSPs. Parts of the IP and EC also show a slightly lower decrease of around 10-20 days. The bottom of the UP and the west of the NW regions show a slight increase in consecutive summer days, with SSP5 showing the largest increase of 5-20 days. The WH, west of the NE and WC regions appear to be unchanged for the NF. When looking at the FF period there is mostly an increase over India, with FF SSP5-8.5 showing the largest increase in consecutive summer days when compared to the historical period. The regions that see the largest increase are north of the NC, parts of NW and northeast of NE across all SSPs, however FF SSP5-8.5 shows much higher areas of increased days in the EC and IP (60-80 days) compared to the other SSPs. A higher concentration of increased consecutive summer days seems to follow the Indo-Gangetic plains for FF. FF SSP1-2.6 and SSP2-4.5 show a slight decrease in parts of the NC and IP regions.

There is little change to the warm day's percent (Fig 2.16) during NF and an increase during the FF period for all SSPs when compared to the historical period. The WC shows the largest increase (1%) in warm days for all NF SSPs. There is a slight decrease in warm days for IP, NC, NW and west of NE regions and a slight increase for WH, east of NE and EC regions. All regions during FF SSPs show an increase in warm days percent. The most affected regions for FF SSP1-2.6 and SSP2-4.5 are the WH, NE and NW regions with SSP2-4.5 showing a larger percentage increase (2-3%) when compared to SSP1-2.6. FF SSP5-8.5 shows the largest increase in warm days percent with most regions showing a 3+% increase. East of the NC shows a slightly smaller increase (2.5-3%) when compared to the other regions. The difference in warm spell days index (Fig 2.17) show very similar spatial patterns as described

above in figure 2.16. Again, there is only a small change during the NF and a much larger increase during FF. The largest increase is seen in FF SSP5-8.5 which shows around 90 more warm spell days when compared to the historical period. FF SSP1-2.6 shows an increase of 30-60 days and FF SSP2-4.5 shows an increase of 50-70 days.

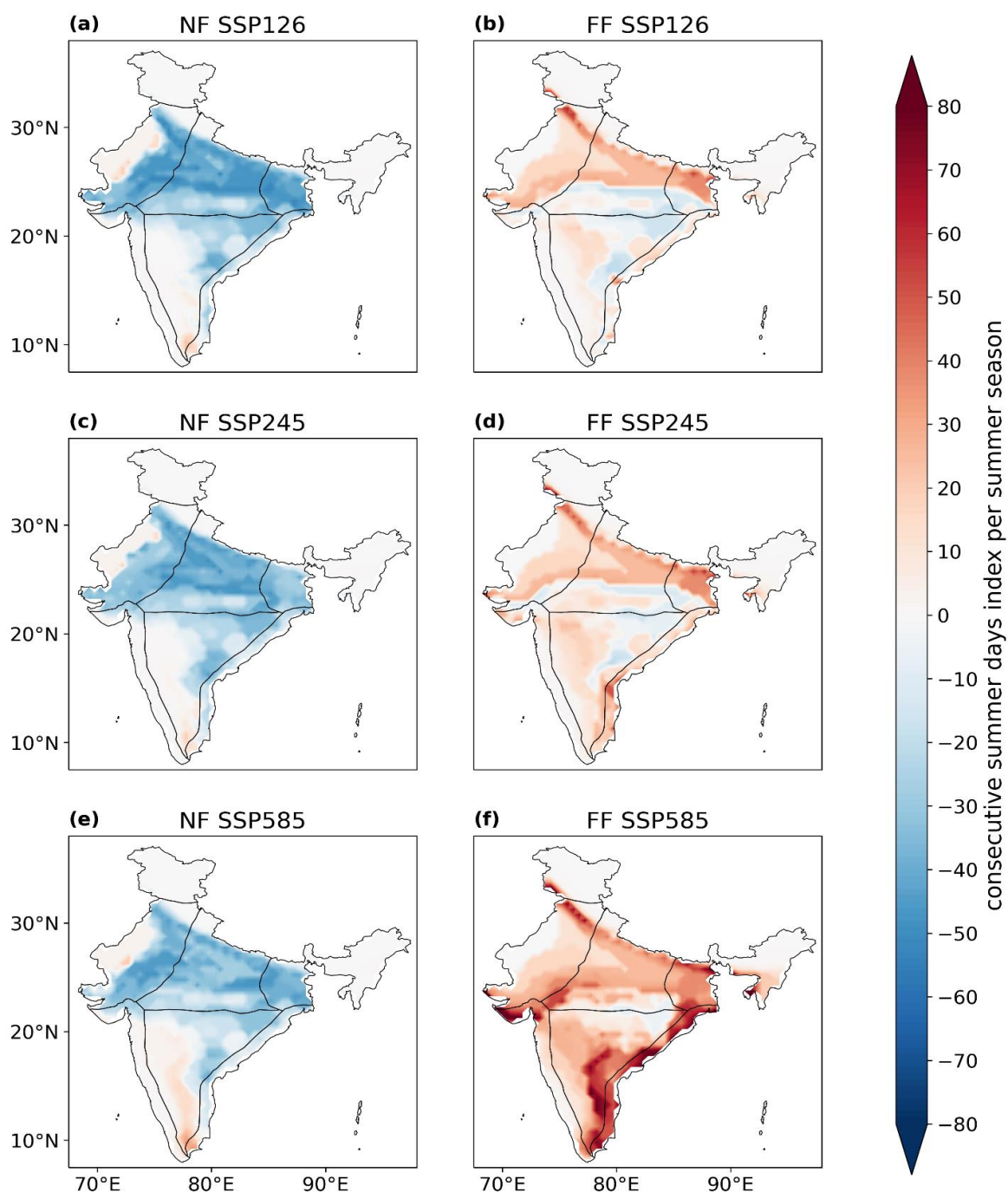


Fig. 2.15 - Consecutive summer days index per summer season difference compared to the ensemble mean of the historical period (1984-2014) for SSP1-2.6 (a, b), SSP2-4.5 (c, d) and SSP5-8.5 (e, f). The first column shows the difference over the NF period (a, c, e) and the second column shows the difference over the FF period (b, d, f).

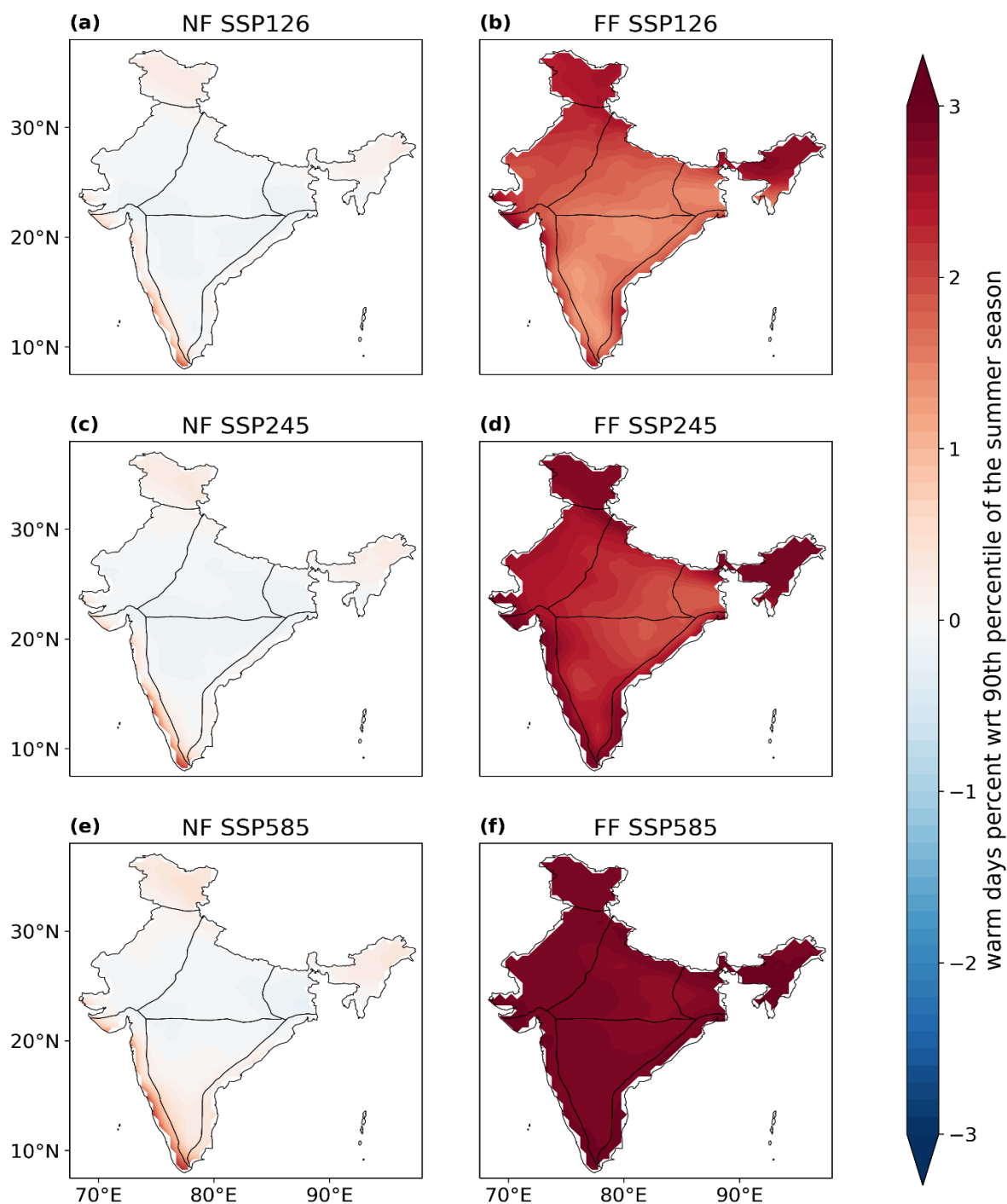


Fig. 2.16 - Warm days percent with reference to the 90th percentile of the summer season difference compared to the ensemble mean of the historical period (1984-2014) for SSP1-2.6 (a, b), SSP2-4.5 (c, d) and SSP5-8.5 (e, f). The first column shows the difference over the NF period (a, c, e) and the second column shows the difference over the FF period (b, d, f).

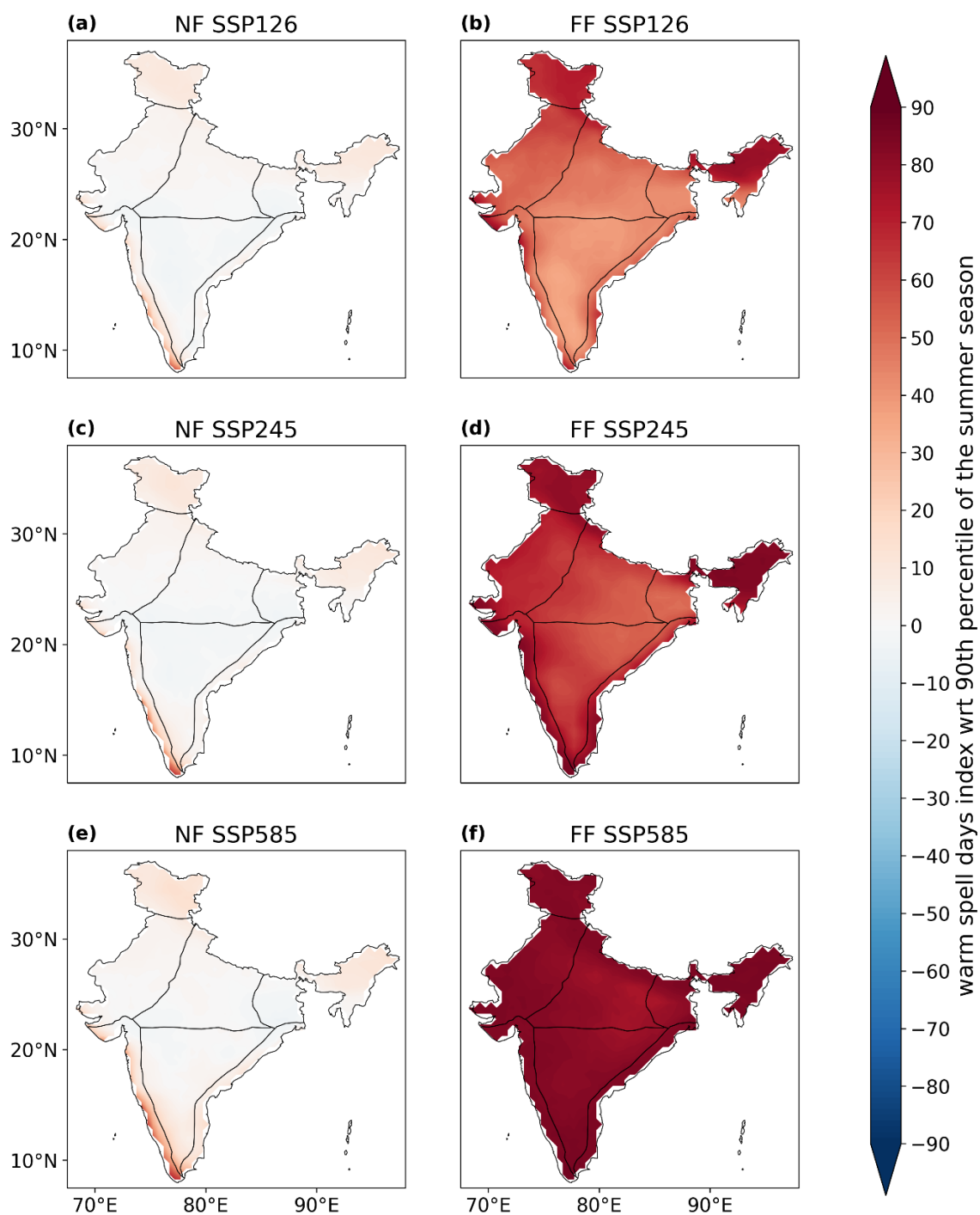


Fig. 2.17 - Warm spell days index with reference to the 90th percentile of the summer season difference compared to the ensemble mean of the historical period (1984-2014) for SSP1-2.6 (a, b), SSP2-4.5 (c, d) and SSP5-8.5 (e, f). The first column shows the difference over the NF period (a, c, e) and the second column shows the difference over the FF period (b, d, f).

Both the heat wave frequency (Fig 2.18, 2.19 and 2.20) and duration (Fig 2.21, 2.22 and 2.23) are projected to increase by the end of the century over most parts of India. We have shown the number of heat waves per summer season for 3 (Fig 2.19), 5 (Fig 2.20) and 7 (Fig 2.18) consecutive days when compared to the historical period. When looking at 3 consecutive days, during the NF most regions (NC, NE, WC, IP, and EC) show no change in the number of heat waves for all SSPs. The WH region is most affected during the NF with around one more heat wave per summer season for all SSPs. There is a slight increase in parts of the NW where the coverage increases from SSP1-2.6 (least coverage) to SSP5-8.5 (most coverage). The same regions are affected for 5 and 7 days with the number of heat waves reducing slightly from 3 (1 day increase) to 7 (0.5-day increase) days. Moving onto the FF the increase in number of heat waves is much greater. The most affected regions for FF SSP1-2.6 are the WH, NW and NC where parts of these regions project around 3 more heat waves per summer season. Other parts of the NW, NC NE, IP and EC show an increase of 2 heat waves per summer season. The least affected regions are the WC, southeast of the NE and southwest of the IP. The number of heat waves increases when comparing SSP1-2.6 to the other two SSPs. FF SSP2-4.5 shows an increase in number of heat waves over most regions, with more parts of the NW, WH, NC and northeast of the NE being the most affected (approx. 3 more heat waves per summer season). For FF SSP5-8.5 almost all regions show a coverage of 3+ more heat waves and the northeast of the NE shows the highest increase approaching 4 more heat waves. The WH region shows less of an increase (1-2 days) when compared to FF SSP1-2.6 and SSP2-4.5. The same patterns emerge with 5 and 7 consecutive day heat waves; however, the number of heat waves reduces with 3 consecutive day heat waves showing the highest increase (up to 4 more days), 5 consecutive heat wave days being in the middle (up to 2.5 more days) and 7 consecutive day heat waves showing the lowest increase (up to 2 more days) in heat wave days. Heat wave duration index (HWDI) is also shown for 3 (Fig 2.22), 5 (Fig 2.23) and 7 (Fig 2.21) consecutive

day heat waves, although there are negligible differences between these figures. All regions except the WH show no increase in HWDI for all NF SSPs and the WH shows an increase of up to 15 more days. Larger increases are seen for all SSPs in the FF with SSP5-8.5 showing the largest increases. The WH region is the most affected with 55, 65 and 70 more days for

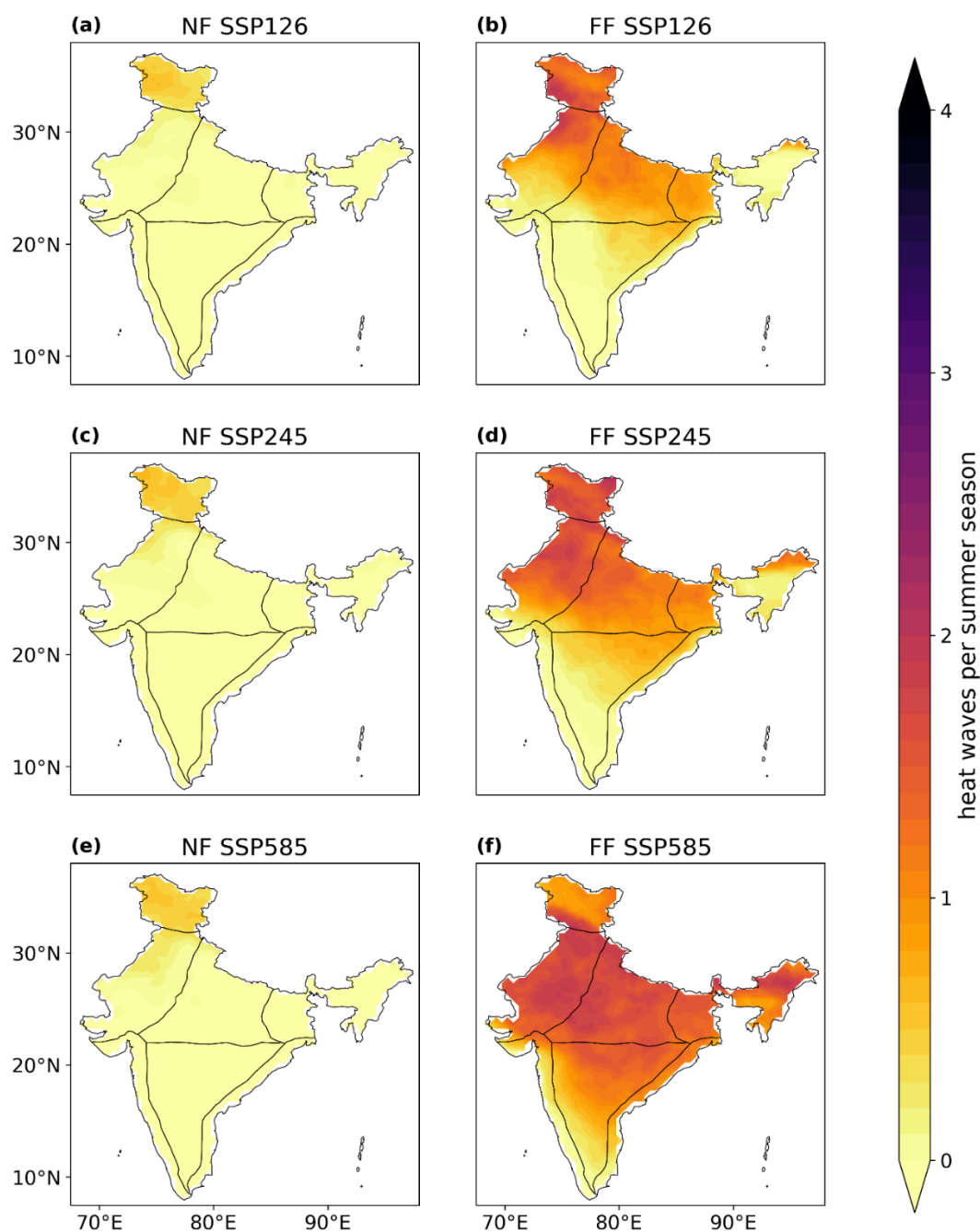


Fig. 2.18 - Heat waves per summer season (where $TX > TX_{norm} + 5^{\circ}C$ for 7 consecutive days) difference compared to the ensemble mean of the historical period (1984-2014) for SSP1-2.6 (a, b), SSP2-4.5 (c, d) and SSP5-8.5 (e, f). The first column shows the difference over the NF period (a, c, e) and the second column shows the difference over the FF period (b, d, f).

SSPs 1, 2 and 5 respectively. The next most affected regions are the NW, NC and NE which affect the most populated areas of India. These regions see an increase of 20, 30 and 50 more days for SSPs 1, 2 and 5 respectively. Whilst the EC, WC and parts of the IP and NE are mostly

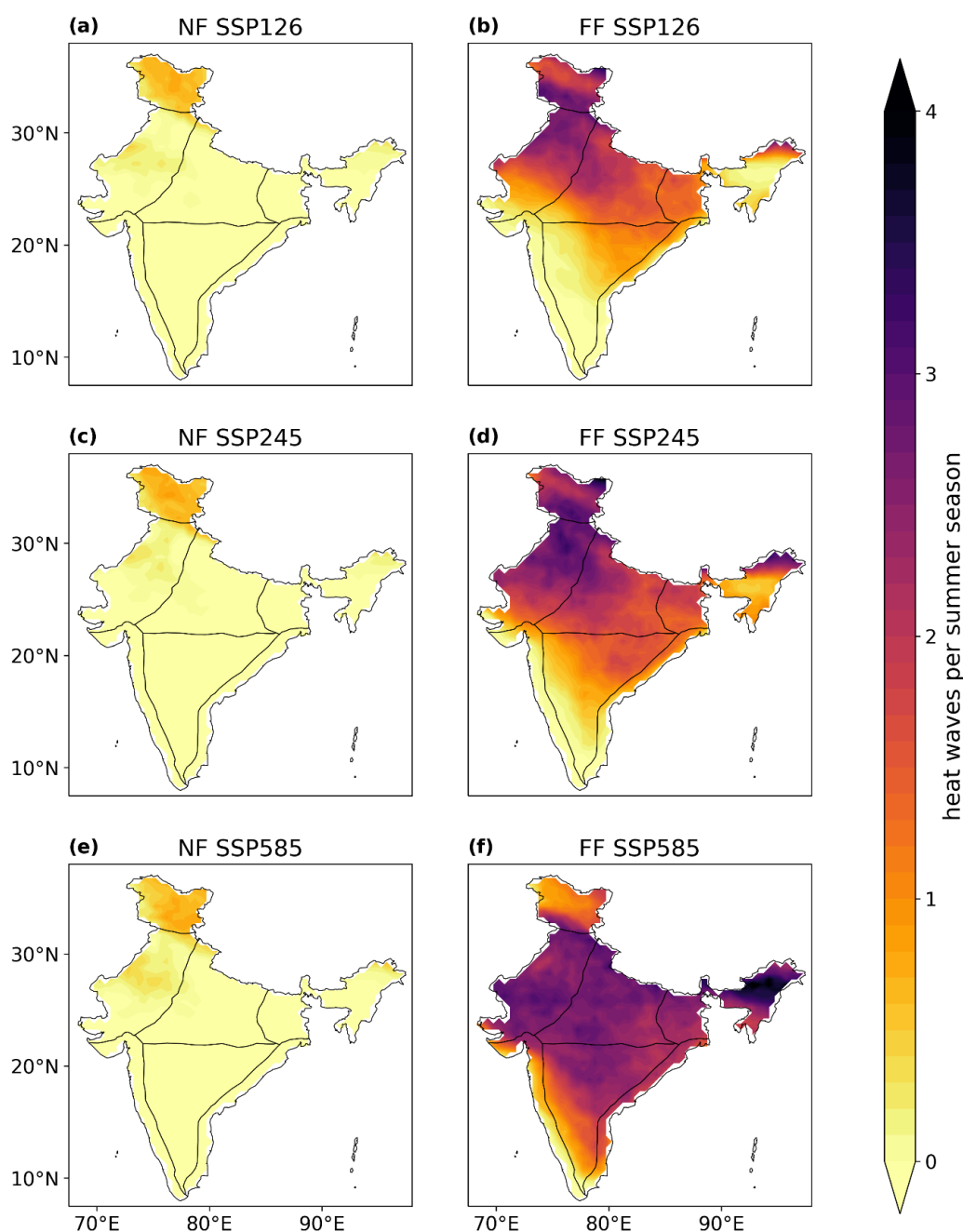


Fig. 2.19 - Heat waves per summer season (where $TX > TX_{norm} + 5^{\circ}C$ for 3 consecutive days) difference compared to the ensemble mean of the historical period (1984-2014) for SSP1-2.6 (a, b), SSP2-4.5 (c, d) and SSP5-8.5 (e, f). The first column shows the difference over the NF period (a, c, e) and the second column shows the difference over the FF period (b, d, f).

unaffected for SSPs 1 and 2, SSP5-8.5 shows that all of India except the WC will have an increase in HWDI.

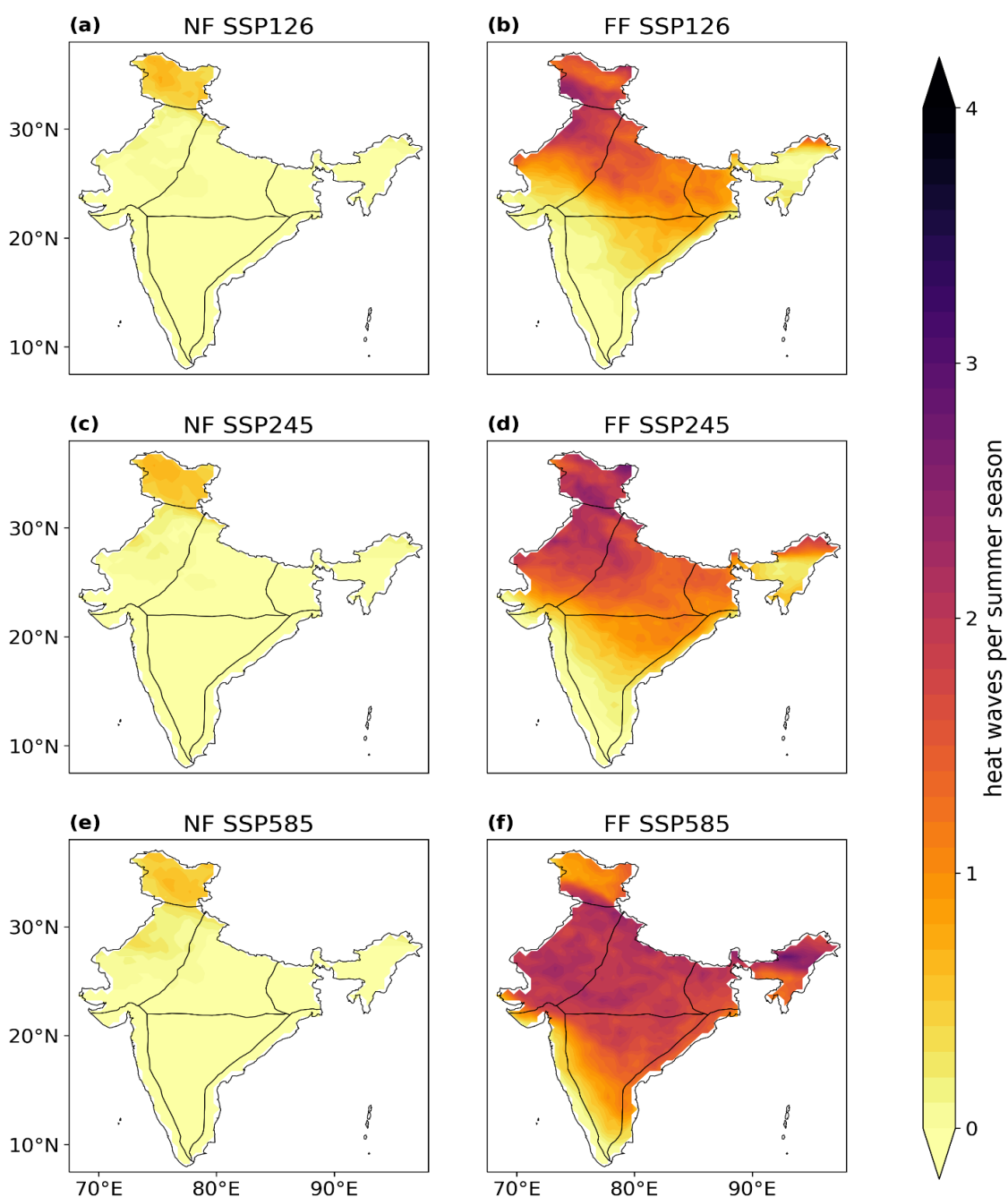


Fig. 2.20 - Heat waves per summer season (where $TX > TX_{norm} + 5^{\circ}C$ for 5 consecutive days) difference compared to the ensemble mean of the historical period (1984-2014) for SSP1-2.6 (a, b), SSP2-4.5 (c, d) and SSP5-8.5 (e, f). The first column shows the difference over the NF period (a, c, e) and the second column shows the difference over the FF period (b, d, f).

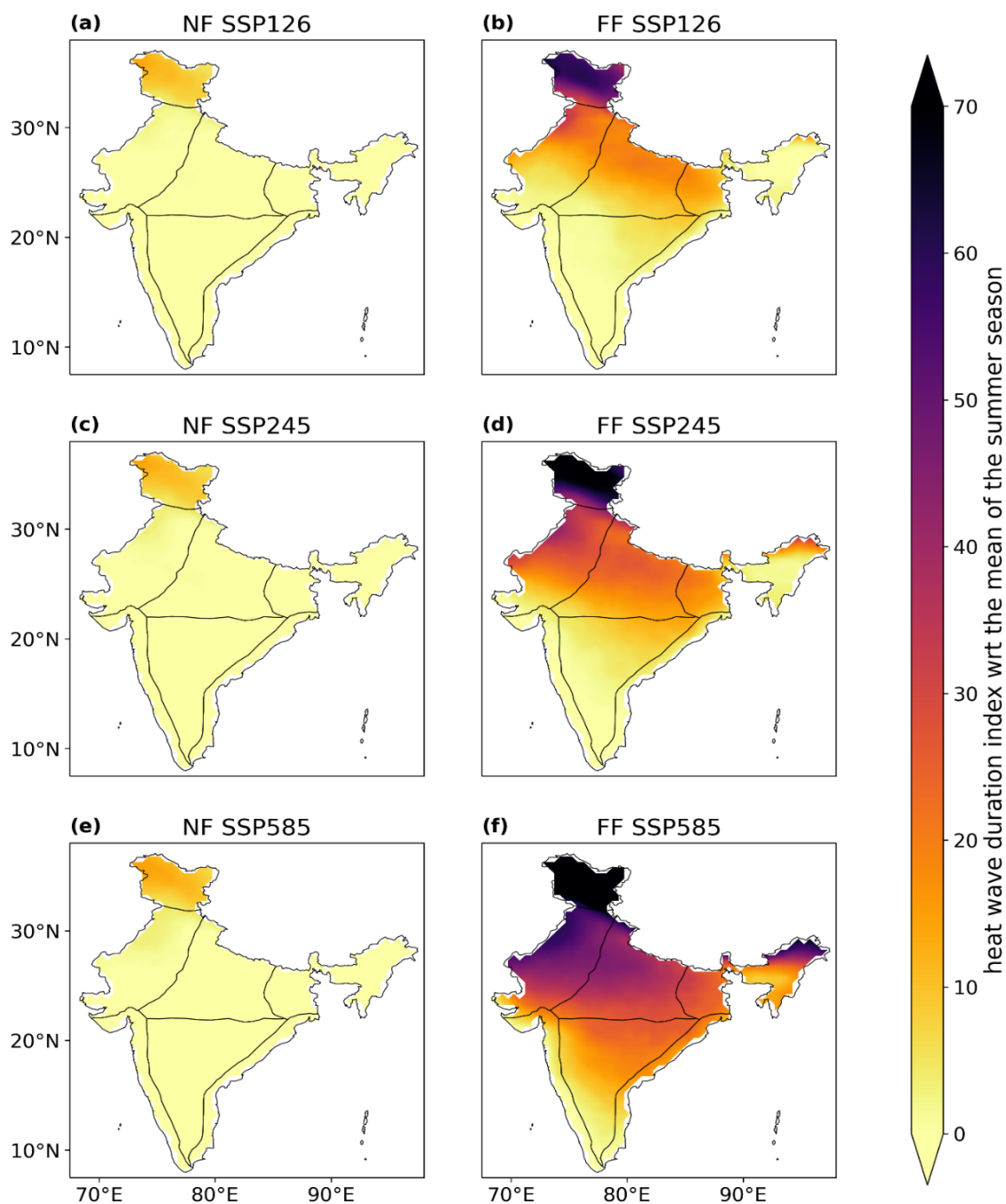


Fig. 2.21 - Heat wave duration index with reference to the mean of the summer season (where $TX > TX_{norm} + 5^{\circ}C$ for 7 consecutive days) difference compared to the ensemble mean of the historical period (1984-2014) for SSP1-2.6 (a, b), SSP2-4.5 (c, d) and SSP5-8.5 (e, f). The first column shows the difference over the NF period (a, c, e) and the second column shows the difference over the FF period (b, d, f).

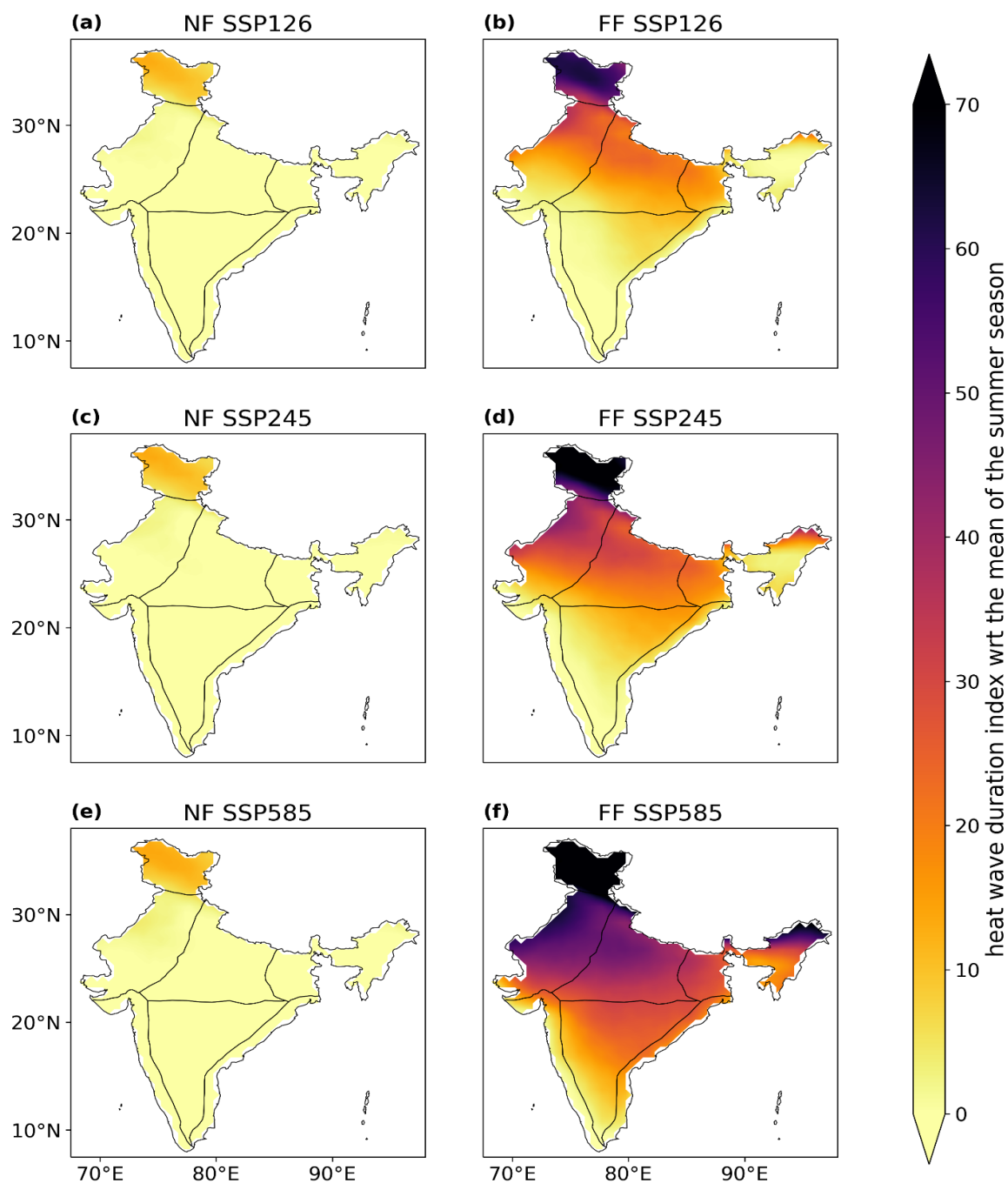


Fig. 2.22 - Heat wave duration index with reference to the mean of the summer season (where $TX > TX_{norm} + 5^{\circ}C$ for 3 consecutive days) difference compared to the ensemble mean of the historical period (1984-2014) for SSP1-2.6 (a, b), SSP2-4.5 (c, d) and SSP5-8.5 (e, f). The first column shows the difference over the NF period (a, c, e) and the second column shows the difference over the FF period (b, d, f).

Overall, the analysis suggests that spatial temperature trends over India, CNRM-CM6 is the best performing GCM, although a lot of the GCMs (CMCC-ESM2, FIO-ESM-2-0, GFDL-ESM4) perform almost as well. When looking at the temporal temperature trends over India HadGEM3-GC31-LL, KACE-1-0G and UKESM1-0-LL perform much better than other GCMs. Our work has shown that the largest increase in future heat wave duration, intensity and frequency is from FF SSP5-8.5. This is comparable to other studies over South Asia who have shown similar results using CMIP5 (Yang et al. 2020) and CMIP6 models (Hamed et al. 2022, Salehie et al. 2022, Ullah et al. 2022, 2023)

2.4 Conclusion

The fidelity of 13 CMIP6 models have been assessed for simulating the temperature over the Indian temperature homogenous regions. A new addition for CMIP6 models compared to previous version is the addition of SSP scenarios which were used to simulate the mean, maximum and minimum temperature up to the end of the century. Our results indicate that:

- CMIP6 models do well at modelling the spatial distribution of temperature over Indian homogenous temperature regions, although they struggle with the colder temperatures of the Western Himalaya and Northeast regions due to the topographic complexity, snow cover and reduced observed values which the coarse resolution of the models fails to capture.
- CNRM-CM6 performs best comparably to other models for spatial temperature over India. HadGEM3-GC31-LL, KACE-1-0G and UKESM1-0-LL are comparably the best performing models for temporal temperature trends over India.
- The MME tends to have a larger warm bias during the JJA period compared to the annual period for mean, maximum and minimum temperature. This could suggest that the models are overestimating warm temperatures during JJA. There is more variation

in the warm and cold biases of the MME per region for the annual period. The IP region has mostly a cold bias for annual temperatures. NC shows a warm bias for Tmax and Tmean but more of a cold bias for Tmin. NW shows a warm bias for Tmax and mostly a cold bias for Tmean and Tmin. The WH and NE show a large cold bias for all temperatures during annual and JJA periods.

- MME outperforms the individual models in terms of the mean biases for different temperature metrics.
- Both annual and JJA temperatures are shown to increase in the NF and FF for mean, maximum and minimum temperatures. The annual maximum temperature is projected to increase by 1.1°C, 1.2°C and 1.6°C for NF and 1.5°C, 2.3°C and 4.1°C for FF SSP1-2.6, SSP2-4.5 and SSP5-8.5 respectively.
- All SSP scenarios project a higher mean, maximum and minimum temperature by the end of the century suggesting that even with mitigation in place, warming is inevitable.
- The mean, maximum and minimum temperature increase for both SSP1-2.6 and SSP2-4.5 seem to level off by the end of the century, whereas SSP5-8.5 continues to rise steadily. This suggests that with sufficient mitigation strategies we can significantly limit the amount of warming over this region by the end of the century.
- Both the frequency and duration of heat waves are shown to increase in the FF with the most populated areas of India being the most affected. The increase shown by SSP1-2.6 is significantly less than what is seen by SSP5-8.5, meaning that effective mitigation can reduce both the frequency and duration of heat waves seen over India by the end of the century.

Fidelity of CMIP6 Models in Simulating Precipitation and Associated Extremes Over India

This chapter is based on the paper:

- Marc Norgate, P. R. Tiwari, S. Das, D. Kumar (2024). On the present and future changes in Indian summer monsoon precipitation characteristics under different SSP scenarios from CMIP6 models. *Climate Dynamics.*, Springer (Accepted, in press).

Abstract

Monsoons are a vital part of the agriculture and economy of India which most of its population rely on for their livelihoods. It still is not clear how climate change will impact precipitation events over India due to the complexity of accurately modelling precipitation. Using twelve Coupled Model Intercomparison Project Six models, we compared their performance to observed data taken from CRU as well as looking at the future changes in precipitation until the end of the twenty first century for the six precipitation homogenous regions over India. The individual models showed varying degrees of wet and dry biases and the ensemble mean of these models showed relatively lesser bias and improved spatial correlation. Out of 12 models, NorESM and MIROC6 models outperform other models in terms of capturing the spatial variability of precipitation over the Indian region. It is also found that due to lesser moisture transport from the adjoining seas represented through vertically integrated moisture transport (VIMT) analysis, there is consistent dry bias across the models. Shared Socioeconomic Pathways (SSPs) were used for future projections and a slight increase in June, July, August, and September (JJAS) precipitation until the end of the century with SSP5-8.5 showing the largest increase. We found an increase in precipitation of 0.49, 0.74 and 1.4mm/day under SSP1-2.6, SSP2-4.5 and SSP5-8.5 in the far future. The northeast region was shown to receive the largest increase in precipitation (2.9 mm/day) compared to other precipitation homogenous regions and northwest will experience largest shift in precipitation. Interestingly, the number of wet days is expected to increase in the northwest region implying more VIMT towards the region. Our results indicate that monsoon precipitation extremes across all the homogenous regions will increase into the future with a higher severity under fossil-fuelled development, although the models still show large biases lowering confidence in our results.

3.1 Introduction

Monsoons affect two thirds of the world's population and are essential for sustainable agriculture and economic development, with a larger impact on lesser developed countries (Zhou et al. 2016). Almazroui et al., (2020) shows that annual mean precipitation is projected to increase into the future, with a greater increase under SSP5-8.5, although there is a relatively large uncertainty due to variations between models. The warming of the Indian Ocean is a likely cause for increased precipitation over India (Turner, 2022). It is difficult to assess how much of the projected increase in precipitation is due to anthropogenic factors and not natural variability (Wang et al., 2013), however later studies generally seem to agree that monsoon rainfall will increase in the future because of a warmer climate caused by GHG emissions (Lau et al., 2013, Menon et al., 2013, Asharaf and Ahrens, 2015, Sharmila et al., 2015). The El Niño-Southern Oscillation (ENSO) has been shown to affect ISM precipitation (Goswami, 1998, Yang and Huang, 2021). The warming of sea surface temperature (SST) is known as El Niño which have been linked to reduced monsoon rainfall (Goswami, 1998, Rasmusson and Carpenter, 1983) and the cooling of SST is known as La Niña which have been linked to increased monsoon rainfall (Halpert and Ropelewski, 1992, Mujumdar et al., 2012). However, there are still gaps in our understanding of these relationships (Rajeevan and Pai, 2007). The Indian Ocean Dipole (IOD) occurs on a local scale (Webster et al., 1999) and has been shown to influence the ISM, with a strong IOD leading to a wetter ISM (Ratna et al., 2020).

CMIP6 models have been shown to better represent clouds and water vapour over tropical oceans (Jiang et al., 2021) although precipitation biases still exist in CMIP6, with a larger overestimation over higher altitudes (Lun et al., 2021). Another addition to CMIP6 is the inclusion of Shared Socio-economic Pathways (SSPs, Riahi et al., 2017) compared to the Representative Concentration Pathways (RCPs, Moss et al., 2010) used in CMIP5. SSPs represent future changes by considering different future emissions and societal changes for five

different future scenarios. CMIP6 has been shown to add value to ISM simulations when compared to CMIP5, with reduced model biases during ISM precipitation (Dutta et al., 2022, Gusain et al., 2020). Although models are improving there are large biases between models when simulating precipitation (Gusain et al., 2020).

The aim of this chapter is to look at the performance of 12 CMIP6 models in simulating precipitation over the 6 India precipitation homogenous regions and the future changes in precipitation over these regions. Large spatial and temporal variability in precipitation exists over all of India which is why we will also be looking at the 6 precipitation homogenous regions, which have been used to represent rainfall in other studies (Dash et al., 2009). Future changes are shown using the latest SSP scenarios added in CMIP6. In addition to the changes in precipitation, the dynamics associated are also presented. Section 2 goes over the methodology and data used, section 3 discusses the results for historical and future time periods and section 4 concludes our results.

3.2 Methodology

3.2.1 Indian Precipitation Homogenous Regions and Observed Data

The six rainfall monsoon homogenous regions have been used in this study (Fig. 3.1), namely the North West (NW), West Central (WC), Central North East (CNE), Peninsular Region (PR), North East (NE) and Himalayan Region (HR). The observed precipitation data is taken from CRU at a resolution of $0.5^{\circ} \times 0.5^{\circ}$ which has been used to evaluate the fidelity of these 12 CMIP6 models. The CRU dataset has been used in many studies and represents precipitation over Indian and South Asian landmass well. ERA5-reanalysis data has been used as the observed dataset when analysing windspeed, humidity and vertically integrated moisture transport over South Asia.

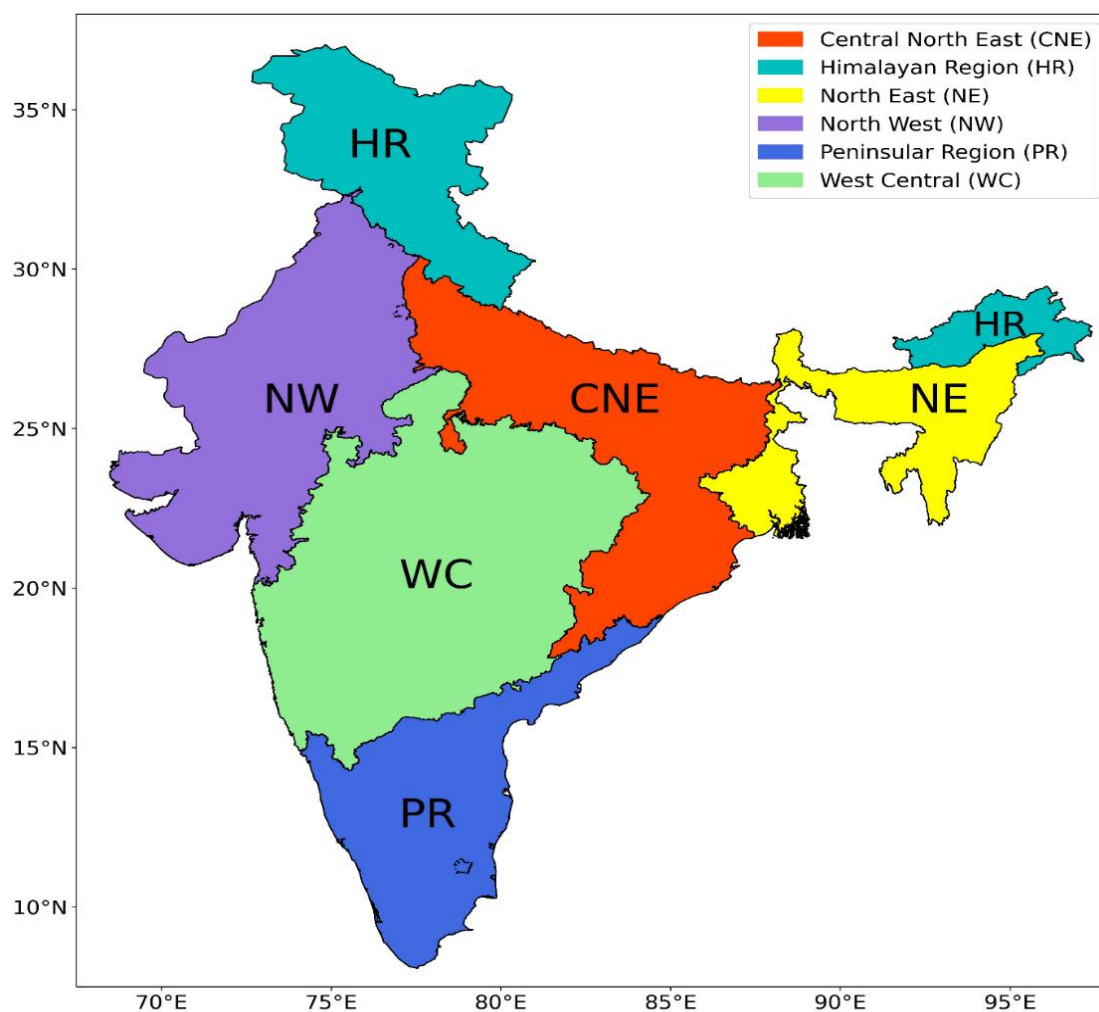


Fig. 3.1 – Six precipitation homogenous regions of India.

3.2.2 CMIP6 Experiments

Precipitation over the India precipitation homogenous regions were modelled using 12 CMIP6 models, the details of these models are shown in Table 3.1. We tested the performance of 17 models originally, however only 12 were chosen for the analysis due to poor performance and data availability. The 12 models mentioned were all chosen due to their positive correlation with the observed data. The CMIP6 data used in this work can be found from the CMIP6 database website (<https://esgf-node.llnl.gov/search/cmip6/>).

Table 3.1 - CMIP6 models used in study

Model	Country	Horizontal Resolution (lon and lat)
CANESM5	Canada	128x64
CESM2	USA	360x180
CMCC-ESM2	Italy	288x192
CNRM-CM6-1	France	362x294
EC-Earth3	Europe	360x180
GFDL-ESM4	USA	360x180
HadGEM3-GC31-LL	UK	192x144
INM-CM5-0	Russia	180x120
KACE-1-0-G	South Korea	192x144
MIROC6	Japan	256x128
NorESM2-MM	Norway	192x96
UKESM1-0-LL	UK	192x144

All models have been re-gridded to match the respective observed grid using the bilinear interpolation method with the Climate Data Operator (CDO, Schulzweida, 2021) for carrying out the analysis. The historical period is considered from 1984 to 2014 for evaluating all the models. CDO was used to calculate the multi-model mean (MME) for all 12 models to reduce biases from individual models (Evans et al., 2000). The MME is the simple mean of all 12 models in this case. To test the fidelity of the models the performance of both the individual models and their MME were compared to the observed precipitation. We calculated the difference between the individual models and MME to the observed data during the historical time period to find the biases of the models and MME. Statistical tests have been carried out at 95% significance using the student-t test.

3.2.3 Future Scenarios and Extreme Precipitation Variables

Three scenarios i.e., SSP1-2.6, SSP2-4.5 and SSP5-8.5 are considered for investigating future changes in the precipitation characteristics during the Indian summer monsoon season. Briefly the SSP1-2.6 represents a sustainable future, SSP5-8.5 represents fossil-fuelled development and SSP2-4.5 represents a middle road (Riahi et al., 2017). The SSPs used represent low (SSP1-2.6), medium (SSP2-4.5) and high (SSP5-8.5) emission scenarios making

SSP5-8.5 the most aggressive scenario in terms of emission. All SSPs represent the future time period 2015-2100 and have been split into near-future (2030-2060) and far-future (2070-2100) to evaluate future changes in precipitation over India. We looked at the projected Indian summer monsoon precipitation for both historical and future time periods. Along with the future changes in the mean precipitation, extreme precipitation indices such as R95, R99, number of consecutive wet days period and wet day index have been examined. The details of the indices are provided in Table 3.2. Further, diagnosis have been carried out to explain the observed future changes in precipitation from dynamic point of view such as changes in winds at 850 hPa and vertically integrated moisture transport (VIMT).

$$VIMT = -\frac{1}{g} \int_{1000hPa}^{100hPa} (qu + qv) dp,$$

Where g is the acceleration due to gravity, q is the specific humidity and u and v are the horizontal and vertical components of the windspeed respectively. The winds at 850 hPa is chosen due to its ability to carry the moisture from adjoining seas i.e., Arabian Sea and Bay of Bengal towards the Indian landmass and VIMT calculates the amount of moisture transported from 1000 to 100 hPa.

Table 3.2 - Extreme precipitation indices definitions calculated using CDO (Schulzweida et al. 2021)

Extremely wet days with reference to the 99th percentile of the reference period	Precipitation percent due to R95p days	Number of consecutive wet days with more than 5 days per time period	Wet days index per time period
The percentage of wet days where the amount of daily precipitation > 99th percentile of the daily precipitation during the historical period.	The percentage where daily precipitation amount > the 95th percentile of daily precipitation during the historical period when compared to the sum of the total precipitation.	The number of consecutive wet days with ≥ 1 mm of daily precipitation that lasts for 5 or more days per JJAS.	The number of days where daily precipitation amount is ≥ 1 mm.

3.3 Results and Discussion

3.3.1 CMIP6 Performance in Capturing ISM Characteristics

The spatial features of JJAS precipitation over India in the observed data portray a maximum over the Western Ghats, Northeast India, Central and Eastern Indian regions, and Himalayan Foothill regions (Fig. 3.2a). There is varying success between the models in representing the historical JJAS precipitation climatology over South Asia (Fig. 3.2). Many of the models can represent these broad spatial features, however a few of them are too dry over the Indian landmass. Although a few of the models do not represent the precipitation hotspots such as the Western Ghats, Himalayan foothills and even the central Indian region, the MME in general outperforms the individual experiments in terms of the spatial distribution. This is also seen in figure 3.3 where we show the biases of the models compared to observations. EC-Earth, HadGEM and NorESM appear to be the best performing models individually and computing the MME of all models shows the best performance. Most models show a dry bias over India, with CanESM5 giving the strongest dry bias (7-9 mm/day) among all the models. The dry bias for JJAS precipitation over India is a known issue with CMIP models, however these biases are shown to improve in CMIP6 compared to CMIP5 (Choudhury et al. 2021, Guilbert et al. 2023). Some models show a large wet bias which is seen mostly over the Himalayan foothills (CESM2, CMCC, MIROC6). The dots in these figures show areas of high confidence which can be seen over the whole region for most figures, except the Northeast of India for the MME and NorESM. The strong dry biases in most of the models affect the MME and major parts of Northern and Northwestern India have dry biases of the order of 3-5 mm/day in them.

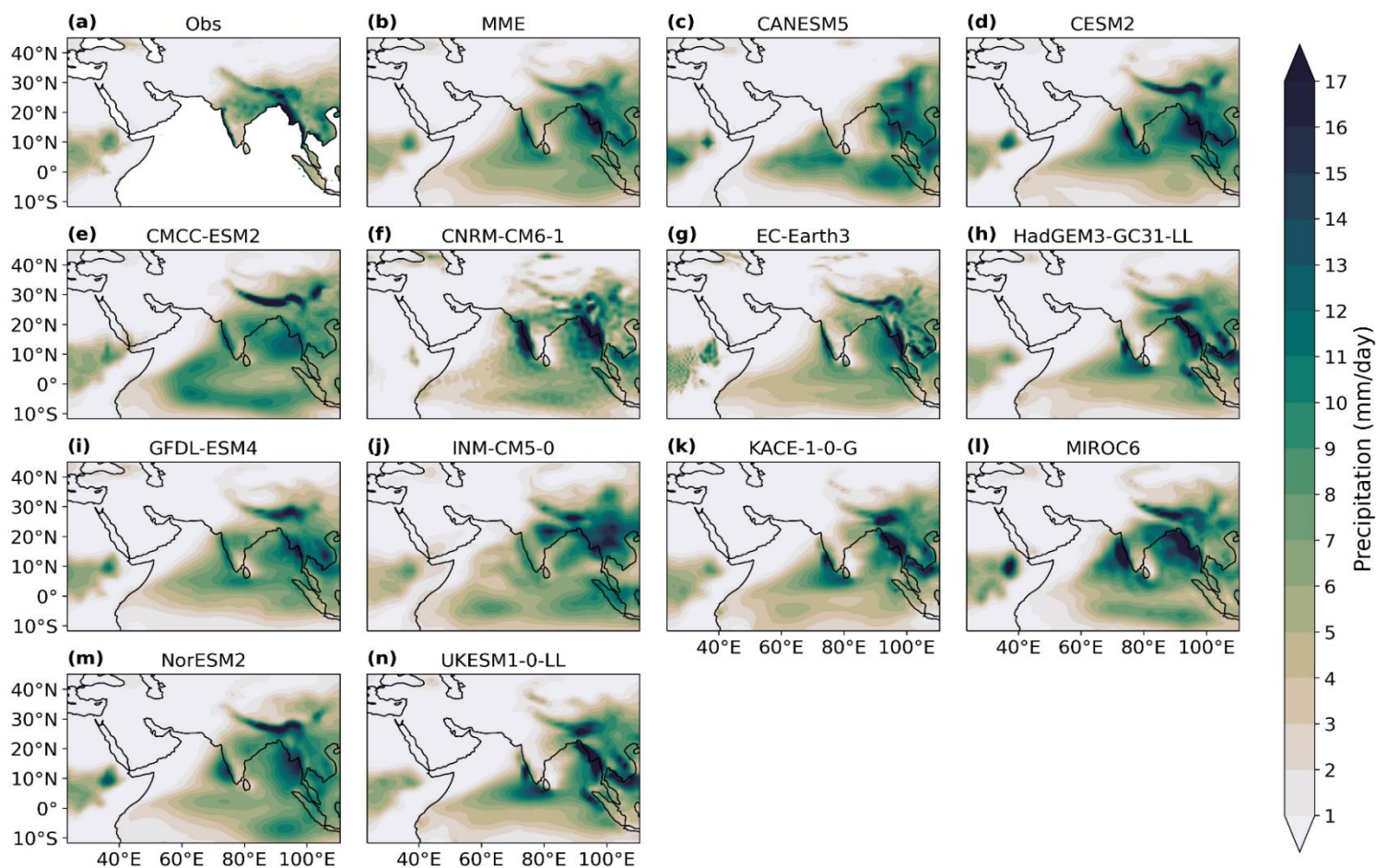


Fig. 3.2 – JJAS precipitation over South Asia (1984-2014) for observed (a), MME (b) and individual models (c-n).

Further, we investigate the model performance for the JJAS daily mean precipitation for individual homogeneous regions using the spatial correlation between the models and the observation. Most of the regions of the Indian precipitation homogeneous regions (Fig. 3.1) show a good spatial correlation when comparing the models and MME to observed values (Fig. 3.4). Most models show a good correlation over CNE with the highest values being 0.8-0.9. CNRM is much worse over this region compared to other models. The models do well across the board when representing the HR. Over half of the models have a correlation between 0.8-

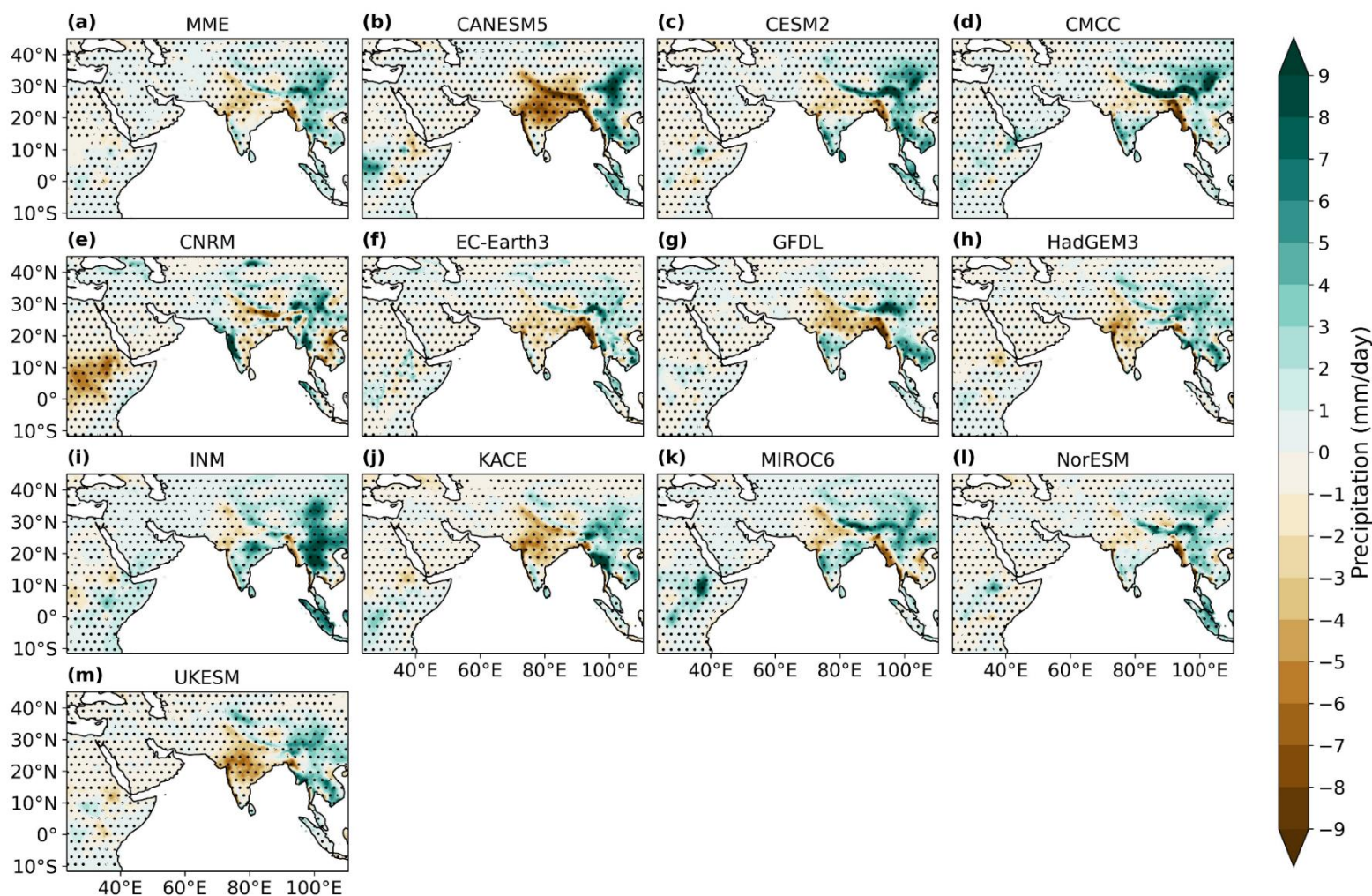


Fig. 3.3 – JJAS precipitation bias over South Asia (1984-2014) for observed (a), MME (b) and individual models (c-n). The dots represent the grid points with significant differences at 95% significance level.

0.9. The NE is the worst represented region by all the models where CanESM5 and CMCC give the lowest values of 0.1-0.2. The NW shows the highest correlation between models and observed with the MME, CESM2, CMCC, GFDL, MIROC6 and NorESM performing the best over this region. CanESM5 shows the lowest correlation over this region. The PR is another well represented region by the chosen models. EC-Earth3 has the highest correlation and INM has the lowest. Finally, the WC is poorly represented and GFDL performs the worst over this region, however EC-Earth is the only model that does very well over this region. The MME consistently performs well over all regions when compared to the individual models highlighting the value of the MME. In general, the MME can capture the spatial patterns of

precipitation over multiple regions with reasonable skill, despite the large spatial variability in the precipitation patterns across the country. Moreover, a general pattern of poor correlation over high rainfall regions such as the NE, and larger correlation values over scanty rainfall regions, is prominent across models. It is important to note that, although the long-term correlations appear robust, there may be differences in the correlation values depending on the period and region under consideration. This variability may indicate interannual to decadal-scale variability in the model results, which might be captured differently across models.

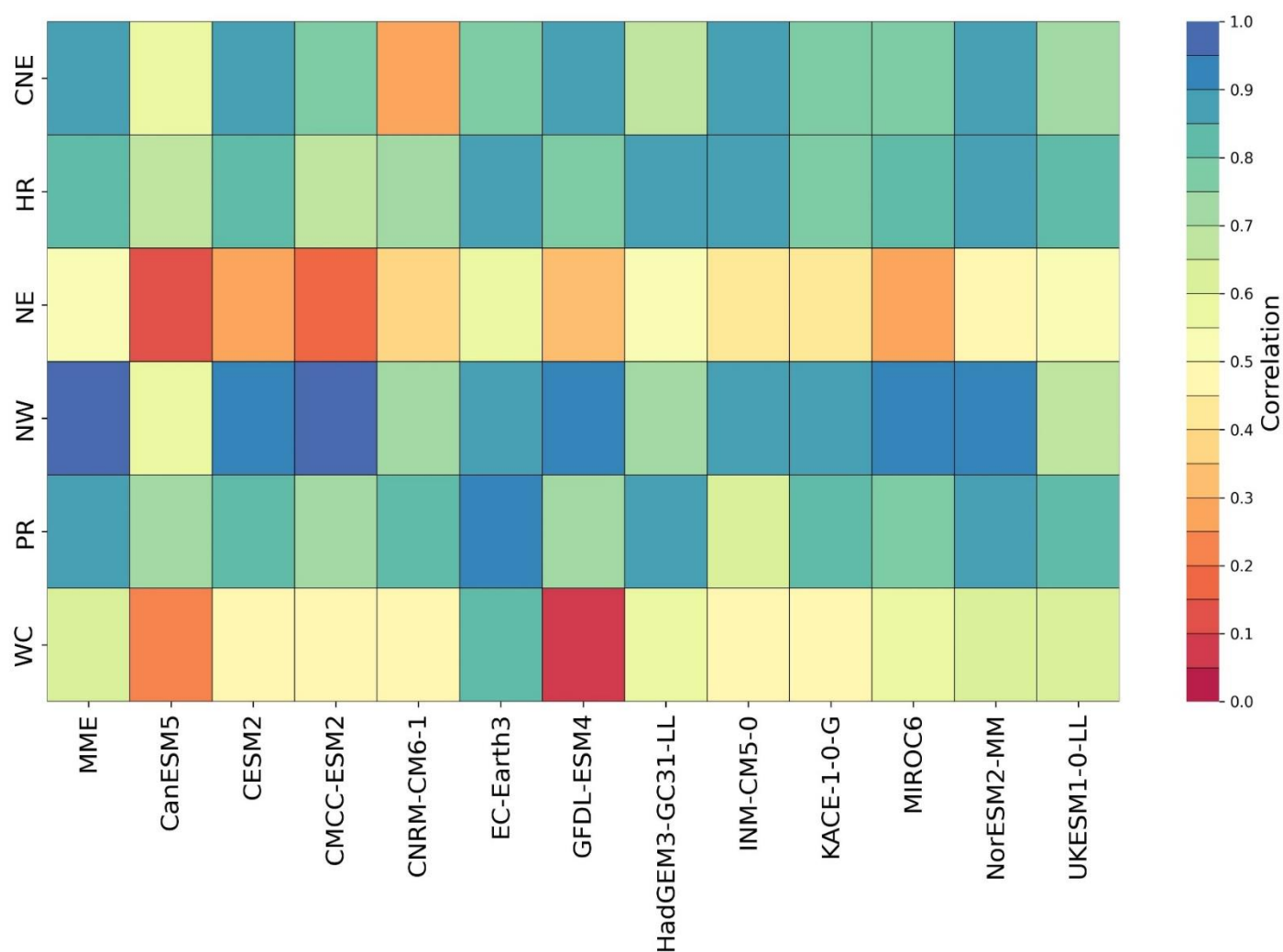


Fig. 3.4 – JJAS precipitation spatial correlation for MME and individual models compared to observed data over each Indian precipitation homogenous region.

We further explore the model's performance in terms of their ability to capture the spatial variability of JJAS precipitation with respect to the observation. Fig. 3.5 illustrates the Taylor diagram comprising of the spatial correlation and normalised standard deviation of the seasonal precipitation. The spatial correlation of seasonal precipitation across the models varies largely with CanESM5 (<0.4) to EC-Earth3 (0.77) and others lying in this broad range. Comparing the standard deviation across models, the model experiments again show a large range of spatial variability compared to the observation. Overall, the NorESM and MIROC6 models outperform other models in terms of capturing the spatial variability of precipitation over the Indian region.

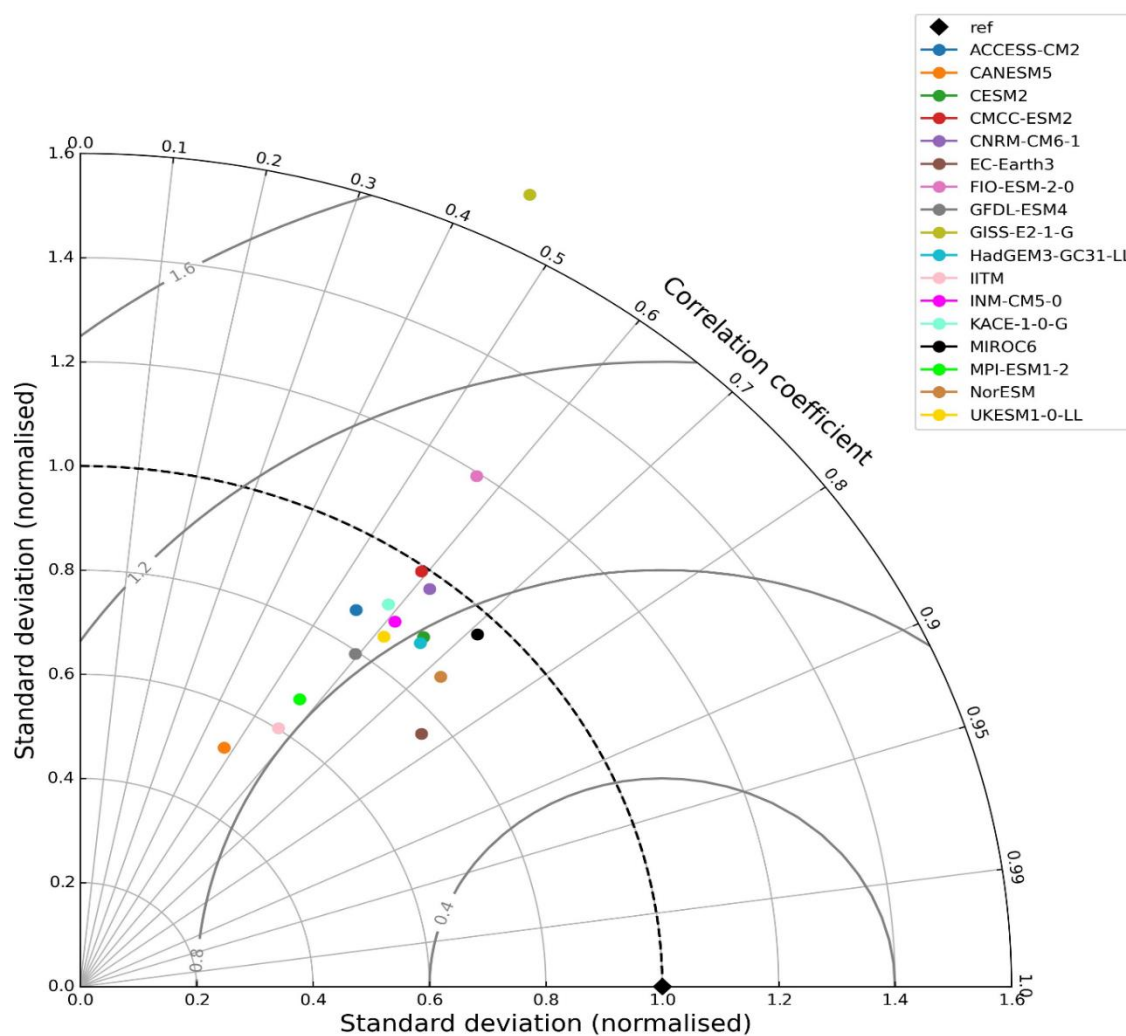


Fig. 3.5 – Taylor diagram for precipitation over India landmass compared to observed data for 17 CMIP6 models.

In terms of simulating dynamic field, we also evaluated spatial distribution of wind at 850 hPa also known as monsoon low level jet. In general, it is one of the semi-permanent features of Indian summer monsoon season. Over South Asia the models generally show a positive bias over most of the region and a negative bias with the south-westerly winds at 850hPa (Fig. 3.6). Some models do not show data over the mountainous regions (Fig. 3.6c, e, g, h, j, k, m) at 850hPa which is why areas such as the Tibetan Plateau are masked. The direction of the South Asian monsoon is captured by the models with varying biases. Over India all models show a positive windspeed bias and in most cases the south-westerly wind shows the most noticeable negative bias, with CanESM5 showing the most extreme negative bias. The MME for specific humidity (Fig. 3.7) shows a mostly negative bias over land and positive bias over the ocean, and the landmass east of India.

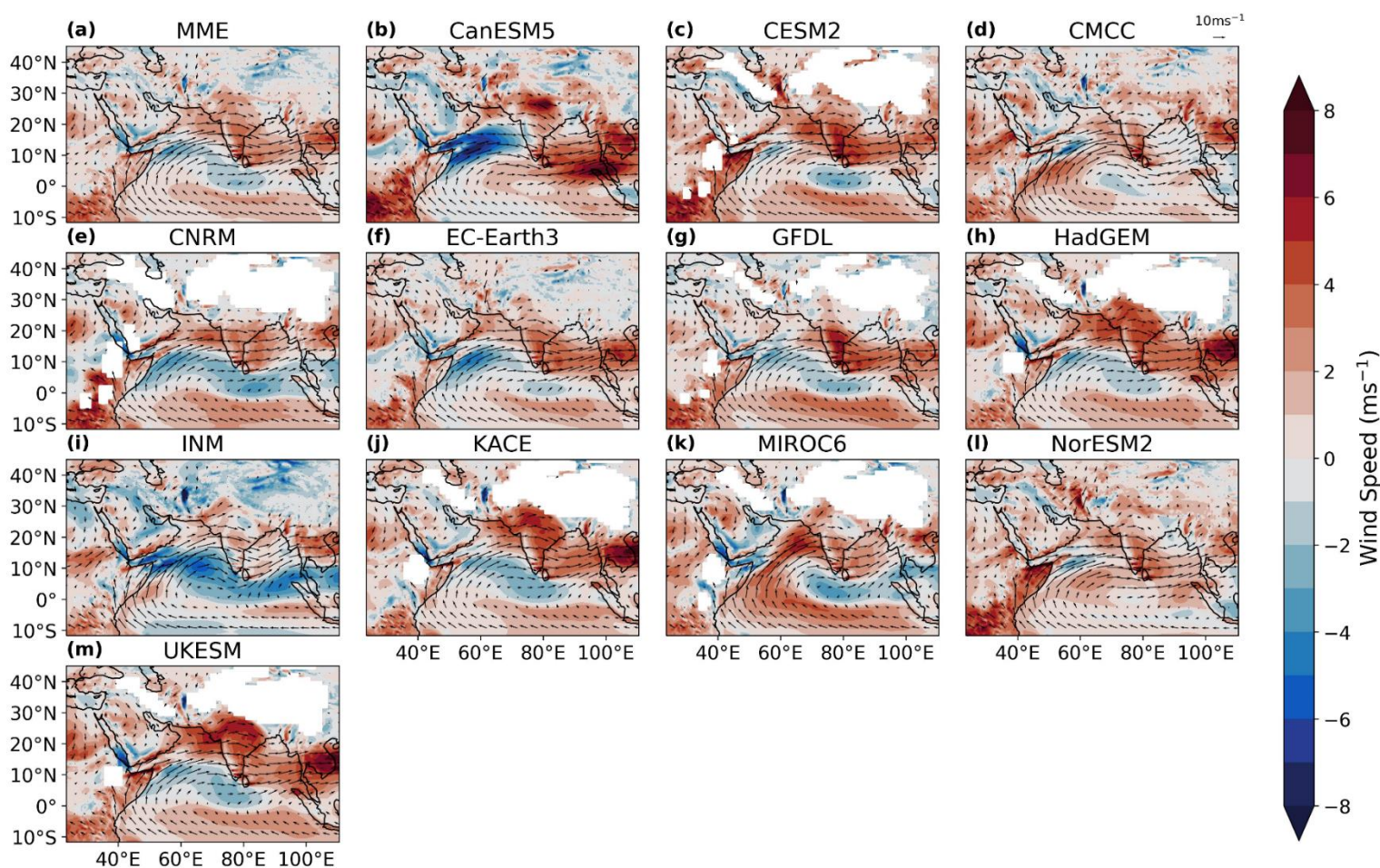


Fig. 3.6 - JJAS windspeed (850hPa) bias over South Asia (1984-2014) for MME (a) and individual models (b-m) compared to observed values from CRU. Arrows show absolute values.

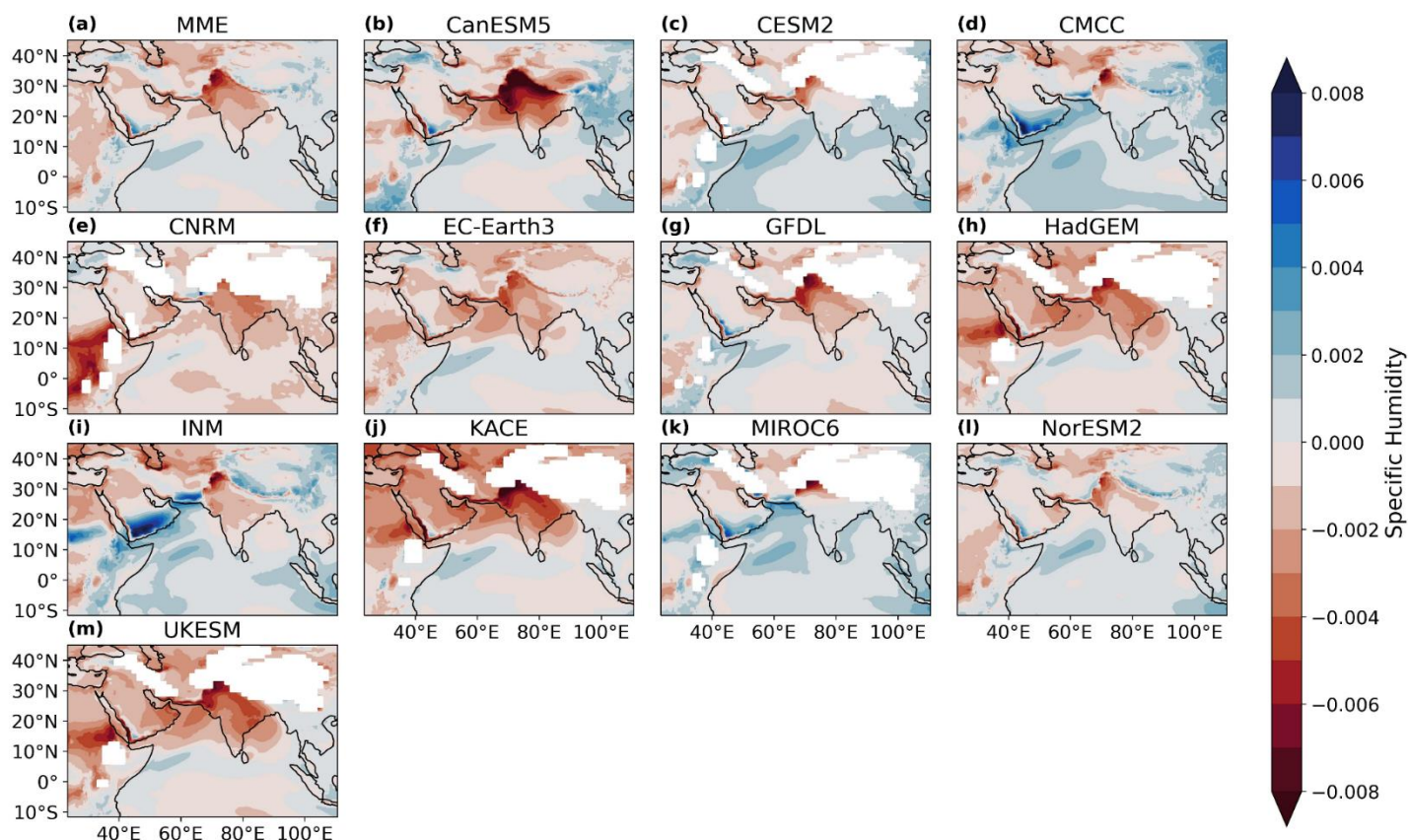


Fig. 3.7 - JJAS specific humidity (850hPa) bias over South Asia (1984-2014) for MME (a) and individual models (b-m) compared to observed values.

Since the moisture transport mechanism from the adjoining seas towards Indian landmass during the Indian summer monsoon season is important, we also checked the vertically integrated moisture transport (VIMT). The models underestimate the larger values of the VIMT which suggests an underestimation of monsoon rainfall over this region during the monsoon season (Fig. 3.8). All models show a negative bias over most of India and a positive bias over the Himalayas. The negative bias over the ocean matches that of the negative bias from the windspeed, although over land VIMT and windspeed biases don't match. The models with a larger negative bias for specific humidity also appear to have a larger negative VIMT bias over India. The negative bias in the VIMT could be the reason for having precipitation dry bias over central part of India. CanESM5 (Fig. 3.8b) shows the largest positive and negative biases compared to all other models for VIMT. The most extreme negative bias

is to the southwest of India and this is the case for most of the models. MIROC6 (Fig. 3.8k) is the only model that shows a positive bias over this area. CMCC (Fig. 3.8d) is the best performing individual model, however there is a relatively large positive bias over northeast India and the surrounding countries comparatively. The MME appears to reduce the magnitude of both positive and negative biases over this region and gives the best VIMT representation overall.

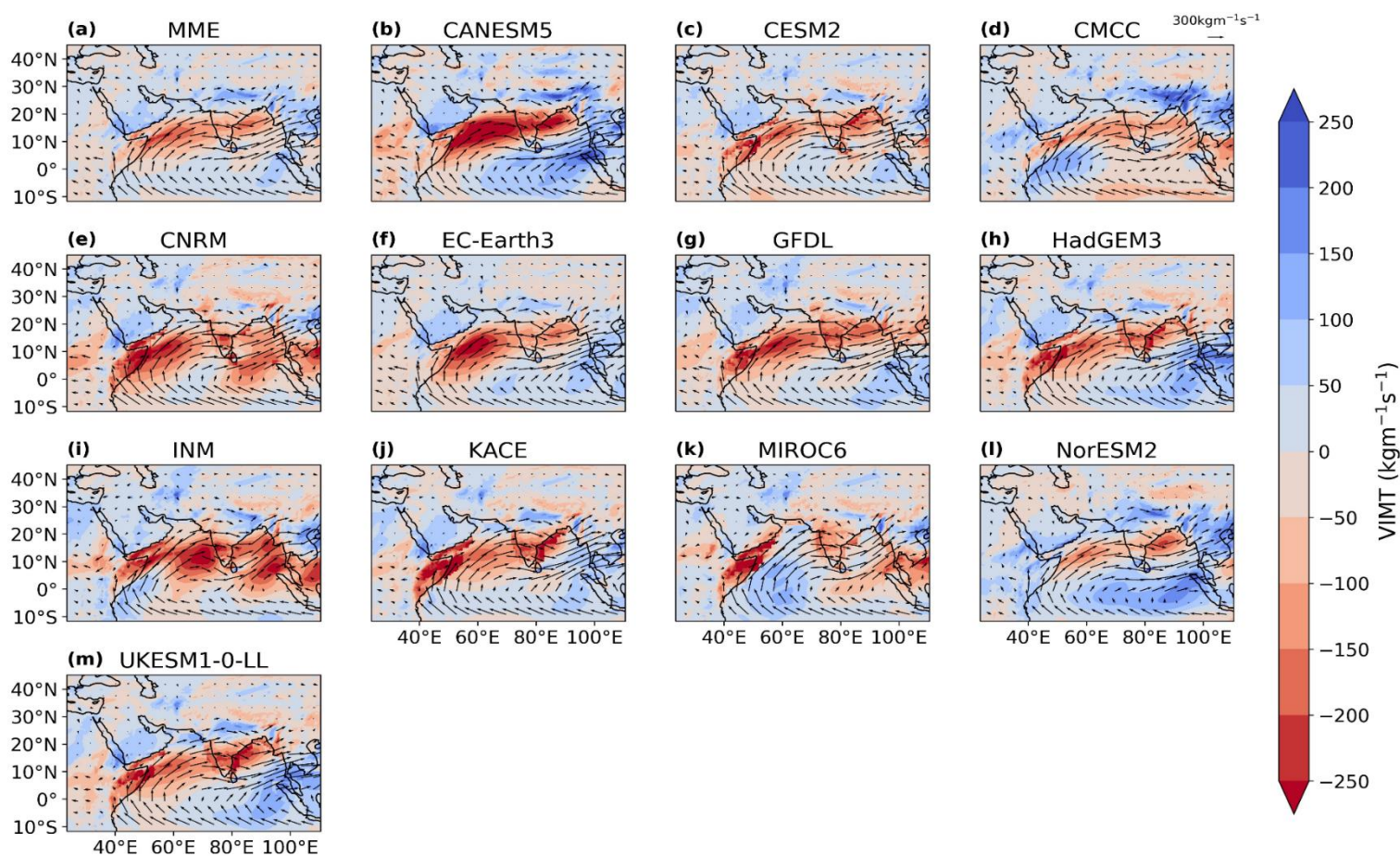


Fig. 3.8 – Vertically integrated moisture transport bias compared to ERA5 for MME (a) and individual models (b-m) over South Asia. The arrows show the absolute values, both bias and absolute values are shown from 1000-100hPa.

3.3.2 Future Changes of ISM Characteristics over South Asia

The spatial changes in the near and far future precipitation during the Indian summer monsoon are shown in Figure 3.9. All SSPs show an increase in precipitation in the NF and FF and FF SSP5-8.5 shows the largest increase overall in the South Asian region (Fig. 3.9). All

figures show a very similar coverage in precipitation changes across most of South Asia where most of the precipitation in the region will increase. When comparing the NF SSPs to the present period, there is not much difference between them. SSP5-8.5 (Fig. 3.9i, j, k, l) has slightly higher extremes than the other two scenarios. Moving to the FF and the changes are much more dramatic. FF SSP5-8.5 (Fig. 3.9l) shows the largest increase, with the West Coast of India, Bangladesh, Nepal, Bhutan and Myanmar receiving over 3mm/day more precipitation in the monsoon season. The west coast of India sees most of the South Asian monsoon precipitation, and this increase suggests that the South Asian monsoon will be more extreme in the far future, with the most extreme scenario being FF SSP5-8.5. This increase in Indian summer monsoon rainfall was also shown by Katzenberger et al. (2021), where all CMIP6 models used in their study as well as the MME showed significant increases in precipitation

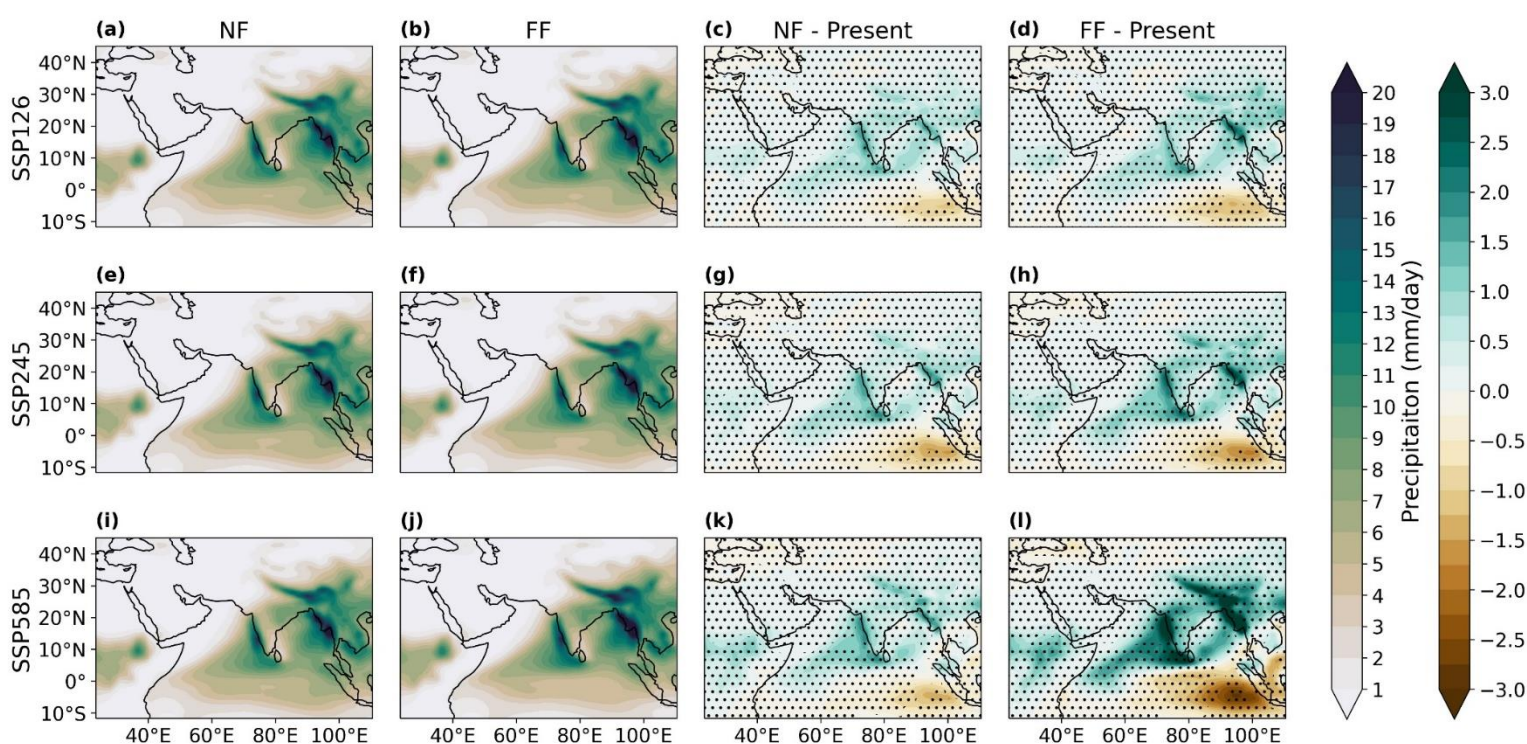


Fig. 3.9 – Mean precipitation difference over South Asia for SSP1-2.6 (a, b, c, d), SSP2-4.5 (e, f, g, h) and SSP5-8.5 (i, j, k, l). The first and second columns show the absolute values for NF (a, e, i) and FF (b, f, j) respectively. The third and fourth columns show the precipitation difference for NF (c, g, k) and FF (d, h, l) respectively when compared to the historical period. The dots represent the grid points with significant differences at 95% significance level.

during FF SSP5-8.5. They also linked this increase in precipitation to an increase in global mean temperature.

The changes in the VIMT in near and far future under various SSP scenarios are shown in Figure 3.10. The FF SSP5-8.5 shows the largest increase in VIMT compared to other SSP scenarios. During the NF (Fig. 3.10 a, c, e) there is little difference between the SSPs. However, in the FF (3.10b, d, f) all SSPs show at least a minor increase in VIMT. The large increase from FF SSP5-8.5 could explain why there is a large increase in precipitation seen in figure 3.9l.

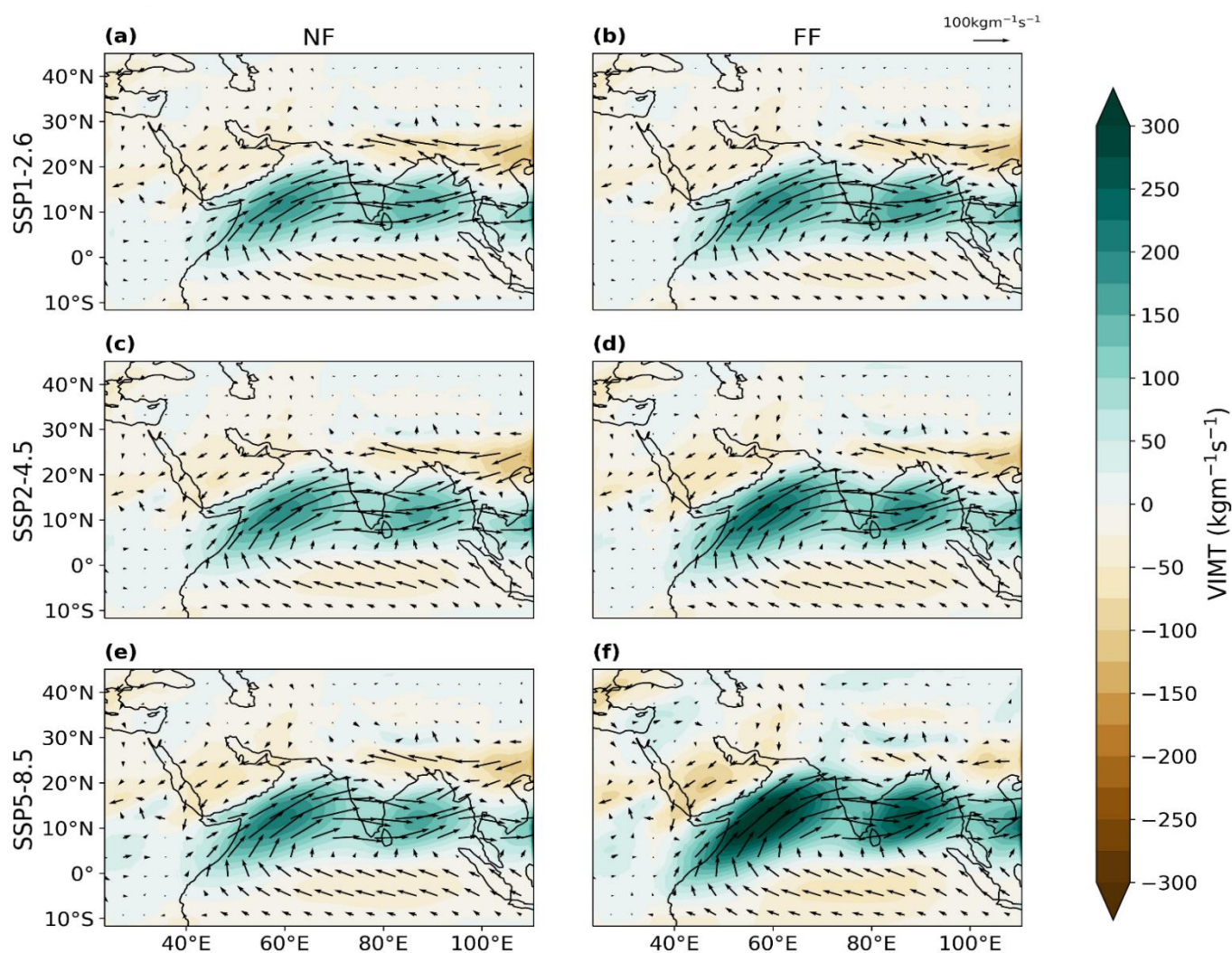


Fig. 3.10 – Vertically integrated moisture transport difference compared to the historical period from 1000-1hPa over South Asia. SSP scenarios SSP1-2.6 (12a, b), SSP2-4.5 (12c, d) and SSP5-8.5 (e, f) are used. The SSPs are split into NF (a, c, e) and FF (b, d, f).

An increase in precipitation can be seen over all India precipitation homogenous regions when comparing the present climate to the SSP scenarios using a gamma distribution (Fig. 3.11) which represents precipitation data well (Wilks, 2011). The MME for the historical period underpredicts precipitation for all regions (Fig. 3.11a, c, d, f) as well as the entirety of India (Fig. 3.11g) except for the PR region (Fig. 3.11e) which is the best represented and the HR region (Fig. 3.11b) where the MME overpredicts precipitation. The SSPs over all regions show an increase in precipitation when compared to the historical period and except for FF SSP5-8.5 there is little difference between the NF and FF SSPs. FF SSP5-8.5 shows the largest shift in precipitation for all regions, the largest shift can be seen over the NE region. For the

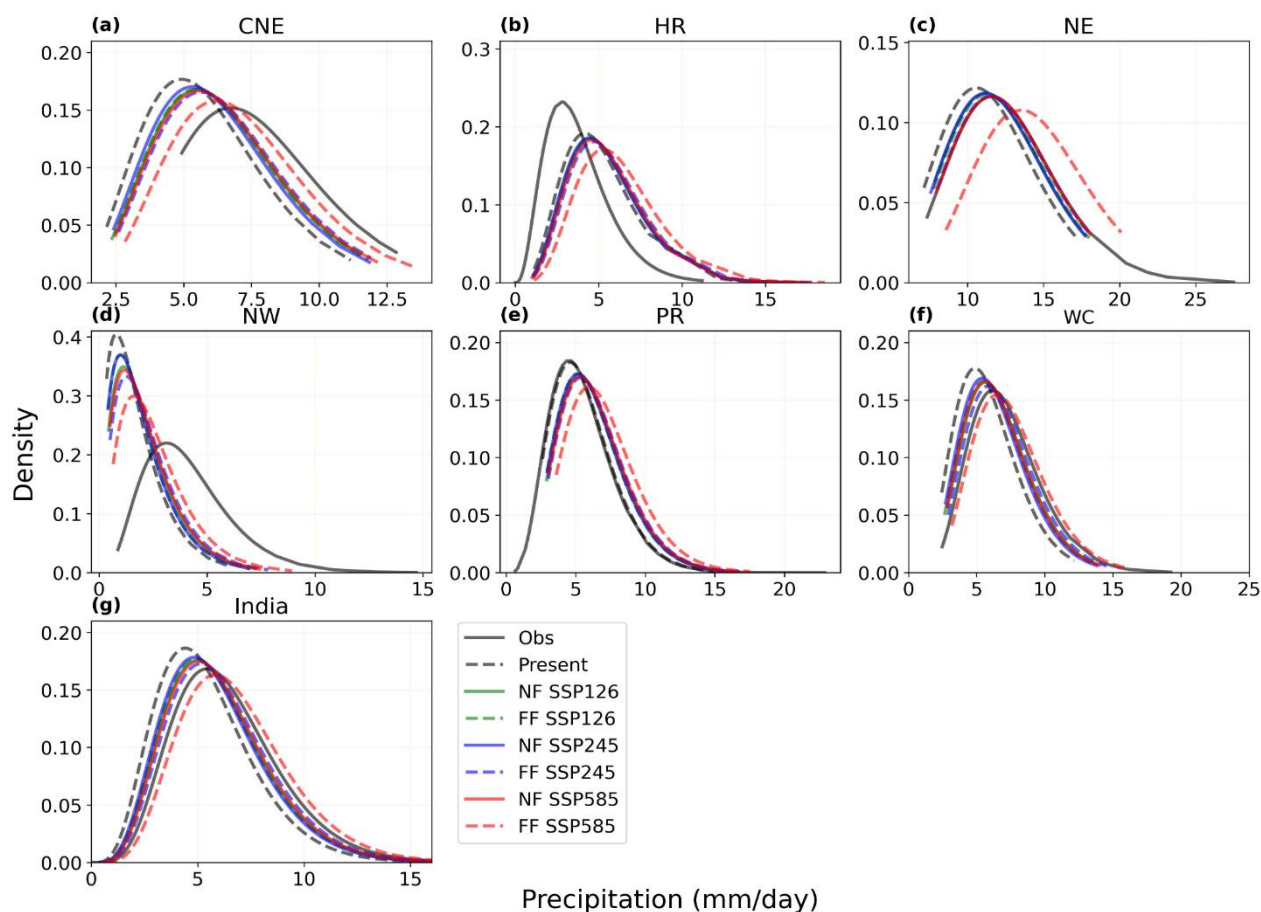


Fig. 3.11 – PDF distribution of precipitation over Indian precipitation homogenous regions (a-f) and India landmass (g). The black lines represent the historical period (1984-2014). The solid and dashed black lines show observed and MME data respectively. For the SSP scenarios green, blue, and red represent SSP126, SSP245 and SSP585 respectively. For the SSPs a solid line shows the NF time period, and a dashed line shows the FF time period.

regions CNE, HR, NE, NW, PR, WC and India, FF SSP585 compared to the historical period shows an increase in precipitation of 1.28, 1.12, 2.9, 0.84, 1.36, 1.63 and 1.4mm/day respectively. FF SSP126 shows an increase of 0.53, 0.03, 0.71, 0.23, 0.56, 0.66 and 0.49mm/day respectively.

There is an increase in precipitation over all the precipitation homogenous regions of India when comparing NF SSP2-4.5 and SSP5-8.5 to FF SSP2-4.5 and SSP5-8.5 respectively (Table 3.3). All percentage increases are compared to the historical period. SSP1-2.6 doesn't

Table 3.3 - Precipitation increase (%) per region compared to historical period (1984-2014)

	CNE	HR	NE	NW	PR	WC
NF SSP126	9.40	6.53	5.52	18.2	11.6	12.9
NF SSP245	6.58	5.59	5.33	10.8	10.1	8.94
NF SSP585	10.6	8.39	8.84	20.9	12.4	12.4
FF SSP126	9.00	6.94	6.35	10.4	9.77	11.0
FF SSP245	11.9	10.3	8.59	25.8	13.6	16.9
FF SSP585	21.4	21.9	25.5	44.6	23.8	27.5

follow this pattern as over the CNE, NW, PR and WC there is a decrease in percent precipitation when comparing NF to FF. The NW will see the largest increase in precipitation going from 10.8% and 20.9% for NF SSP2-4.5 and SSP5-8.5 respectively to 25.8% and 44.6% for FF SSP2-4.5 and SSP5-8.5 respectively. This means that under SSP5-8.5, the NW will see a 23.7% increase when going from NF to FF as well as the largest increase of 44.6% when compared to the historical period. Comparing NF and FF SSP5-8.5 there is an increase of 10.8%, 13.51%, 16.66%, 23.7%, 11.4% and 15.1% for the CNE, HR, NE, NW, PR and WC respectively.

3.3.2.1 Future Changes in JJAS Extreme Precipitation

All SSP scenarios show an increase in extreme wet days (EWD) when compared to the historical period (Fig. 3.12). During the NF, SSP2-4.5 (Fig. 3.12c) shows the smallest increase in EWD's, where most of the NW, WC, and the lower half of the CNE regions show no increase at all. NF SSP5-8.5 (Fig. 3.12e) has the largest increase in EWD compared to the other SSPs, but not by much. The area that sees the largest increase is the southern part of the PR. When

comparing NF and FF SSP1-2.6, there is little difference. The NW region sees a slight decrease in EWD. FF SSP2-4.5 shows an increase over all regions except the northern part of the HR. Now all regions show a minimum 4% increase. Under this scenario, the most affected region is the southern PR with a 14% increase. FF SSP5-8.5 shows the largest increase in EWD. All regions will see an increase in EWD with the most affected regions being the west coast of the

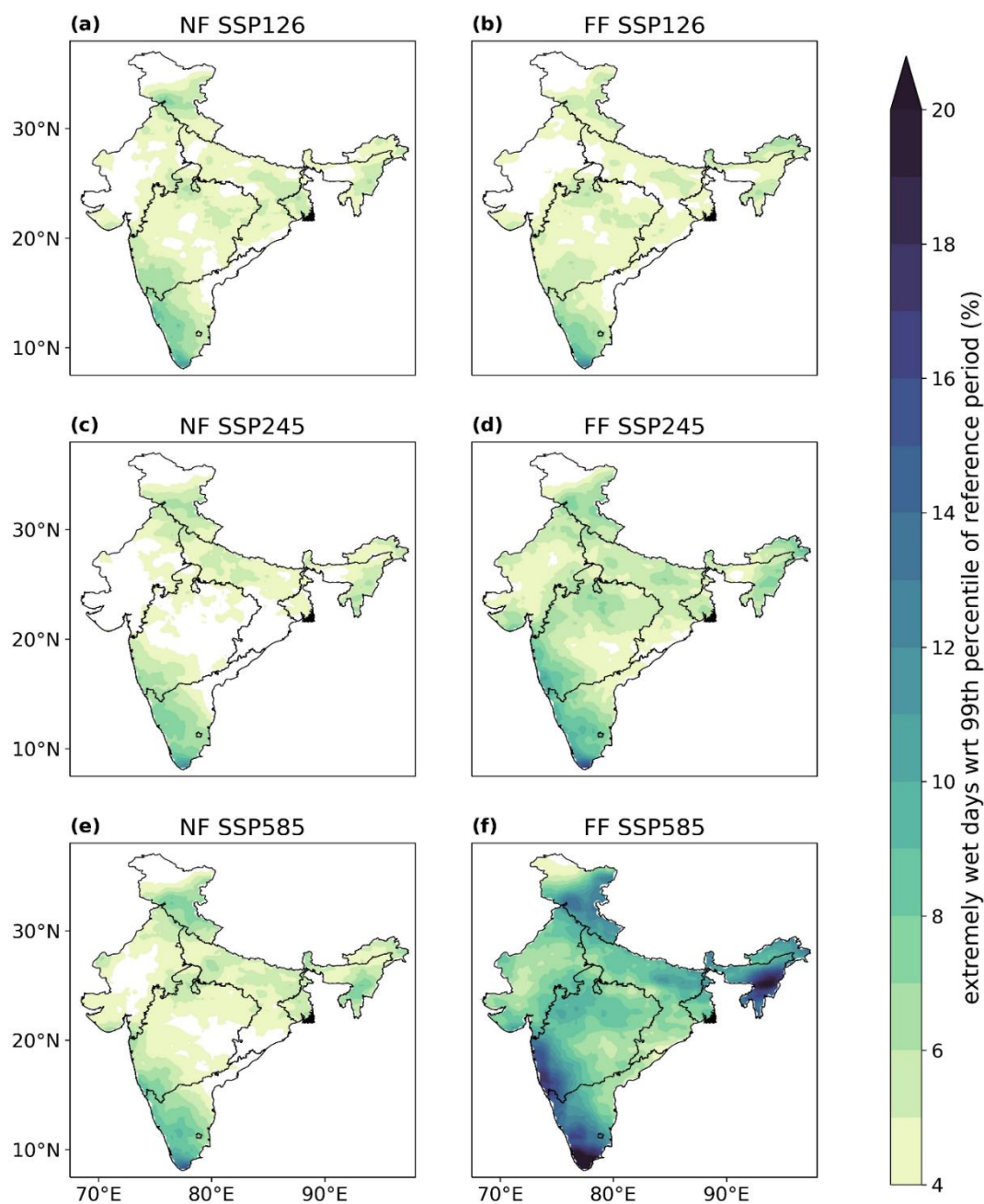


Fig. 3.12 – Extremely wet days with reference to the 99th percentile of reference period (1984-2014). The first column (a, c, e) shows the NF and the second column (b, d, f) shows the FF for SSP126 (a, b), SSP245 (c, d) and SSP585 (e, f).

WC, the west and south coast of the PR and the east of the NE. These regions are showing a >20% increase in EWD. Table 3.4 shows the percentage increase in EWD per region when compared to the historical period. There is very little change between NF and FF SSP1-2.6 for all regions and there is an increase in EWD when comparing NF SSP2-4.5 and SSP5-8.5 to FF SSP2-4.5 and SSP5-8.5 respectively. The largest increase for all regions is from FF SSP5-8.5. When comparing the increase from NF to FF for this scenario, we see a 3.2%, 4.27%, 6.57%, 3.02%, 4.85% and 4.13% for the CNE, HR, NE, NW, PR and WC respectively. This means that the NE will receive the largest increase in EWD from both historical and NF to the FF. When going from the historical to the NF, the PR sees the largest increase in EWD of 6.75%.

Table 3.4 - Extreme wet days difference (%) per region compared to historical period (1984-2014)

	CNE	HR	NE	NW	PR	WC
NF SSP126	4.47	4.48	4.67	4.16	5.80	4.72
NF SSP245	4.23	4.52	4.65	3.86	5.89	4.19
NF SSP585	4.71	5.13	5.63	4.50	6.75	4.68
FF SSP126	4.35	4.47	4.63	3.87	5.68	4.68
FF SSP245	5.21	5.29	5.62	5.14	7.13	5.77
FF SSP585	7.91	9.40	12.2	7.52	11.6	8.81

Similarly, to the previous figure, a much larger increase in precipitation percent due to R95p days can be seen from FF SSP5-8.5 (Fig. 3.13). All NF SSPs show a similar precipitation percent to each other (3.13a, c, e). There is negligible change between NF and FF SSP1-2.6 (3.13a and b respectively). FF SSP2-4.5 shows an approx. 5% increase which seem to affect the same areas. FF SSP5-8.5 shows a dramatic increase in precipitation percent with the most affected regions increasing by over 40%. The most affected regions are the same as figure 3.12 which are also the regions in India that receive the most rainfall per monsoon season.

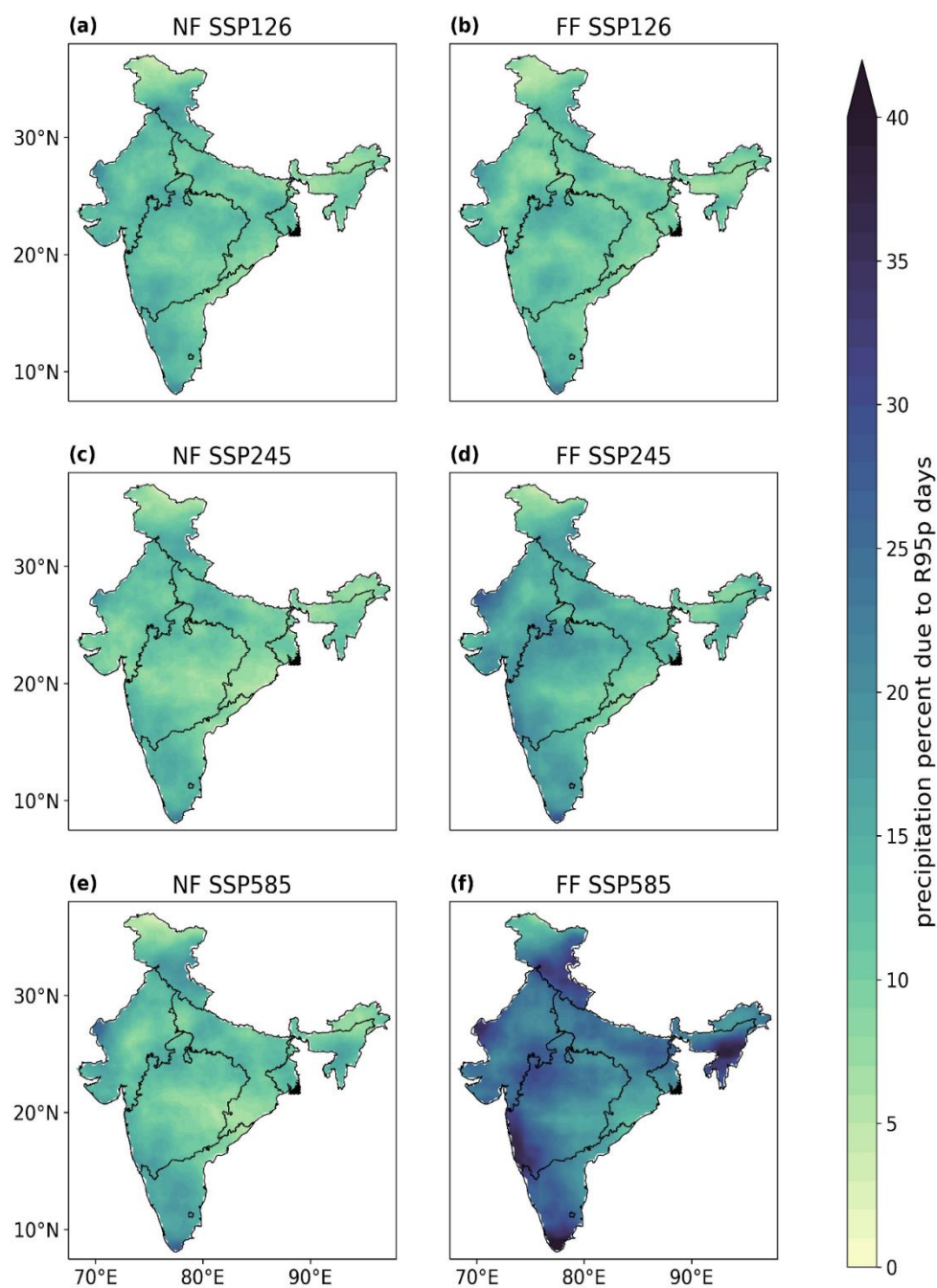


Fig. 3.13 – Precipitation percent due to R95p days. The first column (a, c, e) shows the NF and the second column (b, d, f) shows the FF for SSP126 (a, b), SSP245 (c, d) and SSP585 (e, f).

Although extreme precipitation has been shown to increase, the consecutive wet days (CWD) do not follow this trend for most regions (Fig. 3.14). When looking at the NF SSP2-4.5 and SSP5-8.5 show an increase in CWD over the CNE region whereas under SSP1-2.6 this

region shows a slight decrease. Most regions show no change or a decrease in CWD, however the NW region shows the largest increase for all SSPs. This could be possible due to larger transport in moisture towards the region as discussed in Fig. 3.10 NF SSP5-8.5 has more extreme increases and decreases in CWD compared to the other NF SSPs. There is little change between NF and FF SSP1-2.6. FF SSP2-4.5 shows a similar pattern compared to its NF

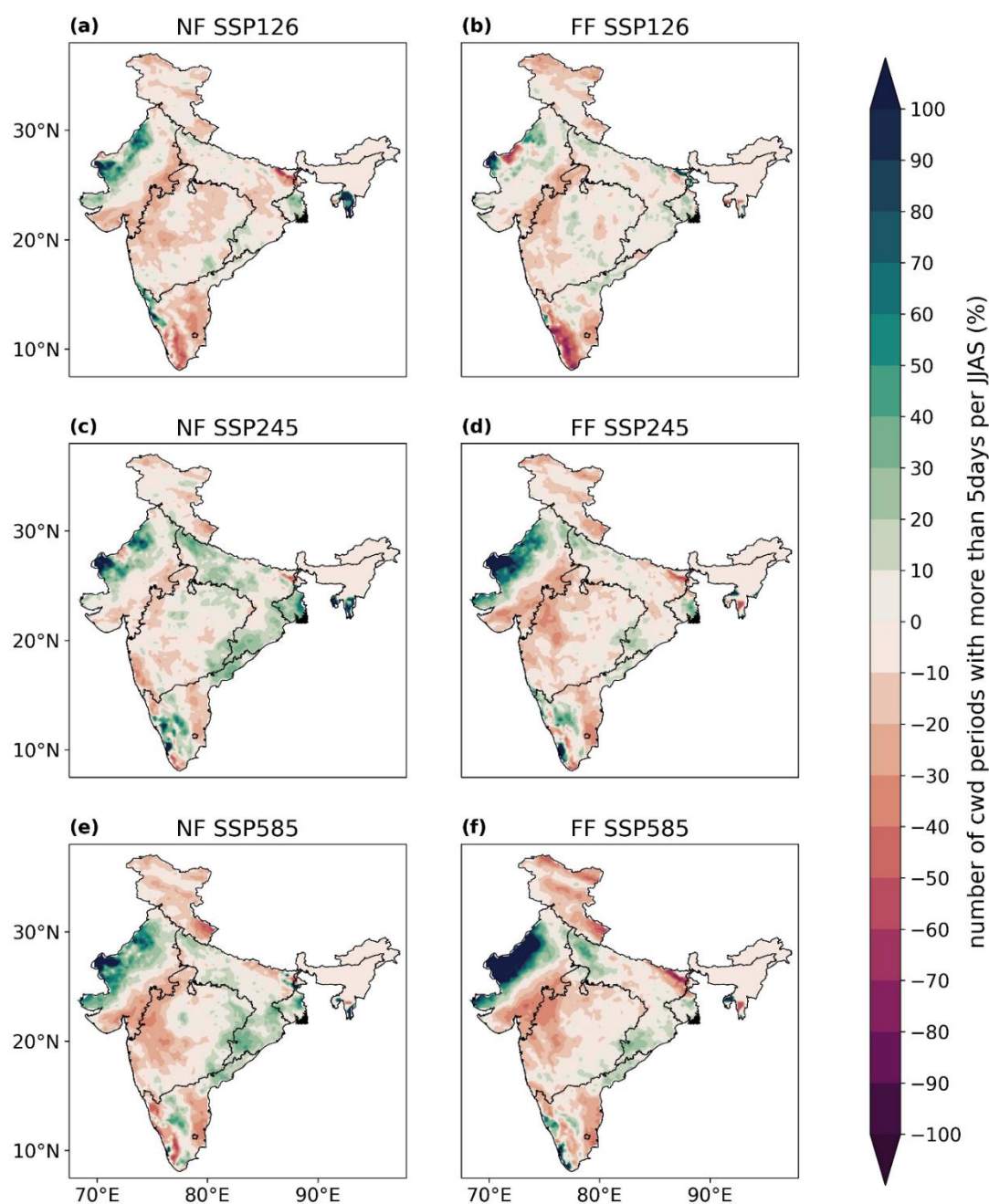


Fig. 3.14 – Percentage difference compared to the historical period for the number of cwd periods with more than 5 days per JJAS season. The first column (a, c, e) shows the NF and the second column (b, d, f) shows the FF for SSP126 (a, b), SSP245 (c, d) and SSP585 (e, f).

counterpart, but with more extreme values. The CNE however changes from a majority increase in CWD in the NF to a slight decrease by the FF. The difference between NF and FF SSP5-8.5 shows similar patterns to SSP2-4.5. FF SSP5-8.5 shows the most extreme increases and decreases in CWD. The most affected region appears to be the NW for an increase in CWD. The southeast of NW, east of PR and HR show the largest decrease in CWD.

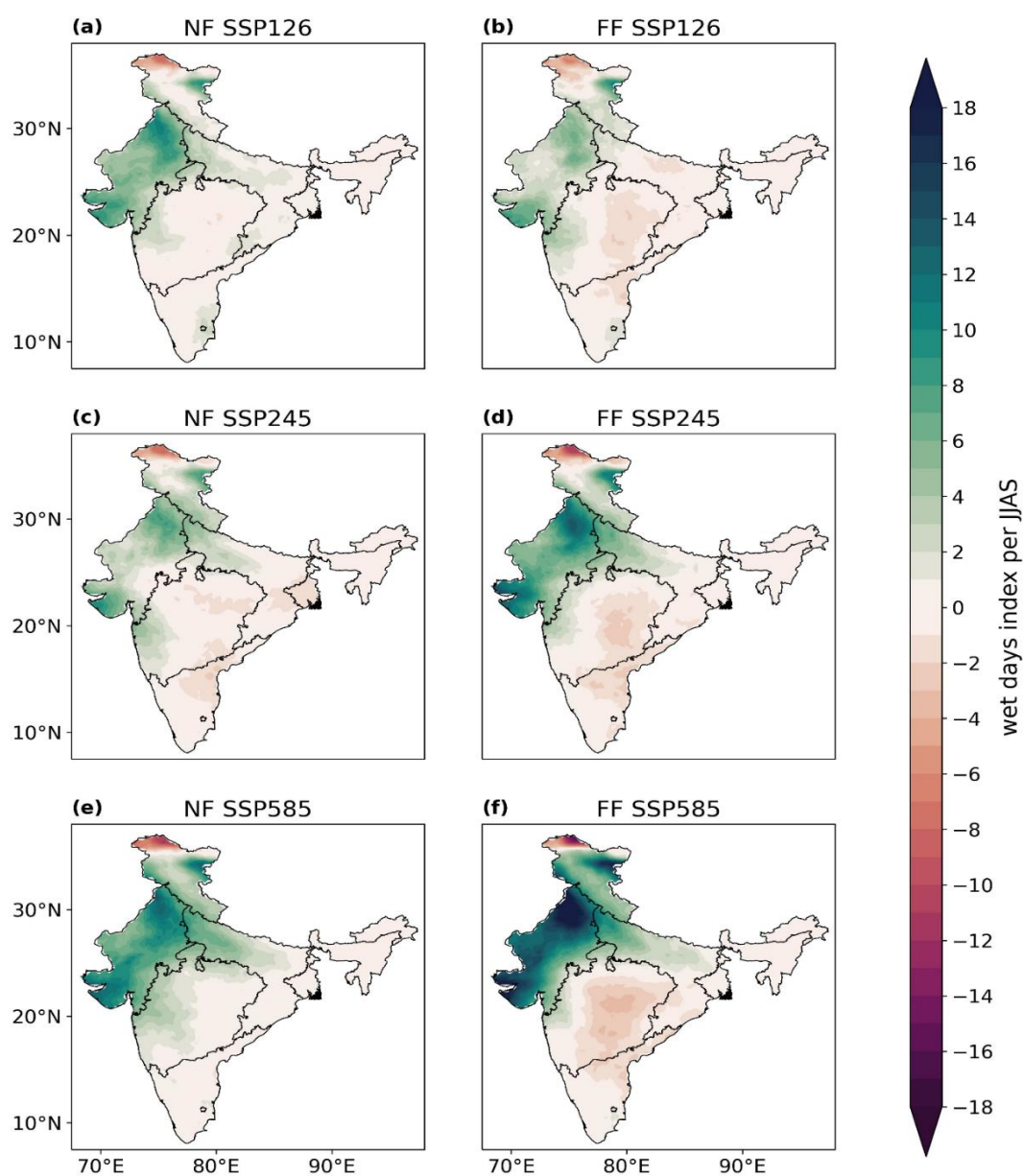
Small changes in emissions appear to have a very large effect on consecutive dry days (CDD) and consecutive wet days (CWD) which can be seen in tables 3.5 and 3.6 respectively. The CDD decrease when comparing the NF to FF SSP5-8.5 for the CNE, HR, NE and NW and increase for the PR and WC. For CWD the CNE, HR, NE, PR and WC decrease and the NW increases. There is a big difference in CDD over the NE and PR for the different SSPs. For CDD in the PR, from NF SSP1-2.6 to SSP2-4.5 we go from a 5.99% decrease to a 35.7% increase. This is also seen over the NE where we see a 55.7% decrease and then a 57.6% increase for SSP1-2/6 and SSP2-4.5 respectively. This is also seen with CWD for these regions. The NE goes from a 9.97% increase to a 26.4% increase and the PR goes from a 15% decrease to a 2.69% decrease for NF SSP1-2.6 and SSP2-4.5 respectively. This suggests that these regions are highly sensitive to changes in emissions.

Table 3.5 - Consecutive dry days difference (%) per region compared to historical period (1984-2014)

	CNE	HR	NE	NW	PR	WC
NF SSP126	-1.24	-0.814	-55.7	-8.84	-5.99	7.03
NF SSP245	-2.20	-3.38	57.6	-6.41	35.7	4.56
NF SSP585	-15.9	-9.32	-3.32	-14.6	-20.0	-5.96
FF SSP126	8.75	3.81	-47.2	-6.63	4.55	8.24
FF SSP245	-4.51	6.55	-9.96	-14.3	55.0	12.1
FF SSP585	-18.6	-17.0	-41.0	-19.8	31.2	13.9

Table 3.6 - Consecutive wet days difference (%) per region compared to historical period (1984-2014)

	CNE	HR	NE	NW	PR	WC
NF SSP126	-2.97	-8.45	9.97	-3.31	-15.0	-8.73
NF SSP245	11.5	-5.11	26.4	1.16	-2.69	-2.29
NF SSP585	7.03	-13.2	12.6	4.17	-8.56	-7.11
FF SSP126	0.876	-9.80	6.71	-1.46	-9.34	-6.04
FF SSP245	0.750	-10.2	6.05	1.23	-8.93	-10.4
FF SSP585	4.32	-18.4	1.65	6.45	-12.6	-10.3

**Fig. 3.15** – Wet days Index per JJAS season over India. The first column (a, c, e) shows the NF and the second column (b, d, f) shows the FF for SSP126 (a, b), SSP245 (c, d) and SSP585 (e, f).

The NW region sees a much larger increase in wet days index (WDI) compared to the other regions (Fig. 3.15). There is little change in most regions in the NF except the NW, HR and west of the CNE regions. For NF SSP5-8.5 the PR sees more of an increase in WDI compared to the other two SSPs. When comparing NF and FF SSP1-2.6 there is little change and FF SSP1-2.6 shows a slight reduction in WDI overall, with the PR decrease being the most noticeable. For FF SSP2-4.5 and SSP5-8.5 the NW and HR see an increase in WDI and SSP5-8.5 shows a much larger increase in comparison. All FF SSPs show the WDI in the PR decrease and the largest decrease is from FF SSP5-8.5.

3.4 Conclusion

In this chapter we compared the performance of 12 CMIP6 models in simulating precipitation over South Asia and the precipitation homogenous regions of India. Using the new SSPs implemented in CMIP6, SSP1, 2 and 5 were used to look at future changes in precipitation. The key findings of this study are listed below:

- CMIP6 models struggle to capture precipitation over India accurately, with large variations between models. However other studies have shown that CMIP6 models improve precipitation simulations when compared to CMIP5 (Choudary 2021, Gusain et al. 2020).
- The MME of the models improves the skill when compared to individual models, improving model results as well as reducing the overall biases compared to individual models. There is still a slight dry bias over India and a wet bias to the east of India.
- All SSPs show an increase in precipitation in the future over India with the largest increase from FF SSP5-8.5 of 1.4mm/day, suggesting that fossil-fuelled development will increase precipitation in the coming century over India. There is a smaller increase in precipitation of 0.49 and 0.74mm/day under FF SSP1-2.6 and FF SSP2-4.5. The NE region will receive

the largest increase in precipitation (2.9mm/day) compared to other precipitation homogenous regions.

- Extreme precipitation has also been shown to increase most dramatically under SSP5-8.5 as well as the VIMT. The most affected regions of India are the PR, WC and NE. The number of wet days will increase over the NW region. This suggests that continued fossil-fuelled development will lead to a more extreme South Asian monsoon approaching the end of the century.
- SSP1.2.6 and SSP2-4.5 increases in precipitation are much less dramatic than SSP5-8.5 meaning that it is possible to lessen the impact given sufficient mitigation strategies are put in place.

Our work only uses CMIP6 models at a coarse resolution which leads to difficulties in simulating the Indian summer monsoon. Applying downscaling and bias correction have been shown to improve precipitation simulations (Konda et al. 2023) and we will be implementing them in our future work.

Customization of RCM Through Sensitivity Experiments

This chapter is partially based on the paper:

- Marc Norgate, P.R. Tiwari, S. Das (2024). Sensitivity experiment with orography, convective and land surface schemes in the regional climate model driven by HadGEM3, *International Journal of Climatology*, Royal Meteorological Society, (To be submitted)

Abstract

This chapter explores the sensitivity of the ICTP Regional Climate Model (RegCM4) to various configurations designed to enhance the simulation of meteorological features in the Indian region. To accomplish this, three sets of sensitivity experiments were conducted over nine distinct years, categorized into wet, normal, and dry conditions. These experiments employed a fine horizontal resolution of 25 km, ensuring detailed and precise modelling. The first set of experiments focused on evaluating the impact of nine different representations of Himalayan orography. This approach was implemented to understand how variations in the orographic features of the Himalayas affect the model's accuracy in simulating precipitation and temperature patterns. The results revealed a direct correlation between orographic height and seasonal mean precipitation, highlighting the critical role of accurate orographic representation in climate modelling. Specifically, a 10% increase in height (P10) led to a 15% rise in precipitation, while a 10% decrease (M10) resulted in a 32% reduction compared to control simulations. The second experiment evaluated four cumulus parameterization schemes—Kuo-AS (SC1), Grell-AS (SC2), Grell-FC (SC3), and Grell-Emanuel (SC4), when simulating precipitation and temperature patterns. Findings indicated that the SC4 outperformed the others, effectively capturing precipitation intensity and distribution in closer alignment with IMD observations. The third experiment compared two land surface parameterization schemes, BATS and CLM, for simulating precipitation and temperature during the JJAS period. The CLM scheme demonstrated superior performance, primarily due to its enhanced representation of soil moisture and surface fluxes. Overall, RegCM4 effectively simulates seasonal meteorological features and upper-air circulations during varying precipitation years. This study highlights the significance of the CLM scheme for improved accuracy in simulations over the Indian region, suggesting a need for future downscaling

experiments to investigate finer-scale physical processes and understand climate extremes under different emission scenarios.

4.1 Introduction

South Asia is among the most vulnerable regions globally to the impacts of climate change, as highlighted by Norgate et al. (2024). Recent evidence indicates a warming trend coupled with a consistent rise in temperature extremes. The prevalence of extreme weather events—such as intense heat, heavy rainfall, flooding, and droughts—negatively impacts various sectors (IPCC 2022). India has a population of over 1.4 billion and is particularly susceptible to climate extremes. Given the critical nature of these challenges, the need for precise climate predictions is paramount. This emphasises the importance of sensitivity in regional model parameterization, as accurately representing local climatic conditions can enhance predictions of climate extremes. Improved parameterization in regional climate models will facilitate better preparedness and adaptive strategies, thereby supporting climate resilience in India amidst a changing climate.

The most significant instruments for generating predictions on a monthly to decadal scale in advance are coupled general circulation models (GCMs). However, these GCMs generally have a coarse horizontal resolution ranging from approximately 100 to 250 km (Tiwari et al. 2014), which are insufficient for accurately representing detailed physical processes and the unique land surface characteristics of particular regions. As a result, they fail to capture the complexities and nuances that are essential for a precise understanding and simulation of local environmental dynamics. Tiwari et al. (2014) conducted an in-depth analysis of the performance of five advanced General Circulation Models (GCMs) in their ability to simulate the interannual variability of precipitation in the Northern Indian (NI) region. Their study revealed that these models displayed a range of proficiency levels, indicating differing degrees

of accuracy and skill in capturing the complex patterns of precipitation variability over this area. This finding underscores the necessity of investigating small-scale physical processes that significantly influence short-term climate fluctuations over the Indian region through the use of regional climate models (RCMs). RCMs, which operate at comparatively higher resolutions, are capable of representing sub-grid scale physical processes at a regional level more effectively. Consequently, these high-resolution regional models are better suited than GCMs for reproducing finer scale information (Giorgi et al., 2012).

It is widely recognized that general circulation models (GCMs) exhibit significant limitations in their representation of orography due to their coarse resolution. This coarse resolution hampers the ability of these models to capture the complex details of mountainous regions, resulting in considerable inaccuracies. Numerous modelling studies have demonstrated that accurately representing orography is essential for determining the spatial distribution of precipitation across various regions globally (Abe et al., 2003; Namias, 1980). Kasahara and Washington (1968) provided an in-depth analysis of the thermal and dynamical effects of orography within the framework of a general circulation model, underscoring the critical importance of precise orographic representation for reliable climate modelling. Their work highlighted the significant impact that mountains and other topographical features have on atmospheric circulation patterns and precipitation distribution. However, these studies predominantly focused on GCMs, leaving a gap in our understanding of how regional climate models (RCMs) perform at sub-grid scales. It is essential to thoroughly examine the role of the Himalayan orography in RCMs for simulating meteorological fields. Such an examination will help to determine whether RCMs, with their higher resolution, can better represent the complex terrain and its influence on local climate, particularly in the context of the Himalayas. This understanding is vital for improving the accuracy of climate predictions and for developing more effective strategies for managing climate-related risks over the Indian region.

Additionally, the cumulus parameterization scheme is a crucial element in numerical models, significantly influencing the representation of sub-grid scale convective processes. The impact of cumulus parameterizations on the precipitation process depends on the specific convective schemes chosen and the domain of interest (Giorgi et al., 2012). Despite its importance, there has been limited research on the sensitivity of different cumulus parameterization schemes using regional climate models (RCMs) to simulate various meteorological fields over the Indian region. Therefore, this study has been undertaken to conduct a comprehensive analysis of this aspect.

Pielke et al. (1990) highlighted the pivotal role that land surface characteristics play in shaping regional and local climates. These characteristics are instrumental in governing the exchanges of heat, momentum, and water between the land and the atmosphere. Such regulation significantly alters the structure of moving synoptic systems, initiates convective activity, and organizes mesoscale circulations. The influence of the land surface extends to a myriad of atmospheric processes. For example, the heat exchange between the land and the atmosphere can modify temperature and humidity profiles, thereby affecting weather patterns and climate. This dynamic interaction underscores the importance of accurately representing land surface characteristics in climate models to enhance our understanding and prediction of climate and weather phenomena. Momentum exchange impacts wind patterns and the movement of air masses. Water exchange, through processes like evaporation and transpiration, can influence precipitation patterns and cloud formation. Given the pivotal role of land surface interactions, advanced land surface parameterization schemes (LSPS) within climate models can potentially enhance prediction accuracy, especially in the Indian region which has complex terrain due to the presence of Himalayas. These advanced schemes aim to more accurately represent the physical processes at the land-atmosphere interface, improving the model's ability to simulate local climate dynamics. Consequently, incorporating sophisticated LSPS into

regional climate models (RCMs) may significantly enhance their skill in predicting climate variations and weather patterns over mountainous areas. Therefore, in this study we have looked into detail about the sensitivity of land surface schemes to study its role on meteorological fields over the Indian region.

Overall, in this chapter, the main objective is to investigate how different representations of orography, convection, and land surface schemes influence the outcomes of the Regional Climate Model version 4.7 (RegCM4), with a specific focus on the Indian region. The sensitivity experiments are conducted across nine distinct years, categorized into wet, normal, and dry conditions, and are performed at a spatial resolution of 25 km. Regarding orography, we explore nine different configurations by adjusting the model's representation of terrain elevation, aiming to understand how these variations impact model performance. The Regional Climate Model is driven by the Hadley Centre Global Environment Model (HadGEM3) from the UK Met Office to simulate meteorological fields over India. Section 4.2 provides a concise overview of the models utilized in this study, while section 4.3 details the datasets used, and the experimental setups employed. The findings and discussions are presented in section 4.4, where we analysed the results derived from the experiments. Finally, section 4.5 offers conclusions drawn from this comprehensive study.

4.2 Methodology

4.2.1 Hadley Centre Global Environment Model Version 3 (HadGEM3)

The global climate model utilized in this study is the UK Met Office's Hadley Centre Global Environment Model (HadGEM3). This model features a coupled atmosphere-ocean configuration, extending vertically to incorporate a well-resolved stratosphere. Moreover, the Earth-System configuration of HadGEM3 encompasses dynamic vegetation, ocean biology, and atmospheric chemistry. The atmospheric component boasts a horizontal resolution of 1.4°

and includes 38 vertical levels. The ocean model's resolution is 1° by 1° , which increases to $1/3^\circ$ at the equator, and it comprises 40 depth levels. Further details of the model can be found at William et al. (2017) and Kuhlbrodt et al. (2018).

4.2.2 Regional Climate Model

The Regional Climate Model version 4.7 (RegCM4) has been developed at The Abdus Salam International Centre for Theoretical Physics in Italy. It is built around a hydrostatic dynamical core that is similar to the Mesoscale Model MM5 (Grell et al., 1993). RegCM4 consists of 24 vertical sigma levels and five of these levels are situated in the lower troposphere as per its standard configuration (Elguindi et al., 2017; Giorgi et al., 2012). Several studies (Tiwari et al. 2016; Pattnayak et al. 2017b) have indicated that RegCM4, utilizing these standard vertical levels, effectively simulates the primary characteristics of the climate, as well as the atmospheric circulations and precipitation patterns over India. RegCM4 includes five main convective parameterization schemes to account for convective precipitation: the modified Kuo scheme (Anthes, 1977), the Grell scheme (Grell, 1993), the MIT-Emanuel scheme (Emanuel, 1991), and a mix scheme that employs the Grell scheme over land and the Emanuel scheme over the ocean (Emanuel and Zivkovic-Rothman, 1999). Detailed descriptions of these schemes are available in the respective references cited. Additionally, this work utilises two land surface schemes, the Community Land Model (CLM; Oleson et al., 2008) and Biosphere-Atmosphere Transfer Scheme (BATS; Dickinson et al., 1993). Table 4.3 shows a concise comparison of these two land surface parameterization schemes.

4.3 Experimental Framework and Data

In this chapter, three meticulously designed sets of sensitivity experiments are presented to investigate how different representations of Himalayan orography, cumulus convection, and land surface schemes affect the simulation of meteorological fields over the Indian region using the RegCM4 model. These experiments are detailed as follows:

- **Role of Himalayan Orography Representations:** This set of experiments examines the influence of nine Himalayan orography representations. This is done by adjusting the orography in the model through increasing and decreasing orography from mean elevation.
- **Sensitivity to Convection Schemes:** This set of experiments focuses on the sensitivity of various cumulus convection schemes that are included with the RegCM4 model.
- **Impact of Land Surface Schemes:** This set of experiments investigates the role of two different land surface schemes in RegCM4.

The model domain of interest covers the area from 15°E to 128°E and from 30°S to 56°N. Over this domain, it consists of 496 (384) grid points along the longitude (latitude). Model integrations are conducted from May 1st to September 30th each year, covering nine distinct years categorized into three wet, normal, and dry years, all at a 25 km resolution. The initial and boundary conditions are derived from the UK Met Office's Hadley Centre Global Environment Model (HadGEM3) with a resolution of 1.4°. The results simulated by the model are validated against ERA-5 data (Hersbach et al., 2020) and Indian Meteorological Department (IMD) gridded precipitation data (0.25° × 0.25°) (Pai et al., 2014). Additionally, apart from the HadGEM3 initial and boundary conditions, the model is also driven with ECMWF reanalysis (ERA5), and similar results were observed. The JJAS seasonal rainfall data for each year is constructed by averaging the rainfall of June, July, August, and September

months. From the seasonal mean precipitation anomalies, extreme years (wet/dry) are selected based on the observed precipitation data from the Indian Meteorological Department (IMD), where years with a standardized precipitation anomaly greater than 10% are classified as wet, and those with less than 10% are classified as dry. Out of the 31 years (1984-2014) of IMD data analysis, a total of 9 distinct years were selected for this study: three wet years (1988, 1995, 1998), three dry years (1986, 2000, 2002), and three normal years (1991, 1996, 2005).

In the first set of experiments, sensitivity studies have been conducted to assess the impact of various Himalayan orography representations on the simulation of precipitation and temperature over the Indian region. These representations include adjustments to the orography by $\pm 5\%$, $\pm 10\%$, $\pm 15\%$, and $\pm 20\%$, labelled as M5, M10, M15, M20, CNTRL, P5, P10, P15, and P20. Here M (minus) represents a decrease in height and P (plus) represents an increase in height. The second set of experiments focuses on the sensitivity to different convective parameterization schemes within the RegCM4 model. The final set of experiments examines the sensitivity to two different land surface schemes, namely the Biosphere-Atmosphere Transfer Scheme (BATS) and the Community Land Model (CLM). The experiments were conducted over the targeted region at a horizontal resolution of 25 km. The model domain and configurations utilised in these sensitivity tests are depicted in Figure 4.1 and described in more detail in Table 4.1. Figure 4.2 depicts the differences in topography between the HadGEM3 and RegCM4 models, highlighting the clearer distinction of the northwest to southeast oriented Himalayan ranges in the RegCM4 model. This model captures the peaks and valleys more distinctly compared to the HadGEM3 model, where these features appear to be less defined. Additionally, Figure 4.3 shows the difference in Himalayan height after increasing the height by 5% (P5), 10% (P10), 15% (P15), and 20% (P20) from the mean (CNTRL) height of the model (Figure 4.1).

Table 4.1 – The RegCM4 configuration used.

Dynamics	Hydrostatics
Convective parameterization	(a) Mix99- Grell over land and Emanuel over ocean (b) Grell with Arakawa and Schubert (Grell-AS) closure (c) Kuo with Arakawa and Schubert (AS) closure (d) Grell with Fritch & Chappell clouser (Grell-FC) closure
Model domain	Resolution =25 km
Planetary Boundary Layer parameterization	Holtslag
Envelop topography treatment	Envelop orography with an increase/decrease from model height of 5%, 10%, 15% and 20%
Radiation parameterization	NCAR/CCM3 radiation scheme
Main Prognostic Variables	u,v t,q and p
Map projection	Rotated Mercator
Vertical co-ordinate	24 sigma levels with terrain-following sigma co-ordinate
Land Surface parameterization	<ul style="list-style-type: none"> • Community Land Model (CLM) • Biosphere-Atmosphere Transfer Scheme (BATS)
Horizontal grid system	Arakawa B

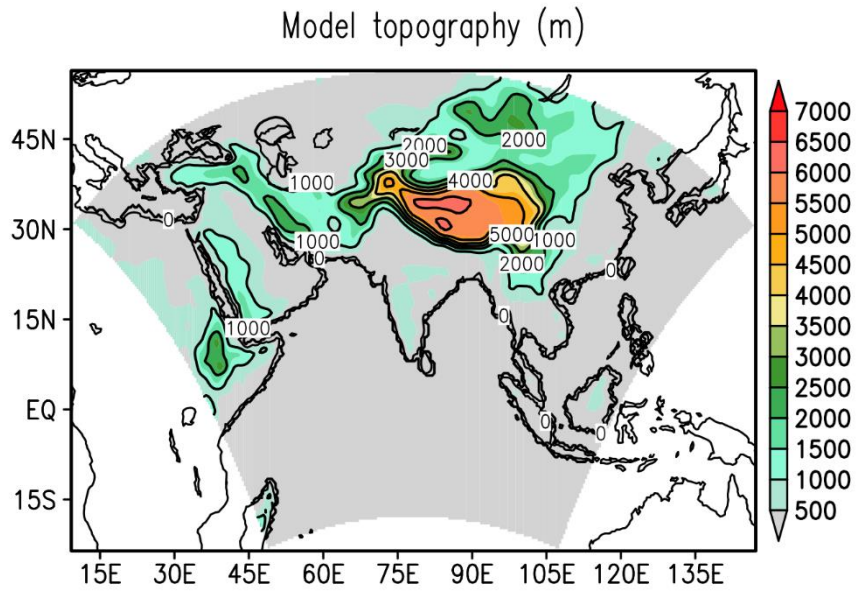


Fig. 4.1 – Model domain and orography (m) as used in RegCM4.

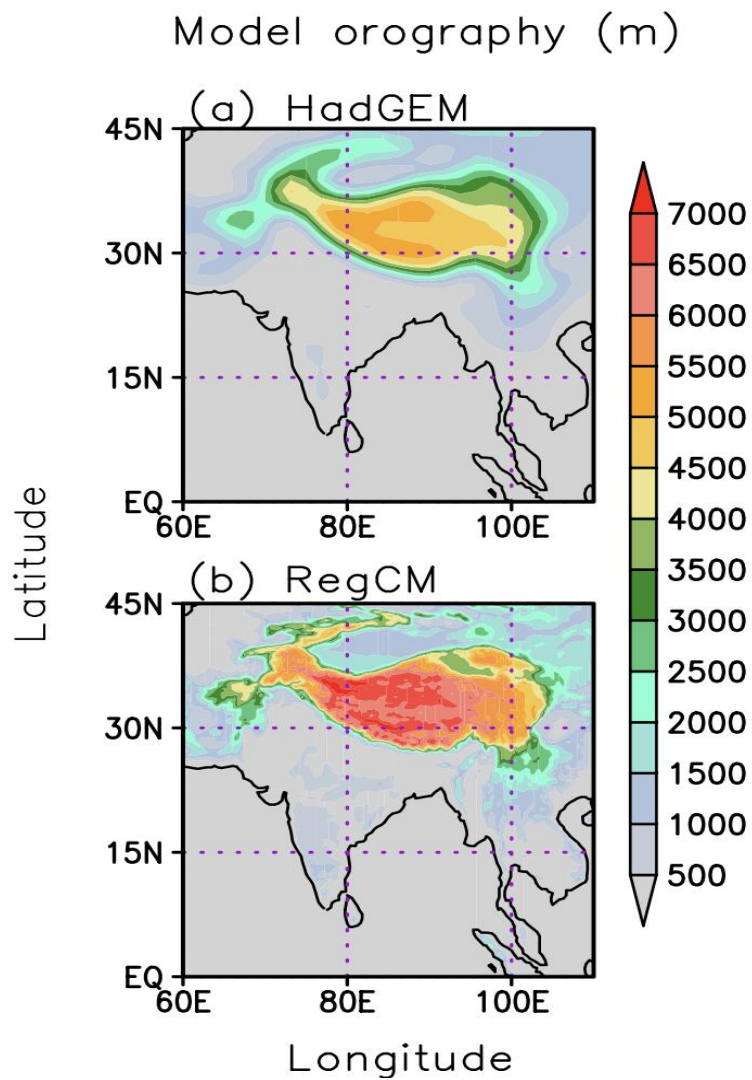


Fig. 4.2 – Model orography (m) from HadGEM3 (a) and RegCM4 (b) models.

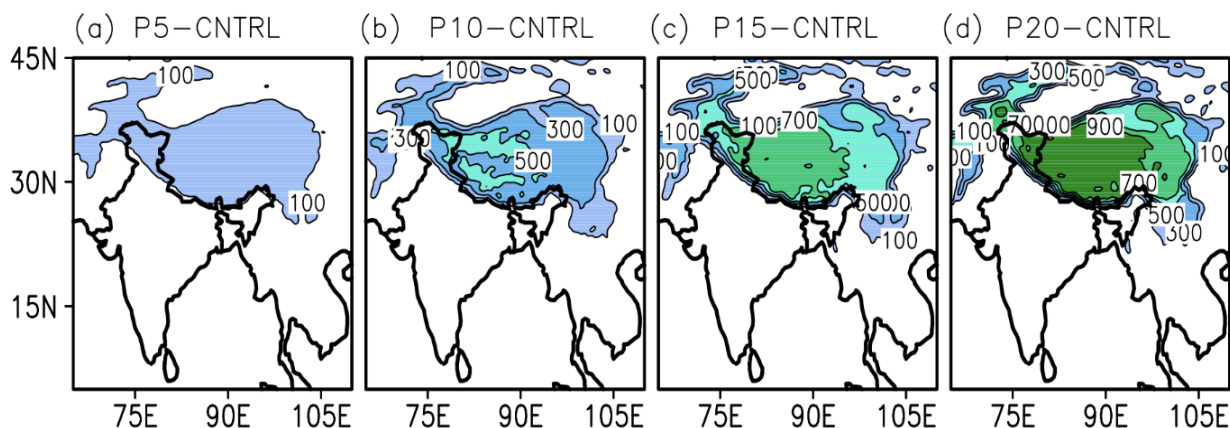


Fig. 4.3 – Difference in height (m) over the Himalayan region between RegCM4 model mean height and a 5% (P5), 10% (P10), 15% (P15), 20% (P20) increase in mean height. There is a contour interval of 100m.

The statistical metrics Equitable Threat Score (ETS), Index of Agreement (IOA), Hit Rate (HR) and False Alarm Rate (FAR) are calculated to evaluate the performance of the model with different orography representations. The formulas for the different statistical techniques are described below:

Equitable Threat Score (ETS): ETS is described as a useful skill metric for estimating model performance (Wilks, 1995) which is defined as:

$$ETS = \frac{H - H_r}{H + F + M - H_r}, \text{ where } H_r = \frac{(H + F)(H + M)}{N}$$

H represents the hits, H_r represents the hits expected by chance, F represents false alarms, M represents misses and N is the total number of events. ETS varies from $-1/3$ to 1. An ETS value equal to 0 indicates no skill and an ETS value equal to 1 indicates perfect skill.

Index of Agreement (IOA): Willmott (1982) stated that the ratio between RMSE and observed climatology are unstable for near zero values. IOA was proposed by Willmott (1982) as an alternative, to correct this issue. IOA (d) is defined as:

$$d = 1 - \frac{\sum_{i=1}^n (O_i - P_i)^2}{\sum_{i=1}^n (|P_i - \bar{O}| + |O_i - \bar{O}|)^2}$$

O_i is the observed value, P_i is the forecast value for the i^{th} year and \bar{O} is the average of observation values. IOA is measured between 0 and 1 ($0 \leq d \leq 1$) with a value of closer to 1 indicating a better forecast from the model.

Hit Rate (HR): This metric gives the fraction of correctly forecasted events. HR is defined as:

$$HR = \frac{H}{H + M}$$

H represents the number of hits and M represents the number of misses. HR ranges from 0 to 1, with a HR equal to 1 indicating perfect prediction skill.

False Alarm Rate (FAR): The fraction of false alarms that occur during the total number of forecasts. This is defined as:

$$FAR = \frac{F}{F + T}$$

Where F represents the a false positive, and T represents a true negative. FAR ranges for 0 to 1, with a FAR equal to 0 indicating perfect prediction skill.

4.4 Results and Discussion

The results of this chapter are split into three sections which look at the sensitivity of RegCM4 simulations, driven by HadGEM3 to different parameterization schemes in simulating temperature and precipitation over India. Himalayan orography representation, sensitivity experiments with four different cumulus convective parameterization schemes and two different land surface schemes.

4.4.1 Himalayan Orography Representation

4.4.1.1 Zonal Moisture Transport

Figure 4.4 shows the seasonal (JJAS) mean differences of zonal moisture transport between wet and dry years at 500hPa. Observed values have been compared to different Himalayan orography representations (M20, M15, M10, M5, CNTRL, P5, P10, P15, P20) that indicate an increase (P) or decrease (M) in orography. There is a significant increase in moisture transport when reducing orography representation, and M20 records the highest values over most of the region. Increasing orography representation appears to reduce moisture transport and produces values that are closer to the observation. This is most noticeable over the middle longitudes which are hugely overestimated by the M experiments. P10 is found to be the best scenario here which is the closest to observed values as further increasing orography representation leads to an underprediction of moisture transport.

4.4.1.2 Precipitation

When comparing the JJAS precipitation of the different orography representations to observed values (Fig. 4.5), P10 shows the best precipitation simulation and is closest to observation. The model simulated the JJAS mean precipitation over nine season (three wet, dry and normal) using the nine different orography representations. It is found that all decreases to orography representation (M5-20) as well as the control and P5 underestimate

precipitation. M20 is shown to give the largest underestimation, and P20 the largest overestimation of precipitation. Here even the control experiment underpredicts precipitation by a significant amount.

JJAS mean precipitation has been averaged over the Western Himalayan region of India (71°E - 84°E and 28°N - 38°N) with the nine different orography representations (Fig. 4.6). It can be seen that increasing the height by 10% (P10) increases the precipitation by around 15% and decreasing the height by 10% (M10) decreases the precipitation by around 32% from the control experiment. A reduction in height would allow a strong prevailing westerly wind to carry more moisture on the leeward side of Himalayas, resulting in less precipitation over the relevant domain.

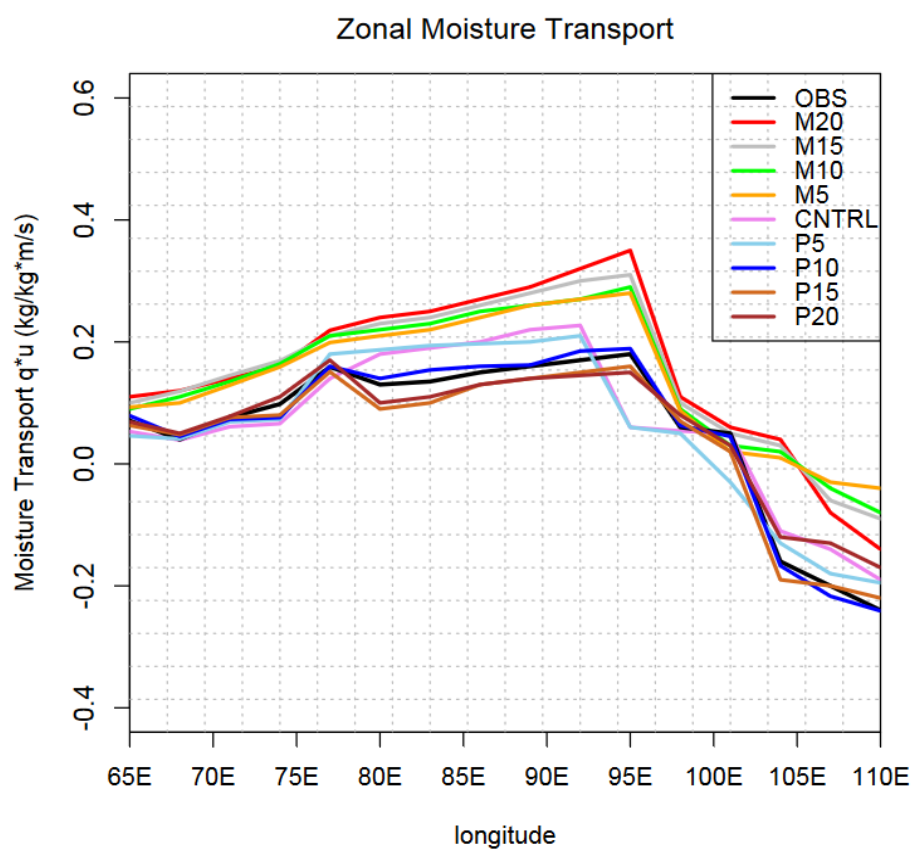


Fig. 4.4 – JJAS differences between wet and dry years for zonal moisture transport at 500hPa. Observation and different Himalayan orography representations (M20, M15, M10, M5, CNTRL, P5, P10, P15, P20) are shown.

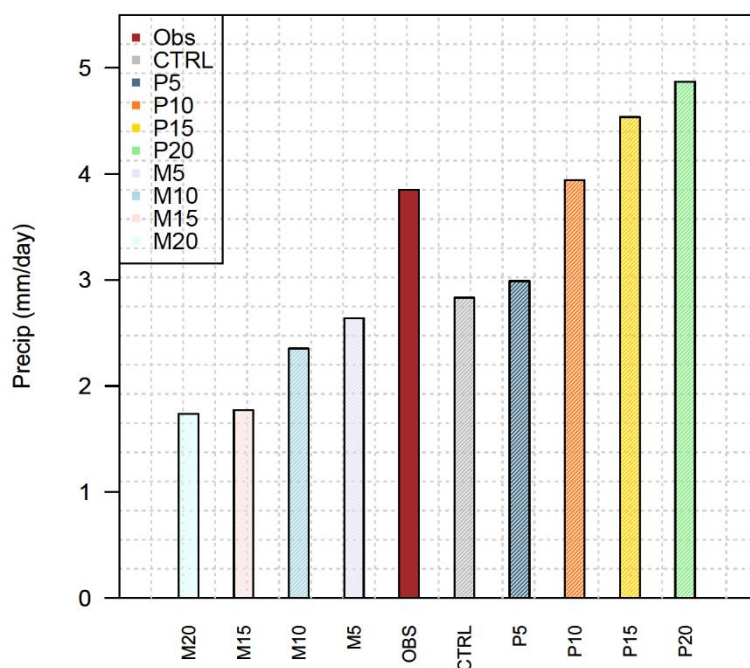


Fig. 4.5 – JJAS precipitation over India using observed and RegCM4 simulations with different Himalayan orography representations (M20, M15, M10, M5, CNTRL, P5, P10, P15, P20) for nine distinct years (three years each for wet, normal and dry).

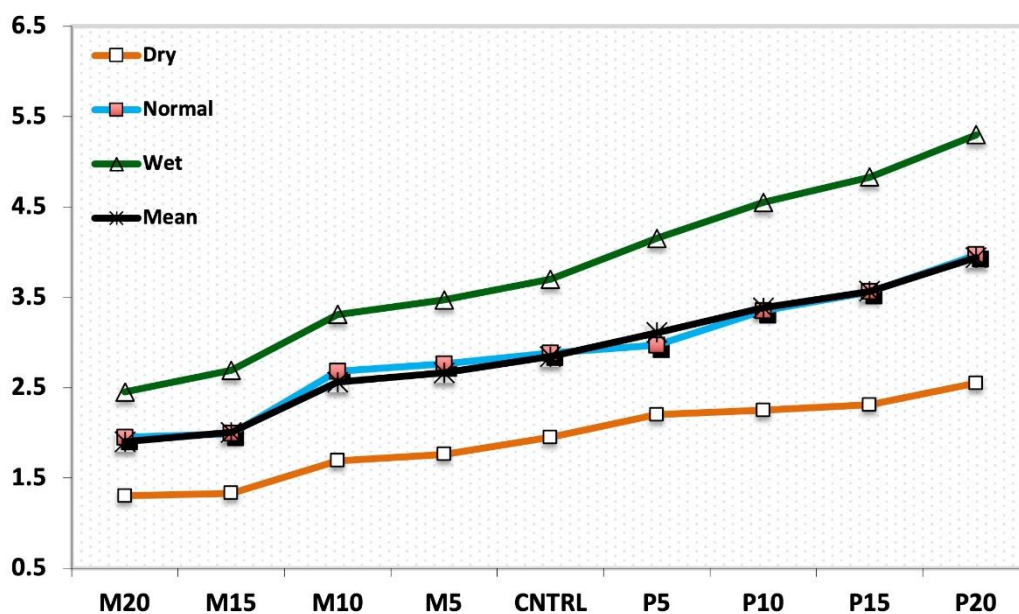


Fig. 4.6 – Western Himalayan (71°E-84°E; 28°N-38°N) area averaged JJAS mean precipitation for different Himalayan orography representations (M20, M15, M10, M5, CNTRL, P5, P10, P15, P20) using RegCM4. The y-axis shows precipitation (mm/day).

The Hit Rate (HR) and False Alarm Rate (FAR) are compared for the nine different orography representations in figure 4.7. A HR of one and a FAR of zero is considered to be the best possible forecast, and it is seen that this varies greatly between the different orography representations. P10 is the best experiment here with a HR of around 0.53 and FAR of around 0.25. It can be seen that decreasing the orography representation lowers the HR and increases the FAR and gets worse the more orography height is reduced. This is worst with the largest reduction in orography (M20). Increasing orography representation is shown to improve upon HR and FAR, however P15 and P20 yield worse results than P10 showing that too large of an increase can negatively impact results.

The Equitable Threat Score (ETS) is calculated for the nine different orography representations in figure 4.8. The ETS has been calculated for days where observed precipitation is greater than 3mm/day. ETS ranges from -0.3 to 1, with 1 being the best possible outcome. M10, M15 and M20 all show an ETS below zero and is worst with the M20 experiment, recording an ETS of -0.24. Increasing the height also increases the ETS and improves up the control height. Once again P10 is the best performing experiment with an ETS of 0.53 and increasing the height beyond this lowers the ETS.

Orography representation is shown to be an important factor to consider with regards to precipitation simulation using RegCM4 over India. Increasing the orography height by 10% (P10) yields the best results and shows improved results in precipitation simulation when compared to the default orography representation in the model.

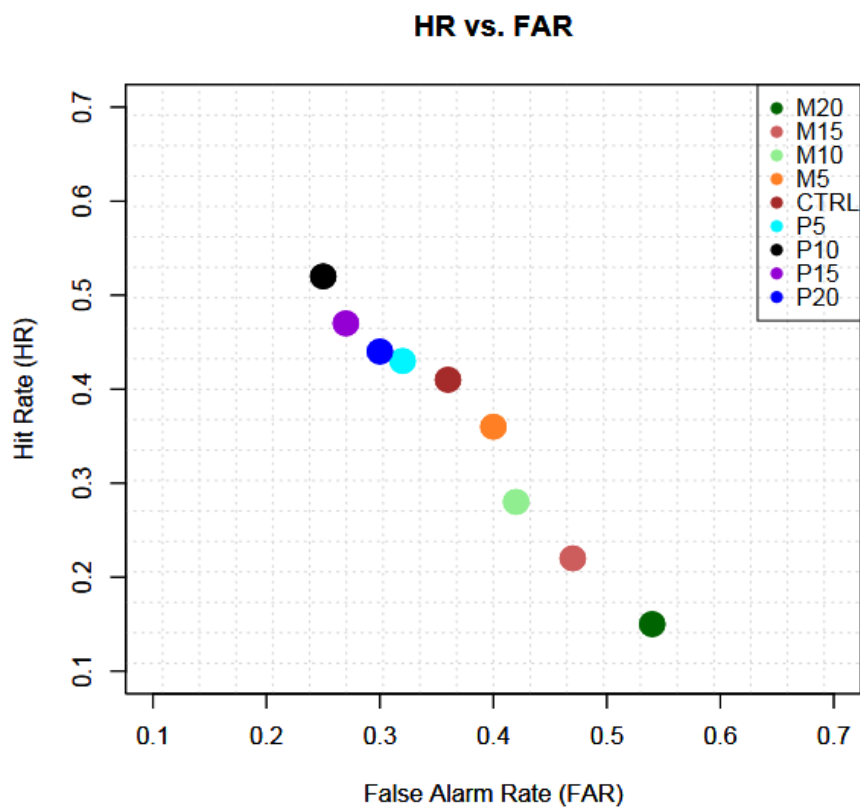


Fig. 4.7 – Hit Rate (y-axis) versus False Alarm Rate (x-axis) for nine different Himalayan orography representations (M20, M15, M10, M5, CNTRL, P5, P10, P15, P20).

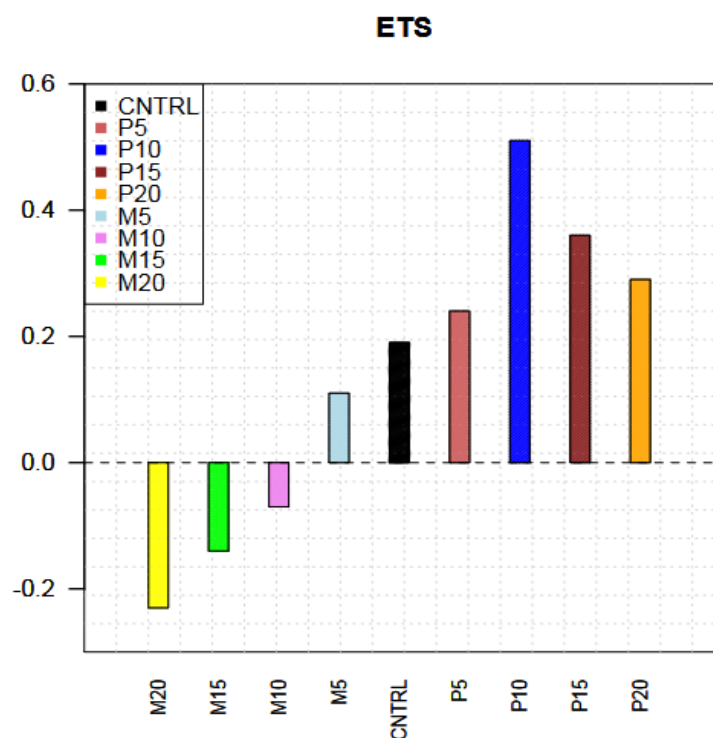


Fig. 4.8 – Equitable Threat Score (ETS) for nine different Himalayan orography representations (M20, M15, M10, M5, CNTRL, P5, P10, P15, P20). ETS is considered for days where the observed precipitation is greater than 3mm/day.

4.4.2 Convective Parameterization Schemes

4.4.2.1 Circulation Features

The RegCM4 simulations have been analysed to study the various meteorological fields and associated patterns for nine different years. The upper air and surface fields are compared with IMD observed data. The sensitivity of convective parameterization scheme experiments are shown in table 4.2.

Vertical pressure velocity (ω) is an important upper air circulation parameter and plays an important role in model dynamics for precipitation simulation. This makes it important to consider the simulations of ω with different cumulus schemes. For this purpose, ω

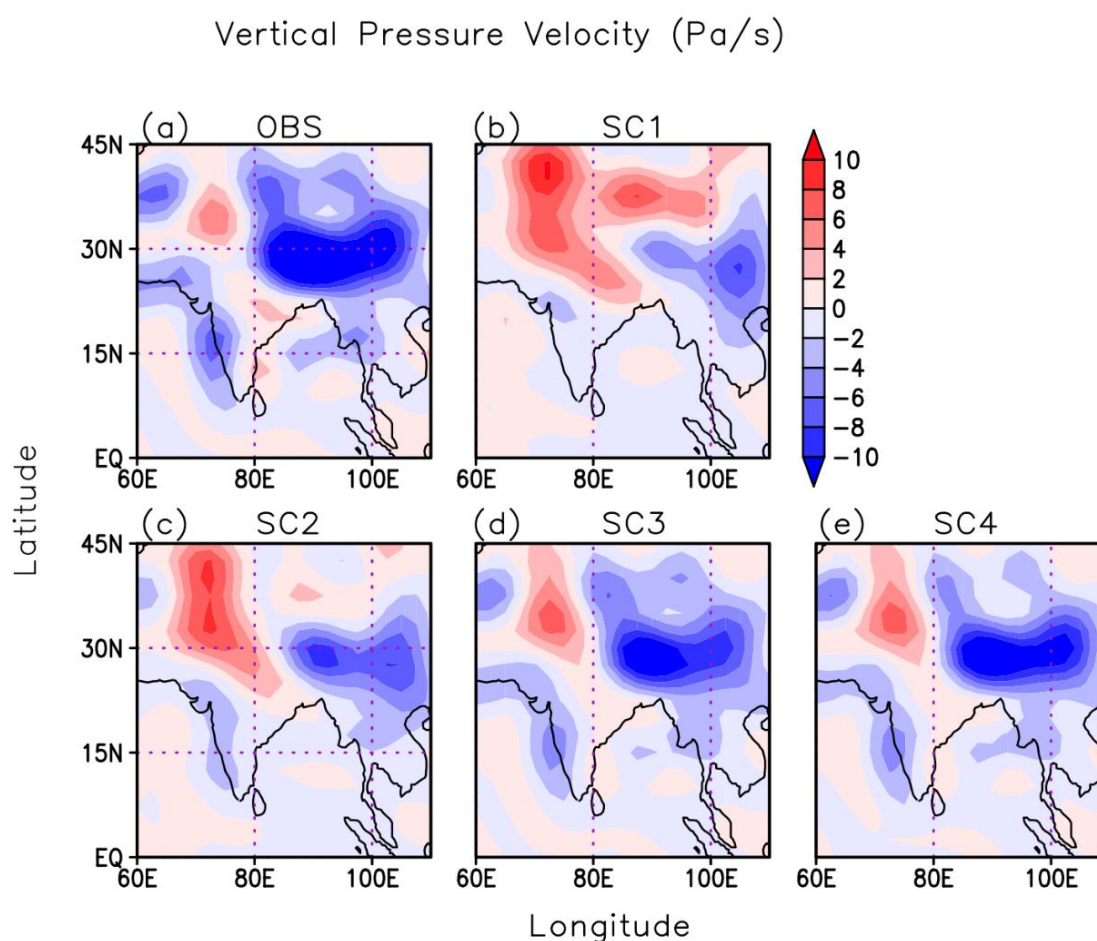


Fig. 4.9 – JJAS mean vertical pressure velocity (Pa/s) at 500 hPa pressure level of Obs (a), RegCM4 simulations at 25km resolution using SC1 (b), SC2 (c), SC3 (d) and SC4 (e) cumulus schemes for a composite (wet-dry) precipitation year.

at 500 hPa obtained from observation and RegCM4 simulations are analysed for composite precipitation years (Fig. 4.9). SC1 and SC2 show a large estimation of omega in the northwest and underestimation of omega in the northeast regions. Observed values show that a negative omega (sinking motion) is stronger over the southwest and northeast regions which is well represented by SC4 and SC3 schemes. Although both of these schemes represent omega well, SC4 is shown to be closer to observation of omega when compared to SC3 over this region.

Table 4.2 – Different cumulus scheme experiments with RegCM4 simulations at a 25 km resolution.

Lateral boundary condition	RegCM4
Hadley Centre Global Environment Model version 3 (HadGEM3)	Kuo cumulus scheme with Arakawa Schubert closure (SC1)
	Grell cumulus with Arakawa Schubert closure (SC2)
	Grell cumulus scheme with Fritsch Chappell closure (SC3)
	Mix99- Grell over land and Emanuel over ocean (SC4)

4.4.2.2 Precipitation

4.4.2.2.1 Precipitation Distribution

The cumulus scheme SC4 is shown to most closely match observations when simulating precipitation for dry, normal and wet years over India (Fig. 4.10). Here the four cumulus schemes (SC1, SC2, SC3 and SC4) are tested against observed values for dry, normal and wet years over the Indian domain. The difference between observed values and SC4 is much smaller than the other schemes, showing the ability of SC4 to capture both precipitation intensity and distribution over India. This is possibly due to the better representation of moisture convergence seen in SC4 when compared to the other schemes.

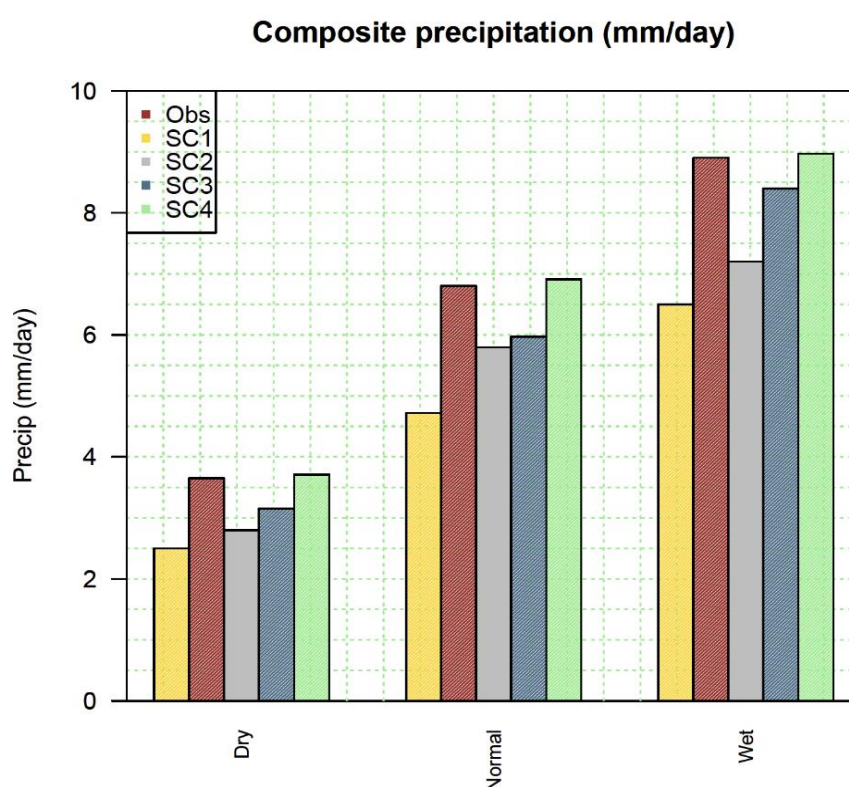


Fig. 4.10 – JJAS mean precipitation over India from observed values and SC1, SC2, SC3, and SC4 cumulus schemes for wet, normal and dry precipitation years.

4.4.2.2.2 Statistical Analysis of Precipitation Simulation in RegCM4

The ability of the four cumulus schemes to represent precipitation over India is shown through the use of a Taylor diagram (Fig. 4.11) and Equitable Threat Score (Fig. 4.12). When comparing the different cumulus schemes, SC4 is shown to perform better in terms of correlation coefficient, root mean square error and standard deviation than the other cumulus schemes. SC3 performs quite well and is not too far away from SC4, whereas SC1 and SC2 perform considerably worse. SC4 is also shown to perform better than the other cumulus schemes through the use of ETS (Fig. 4.12). ETS values are shown for dry, normal and wet years, with an ETS equal to one being the best possible outcome. SC2 struggles the most with precipitation simulations as it is the only cumulus scheme to produce a negative ETS, which is the same for all scenarios. SC4 has the best ETS for all scenarios and performs best during a normal precipitation year with an ETS of 0.54.

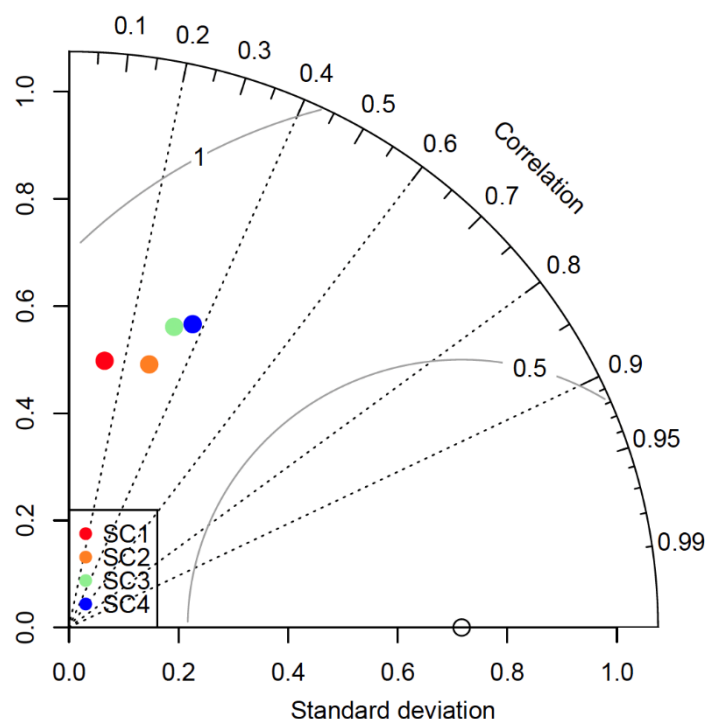


Fig. 4.11 – Taylor diagram showing the correlation coefficient, normalised standard deviation and root mean square error for SC1, SC2, SC3 and SC4 when compared to observed values for JJAS precipitation.

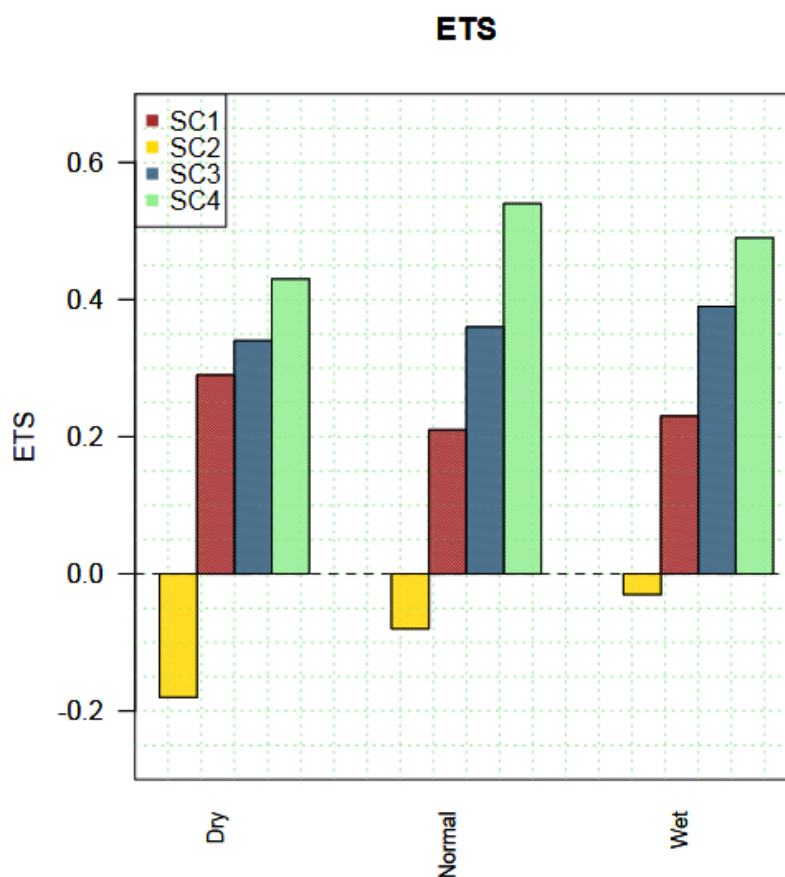


Fig. 4.12 – Equitable threat score (ETS) for precipitation simulations using RegCM4 with SC1, SC2, SC3 and SC4 schemes for dry, normal and wet years.

4.4.3 Land Surface Schemes

Two Land Surface Parameterization Schemes (LSPS) are used to evaluate the sensitivity of land surface when simulating temperature and precipitation over India. The two LSPS used are the Biosphere-Atmosphere Transfer Scheme (BATS) and the Common Land Model version 4.5 (CLM). Details of these two LSPS are shown in table 4.3. The following section compares these two LSPS for use with RegCM4.

Table 4.3 – Land Surface Parameterisation Schemes (CLM and BATS)

Category	CLM	BATS
Treatment of heat and roughness length	Values are updated over bare soil and snow with values from the stability functions	Heat and water vapor roughness lengths are fixed
Soil temperature calculation	The soil temperature is calculated through the use of a ten-layer soil model	It uses a two-layer force-restore model
Land cover/ Vegetation classes	24 vegetation types	20 vegetation types
Vegetation canopy	The canopy is divided into sunlit and shaded fractions as a function of leaf area index	All vegetation in the canopy is treated the same
Surface representation	One vegetation layer with a canopy photosynthesis-conductance model, ten unevenly spaced soil layers and five snow layers	One vegetation layer, one surface soil layer and one snow layer
Calculation of stomatal conductance and photosynthesis rate	The stomatal conductance is calculated separately for sunlit and shaded fractions, and photosynthetic rates are determined within this scheme	No calculation for stomatal conductance or photosynthesis rate

4.4.3.1 Analysis of Soil Moisture and Sensible Heat Flux

Soil moisture during the JJAS period for observed (ERA5) and RegCM4 simulations using BATS and CLM are shown over India (Fig. 4.13). Both RegCM4-BATS and RegCM4-CLM are shown to capture the spatial distribution of soil moisture over India, however RegCM4-CLM values are much closer to observations and RegCM4-BATS shows large underestimations in soil moisture over the region.

Sensible heat flux for observed and RegCM4 simulations using BATS and CLM are shown in figure 4.14. Comparison between the LSPS shows clear spatial difference among the schemes compared to observation. Due to a greater number of vegetation cover/category the RegCM4-CLM is able to capture the fluxes more realistically compared to RegCM4-BATS. This reliable representation of the fluxes helps in better prediction of temperature and precipitation over the Indian region with RegCM4-CLM compared to RegCM4-BATS combination.

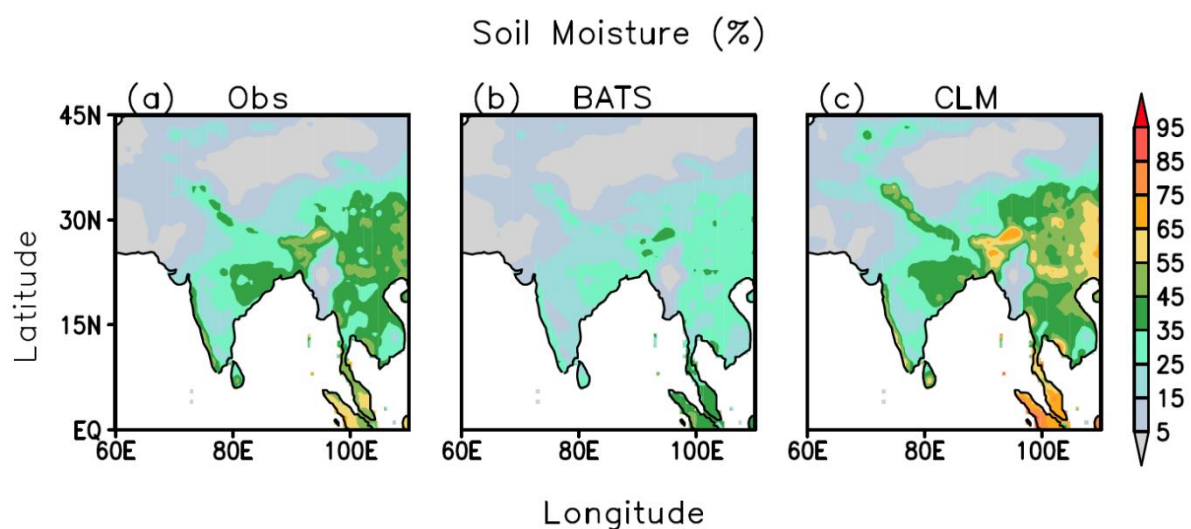


Fig. 4.13 – JJAS average soil moisture for composite precipitation years using observed (a), BATS (b) and CLM (c) schemes.

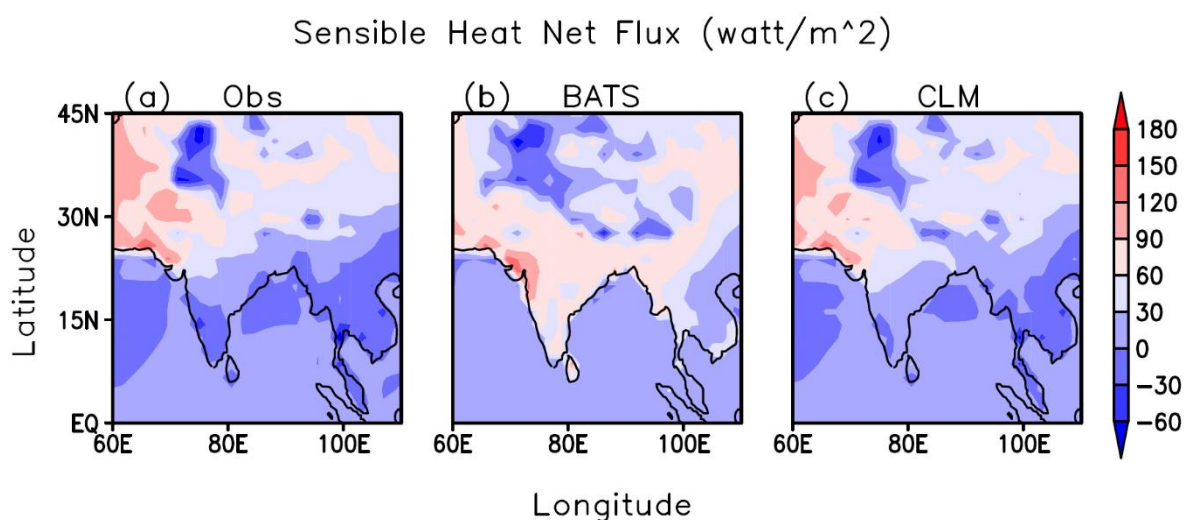


Fig. 4.14 – JJAS sensible heat flux difference for composite precipitation years obtained for observed (a), BATS (b) and CLM (c) schemes.

4.4.3.2 Precipitation Statistical Evaluation

The correlation coefficient (CC) and root mean square error (RMSE) for both BATS and CLM are computed during wet, dry and normal precipitation years (table 4.4). The CLM LSPS outperforms BATS in terms of RMSE and CC for wet, dry and normal years. CLM has a lower RMSE for all scenarios when compared to BATS and the lowest RMSE (1.13) for CLM is seen during a dry precipitation year. CLM also has a high CC for all scenarios compared to BATS and the highest CC (0.46) is during a normal precipitation year.

Table 4.4 – Root mean square error (RMSE) and correlation for wet, dry and normal precipitation years when compared to observed values using BATS and CLM schemes.

		Wet	Dry	Normal
RMSE	BATS	2.14	1.29	2.52
	CLM	1.98	1.13	2.06
Correlation coefficient	BATS	0.29	0.23	0.31
	CLM	0.34	0.37	0.46

Table 4.5 - Skill scores for wet, normal and dry precipitation years over India (where rainfall ≥ 2 mm/day for a wet day).

Year	Land Surface Scheme	IOA (0 to 1)	Bias (0 to ∞)	ETS ($-1/3$ to 1)
Wet	BATS	0.67	1.39	0.14
	CLM	0.78	1.03	0.34
Normal	BATS	0.79	1.43	0.24
	CLM	0.87	1.26	0.36
Dry	BATS	0.53	1.64	0.18
	CLM	0.61	1.51	0.27

The Index of Agreement (IOA), bias and Equitable Threat Score (ETS) have been calculated for RegCM4-BATS and RegCM4-CLM during wet, normal and dry years over India (table 4.5). Here a wet day is classified as a day that is greater than or equal to 2 mm/day. The IOA is better (closer to one) in CLM for wet (0.78), normal (0.87) and dry (0.61) compared to BATS and performs best during the normal precipitation year. Model biases are lower with the CLM scheme for wet (1.03), normal (1.26) and dry (1.51) compared to BATS and shows the lowest bias during the wet precipitation year. ETS is better (closer to one) for wet (0.34), normal (0.36) and dry (0.27) compared to BATS and has the best performance during the normal precipitation year.

These results highlight the improvement in precipitation simulation with the addition of the CLM LSPS and the importance of land surface in precipitation simulation over India.

4.5 Conclusion

This chapter has conducted three different sensitivity experiments with the ICTP Regional Climate Model (RegCM4) at a 25km resolution. The first sensitivity experiment utilises nine different orography representations and their influence on JJAS precipitation simulation. The second sensitivity experiment compares four different cumulus convective schemes in simulating JJAS precipitation. The third sensitivity experiment looks at two different land surface schemes for JJAS temperature and precipitation simulation. The key findings are as follows:

- RegCM4 does well at simulating JJAS mean precipitation over India. Increasing the orography height in the model is shown to also increase precipitation, and decreasing the orography height appears to have the inverse effect. A 10% increase in height (P10) increases precipitation by 15% and a 10% reduction in height (M10) reduces

precipitation by 32% when compared to the control height. P10 is found to best represent precipitation for wet, normal and dry years as increasing orography height further results in leads to an over estimation of JJAS precipitation and lower scores from statistical metrics such as Hit Rate and Equitable Threat Score.

- The Grell over land and Emanuel over ocean cumulus convection scheme (SC4) is found to best represent precipitation. This scheme is best able to reproduce vertical pressure velocity at 500hPa compared to the other tested schemes. JJAS mean precipitation is considerably closer to observations when using SC4 and is able to capture variability between wet, normal and dry precipitation years. Statistical analysis also shows SC4 as the best performing scheme when compared to the three convection schemes.
- Out of the two land surface schemes tested, the Common Land Model version 4.5 (CLM) is considered the better performing scheme. CLM is closer to observed values when simulating soil moisture and sensible heat flux, the latter of which is poorly represented by the Biosphere-Atmosphere Transfer Scheme (BATS). Statistical analysis when simulating JJAS precipitation for wet, normal and dry years shows CLM as being the best performing for all metrics over India.

The importance of orography representation, cumulus convection and land surface has been demonstrated in this chapter. The best performing parameterizations from each of the three sensitivity experiments have been applied to the RegCM4 simulations in the following chapter to allow for a better representation of climate extremes over India.

Dynamical Downscaling of Climate Extremes Over India and Future Scenarios using SSP's

This chapter is partially based on the papers:

- Marc Norgate, P.R. Tiwari, S. Das (2024). On the present and future changes in climate extremes over India using the dynamical downscaling approach, *Quarterly Journal of the Royal Meteorological Society, Royal Meteorological Society*, (To be submitted)
- P. Maharana, D. Kumar, S. Das, P. R. Tiwari., Marc Norgate & V. Raman (2024). Projected changes in heatwaves and its impact on human discomfort over India due to global warming under the CORDEX-CORE framework. *Theor Appl Climatol, Springer* 155, 2775–2786

Abstract

Global Climate Models are useful tool for simulating future climate, however their coarse resolution leads to smaller scale processes not being well represented. Dynamical downscaling through the use of Regional Climate Modelling aims to better represent these small-scale processes and give a more accurate representation of regional climate. Here the RegCM4.7 model was used, driven by HadGEM3-GC31-LL Global Climate Model. Sensitivity experiments were carried out to better fit this model to the Indian region with the addition of orography treatment which adds a 10 % increase from model mean height. The regional model is compared to its driving model during the historical period (1984-2014). For June, July and August maximum, mean and minimum temperature, it was found that the regional model had an improved spatial correlation over all Indian temperature homogenous regions with correlation coefficients as high as 0.99. There was a large improvement over the east coast from HadGEM3 to RegCM4.7 for all temperature variables (0.17 to 0.69 respectively). For June, July, August and September mean precipitation the regional model improved correlation over all regions except for the Himalayan region. Future projections show that maximum temperature is due to increase the most in the far-future when using the Shared Socioeconomic Scenario (SSP), SSP585. Indian is shown to experience more frequent three-, five- and seven-day heat waves, which will have a greater impact on the northern regions. Future mean precipitation changes vary per region with the PR and WC showing the largest increase and the CNE and eastern HR showing the largest decrease. Extremely wet days are shown to increase over all regions, the most impacted being the west coast of the PR and WC. These results show the importance of lowering emissions to prevent a dramatic increase in both extreme temperature and precipitation over India by the end of the century.

5.1 Introduction

The previous chapters highlight the importance of being able to accurately model both temperature and precipitation over India and assess future changes in these variables. These chapters used GCMs which showed valuable insights into future changes in extremes, however due to their coarse resolution, also had relatively large biases. This coarser resolution leads to the GCMs being unable to represent smaller scale processes and this is a known issue in the community (Lun et al., 2021, Tiwari et al., 2014, Zhou et al., 2013.).

This chapter uses dynamical downscaling to try and address the drawbacks of GCMs through the use of the regional climate model RegCM4.7. Various sensitivity experiments were carried out in chapter 4 to try and tailor this model to the Indian region and ultimately better understand the changes in climate extremes over India. Dynamical downscaling uses a reanalysis data or a GCM to drive the RCM and models regional climate at a higher resolution (Giorgi, 2019). RCMs have been used in many studies over many different regions and are valuable tools for assessing regional climate (Ahmadi et al., 2020, Carvalho et al., 2016, Chen et al., 2018, Rajczak et al., 2017, Turco et al., 2017).

CMIP6 models are still relatively new and using them as the driving model for an RCM provides downscaled SSP data which is not readily available. An effort has been made to address the known issues with the more mountainous regions over India with the addition of orography treatment during the parameterization of the RCM. This chapter aims to improve upon the GCM simulations with the use of the newest versions of both GCM and RCMs to give a better understanding of extreme temperature and precipitation over India.

5.2 Methodology

5.2.1 RCM Configuration

The RegCM4.7 regional climate model is used for this chapter over the Indian domain and its relevant temperature and precipitation homogenous regions (described in chapters 2 and 3 respectively). This RCM is from the Abdu Salam International Centre for Theoretical Physics (Elguindi et al., 2017, Giorgi et al., 2012). The configuration used for this model is shown in table 5.1.

Table 5.1 - Configuration of RegCM4.7 model used in the present study

Dynamics	Hydrostatics
Main Prognostic Variables	u, v, t, q and p
Horizontal grid distance	25 km
Map projection	Rotated Mercator map projection
Vertical co-ordinate	Terrain-following sigma co-ordinate
Cumulus parameterization	Grell over land and Emanuel over ocean (SC4)
Land surface scheme	Community Land Model (CLM4.5)
Orography treatment	Envelop orography (10 % increase from model mean height)
Radiation parameterization	NCAR/CCM3 radiation scheme
PBL parameterization	Holtslag
Simulation period	1980-2099
Analysis period	1984-2014, 2030-2060, 2070-2099
Emission pathway	Shared Socioeconomic Pathways (SSPs)- SSP126, SSP245, SSP585
Driving CMIP6 model	Hadley Centre Global Environment Model version 3 (HadGEM3-GC31-LL)

5.2.2 Observed Data and Future Temperature and Precipitation Simulations

The analysis periods are split into three groups, historical (1984-2014), near-future (2030-2060) and far-future (2070-2099). For temperature we only consider JJA periods per year which are the hottest months of the year over India. For precipitation we only consider precipitation during JJAS which is during the ISM and when most heavy precipitation occurs. The RCM was run from 1980-2099 which allowed a spin-up time of 4 years. Allowing a spin-up time removes inconsistencies that are present at the start of RCM model runs (Jerez et al., 2020). For the historical period, the ability of the RCM to simulate maximum, mean and minimum temperature as well as mean precipitation is shown. The observed data used for all temperature variables is from the Climatic Research Unit (CRU, Harris et al., 2017) which has a resolution of 50km. For precipitation the Indian Meteorological Department (IMD, Pai et al., 2014) observed dataset is used, which has a resolution of 25km (the same as the RCM). Both the CRU and HadGEM3 grid size was changed to 25km to match the grid size of the RCM using the CDO (Schulzweida et al., 2021).

Future simulations use Shared Socioeconomic Pathways (Riahi et al., 2017) SSP126, 245 and 585 which represent low, medium and high emission scenarios respectively. For the future time period the variables maximum temperature, mean precipitation, number of consecutive heat waves (3, 5 and 7 consecutive days), heat wave duration index and extremely wet days are shown. Definitions of these variables (except tasmax and pr) are shown in tables 2.2 (heat wave variables) and 3.2 (EWD). These were calculated in CDO using the daily tasmax and daily mean precipitation datasets.

5.3 Results and Discussion

5.3.1 Temperature Extremes using RCM Simulations

5.3.1.1 HadGEM and RegCM4 Historical Analysis

The historical RCM simulations do a good job of capturing tasmax, tas and tasmin over most of the Indian temperature homogenous zones (Fig. 2.1). The models struggle with the WH which shows a large cold bias, which is likely due to the complex topography of this region. For tasmax there is a general cold bias over most regions. A slight warm bias is seen in the NE and a larger warm bias at the south of the EC and IP. When looking at tas, there is also a general cold bias over most regions, however parts of the NW, NE and the southernmost point of the EC do have a small warm bias. tas has less significant grid points

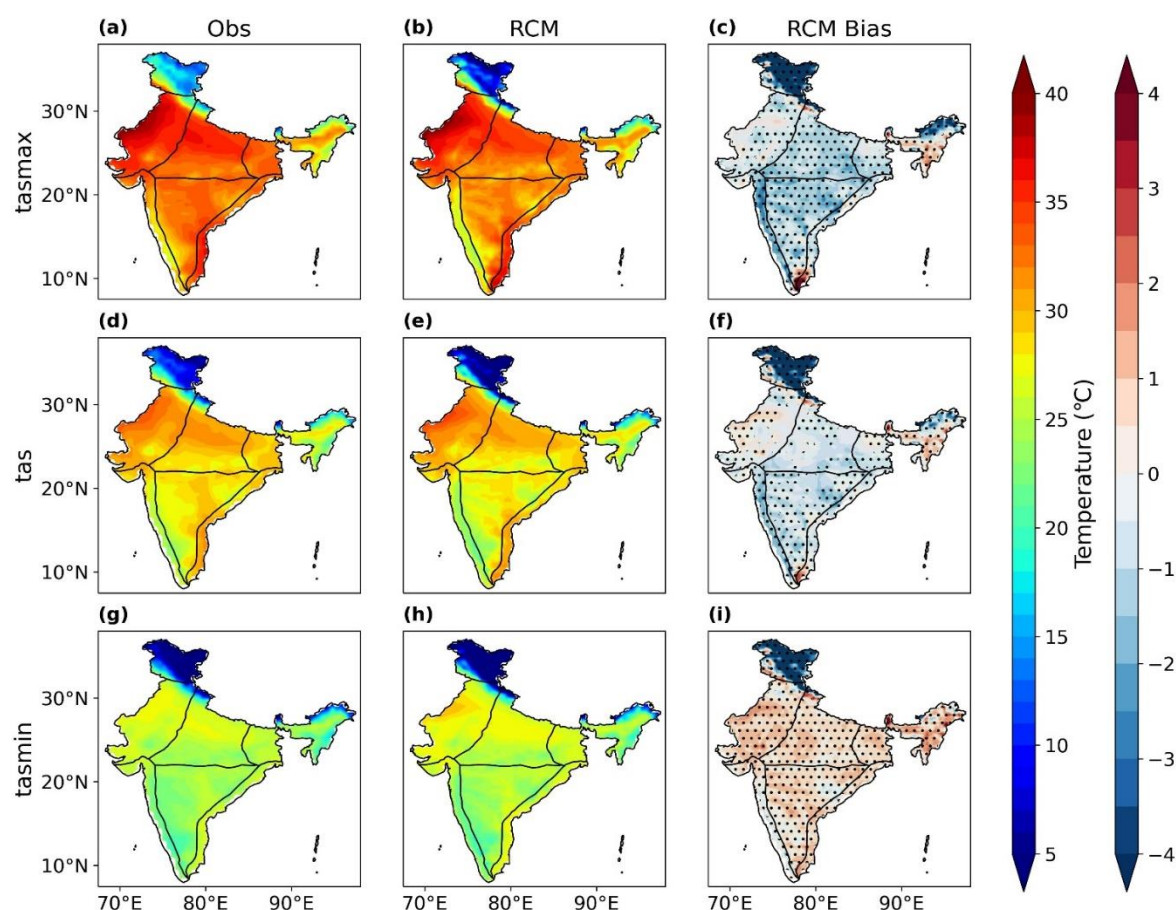


Fig. 5.1 – JJA tasmax (a, b, c), tas (d, e, f) and tasmin (g, h, i) for observed (a, d, g), RCM (b, e, h) and RCM bias (c, f, i) during the historical period (1984-2014). The dots represent the grid points with significant differences at 95% significance level.

than tasmax and tasmin, most noticeably in the NC region. Different from the previous two variables, tasmin shows a warm bias over most regions, except the WH and the WC.

The RCM sees an improvement in CC with the observed dataset for all temperature variables over all homogeneous regions when compared to the CC of the CMIP6 driving model (HadGEM3-GC31-LL). For tasmax (fig. 5.2a), the RCM CC is between 0.9 and 1 for the WH, NW, WC, NE and NC regions. HadGEM3 appears to struggle most over the EC with a CC of 0.17 and the RCM shows a significant increase in CC (0.69) over this region.

Similarly, for tas (fig. 5.2b) the RCM is between 0.9 and 1 for most regions, except EC which is still very high at 0.84. Once again there is a significant improvement in the RCM CC (0.84) over the EC when compared to HadGEM3 (-0.078), which is HadGEM3s worst performing region. The RCM only shows a CC between 0.9 and 1 for tasmin (fig. 5.2c) and once again improves upon HadGEM3 over every region. Overall, the RCM shows a large improvement compared to HadGEM3 over all temperature homogenous regions for all temperature variables with the largest improvements being over the EC, which HadGEM3 has the most difficulty with. For tasmax and tas, the RCM shows the best performance over the NC and worst over the EC, this is almost the same for tasmin, however the WC is tied with the NC for the best CC. Even though the RCM performs best over the NC, the other regions are not far behind and the RCM does an excellent job at representing temperature over the Indian homogenous regions.

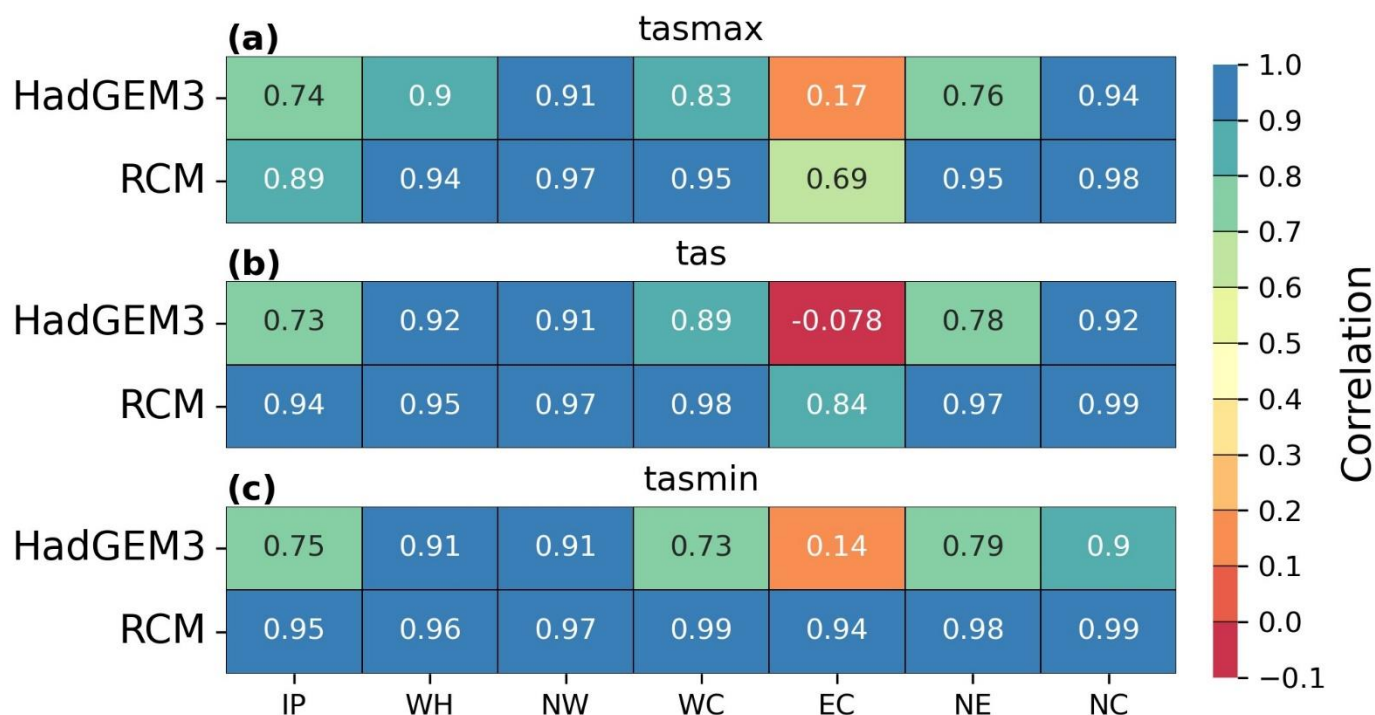


Fig. 5.2 – Spatial correlation coefficient for both the HadGEM3-GC31-LL (1st row) and RCM (2nd row) compared to the observed (CRU) dataset for JJA tasmax (a), tas (b) and tasmin (c) over the Indian temperature homogenous zones for the historical period.

5.3.1.2 RegCM4 Future Projections over India

FF SSP585 shows the largest rightward shift in temperature when compared to all over SSPs and time periods over all homogenous regions (fig. 5.3). The RCM underestimates tasmax during the historical period for all homogenous regions, with the largest bias being seen in the WH (fig. 5.3b) which has a difference of 6°C. The NE is closest to observed values with a difference of 0.3°C. All SSPs over all regions show an increase in tasmax when compared to the present climate, suggesting that warming is inevitable. For all regions FF SSP126 appears to have a lower tasmax when compared to all NF and FF SSPs. This could suggest that sufficient mitigation strategies can reduce the increased tasmax by the end of the century. FF SSP585 shows the largest increase in temperature for all regions, with increases of 4.4°C (IP), 8.8°C (WH), 7.9°C (NW), 3.4°C (WC), 4.9°C (EC), 6.4°C (NE) and 7.8°C (NC) when compared to the present climate. This makes the WH the most impacted region with regards to

increased tasmax, however there are large temperature biases in this region. The NW and NC are also among the regions that see a large shift in tasmax and the biases for these regions are much smaller.

5.3.1.2.1 Future Changes in Heat Wave Characteristics

The number of heat waves per summer season is shown to increase in the future, with FF SSP585 showing the largest increase over the entirety of India (Fig. 5.4, 5.5, 5.6). When looking at 7 consecutive day HWs (Fig. 5.4) the WH and the north of the NW is most affected during the NF, receiving up to 3 more HWs per summer season. The NW, NC and

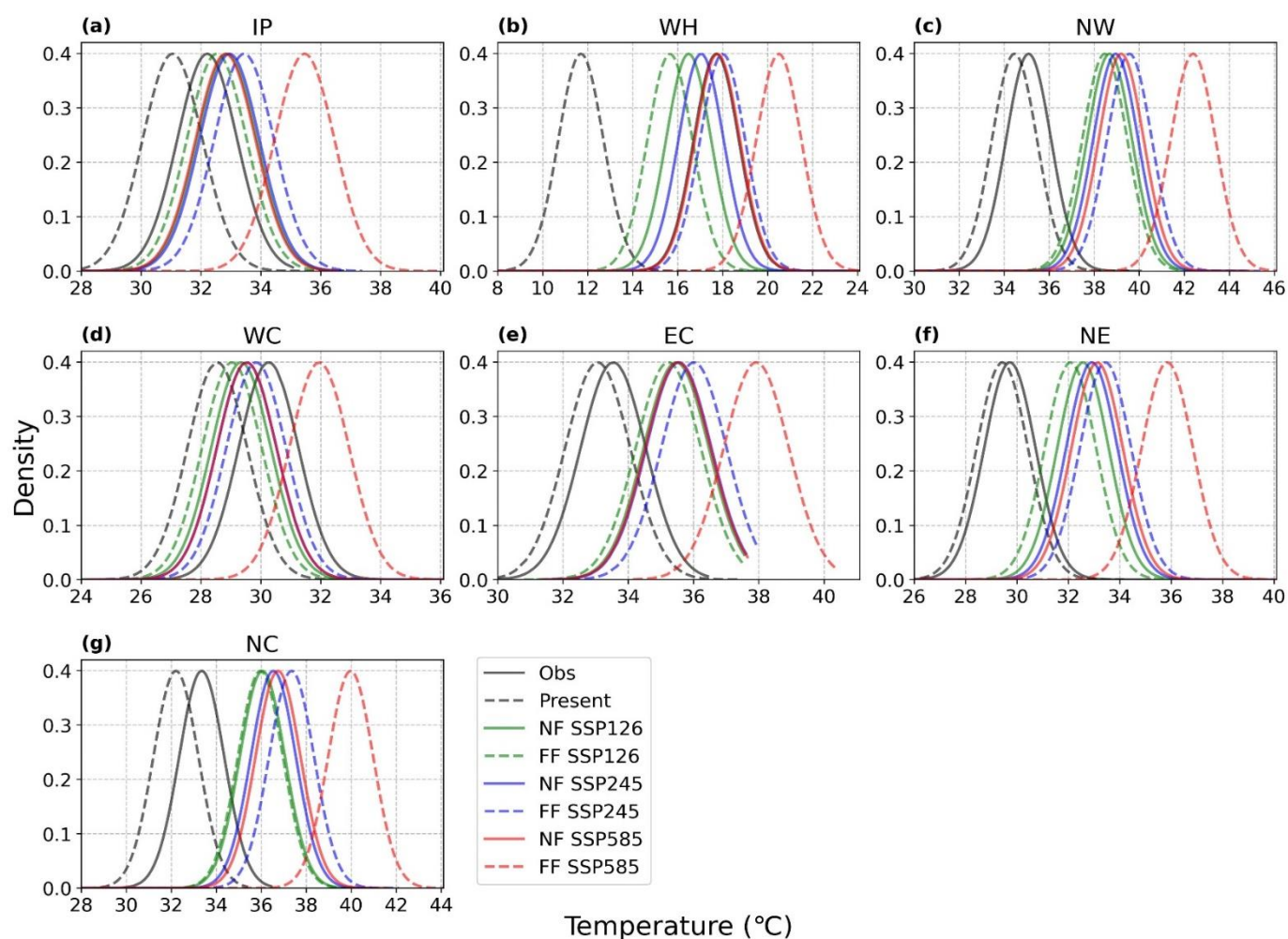


Fig. 5.3 – PDF for JJA tasmax over the Indian temperature homogenous regions during the historical, NF and FF periods using SSP1-2.6 (green), SSP2-4.5 (blue) and SSP5-8.5 (red). The historical period shows both observed values (solid black) and RCM values (dashed black). SSPs show solid lines for NF and dashed lines for FF.

NE are shown to receive between 1 and 2 more HWs when compared to the present climate. The WC is the least affected region showing mostly no increase except a small section near the top of the WC. The IP is least affected during NF SSP585 which is surprising. When looking at the FF, SSP126 sees a reduction in HW coverage when compared to its NF counterpart and is most noticeable over the NE and NW. SSP245 sees an increase in HW number when comparing NF to FF. The WH and north of the NW are most impacted here showing up to 3 more HWs per summer season. FF SSP585 shows the largest increase in HW number. All regions are shown to increase receive more HWs per summer season. The NW, NE and WH are most affected here and have an almost complete coverage of 3 more HWs. Areas that don't receive 3 more HWs are projected to receive an increase of 2 HWs. The IP is now shown to receive 1 more HW and the north of this region is shown to receive 2 more HWs and is now showing more HWs than the other SSPs. The WC which previously showed almost no increase is now showing 1-2 more HWs.

HWs for 5 consecutive days (Fig. 5.5) show a similar trend to the previous figure (Fig. 5.4), but with regions receiving more HWs. Once again NF SSP585 shows the largest increase in HWs compared to other SSP scenarios for most regions, the only exception is the IP. The WH, NW, NC and NE are most affected here with the most impacted areas seeing up to 4 more HWs per summer season. During the FF period SSP126 sees a slight reduction in HW number. Areas in the NC and NE that were seeing 4 more HWs have reduced to 3 and the area of the NW that was most impacted is reducing slightly. SSP245 sees an increase in HW number compared to the NF. The most increase is most noticeable in the NC, NW and WH which now have a larger area showing 4 more HWs and there are some small parts of the WH and NW showing 5 more HWs. FF SSP585 shows the largest increase, especially over the northern

regions. The NE is the most impacted showing a large area with an increase of 5 HWs. Most of the northern regions are now showing an increase of 4 HWs.

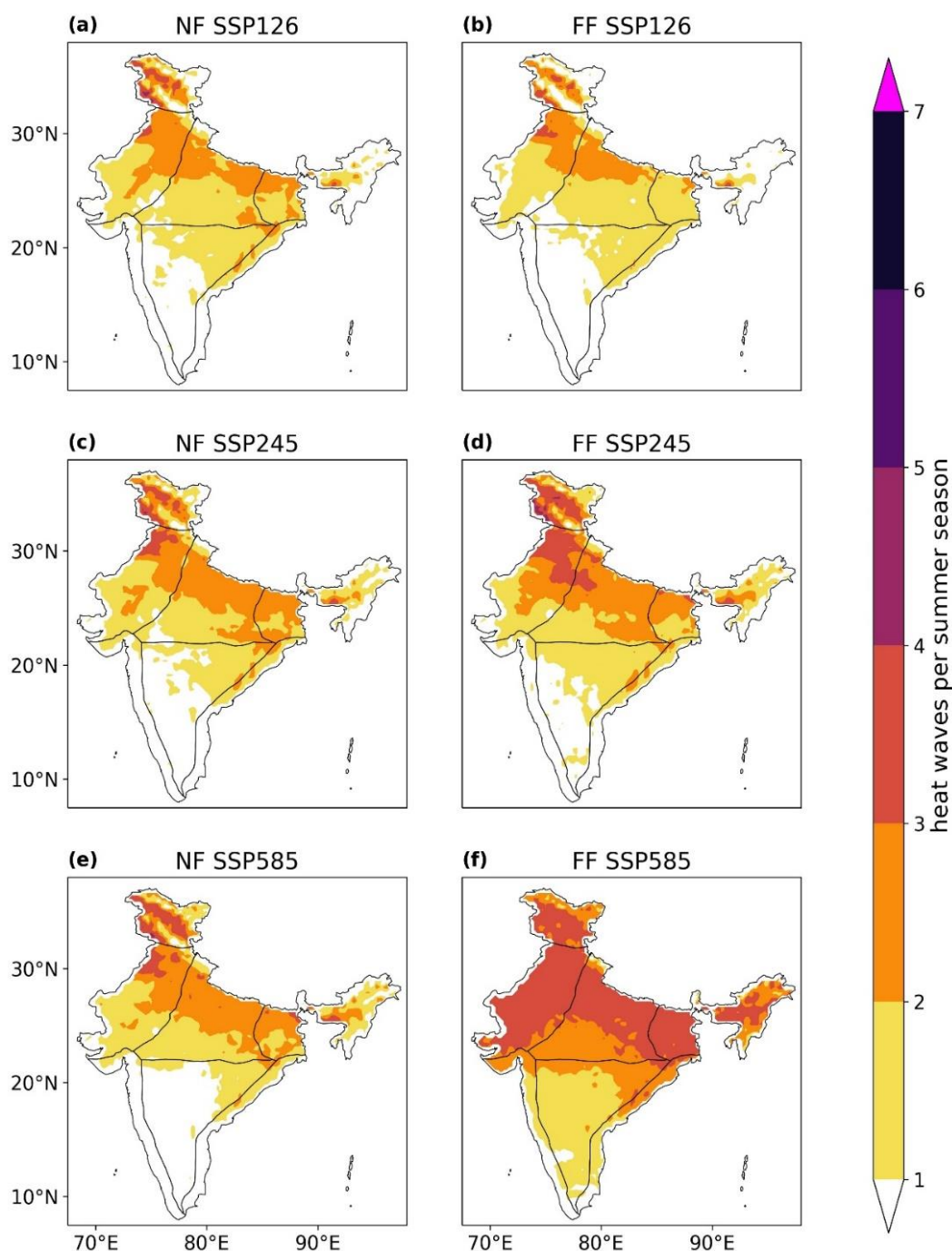


Fig. 5.4 – Heat waves per summer season (where $TX > TX_{norm} + 5^{\circ}C$ for 7 consecutive days) difference compared to the present climate for SSP1-2.6 (a, b), SSP2-4.5 (c, d) and SSP5-8.5 (e, f). The first column shows the difference over the NF period (a, c, e) and the second column shows the difference over the FF period (b, d, f).

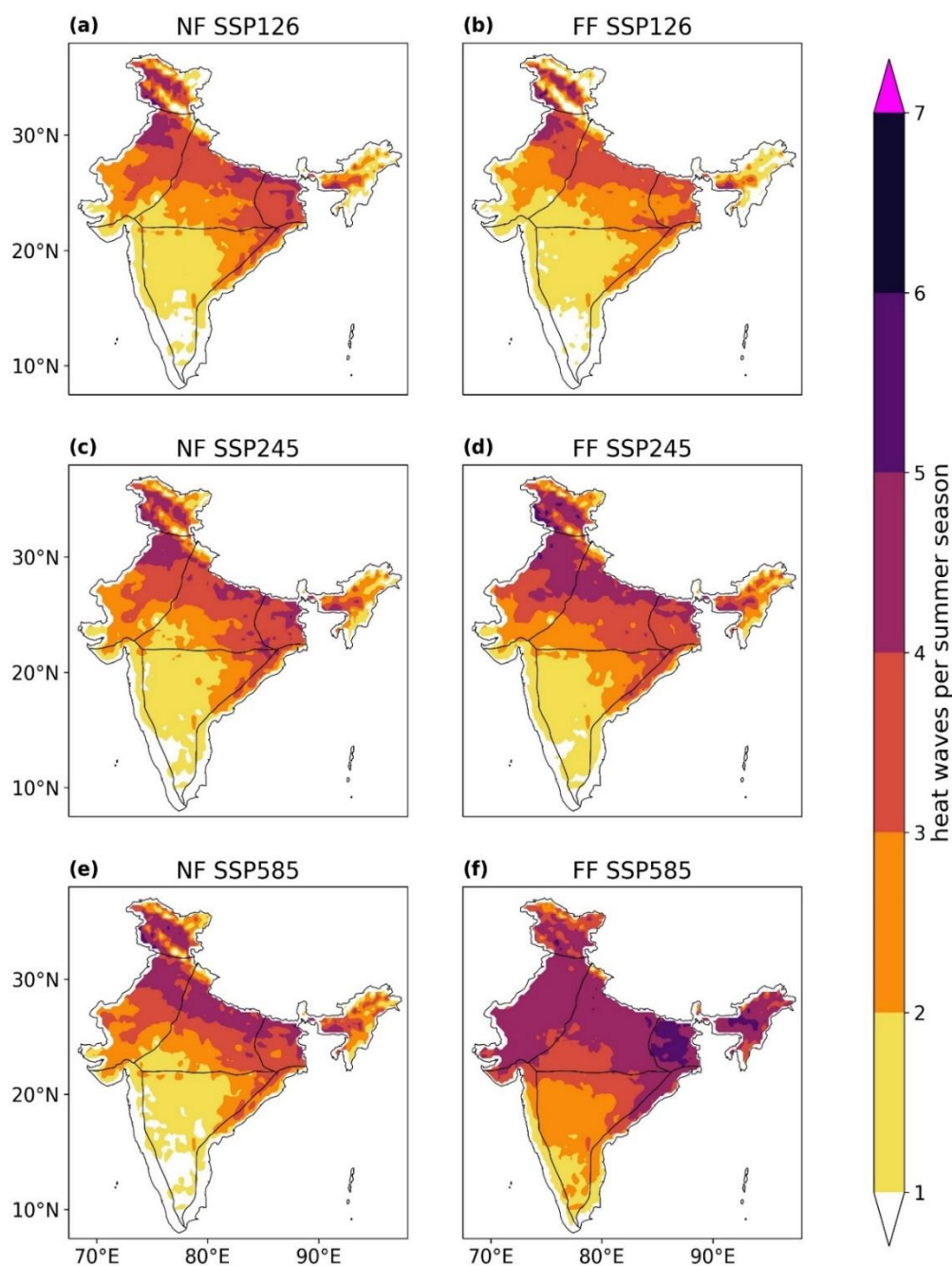


Fig. 5.5 – Heat waves per summer season (where $TX > TX_{norm} + 5^{\circ}C$ for 5 consecutive days) difference compared to the present climate for SSP1-2.6 (a, b), SSP2-4.5 (c, d) and SSP5-8.5 (e, f). The first column shows the difference over the NF period (a, c, e) and the second column shows the difference over the FF period (b, d, f).

3 consecutive day HWs (Fig. 5.6) show the largest increase when compared to the present climate, and once again the largest increase is from FF SSP585. All of India is shown to receive some amount of HW increase. The most impacted regions in the NF are the NE and

NW under SSP126 and SSP245 and show an increase of 7+ HWS. This is the same for SSP585, however a large part of the NC is most impacted here too. Moving onto the FF and SSP126 once again shows a reduction in HW number. There are hardly any more regions receiving 7+ HWS, except a very small part of the NE and WH. The most notable increase for FF SSP245 is over the NC and is shown to increase over all regions. FF SSP585 shows the largest increase over all of India, except the north of the NC which sees a larger increase in FF SSP245. The NC sees a decrease in the north, areas that were shown to have 7+ HWS are now down to 6.

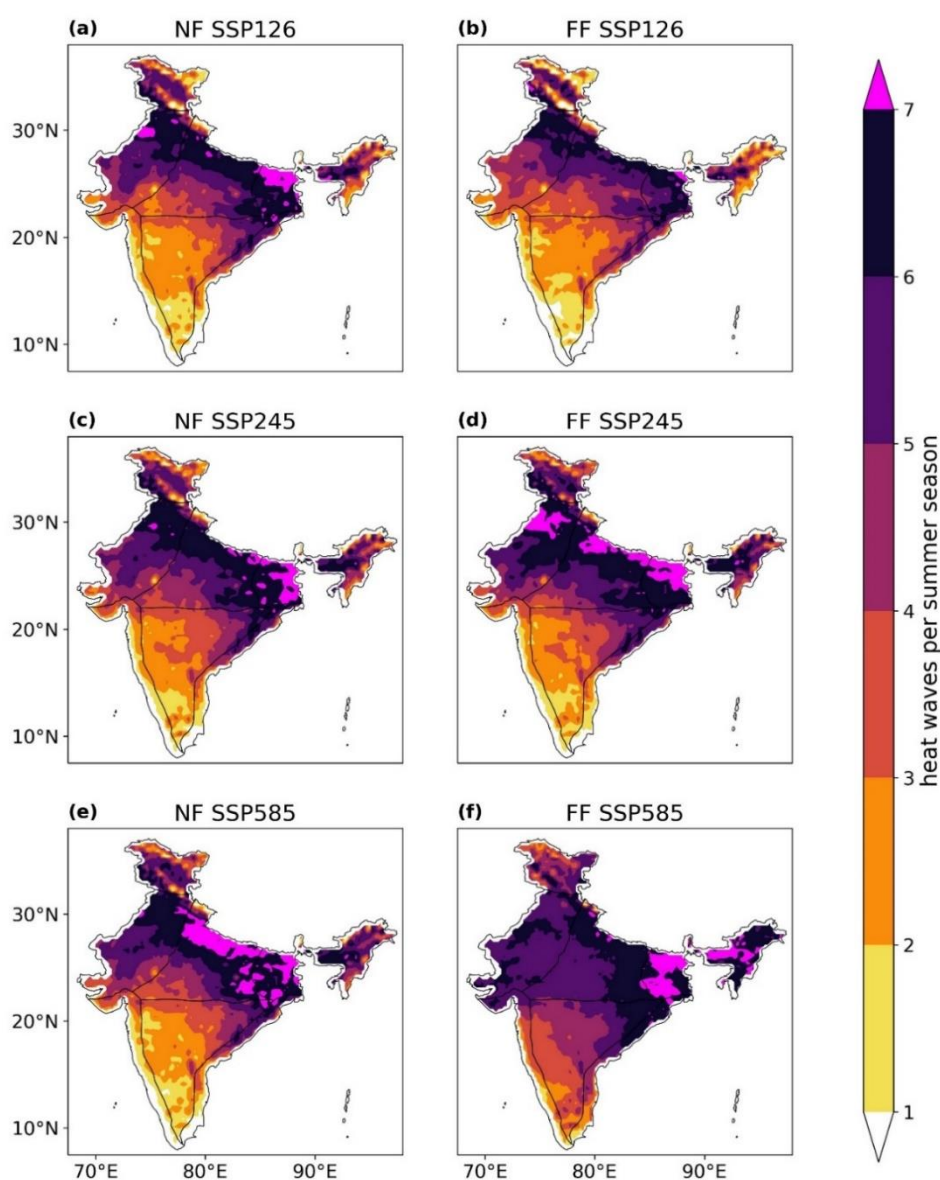


Fig. 5.6 – Heat waves per summer season (where $T_X > T_{Xnorm} + 5^\circ\text{C}$ for 3 consecutive days) difference compared to the present climate for SSP1-2.6 (a, b), SSP2-4.5 (c, d) and SSP5-8.5 (e, f). The first column shows the difference over the NF period (a, c, e) and the second column shows the difference over the FF period (b, d, f).

This could be because of the increase in longer duration HWs under FF SSP585 as seen in figures 5.4 and 5.5, meaning less of the shorter duration HWs. The NE is the most impacted region and sees a very large coverage of 7+ HWs under FF SSP585.

Overall FF SSP585 shows the largest increase in HW number over all of India, as well as an increase in HWs with a longer duration. The NE is generally the most impacted region, but all northern regions show quite a large increase. This is also where the Indo-Gangetic plane is, which is where a large portion of the Indian population resides, meaning this increase in HW frequency and duration will impact a large portion of the Indian population.

The heat wave duration index (HWDI) for 7 consecutive day HWs is shown in figure 5.7 for NF and FF SSP126, 245 and 585. The HWDI for 3 and 5 consecutive days are not shown as they have the same spatial coverage as figure 5.7 with slightly increased values. During the NF there is little different between the SSPs, although SSP245 and SSP585 appear to have a slightly higher HWDI than SSP126. During the NF, the WH is the most impacted region with regards to HWDI. During the FF SSP126 sees very little change. There is a slight increase over the northwest of the NC region. FF SSP245 and SSP585 show an increase compared to their NF counterparts, however the latter is much more significant. The NW, NC, NE and WH are now showing a HWDI of 55+ compared to FF SSP126 which has a maximum value of around 45. The most impacted region is the WH and NW which show values reaching 70 and over.

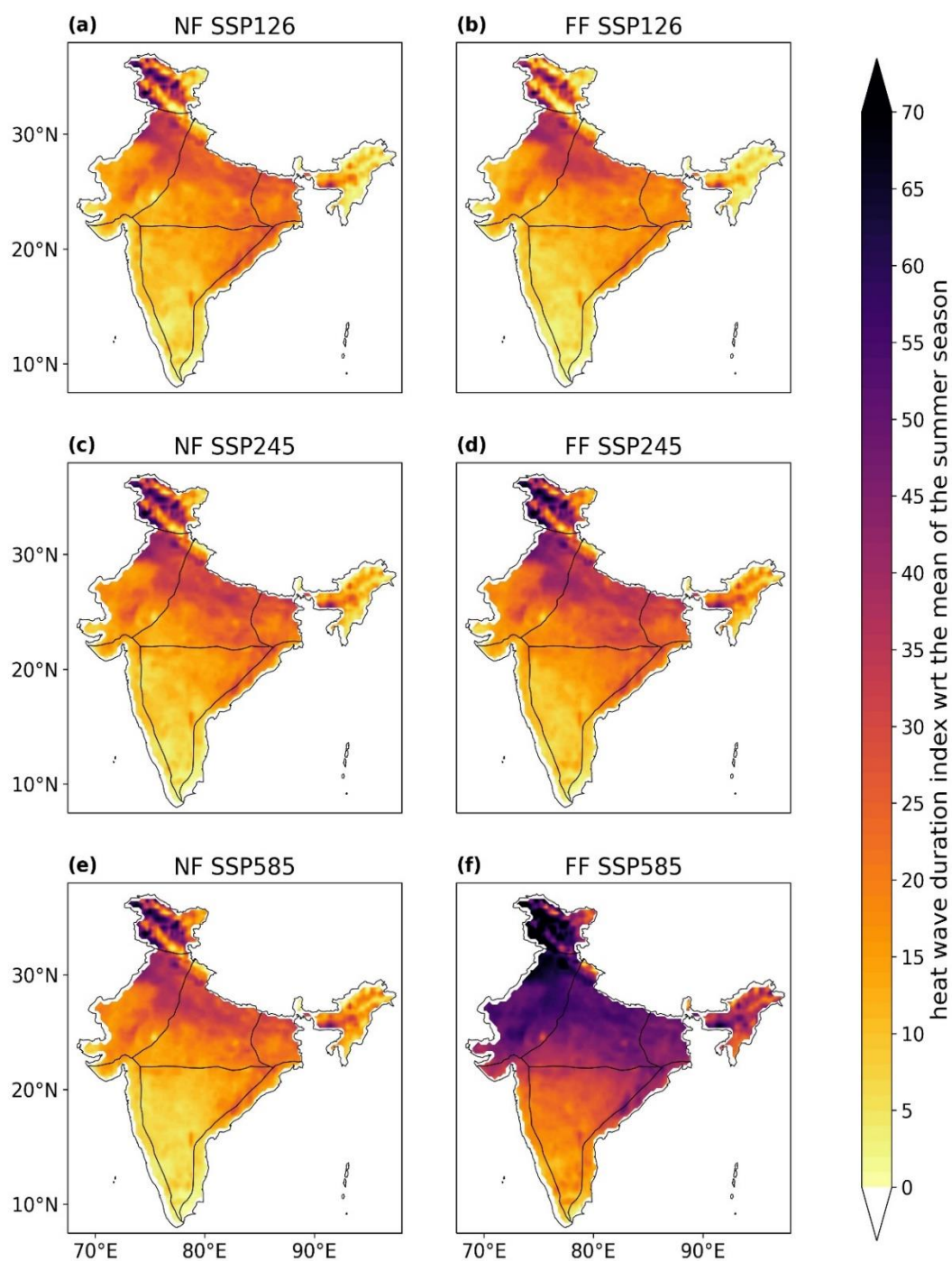


Fig. 5.7 – Heat wave duration index with reference to the mean of the summer season (where $TX > TX_{norm} + 5^{\circ}C$ for 7 consecutive days) difference compared to the present climate (1984-2014) for SSP1-2.6 (a, b), SSP2-4.5 (c, d) and SSP5-8.5 (e, f). The first column shows the difference over the NF period (a, c, e) and the second column shows the difference over the FF period (b, d, f).

5.3.2 Precipitation extremes using RCM simulations

5.3.2.1 HadGEM and RegCM4 Historical Analysis

The RCM mostly does well at representing precipitation over the Indian precipitation homogenous regions (Fig. 3.1) with varying wet and dry biases (Fig. 5.8). The NW region has the lowest biases out of all the regions. This region has a slight wet bias to the north and small areas of a slight dry bias. Conversely The NE and HR show quite a large wet bias. These are the more mountainous regions which suggests why the model struggles. The northwest of the HR shows a slight dry bias but is well represented. All other regions have a small wet bias, except the west coast of the WC and PR which is showing a dry bias. This is also where most of the ISM rainfall occurs in India.

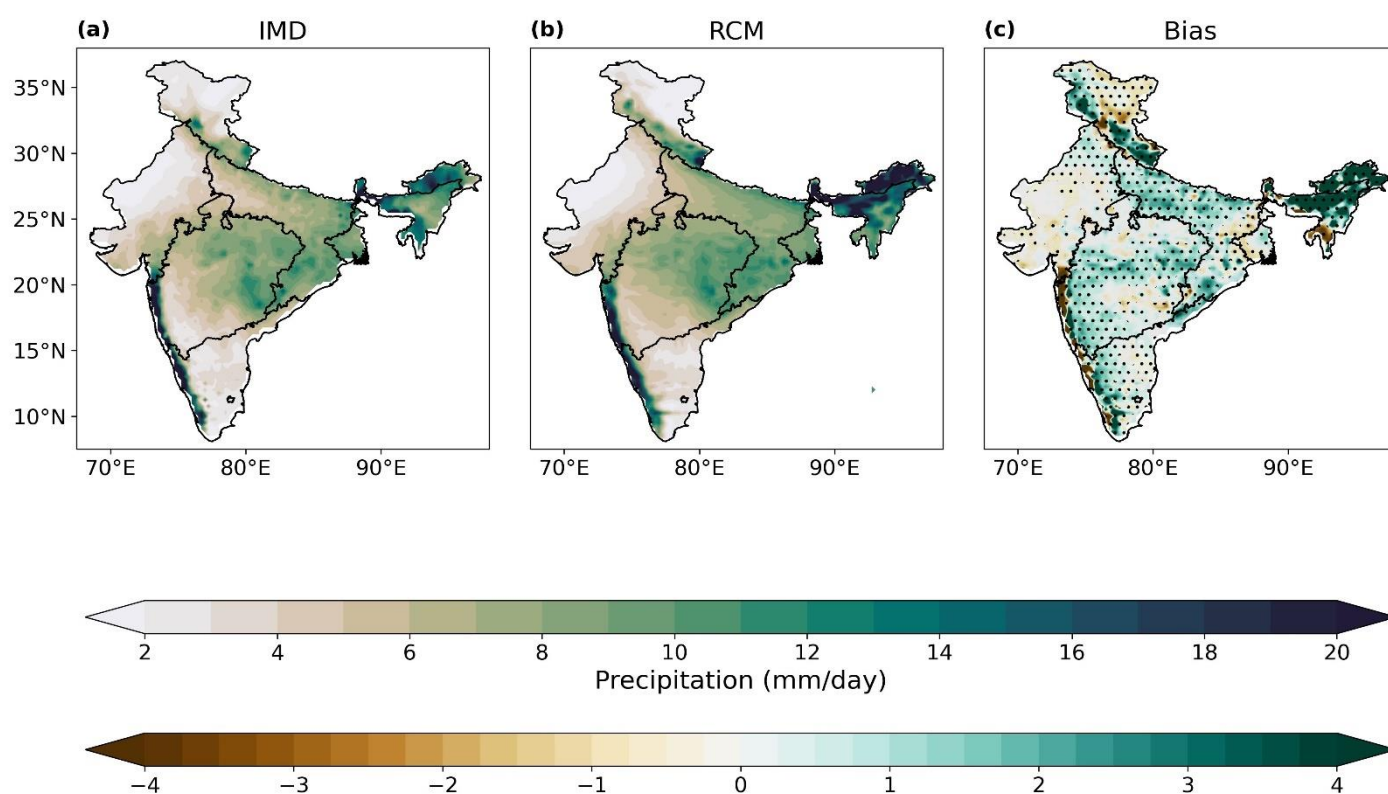


Fig. 5.8 – JJAS mean precipitation over the Indian precipitation homogenous regions for observed (a), RCM (b) and RCM bias (c) for the historical period (1984-2014). Here the observed data is taken from IMD. The dots represent the grid points with significant differences at 95% significance level.

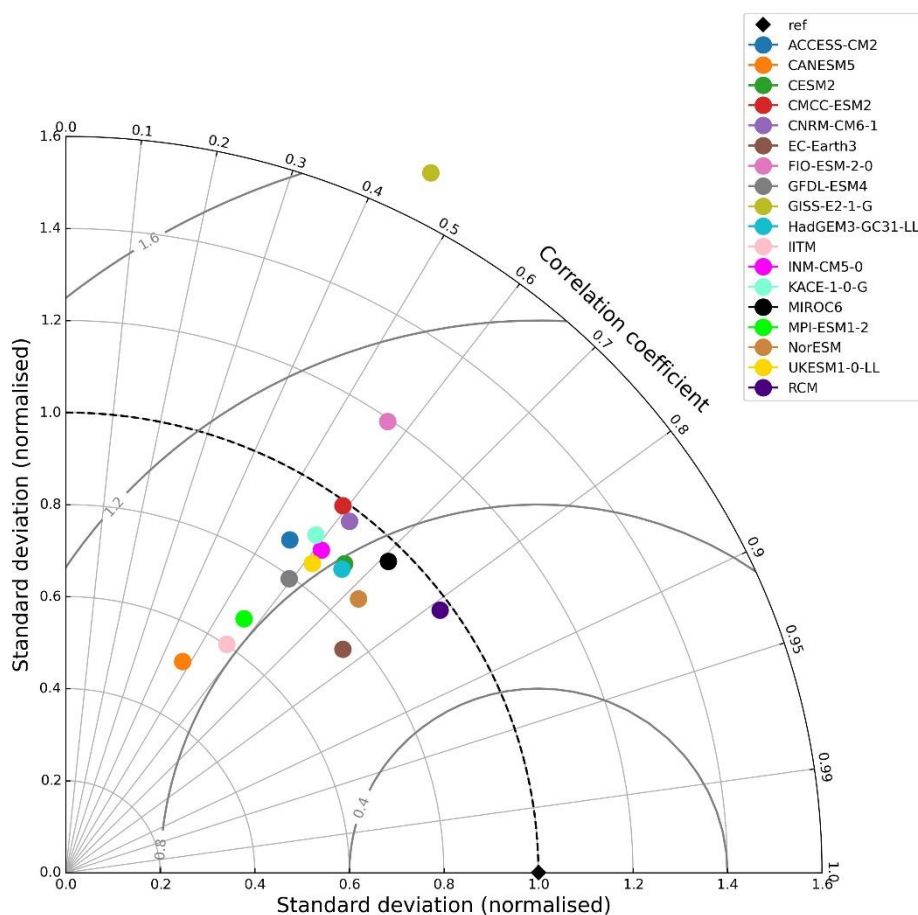


Fig. 5.9 – Taylor diagram showing JJAS mean precipitation over India for the historical period (1984-2014) for 17 CMIP6 models and the RCM compared to the IMD observed dataset.

The RCM outperforms all CMIP6 models when compared to the IMD mean precipitation dataset (Fig. 5.9). The correlation coefficient (CC) of the RCM improves upon all CMIP6 models. The CC of HadGEM3 (the driving model of the RCM) is 0.66, the best performing CMIP6 model (EC-Earth3) has a CC of 0.77 and the CC of the RCM is 0.82. The RCM also has an improved standard deviation (SD) when compared to most CMIP6 models and improves up the SD of HadGEM3. This is once again the same for root mean square error (RSME). Most of the CMIP6 models have an RSME of over 0.8 whereas the RCM has an RSME of 0.6. This figure highlights the importance of downscaling when simulating JJAS mean precipitation over India.

5.3.2.2 Future Changes in Precipitation

Future changes in mean precipitation vary per region and different SSPs seem to have less of an impact on future precipitation (Fig. 5.10 and table 5.2). The CNE shows a large reduction in mean precipitation for all SSPs and the largest reduction (-30.4%) is from FF SSP585. From NF to FF, both SSP126 and 245 increase slightly, whereas SSP585 precipitation reduces further. The HR precipitation change is mixed between SSPs. There is a slight decrease in the NF for SSP126 and 245 and a slight increase for SSP585. During the FF both SSP126 and 245 increase and SSP585 decreases. The NE shows a large decrease for both NF and FF for all SSPs and there is only a small difference between the SSPs. The NW also shows a decrease for all SSPs during the NF and FF. FF SSP585 shows a larger decrease (-28.5%) compared to other SSPs which don't appear to change as dramatically. The PR shows the largest increases out of all regions. During the NF there is a small difference between the SSPs, with SSP585 showing a slightly greater increase (29.1%). During the FF SSP126 decreases by 7.8%, SSP245 stays almost exactly the same (0.1% decrease) and SSP585 increases by 1.5%. The WC also sees increase in precipitation, the largest being from NF SSP585 (17%). Precipitation changes vary dramatically from region to region and it's unclear if the different SSPs have a significant effect on mean precipitation.

Table 5.2 – JJAS mean precipitation increase (%) per region compared to historical period (1984-2014). Positive (negative) values show an increase (decrease) in precipitation.

	CNE	HR	NE	NW	PR	WC
NF SSP126	-24.8	-2.44	-36.4	-18.4	24.4	11.9
NF SSP245	-27.4	-4.93	-36.0	-16.9	25.4	10.4
NF SSP585	-23.1	1.76	-33.7	-14.1	29.1	17.0
FF SSP126	-19.6	5.53	-31.9	-13.0	16.6	10.9
FF SSP245	-23.4	-1.77	-37.4	-11.0	25.3	14.9
FF SSP585	-30.4	-11.6	-39.5	-28.5	30.6	10.8

Generally, mean precipitation is shown to decrease over India and most of the precipitation homogenous regions (Fig. 5.11). The RCM for the historical period does a good job of capturing mean precipitation for most regions but struggles with the HR where it shows a large dry bias. The CNE shows a decrease in precipitation and FF SSP585 shows a slightly larger decrease than the other SSPs. This is the same for the HR and NW. The NE shows a decrease in precipitation, however, there appears to be no difference between the SSPs for NF and FF. The PR shows an increase in precipitation and FF SSP585 shows a slightly larger increase than the other SSPs. FF SSP126 shows a slight decrease. The WC also shows an increase in precipitation; however, the largest increase is from NF SSP585. Over the entirety of India there appears to be a slight decrease in precipitation overall, with FF SSP585 showing a slightly large decrease.

Most of India is shown to experience more extreme wet days (EWDs), however there is little difference between SSPs in the NF and FF (Fig. 5.12). For all SSPs during NF and FF the west coast of the PR and WC and parts of the WH receive the most EWDs (10% and over). There is little difference between the SSPs during the NF, the most noticeable difference is the slight increase in EWDs in the WC for NF SSP585. During the FF SSP126 shows a slight increase in the NW although differences between the two are small. For FF SSP245 the largest increase is seen to the west of the WC. This increase is also seen in FF SSP585 and is slightly greater. It seems that areas that receive the most precipitation during JJAS are projected to receive more EWDs, with SSP585 increasing these EWDs even more.

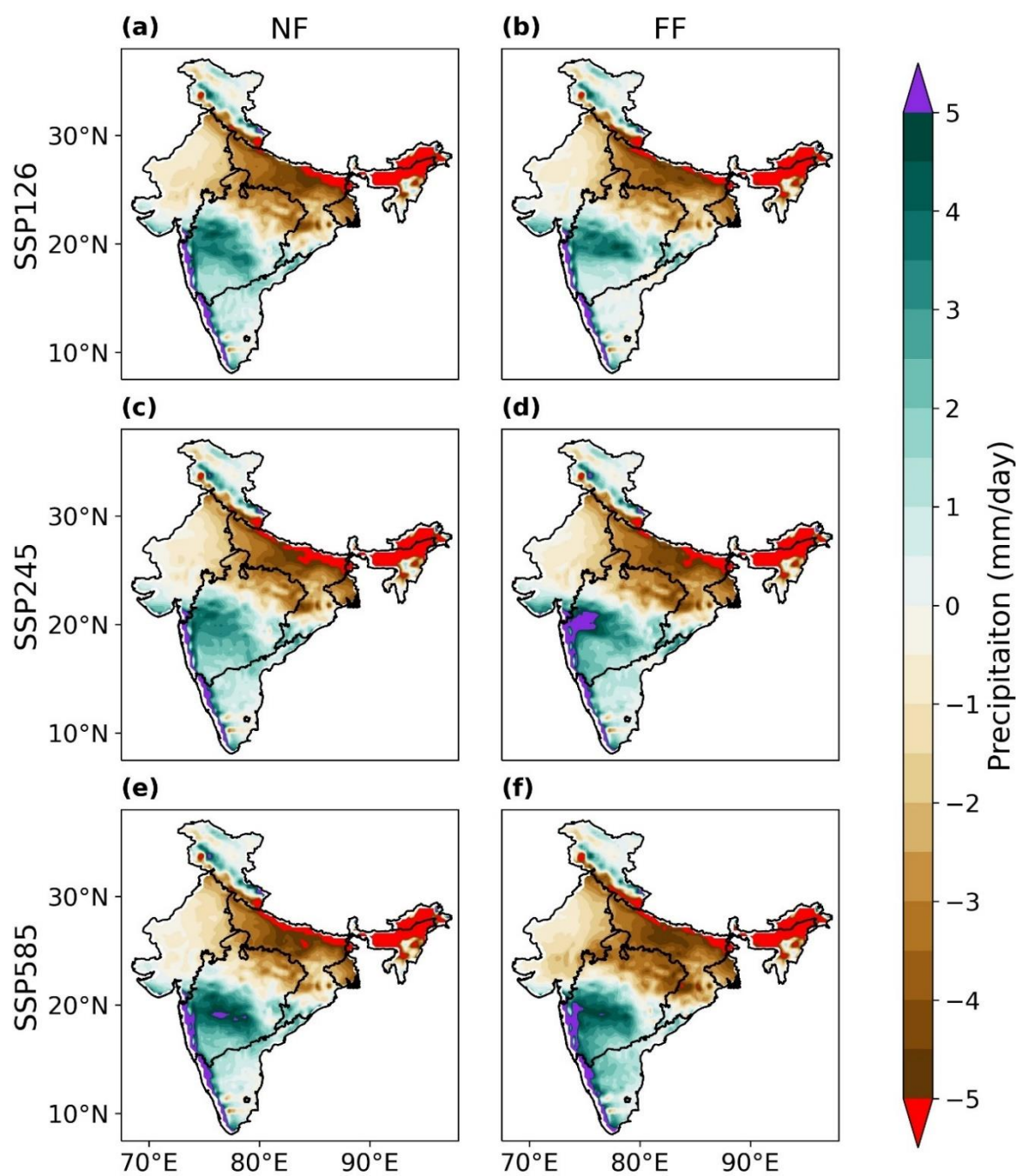


Fig. 5.10 – JJAS mean precipitation difference over Indian precipitation homogenous regions for SSP1-2.6 (a, b), SSP2-4.5 (c, d) and SSP5-8.5 (e, f). The first and second columns show the precipitation difference for NF (a, c, e) and FF (b, d, f) respectively when compared to the historical period.

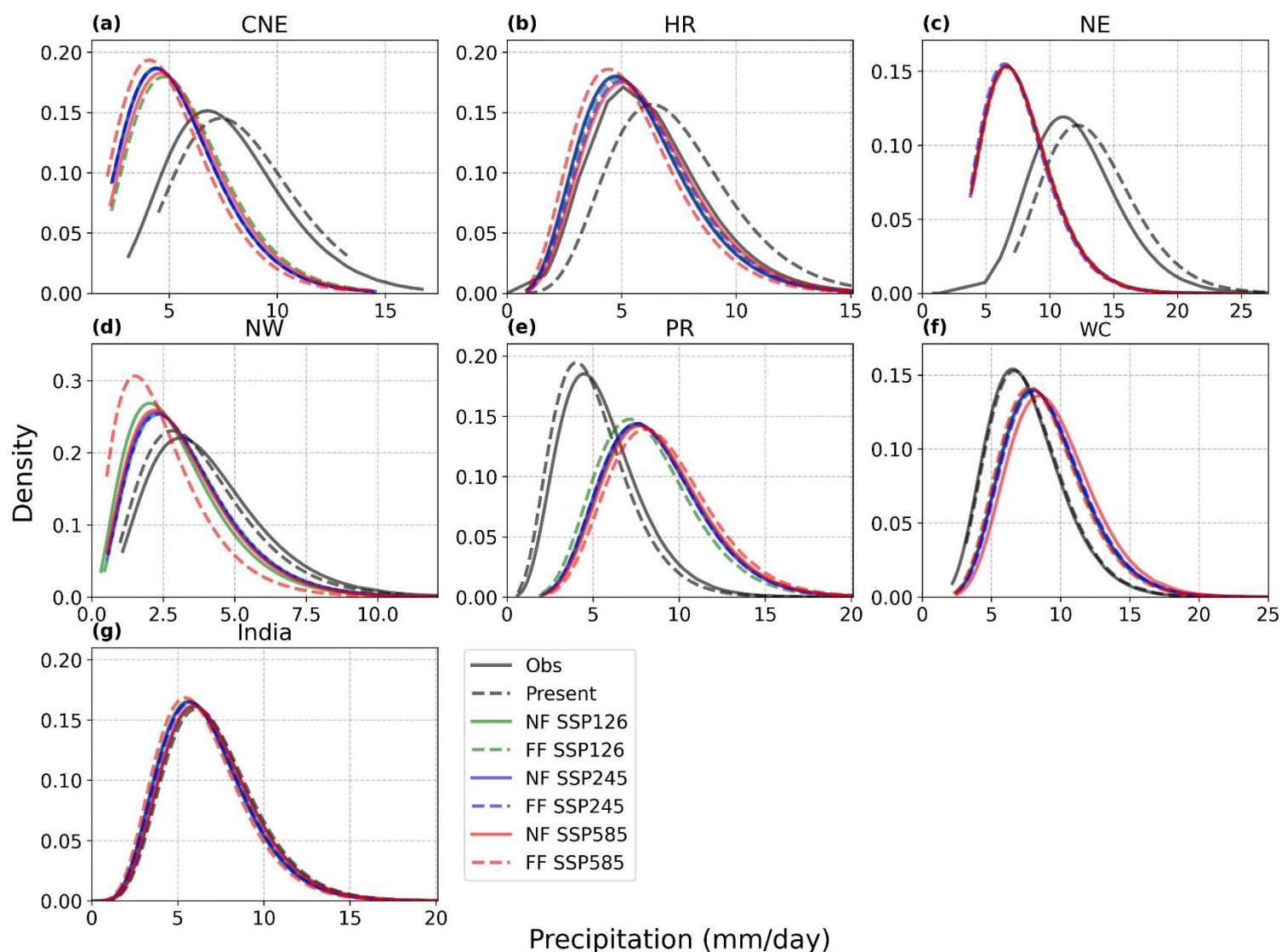


Fig. 5.11 – PDF for JJAS mean precipitation over the Indian precipitation homogenous regions during the historical, NF and FF periods using SSP1-2.6 (green), SSP2-4.5 (blue) and SSP5-8.5 (red). The historical period shows both observed values (solid black) and RCM values (dashed black). SSPs show solid lines for NF and dashed lines for FF.

5.3.2.1.1 Extreme Precipitation

Most of India is shown to experience more extreme wet days (EWDs), however there is little difference between SSPs in the NF and FF (Fig. 5.12). For all SSPs during NF and FF the west coast of the PR and WC and parts of the WH receive the most EWDs (10% and over). There is little difference between the SSPs during the NF, the most noticeable difference is the slight increase in EWDs in the WC for NF SSP585. During the FF SSP126 shows a slight increase in the NW although differences between the two are small. For FF SSP245 the largest

increase is seen to the west of the WC. This increase is also seen in FF SSP585 and is slightly greater. It seems that areas that receive the most precipitation during JJAS are projected to receive more EWDs, with SSP585 increasing these EWDs even more.

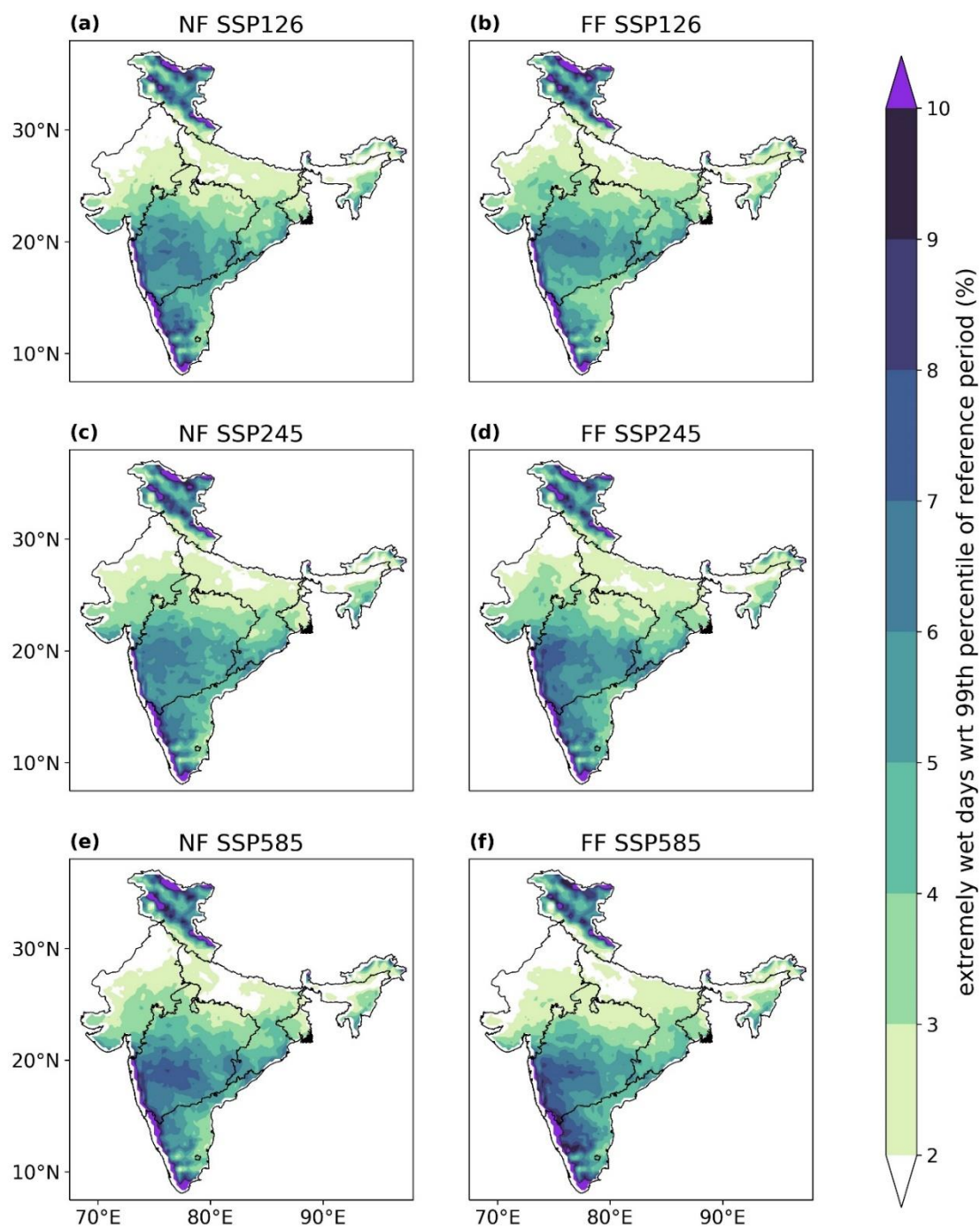


Fig. 5.12 – Extremely wet days with reference to the 99th percentile of reference period (1984-2014). The first column (a, c, e) shows the NF and the second column (b, d, f) shows the FF for SSP126 (a, b), SSP245 (c, d) and SSP585 (e, f).

5.4 Conclusion

RegCM4, driven by HadGEM3-GC31-LL, was used to assess future changes in extreme temperature and precipitation over India during JJA and JJAS respectively, using SSP126, 245 and 585. The performance of the RCM was also compared to HadGEM3-GC31-LL for the historical period. The key findings are as follows:

- The RCM shows a mostly cold bias for tasmax and tas, and a warm bias for tasmin. The biases are relatively small, except for the WH region which shows a large cold bias for all temperature variables.
- Precipitation is well represented by the RCM during the historical period over most regions. There is a large wet bias in the NE and the east part of the HR, which are also the most mountainous regions of India.
- When compared to HadGEM3, the RCM shows an improvement in correlation over all homogenous regions for temperature. For the temperature variables, HadGEM3 struggled with the EC and the RCM showed large improvements over this region.
- The RCM is shown to have an improved correlation coefficient, standard deviation and root mean square error compared to 17 CMIP6 models when simulating mean precipitation over India. This highlights the benefits of downscaling for JJAS precipitation simulation over this region.
- For all temperature homogenous regions, FF SSP585 shows the largest increase in tasmax. All SSPs show an increase in tasmax when compared to the present climate. For FF SP126 all regions except for the NC show a lower increase in tasmax compared to all other NF and FF SSPs. This suggests that although

warming is inevitable, sufficient mitigation strategies could lower this increase by the end of the century.

- All of India is shown to experience more 3-day HWs, with the NE and parts of the Indo-Gangetic plane being most affected. The most affected regions are shown to experience 7 and more HWs per summer season. FF SSP585 does show a slight reduction over the NC, however this could be because FF SSP585 will lead to longer duration HWs in the future. 5-day and 7-day HWs are most extreme with FF SSP585, with the most impacted regions being all the northern regions (NE, NC, NW and WH). FF SSP126 for 3-day and 5-day HWs shows a lower increase in HW frequency compared to the NF.
- From NF to FF there is no change in HWDI when looking at SSP126. There is a small increase in HWDI for SSP245 over the NW and NC. SSP585 shows a large increase in HWDI in the FF over all northern regions (WH, NW, NC, NE).
- Future changes in mean precipitation vary per region. Regions that already receive most of the ISM rainfall (west coast of the WC and PR) are projected to receive the largest increase in precipitation, however this is not true for the NE. The CNE, NE and eastern HR show large reductions in mean precipitation. All regions except for the PR and WC see a decrease in precipitation for all SSPs. There is less of a difference between SSPs for mean precipitation, however FF SSP585 appears to show the biggest difference when compared to the present climate. The only region this does not apply to is the WC where NF SSP585 shows the largest increase.
- Extremely wet days show an increase over almost all of India. The most affected regions are the IP, WC and the western part of the HR. Here the SSPs appear to

have a clearer influence, with FF SSP585 showing a larger increase, particularly over the IP and WC.

This chapter demonstrates the benefits of dynamical downscaling for both temperature and precipitation. The RCM is shown to better represent both variables during the historical period when compared to its driving model. However, there are some large biases, most notably over the Himalayas which the RCM still struggles with. In the future it would be beneficial to look at precipitation on a larger scale, as well as exploring the dynamics (windspeed and VIMT) of the ISM using the RCM.

Conclusion and Future Scope

The main focus of this thesis is to look at future changes in temperature and precipitation over India and its relevant homogenous regions. The fidelity of GCMs was tested for both temperature and precipitation, however the coarse resolution leads to large biases in places, most notably over the Himalayas. This led to the use of RCMs through dynamical downscaling to increase model resolution and better capture small scale processes which the GCMs neglect. The RCM used is the RegCM4.7 from ICTP and RCM data only considers JJA (temperature) and JJAS (precipitation) to look at future changes in these variables when they are most extreme using SSP126, SSP245 and SSP585. All experiments consider three time periods, the historical period (1984-2014), near-future (2030-2060) and far-future (2070-2100). Far-future for the RCM simulations is from 2070-2099.

Chapter 2 evaluates the performance of thirteen state-of-the-art GCMs for annual and JJA temperatures as well as the future changes using different SSP scenarios. A MME of the GCMs was created and has been found to reduce biases overall when compared to observed values, as temperature biases between models vary dramatically. The MME does a good job of capturing tasmax, tas and tasmin over India, but struggles with the Western Himalaya and Northeast regions due to the topographic complexity and snow cover of these regions. These regions are shown to have large cold biases for all temperatures during annual and JJA periods. Spatially CNRM-CM6 is found to be the best performing model, and temporally HadGEM3-GC31-LL, KACE-1-0G and UKESM1-0-LL are found to be the best performing. When looking at the MME, there is a larger warm bias during JJA compared to annual temperature variables, suggesting that models are overestimating summertime temperatures. The annual period shows more variation in biases depending on the region and temperature variable. Annual and JJA temperatures have been shown to increase in the NF and FF for all temperature variables, with the annual maximum temperature showing an increase of 1.1°C, 1.2°C and 1.6°C for NF and 1.5°C, 2.3°C and 4.1°C for FF SSP1-2.6, SSP2-4.5 and SSP5-8.5

respectively. The results of this chapter suggest that warming is inevitable as all SSP scenarios project a higher temperature at the end of the century compared to the present climate. SSP126 and 245 values begin to level off in the FF, whereas SSP585 continues to steadily rise which suggests that sufficient mitigation can limit warming over this region by the end of the century. The frequency and duration of heat waves have been shown to increase in the future and the most impacted areas are also some of the most densely populated regions of India along the Indo-Gangetic plane. This increase in heat wave characteristics is significantly worse when using SSP585, showing the impact of fossil fuels on future heat waves.

Chapter 3 assesses the fidelity of twelve state-of-the-art CMIP6 models and uses the MME of these models to look at future changes in precipitation during JJAS. This period is during the ISM when most precipitation occurs. This chapter considers both the South Asian domain and precipitation homogenous regions of India. Once again there are large variations in biases between models and the MME was shown to decrease these biases. The MME showed a dry bias over most of India, and a wet bias to the east of India. Windspeed and VIMT are also assessed here as they are important components of the ISM. The models can accurately capture the movement of the ISM, however, seem to largely underestimate windspeed and VIMT over the Arabian sea where these variables are strongest, which could explain the dry bias seen by the MME when simulating precipitation. During the future periods, all SSPs showed an increase in mean precipitation over India and this increase is most extreme for FF SSP585 and the Northeast region is found to be most affected. Extreme precipitation variables were also considered and were also found to increase the most for the FF SSP585 scenario and much lower for the other SSPs.

Chapter 4 looks at the customisation of RegCM4.7 through three sensitivity experiments that consider orography representations, cumulus convection schemes and land

surface schemes. The first experiment uses nine different sets of Himalayan orography representations. Here it was found that increasing the height increases mean precipitation and decreasing height has the inverse effect. An increased height of 10% (P10) yields the best results for precipitation representation. The second experiment looked at four different cumulus convection schemes. RegCM4.7 was able to simulate the mean pattern of upper air circulation well and can capture the contrasting features of circulation patterns during wet and dry years. The Grell over land and Emanuel over ocean (SC4) performed best over the Indian region with regards to precipitation simulation. The final experiment considers two different land surface schemes. CLM was found to be the better land surface scheme for both temperature and precipitation simulation over India. When performing long period simulations, the customisation of the RCM was shown to improve temperature and precipitation representation over India. These three experiments lead to a customised and improved RCM to better predict future changes in temperature and precipitation over India.

Chapter 5 uses the customised RCM to assess future changes in temperature and precipitation over India with a focus on extremes. The RCM is compared to CMIP6 models and was found to improve simulations in all regards however biases still remain, most notably over the Himalayan region. Maximum temperature was shown to increase in the future and is most extreme when using the SSP585 scenario in the far-future. SSP126 however, showed a decrease in maximum temperature in the far-future for all regions except for the NC when compared to the near-future. This shows that sufficient mitigation can lessen the impacts of climate change by the end of the century. India was shown to experience longer and more frequent heat waves in the near and far future, with the Indo-Gangetic plane being most affected. This is where most of India's population resides, putting a large amount of people at risk. The increase in heat waves was worse when using SSP585. Future changes in precipitation appear to vary per region. The areas that receive most of the monsoon rainfall along the

Westcoast of India are projected to receive more mean and extreme precipitation in the near and far future. Other parts of the country (CNE, NE and HR) showed a reduction in precipitation and in the far future, SSP585 shows the largest decrease over these regions. Extreme precipitation was shown to increase over most of India for all SSPs and there was a larger increase in the far future over the PR and WC regions using SSP585. While biases still remain in the RCM, a customised RCM is shown to improve temperature and precipitation simulations over India, adding robustness to the future projections. When comparing the results from chapters 2 and 3 to the results from chapter 5, GCMs are found to underpredict heat wave severity and over predict extreme precipitation.

This work emphasises the importance of sufficient mitigation strategies and the urgent need to act sooner rather than later. Actions made in the present day can have a large impact on the end of the century. Climate extremes are shown to worsen when using a high fossil fuel consumption scenario and this impact is lessened with the use of a more sustainable scenario. These climate extremes are shown to impact the most densely populated regions of India. A better understanding of these extremes and better action against these extremes is crucial to lessen the impact of climate change.

A continuation of this work would benefit from the use of ultra-high-resolution modelling over district level to give a more detailed look at increases in extreme temperature and precipitation in the most vulnerable zones. The use of machine learning approaches should be explored to apply downscaling techniques which require significantly less computational resources than dynamical downscaling. This would also allow for ISM simulation over a larger domain and higher resolution to better understand monsoon characteristics in models and further reduce these biases. Data assimilation should be used for short range, high impact climate events.

Appendix

Python Code

Time Average Computation

```
def jjas(month):  
    return (month >= 6) & (month <= 9)  
  
def time_av(sst, month):  
    data = sst.sel(time = month(sst['time.month']))  
    av = data.groupby('time.year')  
    av = av.mean('time')  
    av = av.mean('year')  
    av = av.values.ravel()  
    av = av[~np.isnan(av)]  
    return av
```

Probability Density Function

```
def plot (model, label, colour, line):  
    sort = np.sort(model)  
    ax.plot(sort, norm.pdf(sort, sort.mean()), colour, lw=2, alpha=0.6, label=label,  
linestyle = line)  
    ax.set_ylim([0,0.42])  
    ax.tick_params(labelsize = 14)  
    ax.grid(True, color='grey', linestyle='--', alpha=0.5)  
    return()
```

Spatial Map

```

def create_plot(model_av, model_ds, cru, model_tas, sig, model_name, subplot_number,
               xticks, yticks, domain, label, ytitle,
               colour, bounds, x_label, y_label):

    proj = ccrs.PlateCarree() #ccrs.Robinson() or ccrs.PlateCarree()
    ax = fig.add_subplot(3, 3, subplot_number, projection=proj)
    # Add cyclic point to data
    model_av, lons = add_cyclic_point(model_av, coord = model_ds['lon'])
    # Make a filled contour plot
    global cs
    cs = ax.contourf(lons, model_ds['lat'], model_av, transform = ccrs.PlateCarree(),
                    cmap=colour, levels=bounds, extend = 'both')

    #Lon and Lat ticks
    if x_label == True:
        ax.set_xticks(xticks, crs=ccrs.PlateCarree(), minor = True)
        ax.tick_params(labelsize = 'x-large')
        lon_formatter = LongitudeFormatter(zero_direction_label=True)
        ax.xaxis.set_major_formatter(lon_formatter)
    if y_label == True:
        ax.set_yticks(yticks, crs=ccrs.PlateCarree(), minor = True)
        ax.tick_params(labelsize = 'x-large')
        lat_formatter = LatitudeFormatter()
        ax.yaxis.set_major_formatter(lat_formatter)

    #Define region
    ax.set_extent(domain, crs=proj)

    #Plot Shapefiles
    shape(India_sf)
    ax.set_title(model_name, fontsize = 'xx-large')
    plt.ylabel(ytitle, fontsize = 'xx-large')

```

```

#Add subplot labels

trans = mtransforms.ScaledTranslation(0/72, 5/72, fig.dpi_scale_trans)

ax.text(0.0, 1.0, label, transform=ax.transAxes + trans,
        fontsize='x-large', va='bottom', fontweight = 'bold')

if sig == True:
    stat, p = ttest_ind(cru, model_tas, axis=0, nan_policy='omit')
    plot=p < 0.05
    ax.contourf(model_tas['lon'], model_tas['lat'], plot, 1, hatches=['|.'], alpha=0.06)

return ax, cs

```

Time Series

```

def create_plot(subplot_number, label, time_obs, time_rcm, time_cmip, tas_obs,
               tas_rcm, tas_cmip, min_rcm, min_cmip, max_rcm, max_cmip, title,xlabel, ylabel):
    ax = fig.add_subplot(1, 1, subplot_number)
    plt.title(title, fontsize = 23)
    ax.grid(True, color='k', linestyle='--', alpha = 0.5, zorder = 10)
    ax.plot(time_obs, tas_obs, label = 'Obs', color = 'k', linewidth = 1.7)
    ax.plot(time_rcm, tas_rcm, label = 'RCM', color = 'b', linewidth = 1.7)
    ax.plot(time_cmip, tas_cmip, label = 'CMIP6', color = 'r', linewidth = 1.7)
    plt.ylim(tas_cmip.min() - 1, tas_obs.max() + 1) #remove +/-0.5 for pr
    plt.xlim(1984, 2014.1)
    plt.xticks(np.arange(1984, 2014.1, 2))
    plt.xlabel(xlabel, fontsize = 'xx-large')
    plt.ylabel(ylabel, fontsize = 'xx-large')
    plt.tick_params(labelsize = 'xx-large')
    ax.fill_between(time_rcm, min_rcm, max_rcm, color='b', alpha=0.15, linewidth = 0.6)
    ax.fill_between(time_cmip, min_cmip, max_cmip, color='r', alpha=0.15, linewidth = 0.6)
    ax.plot(time_rcm, min_rcm, color = 'b', linewidth = 0.7, alpha=0.5)
    ax.plot(time_rcm, max_rcm, color = 'b', linewidth = 0.7, alpha=0.5)
    ax.plot(time_cmip, min_cmip, color = 'r', linewidth = 0.7, alpha=0.5)
    ax.plot(time_cmip, max_cmip, color = 'r', linewidth = 0.7, alpha=0.5)

```

Diagonal Correlation Matrix

```
def corr_calc(models, models_name, var_cru):
    results = {}
    a, b = 0, 0
    for i in models:
        for j in regions:
            hom = hom_region(i, j)
            value = time_av(time_slice(hom), jja)
            key = models_name[a] + "_" + regions_names[b]
            results[key] = []
            results[key].append(value)
            b += 1
        a += 1
        b = 0
    corr = {}
    for key in results:
        if re.search("^[^var_cru]", key):
            continue
        else:
            if re.search("IP$", key):
                IP_corr = float(xr.corr(results[key][0], results[var_cru+"_IP"][0]))
                key_corr = key + "_corr_IP"
                corr[key_corr] = []
                corr[key_corr].append(IP_corr)
            elif re.search("WH$", key):
                WH_corr = float(xr.corr(results[key][0], results[var_cru+"_WH"][0]))
                key_corr = key + "_corr_WH"
                corr[key_corr] = []
                corr[key_corr].append(WH_corr)
            elif re.search("NW$", key):
                NW_corr = float(xr.corr(results[key][0], results[var_cru+"_NW"][0]))
```

```
key_corr = key + "_corr_NW"
corr[key_corr] = []
corr[key_corr].append(NW_corr)
elif re.search("WC$", key):
    WC_corr = float(xr.corr(results[key][0], results[var_cru+"_WC"][0]))
    key_corr = key + "_corr_WC"
    corr[key_corr] = []
    corr[key_corr].append(WC_corr)
elif re.search("EC$", key):
    EC_corr = float(xr.corr(results[key][0], results[var_cru+"_EC"][0]))
    key_corr = key + "_corr_EC"
    corr[key_corr] = []
    corr[key_corr].append(EC_corr)
elif re.search("NE$", key):
    NE_corr = float(xr.corr(results[key][0], results[var_cru+"_NE"][0]))
    key_corr = key + "_corr_NE"
    corr[key_corr] = []
    corr[key_corr].append(NE_corr)
elif re.search("NC$", key):
    NC_corr = float(xr.corr(results[key][0], results[var_cru+"_NC"][0]))
    key_corr = key + "_corr_NC"
    corr[key_corr] = []
    corr[key_corr].append(NC_corr)
array = [[0 for col in range(7)] for row in range(2)]
i, j = 0, 0
for x in corr.values():
    array[j][i] = x[0]
    i += 1
    if i == 7:
        i = 0
        j += 1
```

```

array = np.transpose(array)
m_names = ["HadGEM3", "RCM"]
data = pd.DataFrame(array, index = regions_names, columns = m_names)
data = data.transpose()
return data

def heatmap(data, sub_no, c_bar, axcb, params, title, fig_label):
    colour = sns.color_palette("Spectral", 11)
    ticks = np.arange(-0.1, 1.1, 0.1)
    res = sns.heatmap(data, cmap = colour, vmin = -0.1, vmax = 1, linewidths = 0.01, ax = sub_no,
cbar=c_bar, cbar_ax=axcb,
        linecolor = 'black', annot = True, cbar_kws={"ticks":ticks, "label":'Correlation',
'drawedges':True})
    res.figure.axes[-1].yaxis.label.set_size(14)
    res.set_yticklabels(res.get_ymajorticklabels(), fontsize = 14)
    res.set_title(title)
    res.text(0.0, 0.0, fig_label, horizontalalignment='left',
        fontsize=12, va='bottom', fontweight = 'bold')
    if params == True:
        res.tick_params(bottom=False)

```

Vertically Integrated Moisture Transport Calculation

```

def vimt_calc(q, u, v, QU, QV, VIMT):
    a = 0
    b = 1
    n = len(q['plev'])
    for i in range(n-1):
        q2 = q.isel(plev = i+1)
        u2 = u.isel(plev = i+1)
        v2 = v.isel(plev = i+1)
        q1 = q.isel(plev = i)

```

```
u1 = u.isel(plev = i)
v1 = v.isel(plev = i)
p2 = float(q['plev'][b])
p1 = float(q['plev'][a])
qu = (((u1*q1 + u2*q2)/2) * (p1-p2))
qv = (((v1*q1 + v2*q2)/2) * (p1-p2))
vimt = (((u1*q1 + u2*q2)/2) * (p1-p2)) + (((v1*q1 + v2*q2)/2) * (p1-p2))
QU.append(qu)
QV.append(qv)
VIMT.append(vimt)
b+=1
a+=1
QU = np.nan_to_num(QU)
QU_sum = 1/9.81*sum(QU)
QV = np.nan_to_num(QV)
QV_sum = 1/9.81*sum(QV)
VIMT = np.nan_to_num(VIMT)
VIMT_sum = 1/9.81*sum(VIMT)
return QU_sum, QV_sum, VIMT_sum
```

References

Abe M, Kitoh A, Yasunari T (2003) An Evolution of the Asian Summer Monsoon Associated with Mountain Uplift—Simulation with the MRI Atmosphere-Ocean Coupled GCM. *J Meteorol Soc Japan* 81: 909-933.

Acharya N, Chattopadhyay S, Mohanty UC and Ghosh K (2014) Prediction of Indian summer monsoon rainfall: a weighted multi-model ensemble to enhance probabilistic forecast skills. *Meteorological Applications*, 21(3), 724– 732. doi.org/10.1002/met.1400

Agrawal, N., Singh, B. and Vivek Kumar Pandey (2021). Fidelity of Regional Climate Model v4.6 in capturing seasonal and subseasonal variability of Indian summer monsoon. *Dynamics of Atmospheres and Oceans*, 94, pp.101203–101203. doi.org/10.1016/j.dynatmoce.2021.101203

Ahmadi, H., Azizzadeh, J. The impacts of climate change based on regional and global climate models (RCMs and GCMs) projections (case study: Ilam province). *Model. Earth Syst. Environ.* 6, 685–696 (2020). doi.org/10.1007/s40808-020-00721-0

Almazroui, M., Saeed, S., Saeed, F., Islam, M. and Ismail, M. (2020) Projections of Precipitation and Temperature over the South Asian Countries in CMIP6. *Earth Systems and Environment*, 4:297-320. doi.org/10.1007/s41748-020-00157-7

Almazroui M, Ashfaq M, Islam M, Rashid I, Kamil S, Abid M, O'Brien E, Ismail M, Reboita M, Sörensson A, Arias P, Alves L, Tippett M, Saeed S, Haarsma R, Doblas-Reyes F, Saeed F, Kucharski F, Nadeem I, Silva-Vidal Y, Rivera J, Ehsan M, Martínez-Castro D, Muñoz Á, Ali M, Coppola E and Sylla M (2021). Assessment of CMIP6 performance and projected

temperature and precipitation changes over South America. *Earth Systems and Environment*, 5(2): 155–183. doi.org/10.1007/s41748-021-00233-6

Anthes, R.A. (1977). A Cumulus Parameterization Scheme Utilizing a One-Dimensional Cloud Model. *Monthly Weather Review*, 105(3), pp.270–286. doi.org/10.1175/1520-0493(1977)105%3C0270:acpsua%3E2.0.co;2.

Arbuthnott KG and Hajat S (2017). The health effects of hotter summers and heat waves in the population of the United Kingdom: A review of the evidence. *Environmental Health*. 16(S1). doi.org/10.1186/s12940-017-0322-5

Asharaf, S., Dobler, A. and Ahrens, B. (2012) Soil Moisture–Precipitation Feedback Processes in the Indian Summer Monsoon Season. *Journal of Hydrometeorology*, 13:1461-1474. <https://doi.org/10.1175/JHM-D-12-06.1>

Asharaf, S. and Ahrens, B. (2015) Indian Summer Monsoon Rainfall Processes in Climate Change Scenarios. *Journal of Climate*, 28:5414-5429. doi.org/10.1175/JCLI-D-14-00233.1

Ashfaq, M., Cavazos, T., Reboita, M.S. et al. Robust late twenty-first century shift in the regional monsoons in RegCM-CORDEX simulations. *Clim Dyn* 57, 1463–1488 (2021). doi.org/10.1007/s00382-020-05306-2

Bandara JS and Cai Y (2014). The impact of climate change on food crop productivity, food prices and food security in South Asia. *Economic Analysis and Policy*. 44(4): 451–465. doi.org/10.1016/j.eap.2014.09.005

Bøssing Christensen, O., Drews, M., Hesselbjerg Christensen, J., Dethloff, K., Ketelsen, K., Hebestadt, I., & Rinke, A. (2007). The HIRHAM Regional Climate Model. Version 5 (beta).

Danish Climate Centre, Danish Meteorological Institute. Denmark. Danish Meteorological Institute. Technical Report No. 06-17 <http://www.dmi.dk/dmi/tr06-17>

Carvalho, S.C.P., Santos, F.D. and Pulquério, M. (2016). Climate change scenarios for Angola: an analysis of precipitation and temperature projections using four RCMs. *International Journal of Climatology*, 37(8), pp.3398–3412. doi.org/10.1002/joc.4925.

Chen, L., Ma, Z., Li, Z., Wu, L., Jason Peter Flemke and Li, Y. (2018). Dynamical Downscaling of Temperature and Precipitation Extremes in China under Current and Future Climates. *Atmosphere-ocean*, 56(1), pp.55–70. doi.org/10.1080/07055900.2017.1422691.

Choudhury, B.A., Rajesh, P.V., Zahan, Y. and Goswami, B.N. (2021) Evolution of the Indian summer monsoon rainfall simulations from CMIP3 to CMIP6 models. *Climate Dynamics*, 58:2637-2662. doi.org/10.1007/s00382-021-06023-0

Collins, M., R. Knutti, J. Arblaster, J.-L. Dufresne, T. Fichefet, P. Friedlingstein, X. Gao, W.J. Gutowski, T. Johns, G. Krinner, M. Shongwe, C. Tebaldi, A.J. Weaver and M. Wehner, 2013: Long-term Climate Change: Projections, Commitments and Irreversibility. In: *Climate Change 2013: The Physical Science Basis. Contribution of Working Group I to the Fifth Assessment Report of the Intergovernmental Panel on Climate Change* [Stocker, T.F., D. Qin, G.-K. Plattner, M. Tignor, S.K. Allen, J. Boschung, A. Nauels, Y. Xia, V. Bex and P.M. Midgley (eds.)]. Cambridge University Press, Cambridge, United Kingdom and New York, NY, USA

Coppola, E., P. Stocchi, E. Pichelli, J. A. Torres Alavez, R. Glazer, G. Giuliani, F. Di Sante, R. Nogherotto, and F. Giorgi (2021). “Non-Hydrostatic RegCM4 (RegCM4-NH): Model description and case studies over multiple domains”. In: *Geoscientific Model Development Discussions* 2021, pp. 1–25. doi.org/10.5194/gmd-2020-435

-
- Das, S., Giorgi, F., Coppola, E., Panicker, A.S., Gautam, A.S., Nair, V.S. and Giuliani, G. (2021). Linkage between the absorbing aerosol-induced snow darkening effects over the Himalayas-Tibetan Plateau and the pre-monsoon climate over northern India. *Theoretical and Applied Climatology*, 147(3-4), pp.1033–1048. doi.org/10.1007/s00704-021-03871-y
- Dash, S., Kulkarni, M., Mohanty, U. and Prasad, K. (2009) Changes in the characteristics of rain events in India. *J. of Geophys. Res.*, 114,D10109. <https://doi.org/10.1029/2008JD010572>
- Dash, S.K. and Mamgain, A. (2011). Changes in the Frequency of Different Categories of Temperature Extremes in India. *Journal of Applied Meteorology and Climatology*, 50(9), pp.1842–1858. doi.org/10.1175/2011jamc2687.1
- De US, Dube RK and Prakasa Rao GS (2005). Extreme weather events over India in the last 100 years. *Geophys. Union*. 9: 173–187
- DeFries, R., Mondal, P., Singh, D., Agrawal, I., Fanzo, J., Remans, R. and Wood, S. (2016) Synergies and trade-offs for sustainable agriculture: Nutritional yields and climate-resilience for cereal crops in Central India. *Global Food Security*, 11, pp.44-53. doi.org/10.1016/j.gfs.2016.07.001
- Dickinson, R.E., A. Henderson-Sellers, and P.J. Kennedy (Aug. 1993). “Biosphere-Atmosphere Transfer Scheme (BATS) version 1e as coupled to the NCAR community climate model. Technical note. [NCAR (National Center for Atmospheric Research)]”.
- Dileepkumar R, AchutaRao K and Arulalan T (2018). Human influence on sub-regional surface air temperature change over India. *Scientific Reports*, 8(1). doi.org/10.1038/s41598-018-27185-8

- Dippoliti, Daniela, Paola Michelozzi, Claudia Marino, Francesca Dedonato, Bettina Menne, Klea Katsouyanni, Ursula Kirchmayer, Antonis Analitis, Mercedes Medina-Ramón, Anna Paldy, and et al. (2010). “The impact of heat waves on mortality in 9 European cities: results from the EuroHEAT project”. In: *Environmental Health* 9.1. doi.org/10.1186/1476069x-9-37.
- Dobler, A. and Ahrens, B. (2010). Analysis of the Indian summer monsoon system in the regional climate model COSMO-CLM. *Journal of Geophysical Research*, 115(D16). doi.org/10.1029/2009jd013497.
- Dong Z, Wang L, Sun Y, Hu T, Limsakul A, Singhruck P and Pimonsree S (2021). Heatwaves in Southeast Asia and Their Changes in a Warmer World. *Earth’s Future*, 9(7). doi.org/10.1029/2021ef001992
- Dutta, U., Hazra, A., Chaudhari, H.S., Saha, S.K., Pokhrel, S. and Verma, U. (2022). Unraveling the global teleconnections of Indian summer monsoon clouds: expedition from CMIP5 to CMIP6. *Global and Planetary Change*, 215:103873. <https://doi.org/10.1016/j.gloplacha.2022.103873>
- Elguindi, N., Bi, X., Giorgi, F., Nagarajan, B., Pal, J., Solomon, F. et al. (2017) Regional Climate Model RegCM Reference Manual Version 4.7. Tech. rep., The Abdus Salam International Centre for Theoretical Physics.
- Emanuel, K.A. (1991). A Scheme for Representing Cumulus Convection in Large-Scale Models. *Journal of the Atmospheric Sciences*, 48(21), pp.2313–2329. doi.org/10.1175/1520-0469(1991)048%3C2313:asfrcc%3E2.0.co;2.
- Emanuel KA, Živković-Rothman M (1999) Development and evaluation of a convection scheme for use in climate models. *J Atmos Sci* 56(11):1766–1782.

- Evans, R., Harrison, M., Graham, R. and Mylne, K. (2000) Joint Medium-Range Ensembles from The Met. Office and ECMWF Systems. *Monthly Weather Review*, 128:3104-3127. [https://doi.org/10.1175/1520-0493\(2000\)128<3104:JMREFT>2.0.CO;2](https://doi.org/10.1175/1520-0493(2000)128<3104:JMREFT>2.0.CO;2)
- Eyring, V., Bony, S., Meehl, G., Senior, C., Stevens, B., Stouffer, R. and Taylor, K. (2016) Overview of the Coupled Model Intercomparison Project Phase 6 (CMIP6) experimental design and organization. *Geoscientific Model Development*, 9:1937-1958. <https://doi.org/10.5194/gmd-9-1937-2016>
- Falga, R. and Wang, C. (2022) The rise of Indian summer monsoon precipitation extremes and its correlation with long-term changes of climate and anthropogenic factors. *Scientific Reports*, 12, 11985. <https://doi.org/10.1038/s41598-022-16240-0>
- Giorgi, F., Huang, Y., Nishizawa, K. and Fu, C. (1999). A seasonal cycle simulation over eastern Asia and its sensitivity to radiative transfer and surface processes. *Journal of Geophysical Research*, 104(D6), pp.6403–6423. doi.org/10.1029/1998jd200052.
- Giorgi, F., E. Coppola, F. Solmon, L. Mariotti, M. Sylla, X. Bi, N. Elguindi, G. Diro, V. S. Nair, G. Giuliani, U. Turuncoglu, S. Cozzini, I. Guttler, T. O'Brien, A. Tawfik, A. Shalaby, S. Zakey, A. Steiner, F. Stordal, and C. Branković (2012). "RegCM4: Model description and preliminary tests over multiple CORDEX domains". In: *Climate research* 936, p. 577X. doi.org/10.3354/cr01018.
- Giorgi, F., Coppola, E., Solomon, F., Mariotti, L., Sylla, M.B., Bill, X. et al. (2012) RegCM4: model description and preliminary tests over multiple CORDEX domains. *Climate Research*, 52, 7–29. doi.org/10.3354/cr01018

- Giorgi, F. (2019). Thirty Years of Regional Climate Modeling: Where Are We and Where Are We Going next? *Journal of Geophysical Research: Atmospheres*, 124(11). doi.org/10.1029/2018jd030094.
- Gornall J, Betts R, Burke E, Clark R, Camp J, Willett K and Wiltshire A (2010). Implications of climate change for agricultural productivity in the early twenty-first century. *Philosophical Transactions of the Royal Society B: Biological Sciences*. 365(1554): 2973–2989. doi.org/10.1098/rstb.2010.0158
- Grell, G. A. (1993). “Prognostic Evaluation of Assumptions Used by Cumulus Parameterizations”. In: *Monthly Weather Review* 121.3, pp. 764–787. doi.org/10.1175/1520-0493(1993)121<0764:PEOAUB>2.0.CO;2.
- Grenier, H. and C. S. Bretherton (2001). “A Moist PBL Parameterization for Large-Scale Models and Its Application to Subtropical Cloud-Topped Marine Boundary Layers”. In: *Monthly Weather Review* 129.3, pp. 357–377. doi.org/10.1175/1520-0493(2001)129<0357:amppfl>2.0.co;2.
- Gordon, C., Cooper, C., Senior, C. *et al.* (2000) The simulation of SST, sea ice extents and ocean heat transports in a version of the Hadley Centre coupled model without flux adjustments. *Climate Dynamics* **16**, 147–168. doi.org/10.1007/s003820050010
- Goswami, B. (1998) Interannual Variations of Indian Summer Monsoon in a GCM: External Conditions versus Internal Feedbacks. *Journal of Climate*, 11:501-522. https://doi.org/10.1175/1520-0442(1998)011<0501:IVOISM>2.0.CO;2
- Guilbert, M., Pascal Terray and Mignot, J. (2023) Intermodel Spread of Historical Indian Monsoon Rainfall Change in CMIP6: The Role of the Tropical Pacific Mean State. *Journal of climate*, 36:3937–3953. https://doi.org/10.1175/jcli-d-22-0585.1.

-
- Gusain, A., Ghosh, S. and Karmakar, S. (2020) Added value of CMIP6 over CMIP5 models in simulating Indian summer monsoon rainfall. *Atmospheric Research*, 232:0169-8095. <https://doi.org/10.1016/j.atmosres.2019.104680>.
- Haines A, Kovats RS, Campbell-Lendrum D and Corvalan C (2006). Climate change and human health: Impacts, vulnerability and public health. *Public Health*, 120(7): 585–596. doi.org/10.1016/j.puhe.2006.01.002
- Halpert, M. and Ropelewski, C. (1992) Surface Temperature Patterns Associated with the Southern Oscillation. *Journal of Climate*, 5:577-593. [doi.org/10.1175/1520-0442\(1992\)005<0577:STPAWT>2.0.CO;2](https://doi.org/10.1175/1520-0442(1992)005<0577:STPAWT>2.0.CO;2)
- Hamed, M.M., Nashwan, M.S., Shahid, S., Ismail, T. bin, Dewan, A. and Asaduzzaman, M. (2022). Thermal bioclimatic indicators over Southeast Asia: present status and future projection using CMIP6. *Environmental Science and Pollution Research*. doi.org/10.1007/s11356-022-22036-6
- Harris I, Jones PD, Osborn TJ and Lister DH (2013). Updated high-resolution grids of monthly climatic observations - the CRU TS3.10 Dataset. *International Journal of Climatology*, 34(3): 623–642. doi.org/10.1002/joc.3711
- Hashim, J. H. and Z. Hashim (2016). “Climate Change, Extreme Weather Events, and Human Health Implications in the Asia Pacific Region”. In: *Asia Pacific Journal of Public Health* 28.2 suppl, 8S–14S. doi.org/10.1177/1010539515599030.
- Hersbach, H., and Coauthors, 2020: The ERA5 global reanalysis. *Q.J.R. Meteorol. Soc.*, 146, 1999–2049.
- Holton, James R. (2004). *An introduction to dynamic meteorology*. Elsevier academic press.

Im, Eun-Soon, J. S. Pal, and E. A. B. Eltahir (2017). “Deadly heat waves projected in the densely populated agricultural regions of South Asia”. In: *Science Advances* 3.8,e1603322. doi.org/10.1126/sciadv.1603322.

Intergovernmental Panel On Climate Change, World Meteorological Organization and United Nations Environment Programme (1992). *Climate change: the 1990 and 1992 IPCC assessments; IPCC first assessment report overview and policymaker summaries and 1992 IPCC supplement*. Geneva: Wmo.

IPCC, 2001: *Climate Change 2001: The Scientific Basis*. Contribution of Working Group I to the Third Assessment Report of the Intergovernmental Panel on Climate Change [Houghton, J.T., Y. Ding, D.J. Griggs, M. Noguer, P.J. van der Linden, X. Dai, K. Maskell, and C.A. Johnson (eds.)]. Cambridge University Press, Cambridge, United Kingdom and New York, NY, USA, 881pp.

IPCC, 2007: *Climate Change 2007: Mitigation*. Contribution of Working Group III to the Fourth Assessment Report of the Inter-governmental Panel on Climate Change [B. Metz, O.R. Davidson, P.R. Bosch, R. Dave, L.A. Meyer (eds)], Cambridge University Press, Cambridge, United Kingdom and New York, NY, USA., XXX pp.

IPCC, 2013: *Climate Change 2013: The Physical Science Basis*. Contribution of Working Group I to the Fifth Assessment Report of the Intergovernmental Panel on Climate Change (2013). “[Stocker, T.F. and D. Qin and G.-K. Plattner and M. Tignor and S.K. Allen and J. Boschung and A. Nauels and Y. Xia and V. Bex and P.M. Midgley (eds.)]” In: Cambridge University Press Cambridge, United Kingdom and New York, NY, USA.1535.

IPCC, 2014. Climate Change 2014: Synthesis Report. Contribution of Working Groups I, II and III to the Fifth Assessment Report of the Intergovernmental Panel on Climate Change [Core Writing Team, R.K. Pachauri and L.A. Meyer (eds.)]. IPCC, Geneva, Switzerland, 151 pp.

IPCC, 2022: Climate Change 2022: Mitigation of Climate Change. Contribution of Working Group III to the Sixth Assessment Report of the Intergovernmental Panel on Climate Change [P.R. Shukla, J. Skea, R. Slade, A. Al Khourdajie, R. van Diemen, D. McCollum, M. Pathak, S. Some, P. Vyas, R. Fradera, M. Belkacemi, A. Hasija, G. Lisboa, S. Luz, J. Malley, (eds.)]. Cambridge University Press, Cambridge, UK and New York, NY, USA. doi.org/10.1017/9781009157926

Jacob, D., Podzun, R. Sensitivity studies with the regional climate model REMO. *Meteorol. Atmos. Phys.* **63**, 119–129 (1997). <https://doi.org/10.1007/BF01025368>

Jerez, S., López-Romero, J.M., Turco, M., Lorente-Plazas, R., Gómez-Navarro, J.J., Jiménez-Guerrero, P. and Montávez, J.P. (2020). On the Spin-Up Period in WRF Simulations Over Europe: Trade-Offs Between Length and Seasonality. *Journal of Advances in Modeling Earth Systems*, 12(4). doi.org/10.1029/2019ms001945

Jiang, J., Su, H., Wu, L., Zhai, C. and Schiro, K. (2021) Improvements in Cloud and Water Vapor Simulations Over the Tropical Oceans in CMIP6 Compared to CMIP5. *Earth and Space Science*, 8, e2020EA001520. doi.org/10.1029/2020EA001520

Kasahara A, Washington WM (1968) Thermal and Dynamical Effects of Orography on the General Circulation of the Atmosphere, NCAR Manuscript, No. 68-208.

- Katzenberger, A., Schewe, J., Pongratz, J. and Levermann, A. (2021) Robust increase of Indian monsoon rainfall and its variability under future warming in CMIP6 models. *Earth System Dynamics*, 12:367–386. doi.org/10.5194/esd-12-367-2021
- Kiehl, J.T., J.J. Hack, G.B. Bonan, B.A. Boville, and B.P. Briegleb (Sept. 1996). “Description of the NCAR Community Climate Model (CCM3). Technical note”.
- Kitoh, A., Endo, H., Krishna Kumar, K., Cavalcanti, I., Goswami, P. and Zhou, T., 2013. Monsoons in a changing world: A regional perspective in a global context. *Journal of Geophysical Research: Atmospheres*, 118:3053-3065. <https://doi.org/10.1002/jgrd.50258>
- Konda, G., Chowdary, J.S., C. Gnanaseelan and Parekh, A. (2023). Improvement in the skill of CMIP6 decadal hindcasts for extreme rainfall events over the Indian summer monsoon region. *Scientific reports*, 13(1). doi.org/10.1038/s41598-023-48268-1
- Kripalani, R.H., Kulkarni, A., Sabade, S.S. et al. (2003) Indian Monsoon Variability in a Global Warming Scenario. *Natural Hazards*, 29:189–206. <https://doi.org/10.1023/A:1023695326825>
- Krishna Kumar, K., Rupa Kumar, K., Ashrit, R., Deshpande, N. and Hansen, J. (2004) Climate impacts on Indian agriculture. *International Journal of Climatology*, 24:1375-1393. <https://doi.org/10.1002/joc.1081>
- Kuhlbrot, T., Jones, C. G., Sellar, A., Storkey, D., Blockley, E., Stringer, M., Hill, R., Graham, T., Ridley, J., Blaker, A., Calvert, D., Copsey, D., Ellis, R., Hewitt, H., Hyder, P., Ineson, S., Mulcahy, J., Siahann, A., & Walton, J. (2018). The low-resolution version of HadGEM3 GC3.1: Development and evaluation for global climate. *Journal of Advances in Modeling Earth Systems*, 10, 2865–2888. doi.org/10.1029/2018MS001370

- Kumar P, Wiltshire A, Mathison C, Asharaf S, Ahrens B, Lucas-Picher P, Christensen JH, Gobiet A, Saeed F, Hagemann S and Jacob D (2013). Downscaled climate change projections with uncertainty assessment over India using a high resolution multi-model approach. *Science of The Total Environment*, 468-469, pp.S18–S30. doi.org/10.1016/j.scitotenv.2013.01.051
- Lau, W., Wu, H. and Kim, K. (2013) A canonical response of precipitation characteristics to global warming from CMIP5 models. *Geophysical Research Letters*, 40:3163-3169. <https://doi.org/10.1002/grl.50420>
- Li, G. and Xie, S.P. (2012). Origins of tropical-wide SST biases in CMIP multi-model ensembles. *Geophysical Research Letters*, 39(22), doi.org/10.1029/2012gl053777
- Lorenz, Edward Norton (1967). “The nature and theory of the general circulation of the atmosphere”
- Lucas-Picher, P., and Coauthors, 2011: Can Regional Climate Models Represent the Indian Monsoon? *J. Hydrometeor.*, 12, 849–868, doi.org/10.1175/2011JHM1327.1.
- Lun, Y., Liu, L., Cheng, L., Li, X., Li, H. and Xu, Z. (2021). Assessment of GCMs simulation performance for precipitation and temperature from CMIP5 to CMIP6 over the Tibetan Plateau. *International Journal of Climatology*, 41:3994-4018. <https://doi.org/10.1002/joc.7055>
- Mazdiyasni O, AghaKouchak A, Davis SJ, Madadgar S, Mehran A, Ragno E, Sadegh M, Sengupta A, Ghosh S, Dhanya CT and Niknejad M (2017). Increasing probability of mortality during Indian heat waves. *Science Advances*, 3(6). doi.org/10.1126/sciadv.1700066
- Maharana P, Younous A and Pattnayak K (2018). Observed climate variability over Chad using multiple observational and reanalysis datasets. *Global and Planetary Change*, 162: 252-265. doi.org/10.1016/j.gloplacha.2018.01.013

- Medina, S., Houze, R., Kumar, A. and Niyogi, D. (2010) Summer monsoon convection in the Himalayan region: terrain and land cover effects. *Quarterly Journal of the Royal Meteorological Society*, 136:593–616. <https://doi.org/10.1002/qj.601>
- Meehl GA and Tebaldi C (2004). More Intense, More Frequent, and Longer Lasting Heat Waves in the 21st Century. *Science*, 305(5686): 994–997. doi.org/10.1126/science.1098704
- Menon, A., Levermann, A., Schewe, J., Lehmann, J. and Frieler, K. (2013) Consistent increase in Indian monsoon rainfall and its variability across CMIP-5 models. *Earth System Dynamics*, 4:287-300. <https://doi.org/10.5194/esd-4-287-2013>
- Mishra, S.K., Sahany, S., Salunke, P., Kang, I.-S. and Jain, S. (2018). Fidelity of CMIP5 multi-model mean in assessing Indian monsoon simulations. *npj Climate and Atmospheric Science*, [online] 1(1), pp.1–8. doi.org/10.1038/s41612-018-0049-1
- Mitchell TD and Jones PD (2005). An improved method of constructing a database of monthly climate observations and associated high-resolution grids. *International Journal of Climatology*, 25(6): 693–712. doi.org/10.1002/joc.1181
- Mondal S. K., Huang J., Wang Y., Su B., Kundzewicz Z. W., Jiang S., Zhai J., Chen Z., Jing C., Jiang T (2022). Changes in extreme precipitation across South Asia for each 0.5 °C of warming from 1.5 °C to 3.0°C above pre-industrial levels, *Atmospheric Research*, Volume 266,105961,0169-8095, doi.org/10.1016/j.atmosres.2021.105961.
- Moss RH, Edmonds JA, Hibbard KA, Manning MR, Rose SK, van Vuuren DP, Carter TR, Emori S, Kainuma M, Kram T, Meehl GA, Mitchell JFB, Nakicenovic N, Riahi K, Smith SJ, Stouffer RJ, Thomson AM, Weyant JP and Wilbanks TJ (2010). The next generation of scenarios for climate change research and assessment. *Nature*, 463(7282): 747–756. doi.org/10.1038/nature08823

- Mujumdar, M., Preethi, B., Sabin, T., Ashok, K., Saeed, S., Pai, D. and Krishnan, R. (2012) The Asian summer monsoon response to the La Niña event of 2010. *Meteorological Applications*, 19:216-225. <https://doi.org/10.1002/met.1301>
- Namias J (1980) The art and science of long-range forecasting. *Eos Trans. AGU* 61: 449-450.
- Norgate, M., Tiwari, P. R., Das, S., & Kumar, D. (2024). On the heat waves over India and their future projections under different SSP scenarios from CMIP6 models. *International Journal of Climatology*, **44**, 973–995.
- O'Brien, T. A., P. Y. Chuang, L. C. Sloan, I. C. Faloon, and D. L. Rossiter (Mar. 2012). "Coupling a new turbulence parametrization to RegCM adds realistic stratocumulus clouds". In: *Geoscientific Model Development* 5.4, pp. 989–1008. doi.org/10.5194/gmd-5-989-2012
- O'Neill BC, Kriegler E, Ebi KL, Kemp-Benedict E, Riahi K, Rothman DS, van Ruijven BJ, van Vuuren DP, Birkmann J, Kok K, Levy M and Solecki W (2017). The roads ahead: Narratives for shared socioeconomic pathways describing world futures in the 21st century. *Global Environmental Change*, 42: 169–180. doi.org/10.1016/j.gloenvcha.2015.01.004
- Oleson K. W., G. Y. Niu, Z. L. Yang, D. M. Lawrence, P. E. Thornton, P. J. Lawrence, R. Stöckli, R. E. Dickinson, G. B. Bonan, S. Levis, A. Dai and T. Qian, 2008. Improvements to the Community Land Model and their impact on the hydrological cycle. *J. Geophys. Res.* 113, 1021-1026.
- Pal, J.S., Small, E.E. and Eltahir, E.A.B. (2000). Simulation of regional-scale water and energy budgets: Representation of subgrid cloud and precipitation processes within RegCM. *Journal of Geophysical Research: Atmospheres*, 105(D24), pp.29579–29594. doi.org/10.1029/2000jd900415

- Pai, D., Rajeevan, M., Sreejith, O., Mukhopadhyay, B. and Satbha, N. (2014) Development of a new high spatial resolution ($0.25^\circ \times 0.25^\circ$) long period (1901-2010) daily gridded rainfall data set over India and its comparison with existing data sets over the region. *MAUSAM*, 65:1-18. <https://doi.org/10.54302/mausam.v65i1.851>
- Panda S K, Hong M, Dash SK, Jai-Ho Oh and Pattnayak KC (2020). Relative Roles of Eurasian Snow Depth and Sea Surface Temperature in Indian and Korean Summer Monsoons Based on GME Model Simulations. *Earth and Space Sci.* doi.org/10.1029/2020EA001105
- Pattnayak KC, Kar SC, Dalal M and Pattnayak R (2017a) Projections of annual rainfall and surface temperature from CMIP5 models over the BIMSTEC countries. *Global and Planetary Change*, 152:152-166. doi.org/10.1016/j.gloplacha.2017.03.005
- Pattnayak KC, Panda SK, Saraswat V et al. (2017b) Assessment of two versions of regional climate model in simulating the Indian Summer Monsoon over South Asia CORDEX domain. *Clim Dyn.* doi.org/10.1007/s00382-017-3792-9
- Pattnayak KC, Abdel AY, Rathakrishnan KV, Singh M, Dash R and Maharana P (2019) Changing Climate Over Chad: Is the Rainfall Over the Major Cities Recovering? *Earth and Space Sci* 6(7):1149–1160
- Patz JA, Campbell-Lendrum D, Holloway T and Foley JA (2005). Impact of regional climate change on human health. *Nature*, 438(7066): 310–317. doi.org/10.1038/nature04188
- Peixoto, Jos'e P., Abraham H. Oort, Curt Covey, and Karl Taylor (1992). "Physics of Climate". In: *Physics Today* 45.8, pp. 67–67. doi.org/10.1063/1.2809772.
- Perkins SE and Alexander LV (2013). On the Measurement of Heat Waves. *Journal of Climate*, 26(13): 4500–4517. doi.org/10.1175/jcli-d-12-00383.1

- Pielke R. and R. Avissar, 1990. Influence of landscape structure on local and regional climate, *Landscape Ecol.* 4, 133–155.
- Rajczak, J. and Schär, C. (2017). Projections of Future Precipitation Extremes Over Europe: A Multimodel Assessment of Climate Simulations. *Journal of Geophysical Research: Atmospheres*, 122(20), pp.10, 773–10, 800. doi.org/10.1002/2017jd027176.
- Rajeevan, M., and D. S. Pai (2007) On the El Niño-Indian monsoon predictive relationships, *Geophys. Res. Lett.*, 34, L04704, <https://doi.org/10.1029/2006GL028916>.
- Rasmusson, E. and Carpenter, T. (1983) The Relationship Between Eastern Equatorial Pacific Sea Surface Temperatures and Rainfall over India and Sri Lanka. *Monthly Weather Review*, 111:517-528. doi.org/10.1175/1520-0493(1983)111<0517:TRBEEP>2.0.CO;2
- Ratna, S. B., Cherchi, A., Osborn, T. J., Joshi, M., & Uppara, U. (2021) The extreme positive Indian Ocean dipole of 2019 and associated Indian summer monsoon rainfall response. *Geophysical Research Letters*, 48, e2020GL091497. <https://doi.org/10.1029/2020GL091497>
- Ray K, Giri RK, Ray SS, Dimri AP and Rajeevan M (2021). An assessment of long-term changes in mortalities due to extreme weather events in India: A study of 50 years' data, 1970–2019. *Weather and Climate Extremes*, 32: 100315. doi.org/10.1016/j.wace.2021.100315
- Riahi K, van Vuuren DP, Kriegler E, Edmonds J, O'Neill BC, Fujimori S, Bauer N, Calvin K, Dellink R, Fricko O, Lutz W, Popp A, Cuaresma JC, KC S, Leimbach M, Jiang L, Kram T, Rao S, Emmerling J and Ebi K (2017). The Shared Socioeconomic Pathways and their energy, land use, and greenhouse gas emissions implications: An overview. *Global Environmental Change*, 42: 153–168. doi.org/10.1016/j.gloenvcha.2016.05.009

- Rockel, B. and Geyer, B. (2008). The performance of the regional climate model CLM in different climate regions, based on the example of precipitation. *Meteorologische Zeitschrift*, 17(4), pp.487–498. doi.org/10.1127/0941-2948/2008/0297.
- Rohini P, Rajeevan M and Srivastava AK (2016). On the Variability and Increasing Trends of Heat Waves over India. *Scientific Reports*, 6(1). doi.org/10.1038/srep26153
- Salby, Murry L. (2012). *Physics of the atmosphere and climate*. Cambridge University Press.
- Salehie, O., Ismail, T. bin, Hamed, M.M., Shahid, S. and Idlan Muhammad, M.K. (2022). Projection of Hot and Cold Extremes in the Amu River Basin of Central Asia using GCMs CMIP6. *Stochastic Environmental Research and Risk Assessment*. doi.org/10.1007/s00477-022-02201-6
- Sawyer, J. Man-made Carbon Dioxide and the “Greenhouse” Effect. *Nature* **239**, 23–26 (1972). doi.org/10.1038/239023a0
- Schneider, Tapio (2006). “The General Circulation of the Atmosphere”. In: *Annual Review of Earth and Planetary Sciences* 34.1, pp. 655–688. doi.org/10.1146/annurev.earth.34.031405.125144.
- Schulzweida, Uwe, 2021. CDO User Guide (Version 2.0.0). Zenodo. <http://doi.org/10.5281/zenodo.5614769>
- Seo, G., Ahn, J., Cha, D., Suh, M., Min, S., Chang, E., Byun, Y. and Kim, J. (2023). Evaluation of multi-RCM ensembles for simulating spatiotemporal variability of Asian summer monsoon precipitation in the CORDEX-East Asia Phase 2 domain. *International Journal of Climatology*, 43(8), pp.3710–3729. doi.org/10.1002/joc.8054

-
- Sharmila, S., Joseph, S., Sahai, A., Abhilash, S. and Chattopadhyay, R. (2015) Future projection of Indian summer monsoon variability under climate change scenario: An assessment from CMIP5 climate models. *Global and Planetary Change*, 124:62-78. doi.org/10.1016/j.gloplacha.2014.11.004
- Sherwood, Steven C. and Matthew Huber (2010). “An adaptability limit to climate change due to heat stress”. In: *Proceedings of the National Academy of Sciences* 107.21, pp. 9552–9555. issn: 0027-8424. doi.org/10.1073/pnas.0913352107.
- Shahi, N.K., Das, S., Ghosh, S. et al. Projected changes in the mean and intra-seasonal variability of the Indian summer monsoon in the RegCM CORDEX-CORE simulations under higher warming conditions. *Clim Dyn* 57, 1489–1506 (2021). doi.org/10.1007/s00382-021-05771-3
- Shonk, J., 2022. Mechanisms of Climate Change in the Indian Summer Monsoon. [online] *Weather and Climate @ Reading*. Available at: <<https://blogs.reading.ac.uk/weather-and-climate-at-reading/2018/mechanisms-of-climate-change-in-the-indian-summer-monsoon/>> [Accessed 9 August 2022].
- Sinha, P.C., Mohanty, U.C., Kar, S.C. and Kumari, S. (2013). Role of the Himalayan Orography in Simulation of the Indian Summer Monsoon using RegCM3. *Pure and Applied Geophysics*, 171:1385–1407. <https://doi.org/10.1007/s00024-013-0675-9>
- Sivakumar MVK and Stefanski R (2010). Climate Change in South Asia. *Climate Change and Food Security in South Asia*: 13–30. doi.org/10.1007/978-90-481-9516-9_2

-
- Song, J.H., Kang, H.S., Byun, Y.H. and Hong, S.Y. (2009). Effects of the Tibetan Plateau on the Asian summer monsoon: a numerical case study using a regional climate model. *International Journal of Climatology*, 30:743-759. <https://doi.org/10.1002/joc.1906>
- Sousa, Pedro M., David Barriopedro, Ricardo Garc'ia-Herrera, Carlos Ord'oz, Pedro M. M. Soares, and Ricardo M. Trigo (2020). "Distinct influences of large-scale circulation and regional feedbacks in two exceptional 2019 European heatwaves". In: *Communications Earth Environment* 1.1. doi.org/10.1038/s43247-020-00048-9.
- Stouffer RJ, Eyring V, Meehl GA, Bony S, Senior C, Stevens B and Taylor KE (2017). CMIP5 Scientific Gaps and Recommendations for CMIP6. *Bulletin of the American Meteorological Society*, 98(1): 95–105. doi.org/10.1175/bams-d-15-00013.1
- Taylor KE (2001). Summarizing multiple aspects of model performance in a single diagram. *Journal of Geophysical Research: Atmospheres*, 106: 7183–7192. doi.org/10.1029/2000jd900719
- Taylor K, Stouffer R and Meehl G, 2012. An Overview of CMIP5 and the Experiment Design. *Bulletin of the American Meteorological Society*, 93(4): 485-498. doi.org/10.1175/BAMS-D-11-00094.1
- Tiwari, P.R., Kar, S.C., Mohanty, U.C., Kumari, S., Sinha, P., Nair, A. and Dey, S. (2014). Skill of precipitation prediction with GCMs over north India during winter season. *International Journal of Climatology*, 34(12), pp.3440–3455. doi.org/10.1002/joc.3921.
- Tiwari, P.R., Kar, S.C., Mohanty, U.C., Dey, S., Sinha, P., Raju, P.V.S. and Shekhar, M.S. (2016). On the dynamical downscaling and bias correction of seasonal-scale winter

precipitation predictions over North India. *Quarterly Journal of the Royal Meteorological Society*, 142(699), pp.2398–2410. doi.org/10.1002/qj.2832

Tiwari, P.R., Kar, S.C., Mohanty, U.C., Dey, S., Sinha, P.C. and Shekhar, M.S. (2017). Sensitivity of the Himalayan orography representation in simulation of winter precipitation using Regional Climate Model (RegCM) nested in a GCM. *Climate Dynamics*, 49(11-12), pp.4157–4170. doi.org/10.1007/s00382-017-3567-3

Turco, M., Llasat, M.C., Herrera, S. and Gutiérrez, J.M. (2017). Bias correction and downscaling of future RCM precipitation projections using a MOS-Analog technique. *Journal of Geophysical Research: Atmospheres*, 122(5), pp.2631–2648. doi.org/10.1002/2016jd025724.

Turner, A., 2022. *Royal Meteorological Society*. [online] RMetS. Available at: <<https://www.rmets.org/resource/indian-monsoon-changing-climate>> [Accessed 9 August 2022].

Ullah, S., You, Q., Chen, D., Sachindra, D.A., AghaKouchak, A., Kang, S., Li, M., Zhai, P. and Ullah, W. (2022). Future population exposure to daytime and nighttime heat waves in South Asia. *Earth's Future*. doi.org/10.1029/2021ef002511

Ullah, S., You, Q., Ullah, W., Sachindra, D.A., Ali, A., Asher Samuel Bhatti and Ali, G. (2023). Climate change will exacerbate population exposure to future heat waves in the China-Pakistan economic corridor. *Weather and Climate Extremes*, 40, pp.100570–100570. doi.org/10.1016/j.wace.2023.100570

Wang, B., Liu, J., Kim, H., Webster, P., Yim, S. and Xiang, B. (2013) Northern Hemisphere summer monsoon intensified by mega-El Niño/southern oscillation and Atlantic multidecadal

oscillation. Proceedings of the National Academy of Sciences, 110:5347-5352.
doi.org/10.1073/pnas.1219405110

Webster, P., Magaña, V., Palmer, T., Shukla, J., Tomas, R., Yanai, M. and Yasunari, T. (1998) Monsoons: Processes, predictability, and the prospects for prediction. *Journal of Geophysical Research: Oceans*, 103:14451-14510. doi.org/10.1029/97JC02719

Webster, P., Moore, A., Loschnigg, J. and Leben, R. (1999) Coupled ocean–atmosphere dynamics in the Indian Ocean during 1997–98. *Nature*, 401:356-360. doi.org/10.1038/43848

Wilks, D.S. (2011). *Statistical methods in the atmospheric sciences*. Waltham, Ma: Academic Press.

Williams, K. D., Copsey, D., Blockley, E. W., Bodas-Salcedo, A., Calvert, D., Comer, R., Davis, P., Graham, T., Hewitt, H. T., Hill, R., Hyder, P., Ineson, S., Johns, T. C., Keen, A. B., Lee, R. W., Megann, A., Milton, S. F., Rae, J. G. L., Roberts, M. J., Scaife, A. A., Schiemann, R., Storkey, D., Thorpe, L., Watterson, I. G., Walters, D. N., West, A., Wood, R. A., Woollings, T., & Xavier, P. K. (2017). The Met office global coupled model 3.0 and 3.1 (GC3.0 and GC3.1) configurations. *Journal of Advances in Modeling Earth Systems*, 10, 357–380. doi.org/10.1002/2017MS001115

Wilks DS (1995) *Statistical Methods in the Atmospheric Sciences*. Academic Press: San Diego, CA; 467

Willmott CJ (1982) Some comments on the evaluation of model performance. *Bull. Am. Meteorol. Soc.* 63: 1309–1313.

- Yang, Y., Jin, C. and Ali, S. (2020). Projection of heat wave in China under global warming targets of 1.5 °C and 2 °C by the ISIMIP models. *Atmospheric Research*, 244, pp.105057–105057. doi.org/10.1016/j.atmosres.2020.105057
- Yang, X. and Huang, P., 2021. Restored relationship between ENSO and Indian summer monsoon rainfall around 1999/2000. *The Innovation*, 2:2666-6758. doi.org/10.1016/j.xinn.2021.100102
- You, Q., Jiang, Z., Kong, L., Wu, Z., Bao, Y., Kang, S. and Pepin, N. (2016). A comparison of heat wave climatologies and trends in China based on multiple definitions. *Climate Dynamics*, 48(11-12), pp.3975–3989. doi.org/10.1007/s00382-016-3315-0
- Zeng Q, Li G, Cui Y, Jiang G and Pan X (2016). Estimating Temperature-Mortality Exposure-Response Relationships and Optimum Ambient Temperature at the Multi-City Level of China. *International Journal of Environmental Research and Public Health*, 13(3): 279. doi.org/10.3390/ijerph13030279
- Zhang, Yi, Isaac Held, and Stephan Fueglistaler (2021). “Projections of tropical heat stress constrained by atmospheric dynamics”. In: *Nature Geoscience* 14.3, pp. 133–137. doi.org/10.1038/s41561-021-00695-3.
- Zhou, T., L. Zhang, and H. Li (2008) Changes in global land monsoon area and total rainfall accumulation over the last half century, *Geophys. Res. Lett.*, 35, L16707. https://doi.org/10.1029/2008GL034881
- Zhou, T., Song, F. and Chen, X. (2013). Historical evolution of global and regional surface air temperature simulated by FGOALS-s2 and FGOALS-g2: How reliable are the model results? *Advances in Atmospheric Sciences*, 30(3), pp.638–657. doi.org/10.1007/s00376-013-2205-1.

Zhou, T., A. Turner, J. Kinter, B. Wang, Y. Qian, X. Chen, B. Wu, B. Liu, L. Zou, and B. He., 2016. GMMIP (v1.0) contribution to CMIP6: Global Monsoons Model Inter-comparison Project. *Geoscientific Model Development* 9:3589–3604. <https://doi.org/10.5194/gmd-9-3589-2016>

Zhao A, Bollasina MA and Stevenson DS (2019). Strong Influence of Aerosol Reductions on Future Heatwaves. *Geophysical Research Letters*, 46(9): 4913–4923. doi.org/10.1029/2019gl082269